The Development of Novel Fuel Dehydrating Icing Inhibitors

Sonia Liviana Repetto

A thesis submitted in partial fulfilment of the requirements of the University of the West of England, Bristol, for the degree of Doctor of Philosophy

Faculty of Health and Applied Sciences,
University of the West of England, Bristol

July 2014

Abstract

Dissolved water is a normal component of jet fuel which is vapourised during combustion; however, free water is a contaminant that can starve engines, freeze to form ice crystals capable of blocking fuel feeds, support microbial growth, and contribute towards corrosion. Jet fuel may be protected from the potentially hazardous effects of free-water using biocides and corrosion/icing inhibitors. This investigation seeks to identify novel chemical approaches to the dual management of water contamination and ice formation in jet fuel. The strategy of using organic molecules as dehydrating agents remains a relatively neglected solution, perhaps because of the complexity of the physical organic chemistry involved in developing and refining these systems. This Thesis describes our systematic approach towards the development of jet fuel additives which are kinetically fast, selective, lipophilic water scavengers that produce, upon hydrolysis, a hydrophilic ice inhibitor [Fuel Dehydrating Icing Inhibitors (FDII)]. A qualitative and quantitative analysis of the factors influencing the rates of hydrolysis for carefully selected geminal ethers is presented. The mechanistic understanding of the hydrolysis reactions of five and six membered geminal ethers has been consolidated using a combined kinetic ^{1}H NMR, isotopic labelling and computer assisted conformational analyses approach. For the first time, stereoelectronic arguments have been employed to rationalise the rates of hydrolysis of five membered ortho esters. A novel one-pot stereospecific *O*-acylative cleavage of epoxides is presented. It is anticipated that this new synthetic methodology would provide access to novel FDII in the future. Finally, logK_{OW} calculations have been used to predict the partitioning behaviour of FDII, and thereby screen candidate molecules for future study. We believe that FDII represents a novel and versatile approach for protecting jet fuel against the effects of water contamination.

Copyright Declaration

Acknowledgements

I would like to express my gratitude to Professor Norman Ratcliffe and the Faculty of Health and Applied Sciences for giving me the opportunity to return to chemical research after a ten year break. My PhD was funded by the UK Engineering and Physical Sciences Research Council (EPSRC) and Airbus Operations Ltd through the EPSRC Industrial CASE award, for which I am very grateful.

My special thanks go to Dr James Costello, my husband, with whom I have had continued dialogue throughout this work. I would like to thank him for his support, his guidance, and his ability to interpret data and propose new scientific hypotheses. His passion and enthusiasm for science and philosophy is inspirational, although at times exhausting!

Most of the work in this Thesis would not have been possible without the support of colleagues at the School of Chemistry of the University of Bristol; without ever hesitating, they gave their time and energy because of their love of science. I would particularly like to thank Dr Craig Butt and Professor Guy Lloyd-Jones FRS for providing me access to the facilities and resources of the School of Chemistry of the University of Bristol. A great debt is owed to Dr Craig Butt and Paul Lawrence of the NMR service for their continuous support and knowledge, Dr Louise Evans and Nick Taylor for their support in the kinetic and synthetic work, and Stephanie Flynn for the computational work.

My thanks to all my academic and industrial supervisors, Professor Norman Ratcliffe, Dr Benjamin de Lacy Costello and Dr Joseph Lam, for their support. Numerous people deserve thanks; those include the technical staff from the Health and Applied Science Faculty of University of the West of England and the School of Chemistry of the University of Bristol, my office colleagues at The University of the West of England and my laboratory

colleagues at the University of Bristol for their help with the day to day problems.

Many thanks go to the academic staff of Health and Applied Science Faculty of University of the West of England for giving me the opportunity to develop my teaching skills. I also would like to express my gratitude for the opportunity to collaborate with Solange Baena-Zambrana upon the review on the behaviour of water in jet fuel.

Finally, I would like to thank my family and friends for their support and encouragement throughout this study.

“Grazie mille”

Table of contents

List of Abbreviations

AAIB	Air Accident Investigation Branch
ASTM	American Society for Testing and Materials
Bio-SPK	Bio-Kerosene
C_2	180º Rotational symmetry
CI	Chemical Ionisation
CRC	Coordinating Research Council
C_S	Mirror plane symmetry
Def Stan	Defence Standard
EGME	Ethylene Glycol Monomethyl Ether
ESI	Electrospray Ionisation
EtOH	Ethanol
FDII	Fuel Dehydrating Icing Inhibitors
FID	Flame Ionisation Detector
FSII	Fuel System Icing Inhibitors
FSJF	Fully Synthetic Jet Fuel
FT	Fischer-Tropsch
GC	Gas Chromatography
GOST	Gosudarstvennyy Standart (Russian for state standard)
HA	Generic monoprotic acid
HBA	Hydrogen Bond Acceptor
HBD	Hydrogen Bond Donor
HEFA	Hydro-processed Esters and Fatty Acids
IATA	International Air Transport Association
IR	Infrared
k	Rate constant
K_a	Acid dissociation constant
K_{OW}	Octanol-water partition coefficient
m	gradient
M	Molar (mol/L)
m/z	Mass/charge
MM	Molecular Mass

MS	Mass Spectrometry
MsOH	Methanesulfonic acid
NMR	Nuclear Magnetic Resonance
nOe	Nucleaur Overhauser enhancement
PIANO	Paraffins, Isoparaffins, Aromatics, Naphthenes and Olefins
ppm	part per million (1 ppm = 0.0001%)
R^2	Coefficient of determination for linear regression
RH	Relative Humidity
ROH	Generic alcohol
RPA	Relative Peak Area
RT	Retention Time(s)
S_N2	Bi-molecular nucleophilic substitution
SPK	Synthetic Paraffinic Kerosene
TEOF	Triethyl orthoformate
TMOA	Trimethyl orthoacetate
UV	Ultraviolet
Vis	Visible
WS	Water Scavenger
γ/δ-lactones	5/6-Membered lactone ring
σ^*	Anti-bonding orbital
σ_{nb}	Lone pairs of electrons
[ ]	Concentration (mol/L)
1D NOESY	One Dimensional Nuclear Overhauser Effect Spectroscopy

Chapter 1

Jet Fuel

1.1 Introduction

The importance of the aviation industry cannot be overstated; it allows us to compete in the global market-place, create wealth and form an increasingly important role in how we spend our leisure time. On average, every day more than 8 million people fly. In 2013, the total number of passengers was 3.1 billion (IATA, 2013). From the small business jet to the largest passenger carrier, aircraft are powered mostly by gas turbine engines or by piston engines; both generate the energy by burning a fuel-air mixture. Aviation fuels are a mixture of hundreds of hydrocarbon components with no specific detailed chemical composition; however they have the most extensive specifications of all fuels, because of the performance requirements that have been identified over the years (CRC, 2004).

1.2 The Characteristics of Jet Fuel

Worldwide there are three major specifications for civil aviation turbine fuels; the American Society for Testing and Materials (ASTM) D1655, the British Defence Standard (Def Stan) 91-91, and the Russian GOST 10277. These specifications are alike in most respects, but differ significantly in the lower freezing point, flash point, and viscosity, because of the temperature range encountered in different countries. All three specify the minimum, maximum or the range in which the properties of aviation fuels must fall, but none specify the chemical composition of aviation fuels (CRC, 2004). This implies that the variability in chemical composition between aviation fuels could be infinite, and is dependent on the origin of the fuel, the process through which the fuel has been refined, and the nature and number of additives in the fuel. Aviation fuels are mainly derived from straight-run distillates from crude oil (*i.e.,* petroleum-based kerosene jet fuel); however over the years, the industry has in addition approved, after rigorous engine and compatibility testing, both synthetic kerosene, and bio-kerosene fuels (CRC, 2004). A brief overview of the differences and similarities of the three types of kerosene jet fuel is warranted.

1.2.1 Petroleum-Based Kerosene Jet Fuel

Petroleum-based kerosene jet fuel is derived from crude oil, and consists of blends of many different hydrocarbons with carbon chains ranging between 6-16 carbon atoms per molecule (Hemighaus *et al.,* 2006). Crude oils from different fields, and sometimes even different wells in the same field, differ significantly in the individual hydrocarbons present and their proportions (Smith, 1970). Hence, the properties of the same type of fuel are largely dependent on the crude oil from which they are obtained. However, by controlling the refining methods, the refiner can meet the requirements of the various specifications, even when these properties vary from one to another.

Petroleum-based kerosene jet fuel comprises, by volume, between 99% to 99.5% hydrocarbons (CRC, 2004). The hydrocarbons present can be grouped into three broad classes (Hemighaus *et al.*, 2006a):

- Paraffins (or alkanes)
- Naphthenes (or cycloalkanes)
- Aromatics

The proportions of these three classes vary depending upon the source of the crude oil from which the fuel is derived and the refining process; this will also influence the bulk properties of the fuel. Aromatics are limited to monocyclic and bicyclic compounds by the distillation process, and their content is limited to a maximum of 25% v/v with an industry accepted minimum of 8% v/v. Olefins (or alkenes) are generally present only in trace amounts (CRC, 2004). In 2006 a “World Fuel Survey” reported the average chemical composition of the three classes of hydrocarbon within 55 jet fuel samples to be paraffin:napthenes:aromatics = 3:1:1 v/v (Shafer *et al.*, 2006).

The remainder 0.5-1% non-hydrocarbon constituent of petroleum-based jet fuel is composed of hetero-organic compounds containing sulphur, nitrogen and oxygen; the former two being the most common heteroatoms present in

crude oil. These minor components are closely regulated by the fuel specifications as they are considered to be detrimental to the engine and the aircraft fuel system (Goodger, 2000). Sulphur is usually present as mercaptans, sulphides, disulphides, thiophenes. Free sulphur and hydrogen sulphide are corrosive to certain metals in the fuel system. Mercaptans attack cadmium plating and can cause deterioration of some types of synthetic rubbers. Both mercaptan and total sulphur content is limited by the specifications (CRC, 2004). Common and detrimental nitrogen-containing molecules include carbazoles, anilines, pyridines, indoles, and quinolones (Adams *et al.*, 2013). There are no specifications regarding nitrogen compounds. Phenols, peroxides and naphthenic acids are commonly encountered oxygen-containing compounds present in aviation fuels, and they originate in the crude oil (National Research Council, 1997). Phenols are good antioxidants; whereas peroxides have a negative impact on storage stability. Naphthenic acids can cause corrosion of zinc, by forming zinc naphthenates that are soluble in the fuel. Although there is no direct specification limiting the naphthenic acid content, the total acidity limit controls this constituent (CRC, 2004). In order to remove these undesired compounds and meet the target specifications, the raw kerosene may be subjected to either *hydrotreating* (*i.e.,* hydrogenation), *Merox* (*i.e.,* mercaptan oxidation) process and/or clay treatment at the refinery; this will result in a change of the chemical composition of the resultant jet fuel (Hemighaus *et al.*, 2006a). The world's most commonly used fuel for commercial aviation is the petroleum-based Jet A-1. There are at least 23 specifications which govern the performance of Jet A-1, but do not specify the precise chemical composition of the hydrocarbon mixture (CRC, 2004).

1.2.2 Synthetic Paraffinic Kerosene (SPK) Jet Fuel

Synthetic paraffinic kerosene (SPK) jet fuel is currently derived from natural gas using the gas to liquid Fischer-Tropsch (FT) process followed by downstream processing. Coal and biomass are a less widely used alternative to natural gas. The FT process (Scheme 1) converts a mixture of

carbon monoxide and hydrogen into mainly straight chain high molecular weight hydrocarbons (Schulz, 1999).

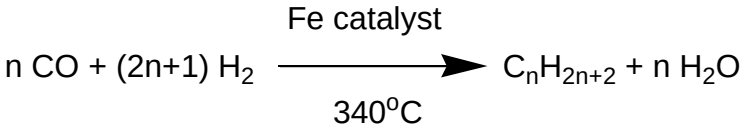

Scheme 1. Fischer-Tropsch process.

The raw product of the FT synthesis must be further processed to meet the specifications; this processing includes cracking the long chains into smaller units and isomerisation to provide the desired properties. This material is then distilled into final products (Hemighaus *et al.*, 2006b). The lack of aromatics and cyclo-paraffins in synthetic kerosenes yields a fuel below the minimum density requirement (Moses, 2008). Aromatics are also necessary for swelling elastomers used in aircraft fuel systems. Hence, the lack of aromatics in the fuel may cause some of these elastomers to shrink, leading to fuel leaks (Hemighaus *et al.*, 2006b). SPK fuel must be blended with petroleum derived jet fuel in order to ensure a minimum aromatic content of 8% v/v (ASTM, 2013). *SASOL* produces an aromatic-containing fully synthetic jet fuel (FSJF) that consists of 50% FT-SPK and 50% synthetic aromatic-containing kerosene. The resulting FSJF meets the aromatics requirements, and it is approved by the international aviation fuel authorities for commercial use in all types of turbine aircraft (Hemighaus *et al.*, 2006b). FT synthesis gives a product virtually free from sulphur, oxygen and nitrogen containing compounds, otherwise found in conventional jet fuel (van der Westhuizen *et al.*, 2011).

1.2.3 Bio-Kerosene (bio-SPK) Jet Fuel

Bio-SPK jet fuels are hydro-processed esters and fatty acids (HEFA) derived from plant oils and animal fats (Maniatis *et al.*, 2013). During the complex process of converting biomass into fuel, plant oils and animal fats are firstly

hydroprocessed to form long-chain paraffinic wax that is later submitted to hydrocracking and isomerisation. As a result, HEFA SPK composition is almost identical to FT SPK (Boeing, 2010). As with FT SPK, aromatics are not found in biomass kerosenes; hence they need to be blended with other types of jet fuels to meet the minimum requirement of 8% v/v of aromatics (ASTM, 2013). Bio-SPKs have been approved by the international aviation fuel authorities, and they have been introduced in commercial aircraft as a 50/50 blend with petroleum derived jet fuels (IATA, 2011).

1.3 The Compositional Analysis of Jet Fuel

Since aviation fuel is a mixture of hundreds of different hydrocarbons, the compositional analysis of a specific batch is extremely challenging. Indeed, modern one-dimensional analytical techniques, such as gas chromatography (GC), cannot separate all the individual compounds present. In an eleven hour gas chromatography experiment, the use of nine coupled 50 m capillary columns was far from sufficient to separate all the hydrocarbon isomers of a fuel sample (Berger, 1996). In fact, the typical GC chromatogram of petroleum has approximately one hundred peaks within a chromatographically unresolved baseline “hump”. GC coupled with mass spectrometric detection (MS) can improve resolution by exploiting the mass analysing second dimension, *i.e*., through extracted ion chromatograms. Nevertheless, the spectrum is the sum of the spectra for each co-eluting component, and this is particularly problematic when the relative concentrations of the co-eluters are dissimilar (Grob & Barry, 2004). A three dimensional separation with GC x GC-MS with two different stationary phases columns increases the identification of minor components and improves the quantitative analysis (Frysinger & Gaines, 1999).

The industry standard (ASTM D1319-03 - Standard Test Method for Hydrocarbon Types in Liquid Petroleum Products by Fluorescent Indicator Adsorption) tests only for total aromatics, olefins, and saturates, in line with the specifications for Jet A-1 fuel, laid out in Def Stan 91-91. The PIANO

(paraffins, isoparaffins, aromatics, naphthenes and olefins) analysis, which uses gas chromatography, is designed to measure the percentage abundance of each of these classes of compound against a standard solution.

1.3.1 GC-MS Analysis of Jet A-1

At the outset of this work, a decision had to be made about whether mechanistic and kinetic studies should be attempted in jet fuel, or whether a simpler surrogate should be used. In any case, a qualitative and semi-quantitative analysis of the Jet A-1 supplied by Airbus (Batch number BIS/HAL/12/035K) seemed appropriate. Experimental details of the GC-MS are presented in Section 10.2, and the resulting chromatogram is shown below in Figure 1.

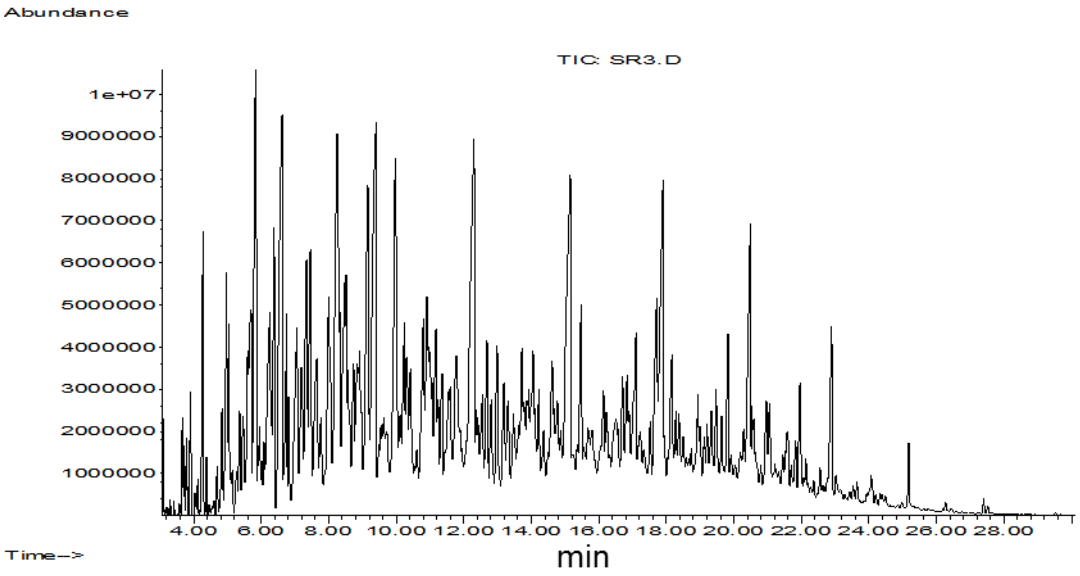

Figure 1. **GC-MS** chromatogram of 10% v/v Jet A-1 in hexane, using a 30m HP-5MS column, with a temperature gradient of 50 to 190 ºC at a rate of 5 ºC/min.

As expected, the sample is largely unresolved and the separation of components is poor; as most of the peaks overlap, only a tentative

identification of hydrocarbons was attempted. The compound identification and corresponding retention times (RT, min.), along with the forward and reverse match quality are reported in Appendix B – a summary of the number of compounds identified for each class is presented in Table 1.

Table 1. Compounds identification in Jet A-1 (Batch BIS/HAL/12/035K).

Class of Compound	*Number of Individual Compounds Identified within Class*
Paraffins	11
Isoparaffins	66
Aromatics	68
Napthenes	64
Olefins	7
Unknown	38

Extracted ion chromatogram technique with ion mass 77 was used to resolve the aromatic content. Background subtraction was applied to improve the identification of many compounds. Because of co-elution, and matches limited to the library spectra, it was not possible to identify 38 compounds; the MS ions (*m*/*z*) of these unknowns are also listed in Appendix B.

To conclude, Jet A-1 is a highly complex solvent in which to study chemical reactions. Although it is possible in principle to chromatographically resolve the components of jet fuels *via* three-dimensional techniques, the issue of co-elution with new potential additives might remain. It is therefore desirable to perform preliminary studies using jet fuel surrogates, which are addressed in the following section.

1.4 Jet Fuel Surrogates

The aviation industry has not defined an standard surrogate for jet fuel; different surrogates have been used depending on the properties which needed to be replicated (Colket *et al.*, 2007). The simplest single component surrogate used is *n*-decane (Dagaut *et al.*, 1994). Two-component surrogates are comprised of *n*-decane and an aromatic component such as trimethylbenzene, xylene or toluene (Guéret *et al.*, 1991). Studies suggest that alkyl substituted aromatics are the preferred aromatic component of jet fuel surrogates (Colket *et al.*, 2007). Three-component surrogates containing *n*-decane, *n*-butyl cyclohexane and *n*-butyl benzene (2:1:1 v/v, respectively) are reported by Natelson *et al.* (2008), which is probably the closest representative of the average composition of jet fuels (Shafer *et al.*, 2006). Although surrogates have included up to twelve components, (Violi *et al.*, 2002; Agosta *et al.*, 2004; Wood *et al.*, 1989), we shall consider using cyclohexane, as it has the added advantage of being available as the d_{12} derivative which is useful for ^{1}H NMR studies.

1.5 Approved Additives for Jet Fuel

The chemical composition of aviation fuel is expected to vary as a result of the diverse range of sources and processes to which the crude starting material is subjected. Consequently, stringent standards governing bulk physico-chemical properties are necessary in order to ensure consistent performance across the industry. This section considers the range of additives sometimes deployed in order to improve the ancillary properties of jet fuel, *i.e.,* thermal and storage stability, lubricity, conductivity, and inhibition of bacterial growth, and ice formation.

In addition to the inherent complexity of jet fuel, one must also be aware of the presences of additives to enhance or maintain properties important to fuel performance or fuel handling. Typically, additives are fuel-soluble chemicals derived from petroleum based raw materials and their function and

chemistry are highly specialised. They produce the desired effect in the part per million concentration range. These additives fall into general categories such as thermal stabilisers, antioxidants, metal deactivators, and de-foamers (CRC, 2004). Additives are used to varying degrees in all petroleum derived fuels, but the situation with aviation fuels is unique in that only those additives specifically approved may be added to jet fuel. All jet fuel specifications list approved additives along with allowed concentrations ranges (Def Stan 91-91, 2011). Some approved additives are required to be added, some are optional, and others are approved for use only by agreement between buyer and seller. Use of additives is the principal difference between commercial and military jet fuels. The static dissipater Stadis® 450 is the only mandatory additive for Jet A-1, whereas military jet fuels will contain three or more additives, such as antioxidants, metal deactivators, fuel system icing inhibitors, because of the high performance requirements (CRC, 2004).

Antioxidants are added to improve fuel storage stability and inhibit formation of peroxides, soluble gums and insoluble particulates, resulting from oxidation reactions. Peroxides can chemically attack sealants in the aircraft fuel systems, gums can lead to engine deposits, and particulates can plug fuel filters (Chevron, 2006). Butyl-phenols, which are mildly acidic ($pK_a \approx 10$) are the only antioxidants approved for jet fuel (Def Stan 91-91, 2011).

Metal deactivators are chelating agents (N,N'-disalicylidene-2-propanediamine), which form stable complexes with metal ions - copper, cadmium, iron, cobalt and zinc – which would otherwise be effective catalysts for oxidation reactions (Def Stan 91-91, 2011).

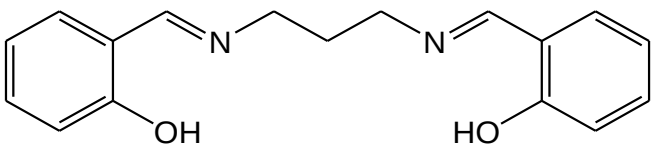

Figure 2. Structure of N,N'-disalicylidene-2-propanediamine.

Lubricity improvers were originally designed as corrosion inhibitors to protect uncoated steel tanks and pipelines from rusting and corrosion caused by water and oxygen (Hemighaus *et al.*, 2006a). It was then discovered that they also improve the lubricity of fuels, and for this reason they are mandatory in all military and some civil turbine fuels (CRC, 2004). They are used to improve the lubricity of severely hydrotreated jet fuels. These compounds are usually long chains carboxylic acids, such as linoleic acid. The polar group adheres to the metal surface, creating a thin layer of the additive on the surfaces (Hemighaus *et al.*, 2006a).

Static dissipaters are added to improve the naturally poor conductivity of fuel, which is why they are also known as conductivity improvers. The only one currently approved is Stadis® 450, produced by Innospec LLC; the maximum concentration permitted is 5 mg/L, and it is mandatory for Jet A-1. Although the composition is well protected by the manufacturer, the safety data sheet reports toluene, solvent naphtha, dinonyl-naphthalenesulphonic acid, isopropanol, quaternary ammonium compound, naphthalene and 1,2,4-trimethylbenzene (Innospec, 2010).

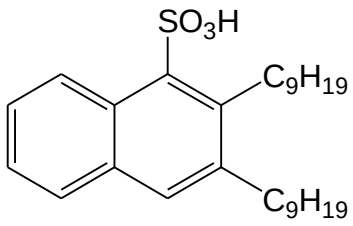

Figure 3. Structure of dinonyl-naphthalenesulphonic acid.

Biocides are added to prevent the growth of microorganisms, which can produce solid films, clog fuel filters, and also generate corrosive by-products (Hill, 2003). Jet fuel is sterilised by the refinery process, because of the high temperatures, yet microorganisms, like bacteria and fungi, can enter the fuel as soon as it is in contact with air and water. Def Stan 91-91 makes no direct reference to biocides. Isothiazolines have been used; an approved

mixture of 5-chloro-2-methyl-4-isothiazolin-3-one and 2-methyl-4-isothiazolin-3-one is commercialised as Kathon^{TM}. Because of their toxicity, water collected from fuel tanks containing biocides need to be appropriately disposed (Hemighaus *et al.*, 2006a).

Fuel System Icing Inhibitors (FSII) are added to prevent ice formation, which could block fuel filters. Most commercial aircraft have heaters on their main fuel filters to melt any ice that is collected. However, many military aircraft do not have these heaters and require FSII. These additives work by dissolving in any free water that forms, thereby lowering the freezing point of the mixture by preventing crystallisation (Hemighaus *et al.*, 2006a). Since ethylene glycol monomethyl ether (EGME) was banned because of its toxicity to humans and the environment, the only FSII currently approved for Jet A, Jet A-1, and military fuels is di-ethylene glycol monomethyl ether (di-EGME) (CRC, 2004). The concentration of di-EGME must be in the range of 0.07 - 0.15% v/v (USA Department of Defence, 2012).

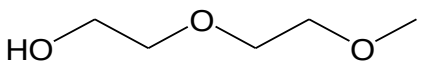

Figure 4. Structure of di-ethylene glycol monomethyl ether.

1.6 Conclusions

The qualitative and quantitative chemical composition of jet fuel varies from batch to batch, depending on the origin of the fuel, the refining process it has been through, and the range of additives used to improve or retain handling performance. Although the composition comprises between 99-99.5% v/v of hydrocarbons, the potential for variation in the remaining fraction could be infinite, and the prospect for reproducibility, when developing and testing novel chemical additives, is more of a challenge. To this end, the use of an appropriate surrogate will ensure reproducible results, and simplified analyses for work on the development of novel FDII.

Chapter 2

Jet Fuel and Water

2.1 Forms of Water in Jet Fuel

Water in aviation fuels can occur in three different forms:

- Dissolved in the fuel.
- As a separate liquid phase (free water).
- Fuel-water emulsion.

2.1.1 Dissolved Water in Jet Fuel

Dissolved water is ordinarily considered to be a constituent of jet fuel, and has no effect on the aircraft fuel system performance as it is vaporised during combustion (Oreshenkov, 2004). Free water and water emulsions are however potentially hazardous and must be avoided (CRC, 2004). The hygroscopic nature of jet fuel refers to its ability to attract moisture from the air. The hygroscopicity of jet fuel is a reversible process that strongly depends on atmospheric conditions such as temperature, humidity and, to a minor extent, the pressure to which the jet fuel is subjected. During a flight, fuel is constantly exposed to changes in temperature, pressure and air humidity through the vent system. As a result there is a continuous process of absorption and spontaneous liberation of water molecules between the liquid and the gas phase (Smith, 1970). However, it has been demonstrated that, over a period of a few months, cyclical temperature changes produce a significant amount of water accumulation in the fuel tanks (Oreshenkov, 2004). Figure 5 outlines the relationship between temperature and water dissolution in jet fuel at 100% relative humidity (RH). Below 100% relative humidity, water dissolution follows Henry's Law. A typical water-saturated petroleum based kerosene fuel contains between 40 and 80 ppm v/v dissolved water at 21°C and atmospheric pressure. If the temperature of the fuel increases, it can dissolve more water. Conversely, if the temperature of the fuel decreases, some of the dissolved water in the fuel will separate as free water (CRC, 2004; Lam *et al.*, 2014).

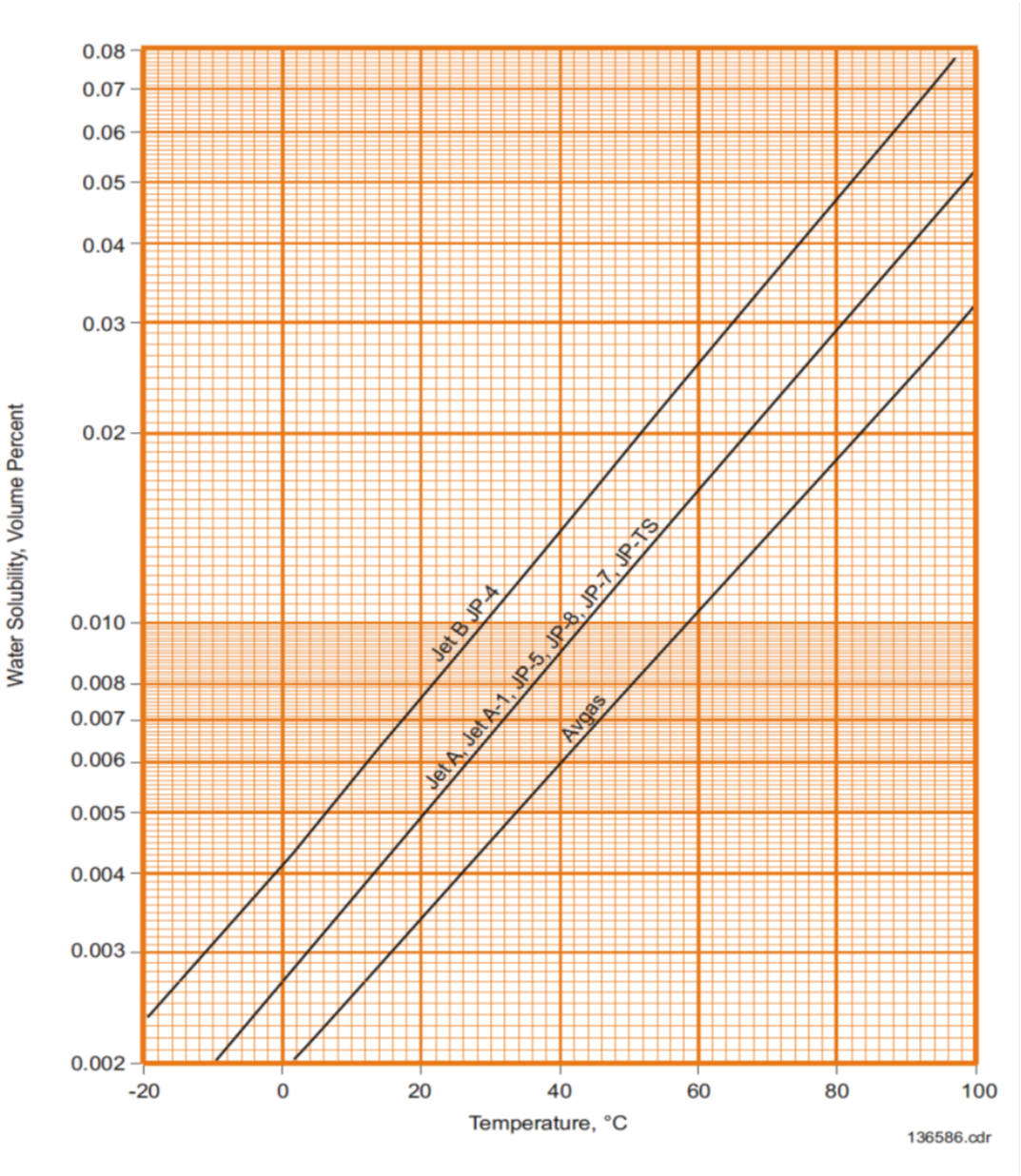

Figure 5. Water solubility *versus* temperature for aviation fuels at 100% RH (CRC, 2004).

The hygroscopic capacity of jet fuel is determined by the water solubility of the individual hydrocarbon components. Because water is sparingly soluble in hydrocarbons, accurate determinations are difficult to achieve, and remains an active and challenging area of research (Oliveira *et al.*, 2007). Experimental observations of water dissolution in hydrocarbons have led to a variety of theoretical models which all require, as a first step, the disruption of the hydrogen bonding networks formed between adjacent water molecules

(Amovilli & Floris, 2003; Economou & Tsonopoulos, 1997; Klamt, 2003; Nilsson, 1986; Oliveira *et al.*, 2007; Ruelle & Kesselring, 1996; Tsonopoulos, 1999, 2001).

The energy associated with dissolving water (*i.e.,* enthalpy of solution) in a range of unbranched alkanes has only a weak dependence on the number of carbons atoms present (*i.e.* $C_7 \rightarrow C_{12}$ = 34.9 ± 1.1 kJ mol^{-1} at 298 K) (Nilsson, 1986). The magnitude of the enthalpy of solution is comparable to the hydrogen bond energy, suggesting that the dissolution of *n* water molecules requires the breaking of *n* hydrogen bonds (Tsonopoulos, 1999). The enthalpy of solution of water in both alkylbenzenes and alkenes decreases by approximately 11 and 2 kJ mol^{-1}, respectively, with respect to alkanes. The energetic cost of disrupting the hydrogen bond network of water is offset by attractive electrostatic interactions with these hydrocarbons. It has long been recognised that extended π electron systems, such as those encountered within alkylbenzenes, form hydrogen bonds with water (Atwood *et al.*, 1991; Feller, 1999; Ruelle *et al.*, 1992). A weaker form of that interaction, between water and the π bond of an alkene, may account for *ca*. 2 kJ mol^{-1} enthalpy reduction (Tsonopoulos, 2001). The formation of attractive electrostatic interactions between water and π-aromatic systems would account for the enhanced solubility of water in alkylbenzenes, relative to both paraffins and naphthenes (Baena-Zambrana *et al.*, 2013). As depicted in Figure 6, water solubility increases with the proportion of aromatic hydrocarbons, but not in a linear fashion. Figure 6 also reflects the behaviour of water solubility in hydrocarbons in general, suggesting that this physical property is non colligative (Krynitsky *et al.*, 1950; Ruelle & Kesselring, 1996).

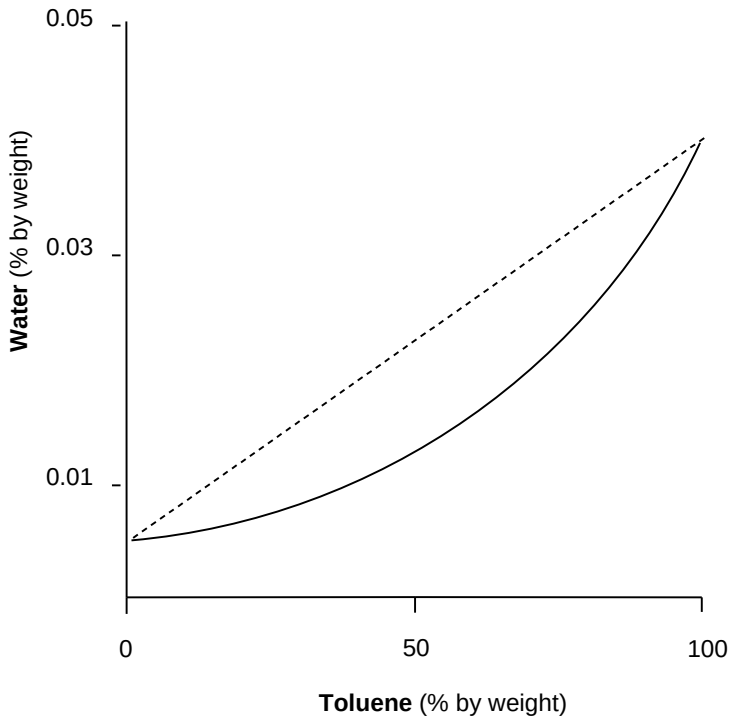

Figure 6. Water solubility in *n*-octane/toluene mixtures at 15.5ºC (Krynitsky *et al*., 1950).

Recent studies have shown that the different refinery treatments of petroleum based kerosene fuels do not have a significant effect on the amount of water absorbed by the fuel (Carpenter *et al.*, 2011). Instead the solubility of water in FT SPK and bio-SPK blends is approximately 25% to 30% lower compared with Jet A-1, because they contain less heteroatoms, aromatics and other polar compounds (Moses, 2008). Jet A-1 containing higher concentration of aromatics are found to have a higher affinity towards water, and tends to shed the greatest quantity of water as the temperature decreases (Lam *et al.*, 2014).

2.1.2 Free Water in Jet Fuel

In jet fuel, free water exists as a separate liquid phase. Since water is denser than jet fuel, free water, under the influence of gravity, will settle to form a lower layer. If jet fuel and water are mixed, normally they will separate again. The speed of the separation and the sharpness of the fuel-

water interface are indications of the fuel's *water separability* (Hemighaus *et al.*, 2006a; Ragozin, 1961). As mentioned above, when water-saturated jet fuel cools, free water separates out, taking the form of many very small droplets sometimes called *dispersed water*. Even if they are not stabilised by surfactants (see Section 2.1.3), the droplets coalesce very slowly because of their small size. The rate of settling of finely dispersed water droplets from fuel is subject to Stoke's Law; giving a direct proportionality to their diameter, and an inverse proportionality to the fuel's density and viscosity (Smith, 1970). A recent study confirmed that, on cooling different jet fuels (Jet A-1, 100% hydroprocessed and 100% Merox jet fuel), the droplets size of dispersed water is 5 µm or below. The cooling rate and the fuel composition don't appear to affect the size of the water droplets (Carpenter *et al.*, 2011). Fuel containing fine water droplets appears cloudy, and there seems to be a correlation between water solubility and optical turbidity (Lao *et al.*, 2011). At freezing temperatures, the separated water may form ice and the dispersed water may form water-fuel slush or small particles of ice and snow suspended in the fuel (Schab, 1960).

Free water is considered a fuel contaminant because, at significant levels it may; support microbial growth, contribute towards corrosion, cause engine starvation if a slug of water is ingested in the engine feed, and increase the risk of filter blocking because of the formation of ice particles at low temperatures. Expanding upon the final point, at high altitudes, and therefore low temperatures, free water may freeze creating fuel flow problems. Ice crystals may occur *via* germs, or crystallites of water molecules (homogeneous nucleation), or germs formed upon foreign particles such as dust, rust or dirt (heterogeneous nucleation). Ultrapure water droplets of micrometer-size remain in a liquid supercooled state when cooled to about -37ºC, before ice nucleates within them homogenously (Murray *et al.*, 2010). Microscopy experiments of water droplets in the micron size range immersed in Jet A-1, demonstrated that fuel does not catalyse ice formation and the droplets froze homogeneously at temperature between -36ºC and -39ºC (Murray *et al.*, 2011). Ice nucleation can be encouraged by the presence of a foreign substrate, like dust, rust, dirt, or ice-

forming nuclei (Shaw *et al.*, 2005). This is called heterogeneous nucleation and it is believed to be the most common process of ice formation in the fuel system. Factors like turbulent flow, impurities and cold metal surfaces in the aircraft feeding system can catalyse the nucleation process of supercooled water droplets at temperatures much higher than those required for homogenous nucleation (Ragozin, 1961).

2.1.3 Fuel-Water Emulsions in Jet Fuel

An emulsion is a mixture of two immiscible liquids in which very small droplets of one (diameter < 100 µm) are dispersed in the continuous phase of the other. In this case the emulsion is formed by water (droplet) in jet fuel (continuous phase). While immiscible liquids normally separate if they have different densities and/or surface tensions, an emulsion can persist for extended time periods. The water-in-oil emulsions can be stabilised by surfactants that congregate at the surface of the droplets, preventing them from coalescing. Molecules, containing both a polar group and a non-polar group within the same molecule, migrate to the interface between the two immiscible liquids, with the polar group interacting with the polar liquid (water) and the non-polar group interacting with the non-polar liquid (jet fuel). These molecules are called surfactants because they are active at the surface between the immiscible liquids. Because they work at the interface, and not in the bulk liquid, trace amounts can affect the properties of a large volume of liquid. Some surfactants found in jet fuel occur naturally in crude oil, such as naphthenic acids and phenols. Others may be introduced in the refining process, such as sulphonic acids, or in the fuel distribution system.

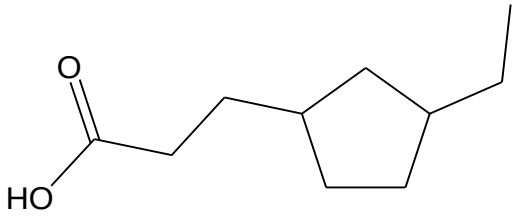

Figure 7. 3-(3-ethylcyclopentyl)propanoic acid; an example of a naphthenic acid.

Surfactants are commonly removed from jet fuel by passing the fuel through clay (*clay treating*). Surfactants can cause problems even if they don't lead to the formation of a fuel-water emulsion. They can impair the ability of a filter/separator to remove free water from jet fuel. Since it is important that only clean, dry fuel is delivered to the aircraft, tests have been developed to detect the presence of surfactants in jet fuel through their ability to stabilise emulsions (CRC, 2004).

2.2 Means of Water Contamination

Free water can enter aviation fuels from numerous sources. Fuel is moved around the UK *via* pipeline networks, rail, ship, road or a combination of these methods; at any point during its transfer from refineries to airports, fuel can pick up free water. Water contamination can also occur during storage, through floating roof tank seals that leak, or during aircraft washing (CRC, 2004). Even if jet fuel enters the aircraft tanks without free water, this does not prevent its formation. Indeed, dissolved water in fuel will precipitate out of solution in the form of micro droplets as the fuel temperature drops through diurnal cycles or during operation as the aircraft climbs to altitude (Lao *et al.*, 2011). Water solubility in Jet A-1 decreases by approximately 2 ppm v/v *per* 1ºC. For example, a temperature change of +20 → -10ºC affords *ca.* 29 ppm v/v of dissolved water to be liberated as free water, which in 100 tons of fuel amounts to 3.62 L (CRC, 2004). A second source is the condensation of atmospheric moisture. As fuel is consumed, air is drawn into the fuel tanks through the vent system; the moisture in the air condenses as it comes into contact with the cold fuel and tank surfaces at the end of a long flight.

2.3 Current Solutions for Water Contamination

Mechanical. The aviation industry uses both hardware and quality control procedures to protect jet fuel from water contamination. Floating roof tanks should have a solid cover over the floating roof and all storage tanks should have drains reaching to the lowest point in the tank. Fuel systems are designed to have a minimum number of low points equipped with drains. Dispersed water is removed from fuel by passing it through water separators and filter units. These components contain fibres with a hydrophilic surface that help to aggregate small water droplets into larger ones, which then are collected through a hydrophobic surface (Hemighaus *et al.*, 2006a).

Ice crystals are prevented from plugging filters in aircraft either by heating the filter, heating the fuel near the filter, or using FSII additives. Airbus and Boeing commercial aircraft also protect their feed pumps using mesh strainers with bypasses; this ensures uninterrupted fuel flow to the engine in the event of mesh strainer blockage. The industry has developed equipment and procedures to mitigate the problems related to water contamination, but challenges remain (CRC, 2004).

Additives. The aviation industry uses a variety of additives to counter the detrimental effects of free water:

- biocides are added to prevent microbial growth
- corrosion inhibitors are used to protect uncoated aluminium tanks and pipelines
- Fuel System Icing Inhibitors (FSII) - added to inhibit ice formation.

Expanding upon the inhibition of ice formation, FSII are hydrophilic substances which will dissolve in free water; in doing so the hydrogen-bonding networks responsible for molecular ordering is disrupted, and the freezing point of water is lowered by preventing crystallisation (Lykov *et al.*, 1989). There is only one additive currently approved for this purpose - di-

EGME (Section 1.5). At the approved concentrations (0.07-0.15% v/v), Trohalaki *et al.* (1999) found that water (0.007% v/v) in jet fuel freezes below -33°C. Di-EGME has also proved to be an effective deterrent to microbial growth (CRC, 2004). The aviation industry has identified several problems related to the interaction of FSII and “wet” fuel, which can actually undermine fuel protection.

- In addition to being hydrophilic, di-EGME is also hygroscopic; this characteristic leads to an uptake of atmospheric water during blending operations which affects its solubility in fuel.

- Di-EGME has a very high water-fuel partitioning ratio: it preferentially dissolves in water. This leads to denser water layers separating under gravity with up to 40-50% m/m of di-EGME. Unless replenished, the jet-fuel is essentially “stripped” of its protection against icing.

- The presence of di-EGME in the water contained within the fuel alters interfacial properties, and can impair the performance of filters. Particularly, the separation efficiency of filter/coalescers can be compromised (Taylor, 2008).

In addition, FSII are toxic at the concentrations required for effective de-icing. Sump water drained from sumps of storage tanks and fuel systems inevitably contain higher concentrations of di-EGME, creating concerns about the handling and disposal of these wastes (Mushrush *et al.*, 1999). FSII are only mildly irritating, but they are rapidly absorbed by the skin. Vapours can cause irritation to the eyes and the respiratory system. Long term effects include damage to the central nervous system, blood, skin, eyes, and kidneys (Pohanish, 2011). Di-EGME is biodegradable in wastewater treatment systems; however concentrations found in sump water could be high enough to disrupt the microbiological process. In the environment, the high oxygen demand required for decomposition results in less available oxygen for aquatic organisms (Meshako *et al.*, 1999).

Over the years many other compounds have been studied as a substitute of di-EGME; however none of them, even the most promising, have gone through the lengthy approval process (Trohalaki *et al.*, 1999; Chang *et al.*, 1998; Mushrush *et al.*, 1999; Zabarnick *et al.*, 2010).

2.4 Conclusions

In jet fuel, water concentrations above the saturation level are potentially hazardous and must be avoided. All approved additives to mitigate the detrimental effects of free water afford their protective properties by dissolving into water, as shown pictorially in Figure 8.

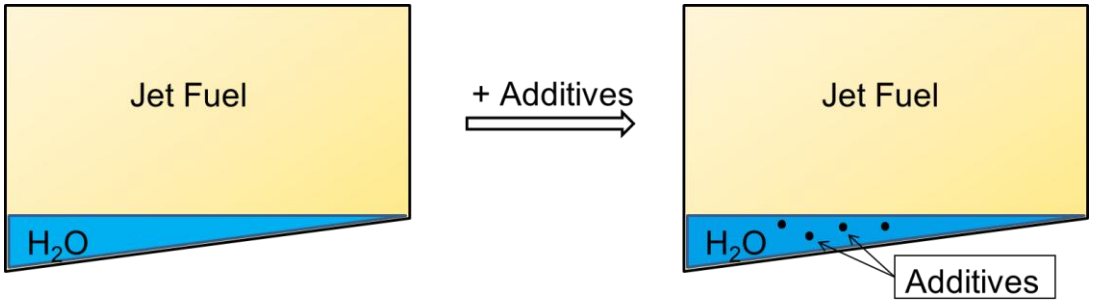

Figure 8. Mode of action for approved additives.

Problems remain particularly regarding ice formation in the fuel tank. When a Boeing 777 crash landed at Heathrow airport in January 2008, the Air Accident Investigation Branch (AAIB) reported that ice in jet fuel is an "industry-wide problem" in aviation, and has emphasised the need for the development of measures to reduce the risk of ice formation in the fuel system (Sleight & Carter, 2010). In fact, the available additives address the problem, but do not necessarily address the root cause.

2.5 Aims and Objectives of the Thesis

An alternative and innovative strategy, which will be explored in this Thesis, is to use an additive which preferentially partitions into jet fuel and consumes water through a fast hydrolysis reaction, as summarised in Figure 9. Such a water scavenger would offer dual protection by affording, as a product of hydrolysis, an ice inhibitor which would preferentially partition into any residual water.

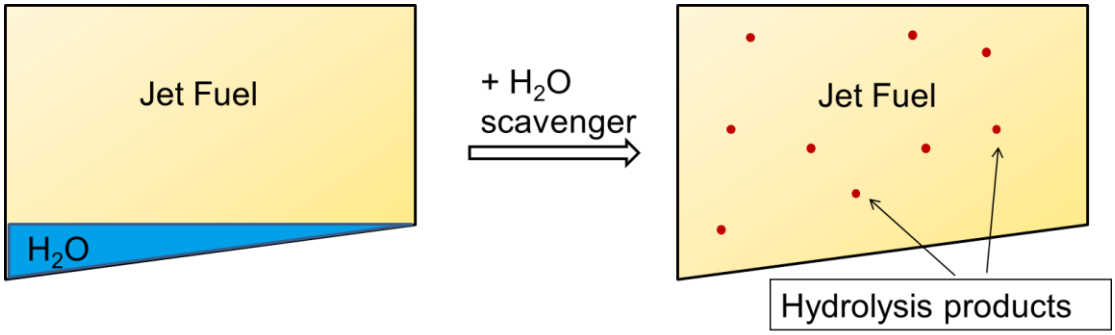

Figure 9. Mode of action for an innovative FDII approach.

Specifically this Thesis seeks to develop a FDII which meets most, if not all of the criteria delineated below.

Selectivity. Jet fuel is a mixture of hundreds of organic compounds; it is therefore critical that the scavenger of choice reacts exclusively with water, which is a notoriously weak nucleophile.

Combustibility. An important consideration here, as both scavenger and by-products must be readily combustible and leave no solid residues.

Atom Economy. Because water is a relatively small molecule (molecular mass MM = 18 g/mol), a relatively large mass of scavenger - assuming a 1:1 reaction stoichiometry - is required to dehydrate the jet fuel. It is important therefore to ensure that the MM of a candidate scavenger is as low as possible, or alternatively possess multiple reactive sites (higher reaction stoichiometry).

Switchable. A selective scavenger which is switchable (*i.e*. on/off) can be stored without degradation (off mode), and yet be activated (on mode) when mixed with fuel. This is best achieved by choosing a process that is catalysed by mild acid, a particular consideration when one recognises that Jet A-1 is mildly acidic (CRC, 2004).

Dual Action. The products of reacting one mole of the scavenger with water would ideally produce one equivalent of FSII for optimum fuel protection.

Fuel/Water Partitioning. A water scavenger must be sufficiently hydrophobic to be soluble in jet fuel, thereby conferring protection - yet the product of the reaction with water must be sufficiently hydrophilic to preferentially partition into residual water to act as an effective FSII.

Cheap & Easy to Synthesise. The production of the water scavenger should be a viable undertaking for manufacturers, and sustainable for the environment.

Environmentally Benign. Both the scavenger and the by-products must be non-toxic for the environment.

Kinetically Fast. Unlike an icing inhibitor, a water scavenger must undergo a chemical reaction at the very low operating temperatures commonly encountered in an aircraft. Such low temperatures can dramatically reduce the kinetic energy of participating molecules, to the point that a chemical reaction slows down or effectively stops. It is necessary then to ensure that the energy barrier to the reaction is small. This ensures a fast reaction even at low temperatures, which corresponds to a high rate constant.

Before addressing the complex task of examining and exploiting hydrolysis reactions in jet fuel, the solution requires disassembling into separate tasks, perhaps the most important being the identification of the most effective analytical method for measuring water levels in jet fuel.

Chapter 3

Measuring Water in Jet Fuel

3.1 Introduction

The aim of the project is to identify, and more importantly optimise the performance of water scavengers in jet fuel. It is important then, to establish a simple, accurate method to measure small concentrations of water in all of its possible forms (*i.e.* dissolved, free, and/or emulsions). Furthermore, the analytical method must be rapid, relatively robust, and it should not interfere with the hydrolysis reactions of a water scavenger.

3.2 Water Content *via* the Karl Fischer Titration

Karl Fischer titration (KF) is the industry standard to determine the water concentration in jet fuels (ASTM D6304, 2007). The method, developed by the German chemist Karl Fischer in 1935, employs an iodine solution, which consists of iodine, sulphur dioxide and an organic base dissolved in anhydrous methanol. The traditional base used was pyridine, but because of its toxicity it has been replaced by imidazole. The redox reaction, which consumes one molecule of water for each molecule of iodine, is shown below in Scheme 2.

$$I_2 + SO_2 + CH_3OH + 3C_3H_4N_2 + H_2O \rightarrow 2C_3H_4N_2H^+ I^- + C_3H_4N_2H^+ CH_3OSO_3^-$$

Scheme 2. Karl Fischer titration

For samples with high concentrations of water, a volumetric method is used in which the sample is added to the titrant; for samples with low concentrations of water a coulometric method is used in which the iodine is generated electrochemically. The presence of unreacted iodine, visually detectable from its brown colour, signals the end point. For better accuracy, the unreacted iodine is measured electrochemically by two platinum electrodes; the potential required to keep the current constant changes sharply signalling the end point, this method is called bi-amperometric (Kenkel, 2002).

The major components of jet fuel and the additives do not interfere with the KF. As the amounts of mercaptan are limited by Jet A-1 specification to 30 ppm m/m, they are likely to lead to appreciable errors when the water concentration is low (CRC, 2004). As might be expected for an analytical technique based upon a redox reaction, compounds with oxidising or reducing functionalities have been shown to interfere with the measurements (Mendham *et al.*, 2006). This constitutes a significant drawback when contemplating examining the progress of a water scavenging system based upon organic molecules. The technique is also destructive, requiring approximately 2 mL per analysis. Therefore it is necessary to perform experiments on a relatively large scale.

3.3 Water Content *via* Infrared Spectroscopy

A preliminary study to explore the capacity of IR-spectroscopy for the measurement of water in jet fuel was performed as part of this work (for experimental details, see Section 10.3). Liquid water has two main absorptions in the mid IR region; the s*tretching* band, which is generated by the overlap of the symmetric and asymmetric stretch (3280 cm^{-1} and 3490 cm^{-1}, respectively), and the *bending* band at 1644 cm^{-1}. Rotations in the liquid phase tend to be restricted by the formation of hydrogen bonds between water molecules (Eisenberg & Kauzmann, 2005). Hydrogen bonding is the reason why the spectra of the same amount of water in the gas, liquid and solid phase are very different, as shown in Figure 10 (Chaplin, 2014).

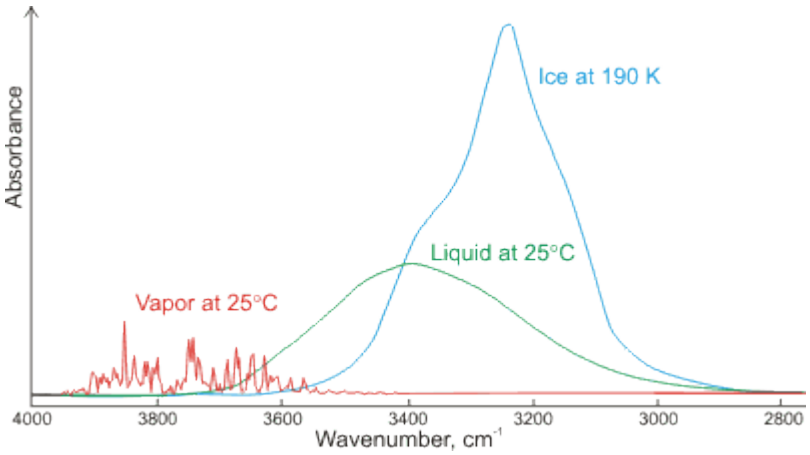

Figure 10. The IR spectra of the same amount of gas, liquid and solid water (Chaplin, 2014).

The hydrogen-bonding capacity of the environment around a molecule of water will influence both the frequency and the sharpness of the IR absorbance. Decreasing the hydrogen bonding strength of the solvent leads to a shift of the *stretch* band to a higher frequency (Ohno *et al.*, 2005). Therefore the vibrational frequencies of water in hydrocarbons are in the following order paraffins > olefins > aromatics > pure water. In fact, the asymmetric stretch of water is at 3710 cm^{-1} in decane, at 3697 cm^{-1} in 1-heptene, and at 3675 cm^{-1} in toluene (Conrad & Strauss, 1987; Seidov & Prokhvatilova, 2008).

The sample temperature also has an impact on the spectrum, and with decreasing temperature the water spectrum approaches that of the ice spectrum. In supercooled water at -35 ºC, the absorbances are shifted to frequencies 70 cm^{-1} lower compared to 25 ºC, and there is an increase of 30% in the intensity of the O-H stretch (Wagner *et al.*, 2005). As in the case of pure water, temperature has an effect on the absorption band of water in organic solvents, because of the changes of the intermolecular interaction between the molecules. The intensities of the absorption bands of water dissolved in aromatic compounds decrease with an increase in temperature, whereas the frequencies increase with an increase in temperature. Even

one degree difference can create an increase in the error of the water concentration measurements (Seidov & Prokhvatilova, 2008). Another important factor to take into consideration is that other molecules possessing an -OH group, such as an alcohol, will have the same vibrational band as water when they are inter-molecularly hydrogen bonded. As part of this work, the IR spectrum of anhydrous jet fuel was measured and is presented in Figure 11.

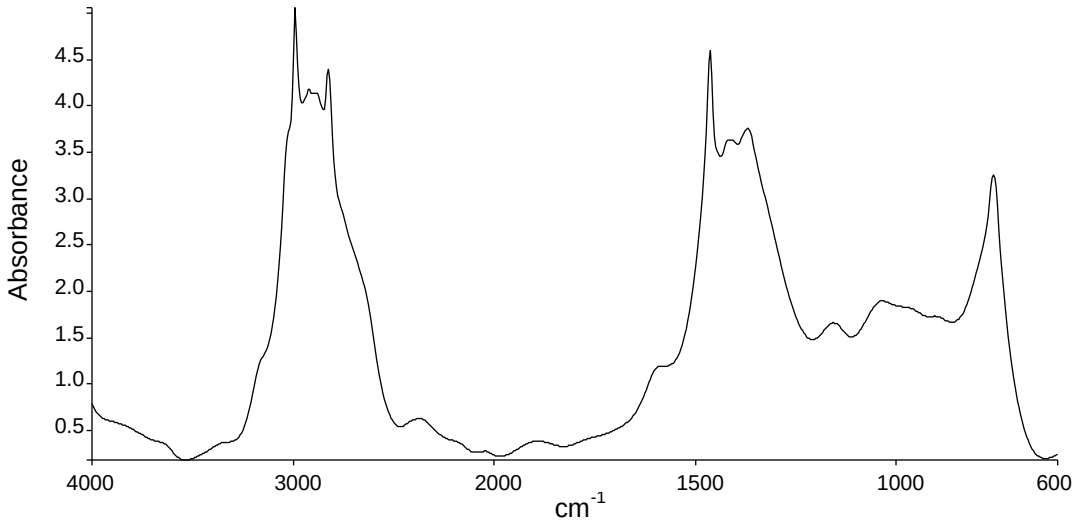

Figure 11. IR Spectrum of Anhydrous Jet A-1 at ambient T=20 ºC.

As one can see, the C-H band (3100-2800 cm^{-1}) is very strong and can obscure the water absorption band (see Figure 10); so the IR spectra of progressively “wetter” samples of jet fuel were recorded using anhydrous jet fuel as background. A typical spectrum of a water standard will vary depending on the water concentration; at low concentrations it is possible to see the two stretching bands separated, whereas at higher concentrations the two stretching bands overlap because of the higher formation of hydrogen bonding. Examples are reported in Figure 12 and 13.

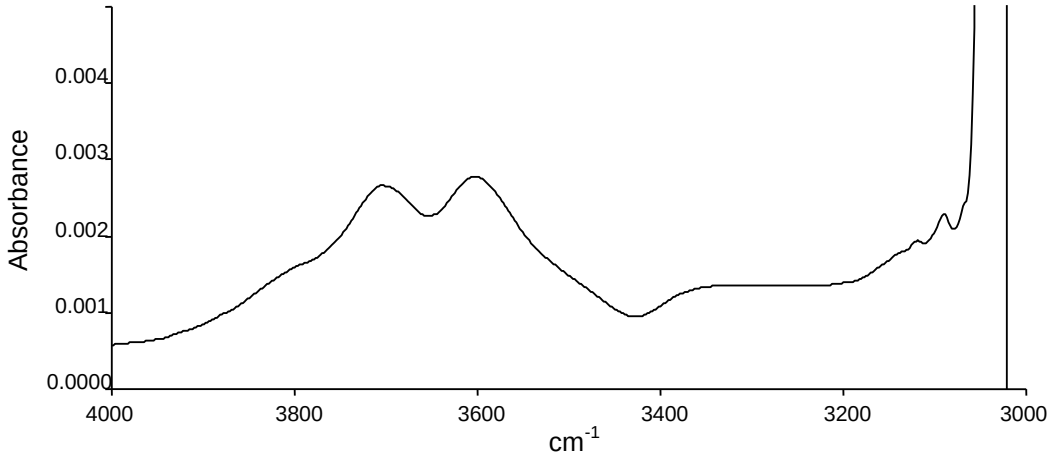

Figure 12. The IR spectrum of Jet A-1 with 0.001% v/v of water at ambient T=20 ºC (below saturation limit).

This implies that the absorbance peaks shift in wavelength depending upon water concentration. However, it is possible to correlate the maximum absorbance height with water concentration (Figure 14). For standards with visible separation of the two stretching bands the average of the two absorbances were plotted. Above 2000 ppm v/v of water the linearity ceases probably because it is difficult to keep a large amount of undissolved water in suspension in jet fuel.

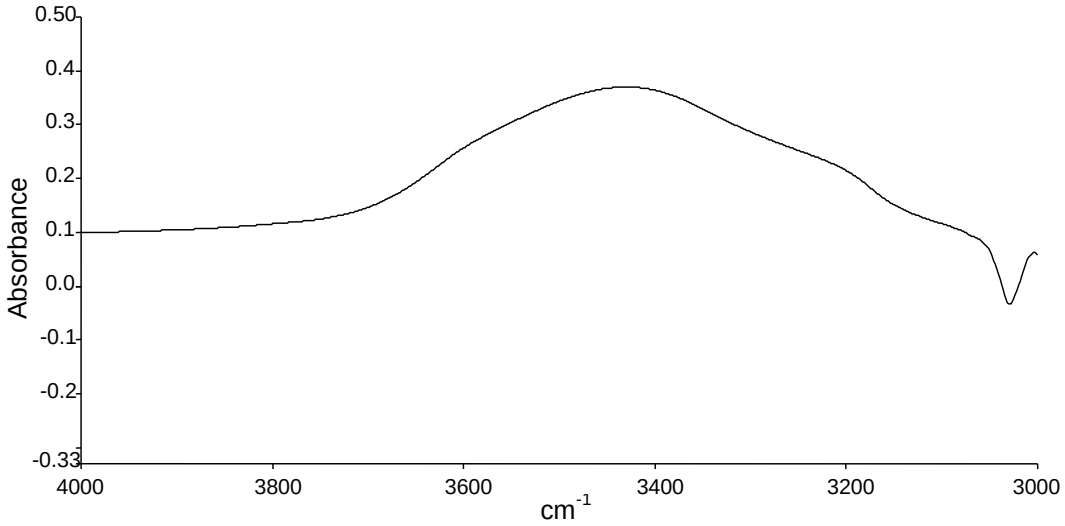

Figure 13. The IR spectrum of Jet A-1 with 0.1% v/v of water at ambient T=20 ºC (above saturation limit).

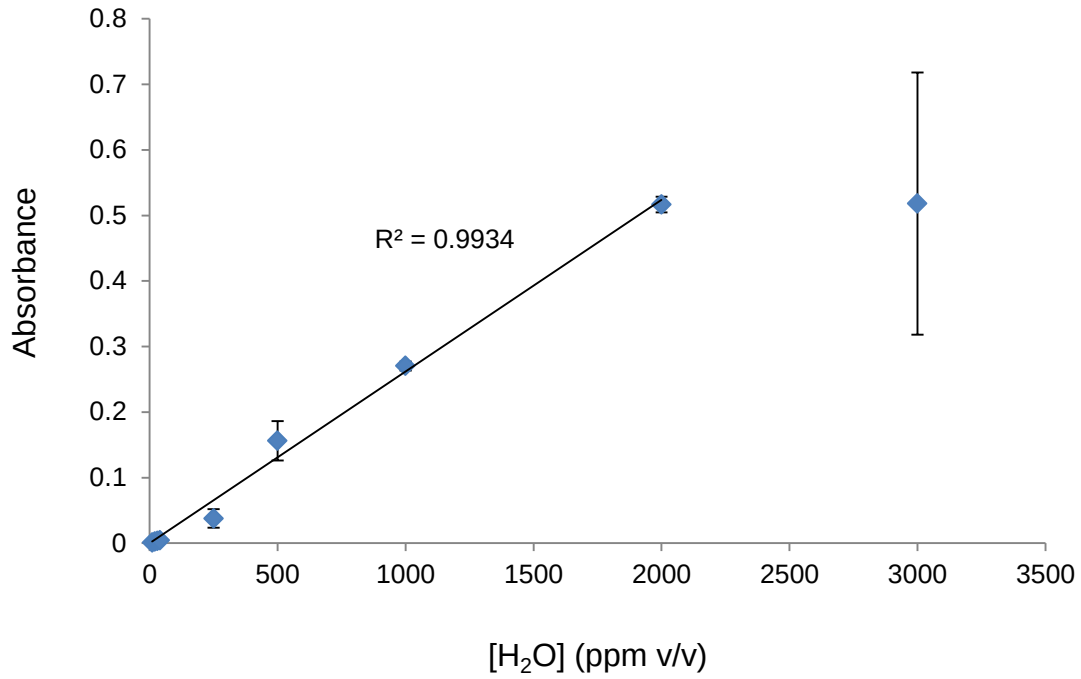

Figure 14. The corrected values for the absorbance of the OH stretch (frequency = 3426-3709 cm^{-1}), *versus* concentration in the IR spectra of water dispersed in Jet A-1 *via* ultrasonication.

In conclusion, it is possible to measure the concentration of water in jet fuel by IR spectroscopy; however it is important to maintain a constant temperature during the experiment, and it is necessary to use dry jet fuel as a reference to correct for other overlapping vibrational bands. The method has further difficulties because, as in the case of KF, when water exceeds the saturation concentration, the formation of non-homogenous micro-emulsions influences the result of the analysis. In this study only a small proportion of the sample is monitored because of the pathlength of the IR cell (1 mm); a longer pathlength should reduce attendant errors associated with micro-emulsions stability and homogeneity. Further studies are necessary to quantify the accuracy and reproducibility of the method and the range of linearity of absorbance versus concentration.

3.4 Water Content *via* Settling Rate

Fuel appears cloudy if suspended water is present; the degree of cloudiness increases with the amount of suspended water present (Schab, 1960). It seemed logical therefore, to explore UV-Vis spectroscopy as a means of quantifying water in jet fuel (for experimental details, see Section 10.4). As a correlation between absolute water concentrations and absorbance was not observed here;this is possibly because of the non-homogeneity of the water-fuel emulsions. The change in absorbance with time for a given concentration of water was examined instead. In principle, the time necessary for a water-fuel emulsion to settle will depend on the water concentration, the size of the water droplets formed, the fuel depth-surface area ratio, and the eddy currents formed in the fuel (Schab, 1960). Water dispersions were created by ultrasonication, which has been shown to afford droplets <30 µm in diameter (Taylor *et al.,* 2011). The rate of change of absorbance at 370 nm – which is proportional to settling - as a function of water concentration, is presented in Figure 15. All curves represent the average absorbance *versus* time for the various water-fuel emulsions (100-1000 ppm v/v) with corresponding error bars. As is clear in Figure 15, the absorbance measured immediately after sonication is statistically different for each water concentration during the first 50 minutes. Thereafter, error bars overlap, and differences become less significant. It is also clear that the standard deviation increases dramatically with higher water concentrations (*i.e.,* 1000 *versus* 750 ppm v/v), because of the non-homogeneity of the water-fuel emulsions.

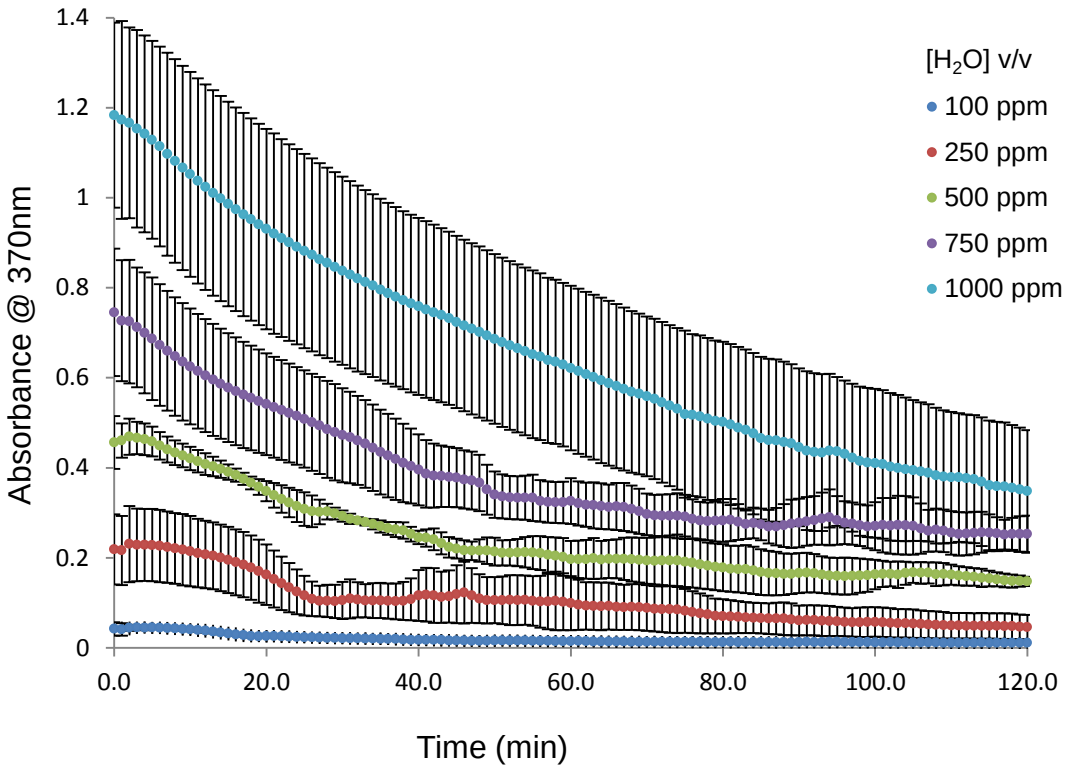

Figure 15. Average settling curves for varying H_2O concentrations in Jet A-1 dispersed by ultrasonication.

As one might expect, the rate of change for absorbance decays with time, wherein larger droplets coalesce and settle out of solution initially, leaving behind smaller dispersed droplets; the smaller droplets settle at a much slower rate (CRC, 2004). This behaviour is further supported by the observation that the rates for settling appear to change approximately every 20 minutes. For example, at a concentration of 100 ppm, the gradient of the curve at t = 0-20 min. is 1.3 x 10^{-3}, and 0.4 x 10^{-3} at t = 20-40 min. Indeed, there is an excellent linear correlation between the initial rate (*i.e.,* t = 0-20 min. R^2 = 0.9936) of settling, and water concentration throughout the range 100-1000 ppm, as depicted in Figure 16.

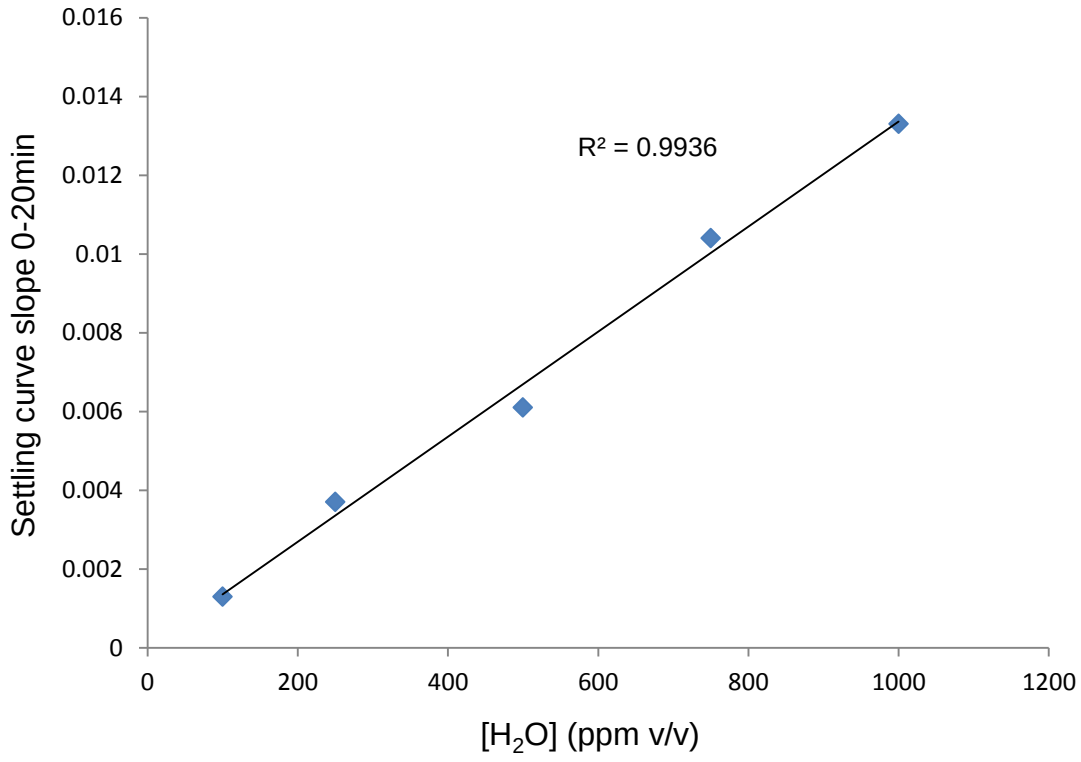

Figure 16. The initial rate of change (t = 0-20 min) for the settling curve of water droplets dispersed in Jet A-1. Samples prepared *via* ultrasonication and recorded *via* UV-VIS spectroscopy at 370 nm

In conclusion, the initial rate at which water/jet fuel emulsions settle was found to be proportional to the initial water concentration within the range studied (*i.e.* 100-1000 ppm v/v), suggesting that a UV-Vis spectrophotometric method presents itself as a method for monitoring water concentrations in jet fuel with some promise, especially for *in situ* monitoring of water concentrations in the fuel tank. As in the case of KF and IR, when water exceeds the saturation concentration, the formation of non-homogenous micro-emulsions influences the accuracy of the analysis. Further studies are necessary to quantify the accuracy and reproducibility of the method and the range of linearity of resultant settling curve *versus* concentration. A correlation between the droplet size distribution and the gradient of the settling curve could also prove useful.

3.5 Water Content *via* Gas Chromatography

In 1991, Chen & Fritz published a GC method for determining the concentration of water in a variety of samples utilising the rapid, acid catalysed reaction with triethyl orthoformate (Chen & Fritz, 1991). The method was found to be reliable with a range of hydrophobic organic solvents, including cyclohexane, benzene, decane, and solid samples; the authors reported accuracies usually in excess of the Karl Fischer method. The method relies upon the indirect determination of water *via* the GC measurement of ethanol (EtOH), a volatile side-product liberated *via* the acid-catalysed stoichiometric reaction of water with ortho ester **1** (Scheme 3).

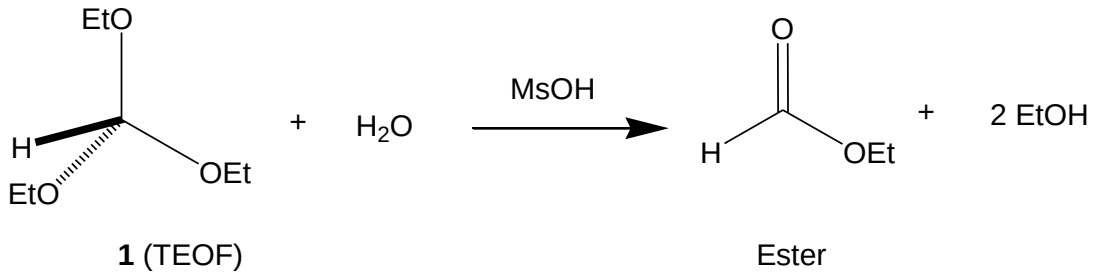

1 (TEOF) Ester

Scheme 3. Hydrolysis reaction of triethyl orthoformate (**1**) in the presence of methanesulfonic acid (MsOH).

This GC method of Chen & Fritz was repeated in these laboratories upon cyclohexane in order to ensure reproducibility, and was then adapted for measuring water in jet fuel (for experimental, see Section 10.5). Importantly, and as confirmed by GC-MS, the products of the hydrolysis of **1** (*i.e.*, the volatile analytical markers ethanol and ethyl formate), and the internal standard (3-methylpentane), all elute before the components of jet fuel (Figure 17). The retention times for ethanol and 3-methylpentane (internal standard) were 1.69 and 1.8 min, respectively. For each water standard, the relative peak area (RPA) of ethanol was calculated by dividing the ethanol peak area by the internal standard peak area.

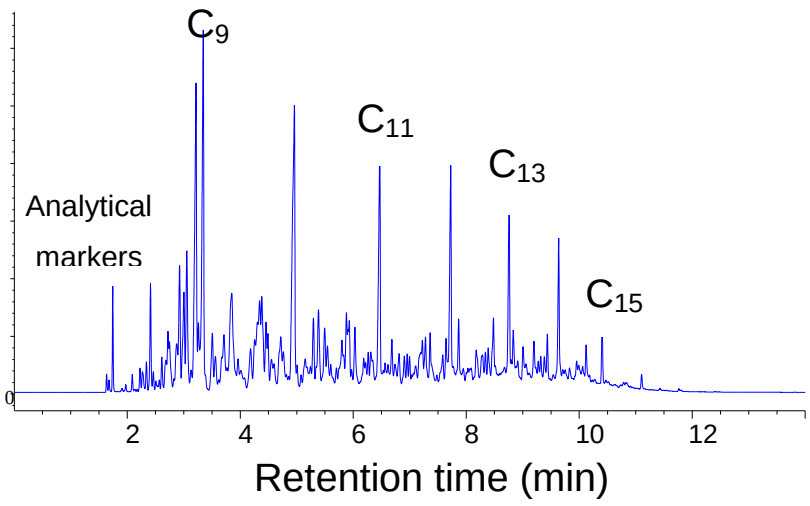

Figure 17. A typical GC-FID chromatogram of the analytical markers ethanol and ethyl formate in Jet A-1. A 30m HP-5MS column was used, with a temperature gradient of 80 to 240 ºC at a rate of 20 ºC/min.

To correct for atmospheric and residual water present in the reactant solution, the RPA of the reactant solution was subtracted from each ethanol RPA. A calibration curve was plotted, and is presented in Figure 18.

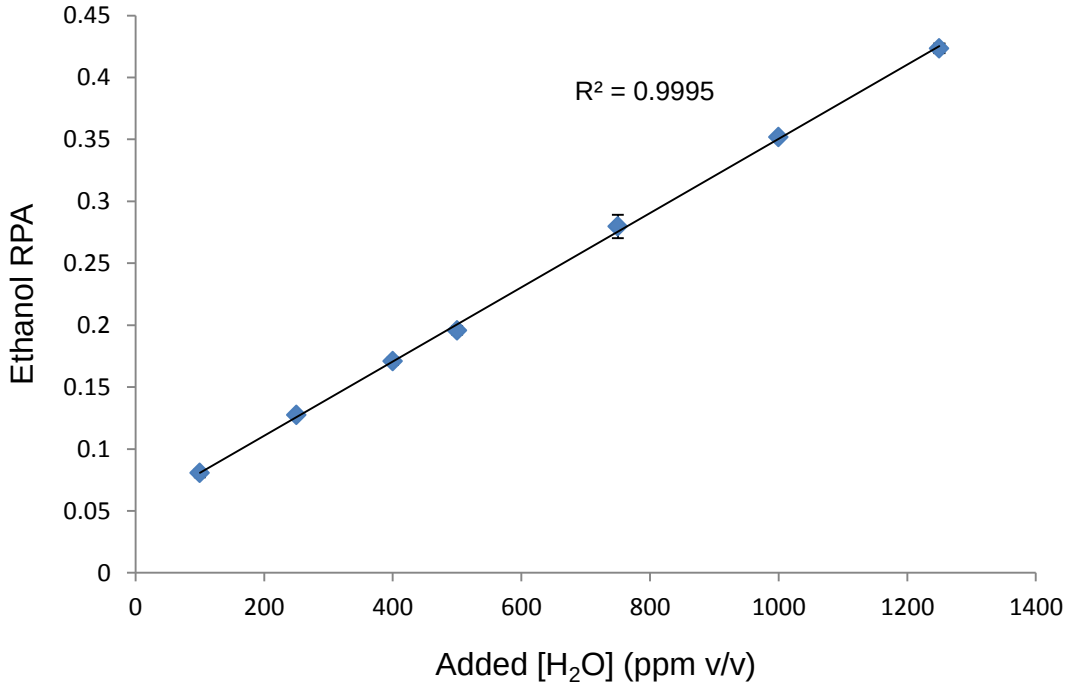

Figure 18. Calibration curve for Jet A-1, obtained from the GC-FID responses of the ethanol produced, with respect to water concentration.

As can be seen, an excellent linear correlation (R^2 = 0.9995) exists between the ethanol RPA and water concentration in Jet A-1 in the concentration range examined (100 - 1250 ppm v/v). The gradient (m = 3 x 10^{-4}) is in excellent accordance with the gradient obtained for the analysis in cyclohexane (m = 3 x 10^{-4}). The linearity and the gradient of the calibration curve demonstrate that the GC method reported here constitutes a new method for the determination of the water content in jet fuel (Repetto *et al.*, 2013). Furthermore, the analytical technique illustrates the effectiveness of using an ortho ester functionality (*i.e.,* triethyl orthoformate) as a dehydrating agent for Jet A-1 in acidic conditions.

3.6 Conclusions

Alternative methods to determine the concentration of water in jet fuel have been briefly considered. From these preliminary results, IR and UV-VIS spectroscopy appear to be potentially useful techniques. However, further studies are needed to establish the accuracy and reproducibility of these methods. Non-destructive techniques for measuring the water content of jet fuel could be important for *in situ* measurements of water in the fuel tank of an aircraft. For our purposes, the GC method appears to be the ideal approach, particularly because it illustrates the effectiveness of using triethyl orthoformate as a dehydrating agent for Jet A-1. It also demonstrates that the hydrolysis reaction of triethyl orthoformate in jet fuel is complete and irreversible under these conditions.

Chapter 4

Towards Fuel Dehydrating Icing Inhibitors

4.1 Introduction

To date, the approaches used to protect jet fuel from the potentially hazardous effects of free-water during the flight include the use of heated filtration systems, and/or additives such as FSII, biocides and corrosion inhibitors. A 1959 US Patent proposed the use of an organic dehydrating agent (2,2-dimethoxypropane) which when reacted with water formed a by-product that provided some additional protection against gum formation (Wood & Hopkins, 1959). The effectiveness of organic dehydrating agents (or water-scavengers), such as the ketal 2,2-dimethoxypropane, is complicated by the inherent reversibility of the hydrolysis reaction which leads to equilibrium mixtures of scavenger and free water (Kesslin and Bradshaw, 1966). This strategy remains relatively neglected, perhaps because of the complexity of the physical organic chemistry involved in these systems. It is proposed here that, alternative organic reagents with well characterised hydrolysis reactions, such as acetals, ketals, ortho esters, and ortho carbonates, present themselves as ideal candidates for investigation as potential scavengers for water in jet fuel. Also the hydrolysis products of these compounds will potentially possess the properties of an efficient FSII, which will then protect the jet fuel against any remaining water contamination.

The use of acetals and ketals derived from sugar mannose has been explored by Mushrush and co-workers. These compounds were proven to show comparable icing inhibitor characteristics to di-EGME, were stable in jet fuel for up to 2 years, and importantly were found to be environmentally benign and relatively nontoxic at the necessary concentration (Mushrush *et al.*, 1997, 1999). It has also been demonstrated, with the GC method reported in Section 3.5, that ortho esters are effective dehydrating agents for jet fuel in acidic conditions. In order to develop a solution to such a complex cascade of processes, it is necessary to break the problem into its constituent parts.

4.2 Candidate FDII

Acetals, ketals, ortho esters, and ortho carbonates appear at first glance to meet many of the criteria outlined in Section 2.5, wherein they possess the appropriate levels of selectivity, and stability for our purposes. Strategically, one would consider using cyclic acetals, ketals, ortho esters, or ortho carbonates because the products of hydrolysis resemble the FSII di-EGME, insofar as they would be bi-functional, possessing *both* hydrogen bond donors (*i.e.,* HBD include the –OH function), and acceptors (*i.e.,* HBA include the C=O, and –OMe function) within an aliphatic backbone. Both five- and six-membered derivatives **2-9** presented in Schemes 4 and 5 were considered, along with anticipated hydrolysis products (Wyatt & Warren, 2013). Acetals and ketals **2-6** are reported in Scheme 4. The *endo*-cyclic acetal **2**, which incorporates all hetero atoms within the ring, will afford a glycol along with an aldehyde. The former are effective de-icers though notoriously toxic to the environment; the latter will form the corresponding carboxylic acids under mildly oxidising conditions. The *exo*-cyclic acetal **3**, which incorporates only one hetero atom within the ring, affords in the first instance a hydroxy aldehyde, which is readily oxidised to the corresponding carboxylic acid. On this basis, acetals were eliminated from consideration as candidate FSII because, whilst carboxylic acids can be expected to increase the rate of the hydrolysis reactions, they are undesirable from the perspective of corrosion. The *endo*-cyclic ketal **4** again affords glycols, along with the corresponding ketone which is oxidatively robust compared to an aldehyde; thereby ensuring that there are no corrosive side-products of the hydrolysis. The promising *exo/endo*-cyclic ketals of type **5** afford a bi-functional hydroxy ketone possessing both HBD and HBA sites with a minimum of five or six aliphatic carbon centres, comparing favourably with the FSII di-EGME. Finally, *exo*-cyclic ketals of type **6** are expected to afford cyclic ketones which are mono-functional, possessing just a single site for hydrogen bonding. Both **5** and **6** afford alcohols as a bi-product, which are highly combustible de-icers.

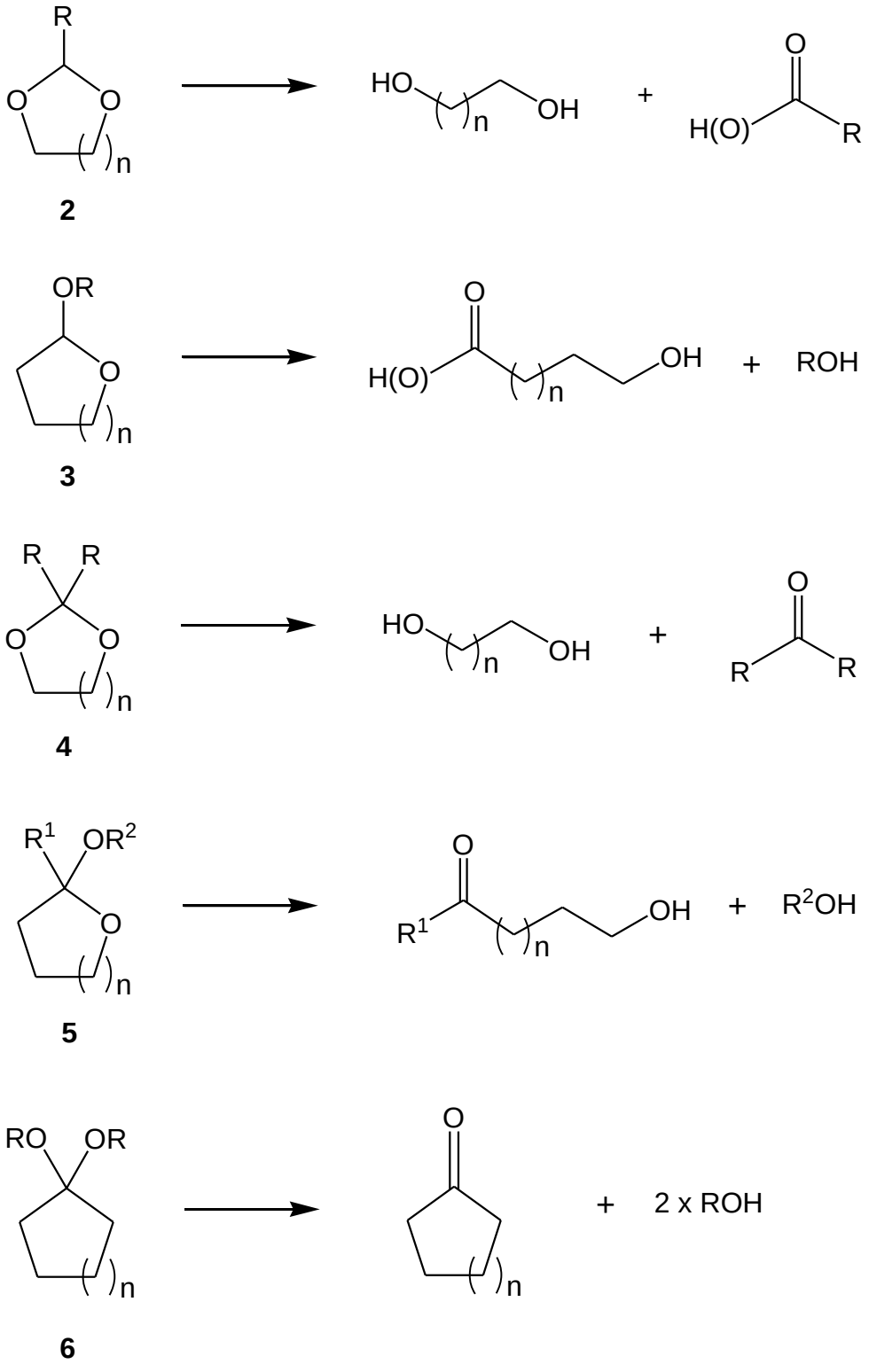

Scheme 4. The acid catalysed hydrolysis reactions for cyclic acetals and ketals (n = 1 or 2).

Ortho esters and ortho carbonates **7-9** are reported in Scheme 5. The promising class of *endo*-cyclic ortho esters of type **7** afford a bi-functional hydroxy ester possessing one HBD (*i.e.,* -OH) and two HBA sites [*i.e.,* -OC(=O)] with a minimum of four or five aliphatic carbon centres, comparing very favourably with the FSII di-EGME in terms of molecular similarity and atom economy. The promising *exo*-cyclic ortho esters of type **8** afford a mixture of γ/δ-lactones and hydroxy esters, which depends upon *p*H and reaction times (Deslongchamps *et al.*, 1985). Finally, hydrolysis of ortho carbonates of type **9** leads to a cyclic carbonate, which may spontaneously decompose to afford toxic ethylene glycol, water and carbon dioxide.

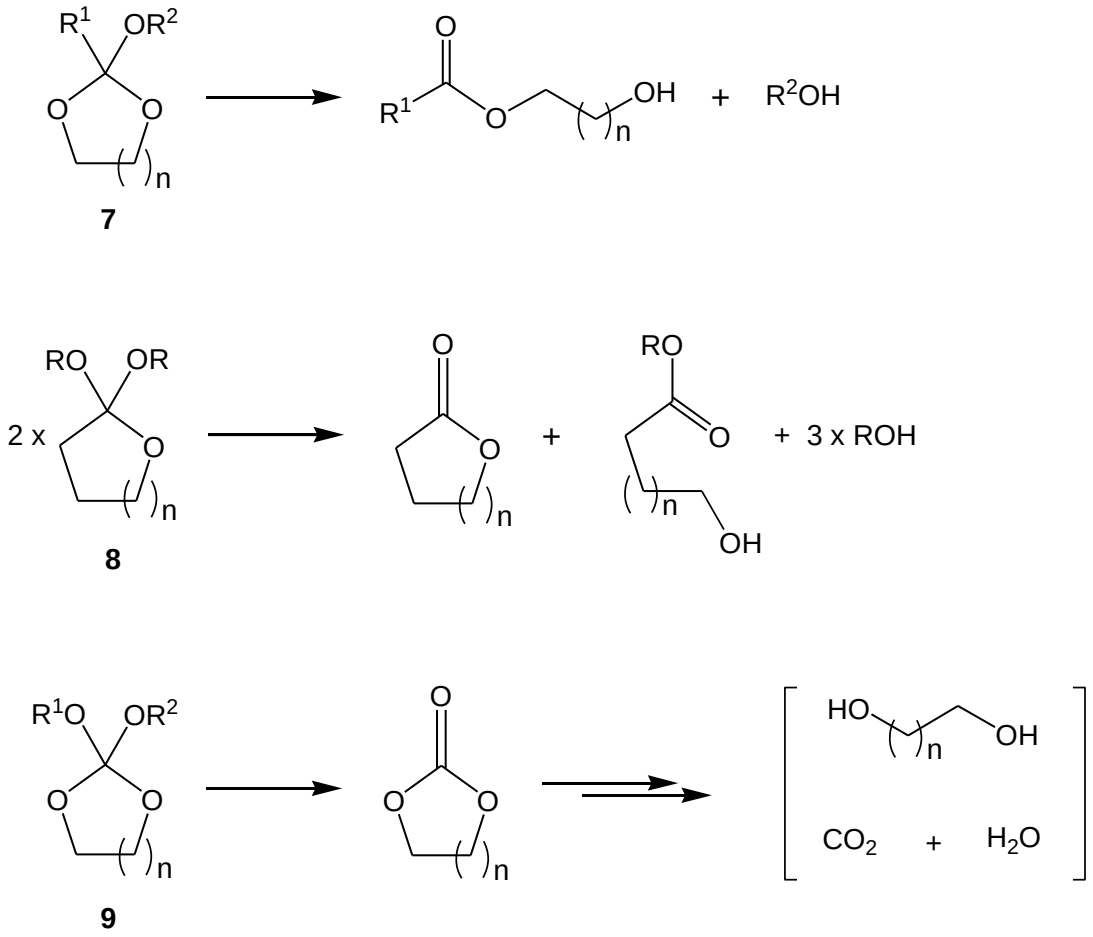

Scheme 5. The acid catalysed hydrolysis reactions for cyclic ortho esters, and ortho carbonates (n = 1 or 2).

In conclusion, having reviewed the structural characteristics of cyclic acetals, ketals, ortho esters, and ortho carbonates for their potential as FDII, the *exo/endo*-cyclic ketals of type **5**, and both *endo*- and *exo*-cyclic ortho esters of type **7** and **8**, respectively present themselves as promising candidates for a dual purpose additive, meeting the criteria outlined earlier. The next step was to perform a preliminary study to examine the feasibility of using the inherent acidity of jet fuel to catalyse the hydrolysis reaction.

4.3 Proof of Concept

Since a strong acid catalyst is undesirable inside the fuel tank of an aircraft, it was necessary to establish whether the inherent acidity of jet fuel is sufficient to catalyse the hydrolysis reaction of ketals and ortho esters. Jet fuel is mildly acidic because it contains mixtures of cyclohexyl and cyclopentyl carboxylic acids *i.e.*, naphthenic acids (CRC, 2004). Indeed, the batch of Jet A-1 used for the analyses outlined in this Thesis is reported to be 0.01 mg KOH/g by ASTM D3242 (S.G.S. Oil, 2012). In order to examine the capacity of ketals and ortho esters to dehydrate jet fuel in the absence of added acid, the GC method described earlier in Section 3.5 was repeated in the absence of methanesulfonic acid (for experimental details, see Section 10.5). It seemed logical to examine the relative extent of hydrolysis of TEOF **1** in the absence of acid, with respect to the corresponding acid catalysed process reported earlier (Section 3.5). The extent of the hydrolysis reaction of **1** in jet fuel at T = 20°C within the first 30 minutes after the addition of the ortho ester, across the concentration range 100-1250 ppm are shown in Figure 19. Strikingly, in the absence of both added water and acid, TEOF **1** is hydrolysed to the same extent as the acid catalysed process. With the addition of progressively greater amounts of water to Jet A-1, the extent of ortho ester hydrolysis decreases to 30-15% thereby indicating some relationship between the rate of hydrolysis and acid concentration.

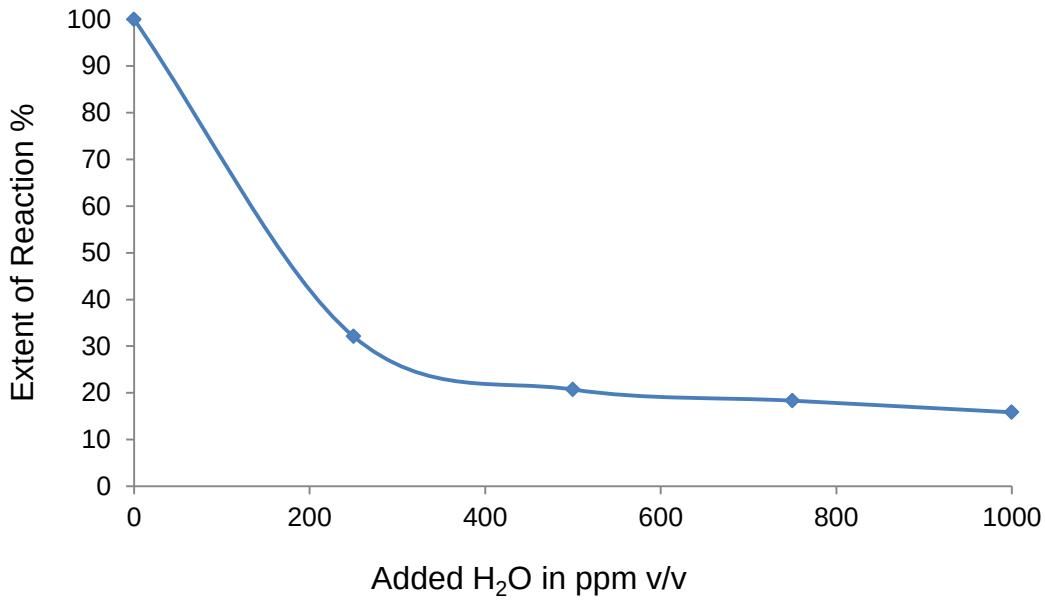

Figure 19. Extent of the hydrolysis reaction of TEOF **1** in Jet A-1 after 30 min at ambient T=20 ºC. The plot was obtained by comparing the GC-FID responses of the ethanol produced with respect to water concentration, both with and without added methanesulfonic acid.

4.4 Conclusions

Geminal ethers of the type **5**, **7** and **8** have been identified as promising FDII which appear to meet many if not all of the criteria outlined in Section 2.5. Furthermore, the ortho ester functionality *i.e.,* **1** is demonstrably effective as a fuel dehydrating agent to such a degree that it constitutes the basis of a new method for the determination of water in aviation fuel. The inherent acidity of Jet A-1 is clearly sufficient to catalyse the hydrolysis of an ortho ester. The relationship between the role of the acid, the extent, or rate of hydrolysis, and the molecular structure of geminal ethers **5**, **7** and **8**, constitute the remainder of the discussion in the following chapters of this Thesis.

Chapter 5

The Factors Governing the Rate of FDll Hydrolysis

5.1 Introduction

A generic reaction for the acid catalysed hydrolysis of geminal ethers (*i.e.,* acetals, ketals, ortho ester, and ortho carbonates) is presented in Scheme 6. The overall reaction is reversible, but in an excess of water the equilibrium is driven to the carbonyl and alcohol products. Though easily stated, the mechanism for the cleavage of two RO─C bonds, the addition of a molecule of water, and several proton-transfer reactions constitute a surprisingly complex process (Fife, 1972; Cordes & Bull, 1974; Carey & Sundberg, 2007).

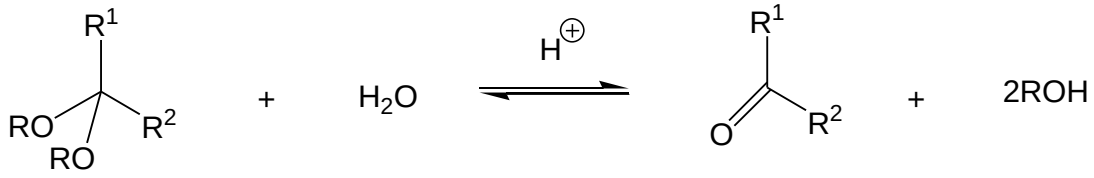

Scheme 6. The general equation for the hydrolysis of acetals ($R^{1\text{-}2}$ = H/alkyl/aryl), ketals ($R^{1\text{-}2}$ = alkyl/aryl), ortho esters (R^1 = H/alkyl/aryl, R^2 = OR), and ortho carbonates ($R^{1\text{-}2}$ = OR).

Specifically (Figure 20), the hydrolysis process for a generic geminal ether *may* be initiated by the delivery of H^+ from the conjugate base[†1] A^- (*i.e.,* bond cleavage step α) along the trajectory of a hydrogen bond (*i.e.,* bond formation step β), to form a charged intermediate (Fife, 1972; Guthrie, 1980; Jensen & Wuhrman, 1983; Kresge *et al.*, 1983; Buckley & Oppenheimer, 1996; Zanette *et al.*, 2003). The displacement, or simply replacement, of the "RO–" fragment (*i.e.,* bond cleavage, step γ) by water (*i.e.,* bond formation step δ) may also be mediated *via* a change in hybridisation of the central carbon atom (*i.e.,* $sp^3 \leftrightarrow sp^2$ ε; Figure 20) (Fife, 1967; Young *et al.,* 1980; Jensen & Wuhrman, 1983).

[†1] The conjugate base of H^+ in water is the hydroxonium cation H_3O^+.

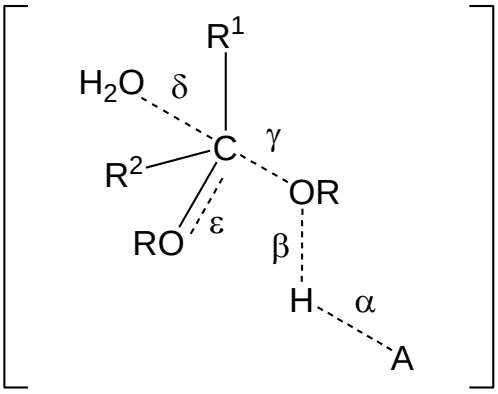

Figure 20. Bond breaking and formation stages in the acid (HA) catalysed hydrolysis reactions of geminal ethers.

The debate about the factors influencing the overall rate of reaction, and the sequence/synchronicity of events α–ε has failed to produce a consensus (Richard *et al.*, 1999; Kirby *et al.*, 2000; Zanette *et al.*, 2003). Although variables such as solvent (Young *et al.*, 1980), the pK_a of the acid catalyst (Guthrie, 1980), the basicity of –OR groups (Kankaanperä, 1969; Cordes & Bull, 1974; Lahti & Kauppi, 1986), stereoelectronic effects (Deslongchamps *et al.*, 2000), and the impact of substituents $R^{1\text{-}2}$ upon the formation (Jensen & Wuhrman, 1983; Kresge *et al.*, 1984; Wiberg *et al.*, 1985; Lahti, 1987; Fife *et al.*, 1996; Zanette *et al.*, 2003) and reactivity of charged intermediates (Richard *et al.*, 1999) have all attracted scrutiny across the range of geminal ethers, a unified and coherent mechanistic model has yet to emerge.

The hydrolysis of ortho esters has attracted particular attention because it is a good model for the cleavage of glycosidic bonds in biological systems (Buckley & Oppenheimer, 1996). As discussed earlier, ortho esters are potential water scavengers for jet fuel (Chapter 4). In order to optimise performance, an understanding of the dominant mechanistic pathway for the hydrolysis of these compounds must be arrived at. In the first instance, the role of the acid catalyst and any implications for the design of a scavenging system must be investigated. Later, the influence of molecular structure upon the relative rates of hydrolysis for a range of geminal ethers will be considered (see Chapter 6).

5.2 The role of the acid catalyst

Since a strong acid catalyst is undesirable inside the fuel tank of an aircraft, it is important to determine the dominant bond making/breaking steps associated with acid catalysis. Formation of the dialkoxy carbenium ion **14** *via* either specific or general acid catalysed protonation of a generic ortho ester **10** is presented in Scheme 7. A strong acid will undergo fission of the α bond prior to the formation of bond β, *i.e.,* specific acid catalysis (Figure 20). A weak acid will form bond β prior to fission of bond α *i.e.,* general acid catalysis (Figure 20). In the case of general acid catalysis, H-A delivers a proton to an oxygen atom of the ortho ester *via* **12**, which then eliminates a molecule of alcohol ROH to give **14** with an overall rate constant k_{HA}. In the case of specific acid catalysis, **10** is protonated (**11**) to give **14** after the elimination of ROH with an overall rate constant k_{H+}. It is generally considered that the decomposition of **13** to form the water scavenging dialkoxy carbenium ion **14** is the rate limiting stage (Cordes & Bull, 1974; Wenthe & Cordes, 1965). In both mechanistic pathways, the cation **14** is rapidly hydrated and collapses to form ester **15** through several steps, and the ultimate elimination of a second molecule of ROH (Scheme 7). For all but the strongest acids both pathways will be operative; therefore it is necessary to determine the magnitude of the rate constants associated with the simultaneous processes k_{H+} and k_{HA}.

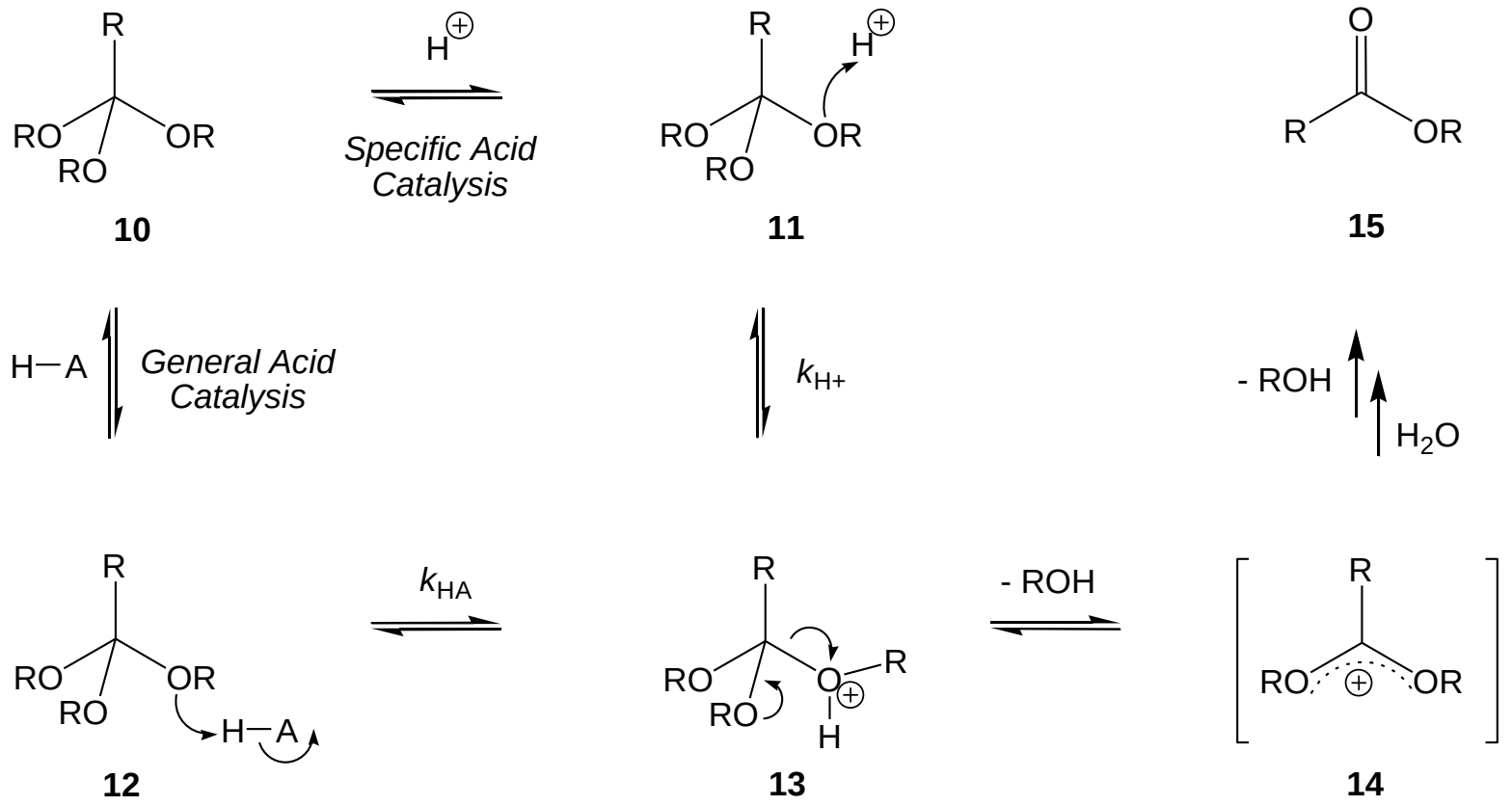

Scheme 7. General and specific acid catalysed pathways for the hydrolysis of ortho esters.

Since several consecutive mechanistic steps are being scrutinised, the mathematical treatment of the kinetic expressions for each individual step becomes impractical; therefore a steady-state approximation is necessary in order to simplify the kinetic treatment. Water is in excess, therefore it is safe to assume that $\delta[H_2O]/\delta t = 0$. Intermediates **13** and **14** are highly reactive, and so their concentrations will be small compared to those of the reactants and the products (*i.e.,* δ[**13**]/δt and δ[**14**]/δt = 0). The intermediacy of aliphatic **13** or **14** could not be detected by NMR spectroscopy in this work, or by using UV in the work of others (Kresge *et al.*, 1979a). The kinetic expression therefore reduces to Equation I (Cox, 1994).

$$rate = k_{obs}[\mathbf{10}] \qquad \text{(I)}$$

As the overall rate of reaction (equation I) is a summation of both processes described by k_{H+} and k_{HA}, the rate constant k_{obs} is therefore proportional to the concentration of both associated and dissociated acids (Equation II).

$$k_{obs} = k_{H+}\,[H^+] + k_{HA}[HA] \qquad \text{(II)}$$

As discussed earlier (Chapter 1), jet fuel is mildly acidic, and in the presence of polar solvents such as water, the extent of the acid dissociation will be proportional to the acid dissociation constant (K_a) of the individual acids present (Equation III).

$$K_a = \frac{[H^+][A^-]}{[HA]} \qquad \text{(III)}$$

By exploiting the constancy of K_a and varying the numerators (*i.e.,* $[A^-]$ 2.0 → 0.1 and *p*H 5.07 → 3.74) whilst maintaining [HA] constant (*i.e.,* 0.192 mol/L), it is possible to determine k_{H+} and k_{HA}. In fact if [HA] is kept constant, Equation II becomes equivalent to that of a straight line and k_{H+} and k_{HA} may be determined by plotting k_{obs} *vs* $[H^+]$. The value of k_{obs} may be obtained experimentally by monitoring the change in concentration of **10** over time, according to the integrated rate law (Equation IV) (Atkins & de Paula, 2006).

$$\ln[\mathbf{10}]_t - \ln[\mathbf{10}]_0 = -k_{obs}t \qquad \text{(IV)}$$

^{1}H NMR spectroscopy is the technique of choice for studying dynamic processes in solution (Potts & Schaller, 1993). Initial experiments using apolar solvents such as cyclohexane-d_{12} (a reasonable surrogate for jet fuel – see Section 1.4) with water, led to the formation of emulsions; the concomitant line broadening made meaningful analyses impracticable. However, if one makes the reasonable assumption that reactions will occur at or near the fuel-water phase boundary, then a relatively apolar yet water-miscible solvent, such as acetone-d_6, presents itself as an appropriate matrix for our purposes. Throughout these kinetic studies H_2O was used, instead of D_2O which is invisible to the ^{1}H NMR experiment; firstly because the scavenger will encounter H_2O and not D_2O in a fuel tank, and secondly to avoid the inevitable mechanistic complications attending kinetic isotope effects (Wenthe & Cordes, 1965; Lahti, 1987).

Our choice of HA for these studies was acetic acid, because it possesses a dissociation constant (AcOH, K_a = 1.75 x 10^{-5} mol/L) of the same order of magnitude as the aliphatic carboxylic acids generically known as naphthenic acids, which are an unspecific mixture of both cyclopentyl and cyclohexyl carboxylic acids already present in jet fuel (see Section 1.2.1).

Five buffered solutions with a constant [AcOH] yet different [H^+] were prepared by varying the amount of sodium acetate (AcONa). For the purpose of this study, attention was switched from the aldehyde derivative TEOF (**1**, Scheme 3) which was used for the proof of concept study, to the presumably faster reacting keto-derivative trimethyl orthoacetate (TMOA) (**10**, Scheme 7 where R = -CH_3) for reasons of atom economy (*i.e.,* 20% less MM) (Kresge *et al.*, 1983). For each buffered solution a k_{obs} was obtained and the results are presented in Table 2.

Table 2. Experimentally determined k_{obs} for trimethyl orthoacetate (TMOA – **10**, Scheme 7 where R = -CH_3) (T = 22ºC).

[AcOH]/[AcONa]	$[H^+]$ (M)	k_{obs} (s^{-1})
0.486	$8.51x10^{-6}$	$2.64x10^{-5}$
1.000	$1.75\ x10^{-5}$	$3.95x10^{-5}$
2.918	$5.11\ x10^{-5}$	$5.92x10^{-5}$
4.000	$7.00\ x10^{-5}$	$6.99x10^{-5}$
10.378	$1.82\ x10^{-4}$	$13.4x10^{-5}$

From these data, k_{obs} *v.* $[H^+]$ may be plotted (Figure 21) and a straight line fitted (y = 0.6 x + $2.6x10^{-5}$; R^2 = 0.994) from which values for the gradient of the slope and y-intercept afford k_{H+} = $6x10^{-1}$ $M^{-1}s^{-1}$ and, k_{HA} = $1.4x10^{-4}$ $M^{-1}s^{-1}$, respectively. It is clear that the pathway catalysed by dissociated acid H^+ (specific acid catalysis – Scheme 7) is approximately 4300 times faster than the pathway catalysed by undissociated AcOH, within the *p*H range studied here (3.7 → 5.0), *i.e.*, k_{H+} ›› k_{HA} (Repetto *et al.*, 2013).

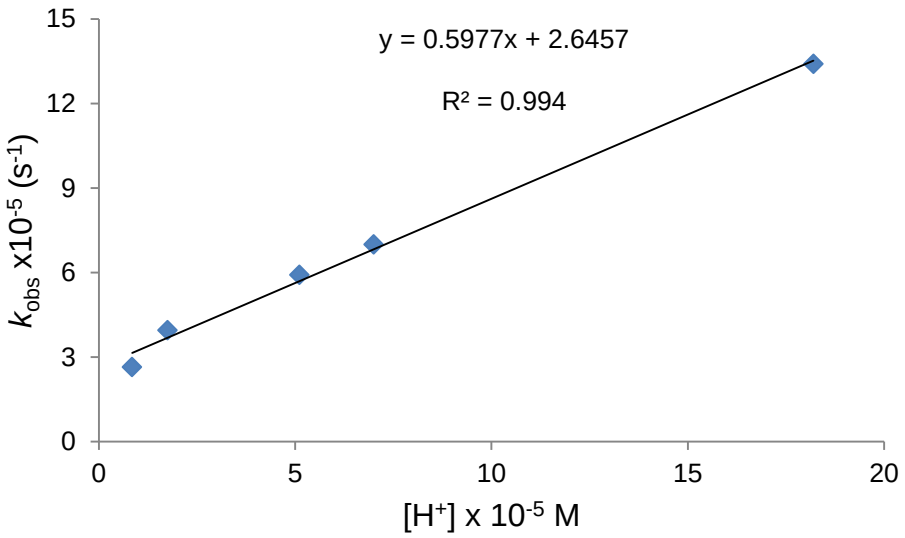

Figure 21. A plot of k_{obs} *vs*. $[H^+]$ for trimethyl orthoacetate (TMOA) **10**.

In conclusion, the significant difference in the experimentally determined rate constants for the hydrolysis of an ortho ester by both dissociated H^+ and associated HA acids has important implications for the partitioning behaviour of a scavenger across the fuel-water interface (Figure 22). Associated - relatively weak - acids (HA), such as naphthenic acids, tend to reside in the apolar environment of jet fuel, unlike the hydrophilic hydroxonium cation which by definition prefers the polar environment of free water. The aim is to design a water scavenger (WS) which preferentially partitions into the lipophilic fuel phase (*i.e.,* $K_{ow} = [WS]_{octanol}/[WS]_{water} > 0$, Figure 22) – which in the case of an ortho ester means that here, it may only undergo a slow hydrolysis reaction with dissolved water – thereby ensuring fuel protection. However, at the phase boundary with free water, the water scavenger may encounter dissociated acid H_3O^+ and subsequently undergo a rapid hydrolysis reaction - thereby consuming free water.

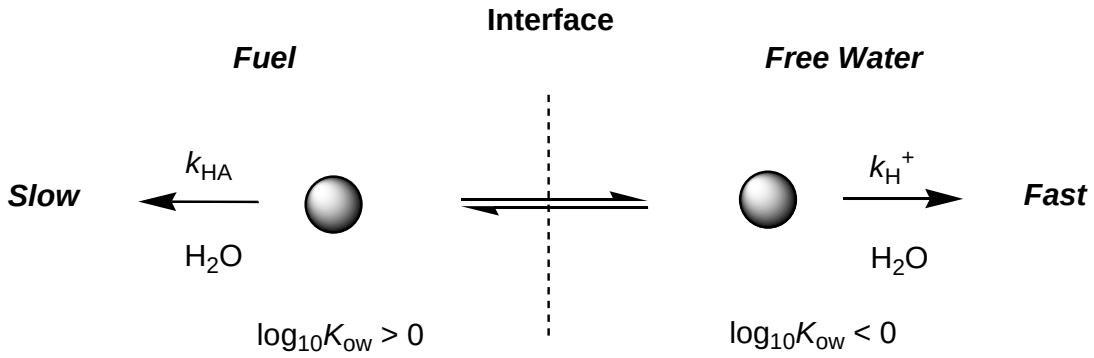

Figure 22. Fuel-water partitioning and the implications for acid catalysed hydrolysis. The water scavenger is represented as a sphere.

5.3 The impact of FDII structure upon the rate of reaction

A deeper qualitative understanding of the structural factors influencing the rate of hydrolysis is necessary in order to optimise FDII performance without recourse to concentrated acid catalysts. Attention will focus upon promising FDII candidates belonging to the group of endo-cyclic ortho esters of type **7** (Scheme 8). It is generally accepted that the specific acid catalysed hydrolysis of ortho esters proceeds *via* a three-stage mechanism (McClelland *et al*., 1988). For illustrative purpose, a generic 2-alkoxy-2alkyl-1,3-dioxolane **7** is considered (Scheme 8).

***Stage 1*.** The first stage involves the generation of a 1,3-dioxolan-2-ylium cation **16** (the name is derived from the parent heterocyclic 1,3-dioxolane), which is in principle a reversible process. Because of the reaction conditions ordinarily employed (*i.e.,* an excess of water as nucleophile), the reverse reaction with ROH (*i.e., k_{-1}*) is considered to be negligible, thereby rendering this step effectively irreversible. It has been established that cyclic ortho esters, and in particular those derived from 1,3-dioxolanes, initially undergo exclusive cleavage of the exocyclic alkoxy group (Kresge *et al.*, 1984). In reviewing the case of ortho esters, Kresge *et al.,* suggested two mechanistic extremes for stage 1 (Kresge *et al.*, 1974, 1984). A *concerted* catalysed process, wherein the ─OR group undergoes protonation as the $C^{\cdots\cdots}O(H)^{+}R$ bond begins to undergo cleavage. The alternative *stepwise* process, involves the C─OR bond spontaneously cleaving at a rate similar to that of RO^{-} protonation by H_3O^{+}. The latter describes a spontaneous, uncatalysed hydrolysis. In the case of 1,3-dioxolanes, the concerted mechanism is believed to dominate (Kresge *et al.*, 1979b); however Guthrie (Guthrie, 1980) asserts that ortho esters are in fact delicately poised between stepwise and concerted processes, as evidenced by aryl dimethyl orthoformates (Lahti, 1987) for which both mechanisms are known to be operational, depending upon the substituents upon the aryl group.

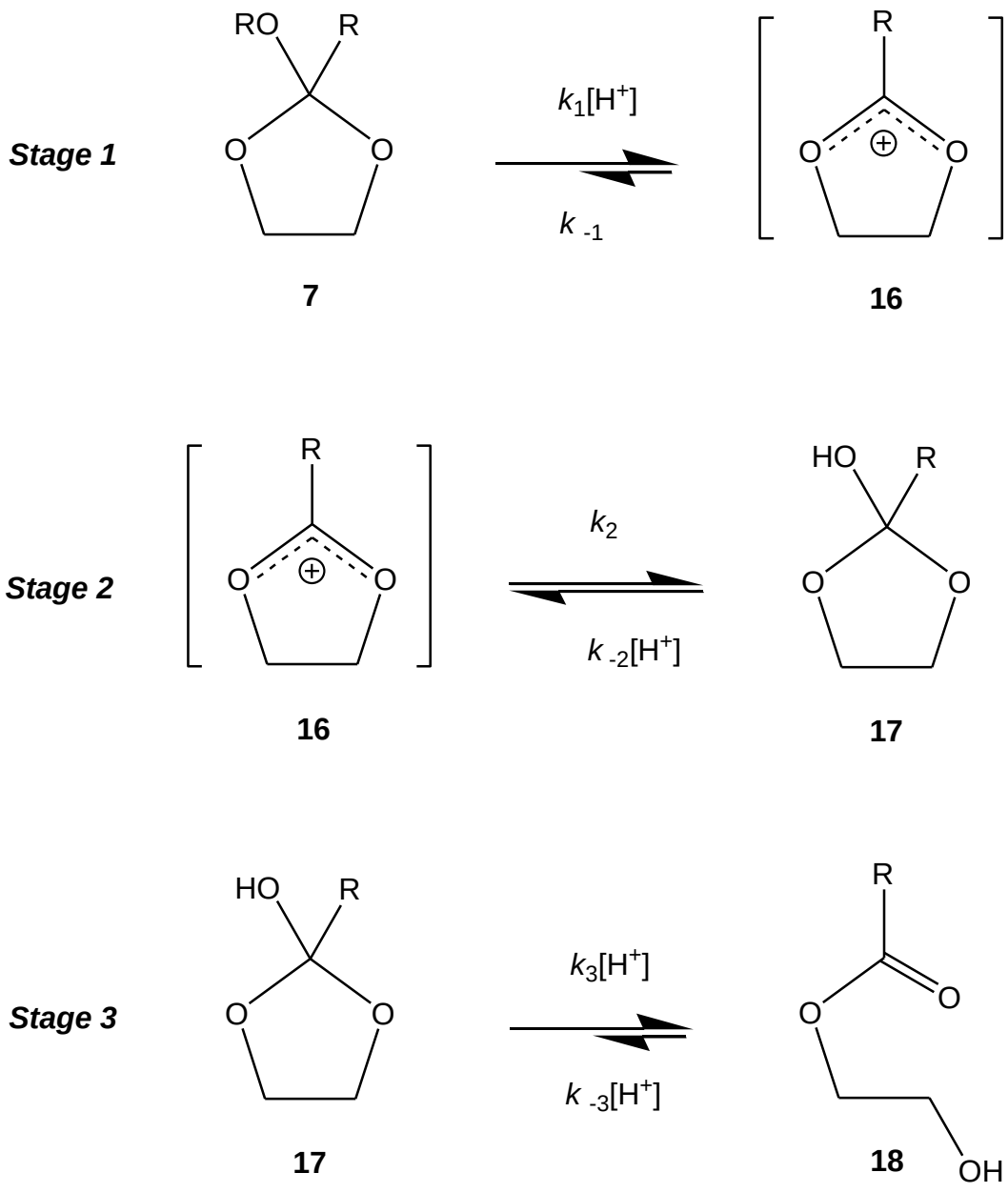

Scheme 8. The three-stage mechanism for the specific acid catalysed hydrolysis of cyclic ortho ester **7**.

A graphical analysis of anticipated substituent effects in terms of a simplified Jencks-More-O'Ferrall diagram is presented in Figure 23 (Jencks, 1972). The diagram shows only those steps leading to the generation of 1,3-dioxolan-2-ylium cation **16**, because in water and at low pH (*vide supra*), stage 1 is assumed to be rate limiting. The pathways **A** → **D** indicate contribution from either a catalysed (*via* corner **B**) or spontaneous (*via* corner **C**) process. It has been proposed that the formation of hypothetical

intermediates corresponding to corner **B** for acetals is energetically favourable (Zanette *et al.*, 2003). As the basicity of ortho esters and acetals are comparable (*i.e.,* pK_a ≈ -7→ -4) (Cordes & Bull, 1974; Kankaanperä, 1969) it is assumed by analogy that intermediates at corner **B** are also energetically favourable for ortho esters. However, unlike both cyclic acetals and ketals, orthoesters may form a delocalised 1,3-dioxolan-2-ylium cation **16**, which provides a significant contribution from the ion pair in corner **C** as depicted in Figure 23. Additionally, ortho esters possessing a good leaving group (RO^-), such as the conjugate base of a relatively strong acid (*i.e.,* ArO^- with pK_a ≈ 10), leads to spontaneous hydrolysis *i.e.,* corner **C** (Lahti, 1987). Furthermore, sterically demanding R^1/R^2 groups are expected to increase the energy of species at corners **A** and **B** relative to **C/D**. It is proposed therefore that shifting the transition state along the **A** → **C** coordinate will accelerate the overall rate of hydrolysis. The role of anomeric effects (*i.e.,* corner **C**) (Deslongchamps, 1975; Wiberg *et al.*, 1985) upon the overall rate of reaction of 1,3-dioxolanes has yet to be investigated, and will be addressed in due course.

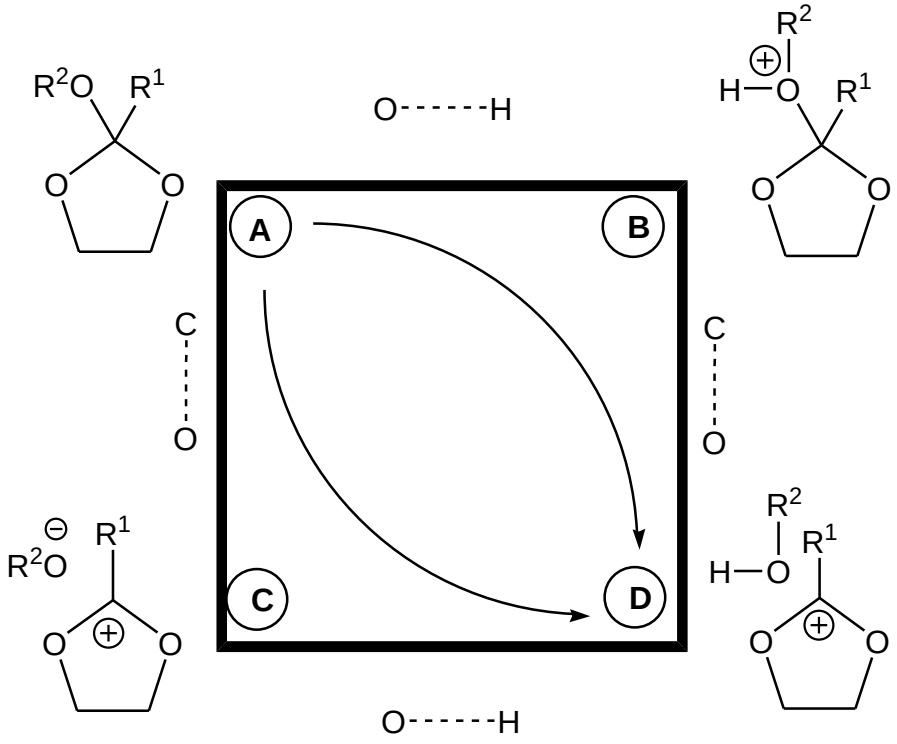

Figure 23. A simplified Jencks-More-O'Ferrall diagram indicating either a catalysed (*via* corner **B**) or spontaneous (*via* corner **C**) process.

Stage 2 of the mechanism (Scheme 8) is the reaction of the water scavenging 1,3-dioxolan-2-ylium cation **16** with H_2O to afford the 2-hydroxy-1,3-dioxolane **17** (*i.e.,* k_2), which may undergo the reverse, acid catalysed elimination of H_2O (*i.e.,* $k_{-2}[H^+]$) to afford **16**; the overall equilibrium constant for stage 2 is $K_2 = k_2/k_{-2}[H^+]$. Presumably, one would expect some if not all of the factors which impact upon $k_1[H^+]$ to influence $k_{-2}[H^+]$.

1,3-Dioxolan-2-ylium cations are an important subset of the widely encountered dialkoxy/hydroxyl-substituted carbenium ions. Their existence as transient species – named acetoxonium ions – was first proposed by Winstein and Buckles in 1942 in order to account for the rate enhancements and stereoselectivities associated with the solvolysis of 2-acetoxy-3-bromobutanes and 1-acetoxy-2-bromocyclohexanes (Winstein & Buckles, 1942). The transformation from purported reactive intermediate to stable, characterisable carbocation was initiated in 1955 when Meerwein was the first to succeed in isolating 1,3-dioxolan-2-ylium ions of type **16** as stable materials co-crystallised with non-polarisable anions such as $SbCl_6^-$ or BF_4^- (Meerwein *et al.*, 1955). The ^1H NMR spectra of these cations were obtained by Winstein and co-workers in the 1960's (Winstein *et al.*, 1963), and work continues in order to understand the reactions and properties of this important class of cation (West *et al.*, 1998).

1,3-Dioxolan-2-ylium cations **16** are ambident (Scheme 9). They can react with a nucleophile at C(4/5) to afford the thermodynamically controlled acyclic ester **19**, or *via* C(2) to form the kinetically controlled cyclic 1,3-dioxolane **20**. If the 1,3-dioxolane **20** can establish an equilibrium with the 1,3-dioxolan-2-ylium cation **16** then the kinetic product may ultimately be transformed to the thermodynamically preferred **19**. However, when the nucleophile can undergo a change in valency, as in the case of H_2O, ring opening of **20** may occur to afford acylic **21** directly. Nucleophiles favouring the C(2) pathway include alkoxides to afford ortho esters, halides, cyanides, and hydrides (Pittman *et al.*, 1972). In the case of water, it is not possible to distinguish between the C(2) and C(4/5) pathways as the products are **19** and **21**, which are identical hydroxy esters. The stereoselectivity attending

the C(4/5) ring-opening reactions of **16** has led to their extensive use in the field of carbohydrate chemistry for the introduction of new groups into sugars *via* neighbouring group cyclisation's (Paulsen, 1971).

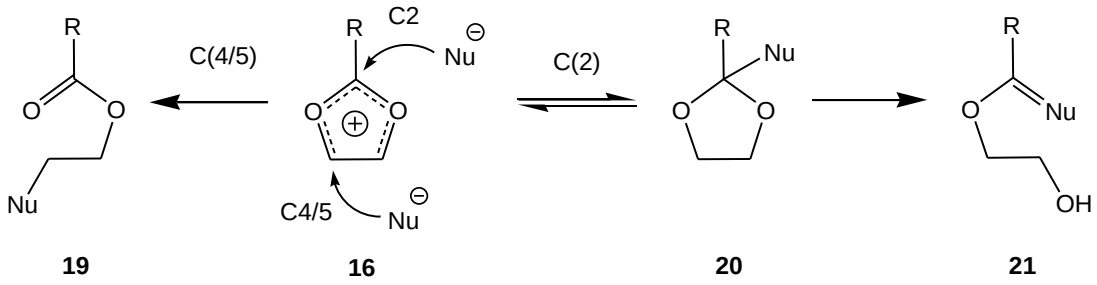

19 **16** **20** **21**

Scheme 9. The ambident nature of the 1,3-dioxolan-2-ylium cation **16**.

To understand, and perhaps more importantly to predict the reactivity of 1,3-dioxolan-2-ylium cations with water, a brief examination of how the solid-state structure varies with substituents is warranted. The value of examining the crystal structures of a series of closely related molecules is well established (Buergi & Dunitz, 1983). A search of the 2014 release of the Cambridge Structural Database (Allen, 2002) for molecules possessing the core 1,3-dioxolan-2-ylium ring identified five closely related systems: DOXYLP (Paulsen & Dammeyer, 1976), PEXSAM (Childs *et al.*, 1993), PEXSIU (Childs *et al.*, 1993), OXCLI (Caira & de Wet, 1981), and PEXSUG (Childs *et al.*, 1993). These structures are presented along with their REFCODEs in Table 3.

Table 3. Structures and REFCODEs for the X-ray crystal structures of closely related 1,3-dioxolan-2-ylium ring systems.

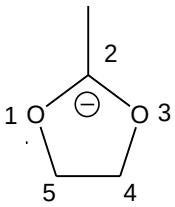	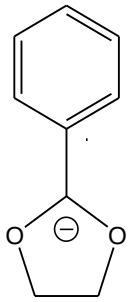	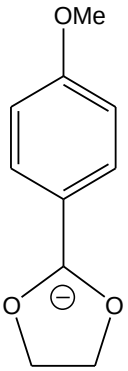	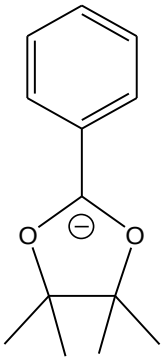	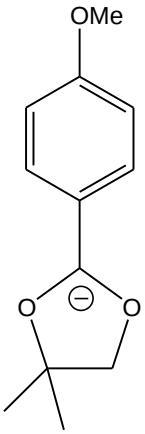
DOXYLP	PEXSAM	PEXSIU	OXCLI	PEXSUG

As is evident from Figure 24, the five membered ring of a 1,3-dioxolan-2-ylium cation is planar, possessing relatively long O(3)─C(4)/O(1)─C(5) bonds compared to that of the corresponding C─OC(O) bond of an ester *i.e.,* >1.45 Å. The average O(1/3)─C(2) distances are intermediate in length between those of a double O=C and single O─C bond of an ester (Childs *et al.*, 1993). The aryl rings of structures PEXSAM, PEXSIU, OXCLI and PEXSUG lie almost coplanar with the plane of the five membered 1,3-dioxolan-2-ylium ring, suggesting that the observed conformations facilitate effective conjugation between the C(2) substituents of the 1,3-dioxolan-2-ylium system.

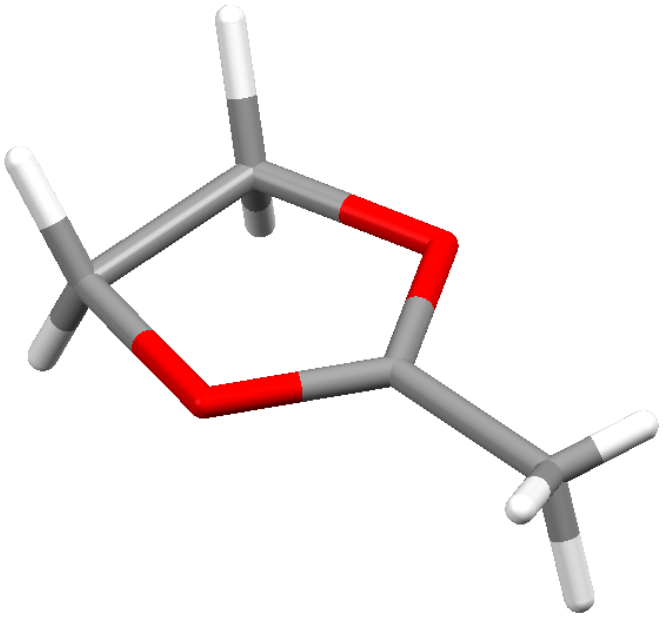

Figure 24. The X-ray crystal structure of the 2-methyl-1,3-dioxolan-2-ylium cation (DOXYLP). The ClO_4^- counterion has been omitted for clarity (Paulsen & Dammeyer, 1976).

Importantly, the O(1)─C(5) and O(3)─C(4) bonds in the 1,3-dioxolan-2-ylium cations exhibit a significant dependence upon the C(4/5) substituents. For unsubstituted structures DOXYLP, PEXSAM and PEXSIU the average O─CH_2 bond length is 1.474 Å. The cation with symmetrically disposed alkyl substituents upon C(4/5) (*i.e.,* OXCLI) contains significantly longer O(1/3)─C(5/4) bonds (*i.e.,* 1.525 Å) (Childs *et al.*, 1993). In the asymmetrically substituted structure PEXSUG, one observes a longer [O─$C(CH_3)_2$ = 1.509 Å], and shorter (O─CH_2 = 1.458 Å) bond, which may be accounted for by considering an ionic contribution towards the more substituted carbon atom. The electron-releasing methyl groups would readily support a partial positive charge upon the carbon atom, allowing us to consider a third contribution towards the customary resonance structures for 1,3-dioxolan-2-ylium cations, as depicted in Figure 25c (Pittman *et al.*, 1973).

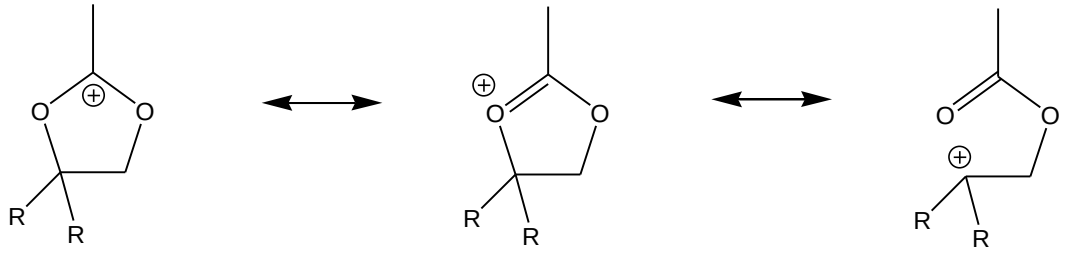

Figure 25. Resonance contributions to the 1,3-dioxolan-2-ylium cation.

To conclude, X-ray crystallographic analyses suggest that alkyl substituents upon atoms C(4/5) support a separation of charge along the O(1/3)─C(5/4) bonds, as depicted by a third resonance structure (Figure 25c). This in principle increases the stability of the 1,3-dioxolan-2-ylium cation and the susceptibility to C(4/5) attack.

Stage 3. Finally, the acid catalysed (*i.e.,* $k_3[H^+]$) cleavage of 2-hydroxy-1,3-dioxolane **17** affords the hydroxy ester **18** (Scheme 8). In the case of an acyclic *hemi* ortho ester derived from an acyclic ortho ester, the reverse process described by k_{-3} may be essentially ignored because the eliminated alcohol will be highly diluted in the solvent, thereby rendering this step essentially irreversible, even under highly acidic conditions. For this reason, $k_3 > k_1$ for acyclic geminal ethers *i.e.,* stage 1 is invariably rate limiting. In contrast to acyclic systems, cyclic 2-hydroxy-1,3-dioxolanes **17** undergo the ring cleavage described by k_3, to afford the hydroxyl carbonyl derivative **18,** which is more likely to undergo rapid cyclisation, described by k_{-3}, as the nucleophile is tethered to the ester. Indeed, the cyclisation of the hydroxy esters derived from both 1,3-dioxolane and 1,3-dioxane systems, undergo favourable 5- and 6-exo-trig cyclisation's, respectively (Baldwin, 1976). It stands to reason that, as the acid concentration increases, so the cyclisation step described by k_{-3} may become more dominant, though not necessarily linearly proportional to $[H^+]$ (McClelland *et al.*, 1979). The implications of an increasingly dominant k_{-3} term with decreasing *p*H, is that overall stage 3 *appears* to becomes rate limiting. The apparent switch in rate limiting step accompanying variance in *p*H is graphically presented in Figure 26.

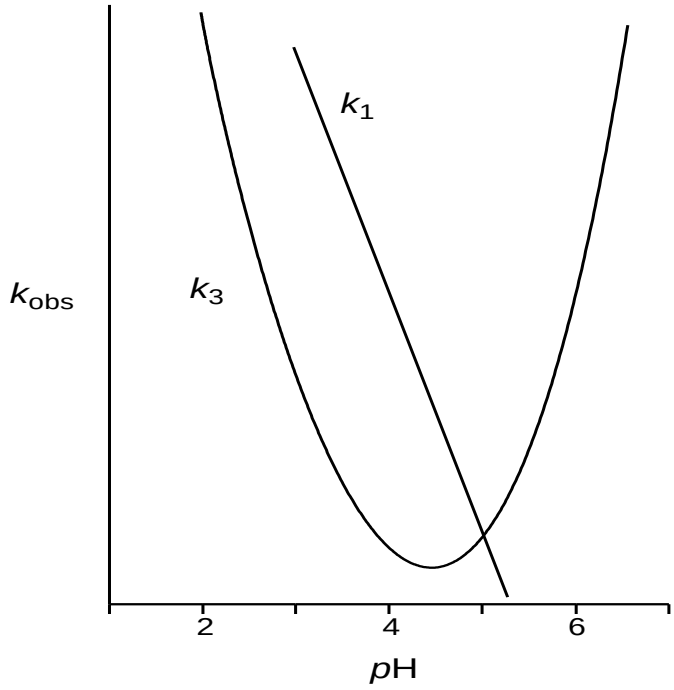

Figure 26. Rate profiles of k_1 and k_3 for the hydrolysis of cyclic ortho ester (Kresge *et al.*, 1979b; McClelland *et al.*, 1988).

Experimental evidence for this switch in rate determining stage throughout a *p*H range of approximately 4-6 for 1,3-dioxolanes has been previously noted by McClelland *et al.* (1988). However, these workers erroneously propose the operation of an additional base catalysed mechanism at higher *p*H in order to explain their data, thereby introducing a $k_3[HO^-]$ term into the rate law (McClelland *et al.*, 1988). One cannot rule out rate acceleration derived from excess conjugate base of the buffer (*i.e.,* HPO_4^{-2}, H_2PO^- or AcO^-). If this were so, the inclusion of a $k_3[A^-]$ term would more accurately represent the rate law here. As discussed earlier (Section 5.2), the goal of the project is to identify FDII which do not require strong acids for hydrolysis, preferring instead the much milder conditions associated with *p*H ≈ 5-6. A consequence of this self-imposed criterion is that under these conditions, a mechanistic "cross-over" occurs, such that k_1 and k_3 may be of similar magnitudes.

5.4 Conclusions

Detailed kinetic measurements using ^{1}H NMR spectroscopy have established that ortho esters are rapidly hydrolysed by dissociated acid catalysts, whilst a much slower process occurs with an associated acid catalyst. The implications for the development of a water scavenger are that lipophilic ortho esters will hydrolyse slowly in jet fuel, yet rapidly at the interface with free water. Further developments are therefore focussed upon acid catalysis using dissociated acids.

A qualitative summary of the key structural features of a FDII which can be manipulated in order to accelerate the rate of hydrolysis is presented in Figure 27. Sterically demanding R^1 and R^2 substituents are expected to lead to acceleration in the rate of reaction because of the concomitant release of strain in the ring system. A good leaving group (*i.e.,* when R^2O^- is the conjugate base of a strong acid) promotes spontaneity in the formation of the carbocation. Furthermore, an inductively donating R^1 will also promote carbocation formation. Inductively electron donating, and perhaps even sterically demanding R^3 may also support the stability of the developing carbocation and thereby accelerate the overall rate of hydrolysis. The rate accelerating potential of carefully chosen substituents R^{1-3} applies equally to the case of both five (n = 1) and six (n = 2) membered rings. In the case of the latter, rate accelerations are expected to accompany stabilising anomeric effect (Deslongchamps, *et al.,* 2000); what is yet to be understood is the role of the anomeric effect in the hydrolysis reaction of 5-membered rings.

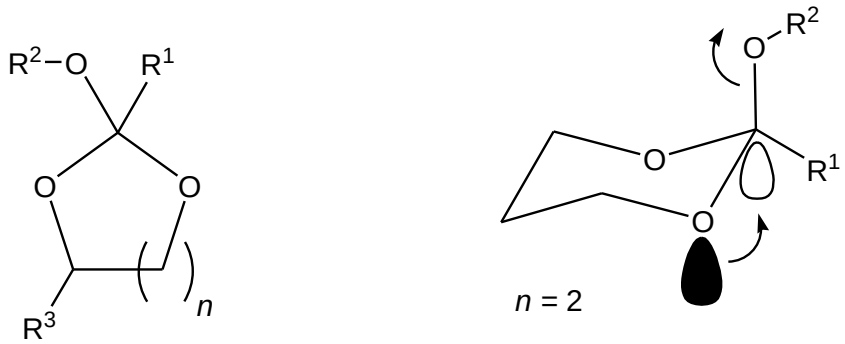

Figure 27. Structural features for accelerating the rate of hydrolysis of FDII.

Chapter 6

The Relative Rates of FDII Hydrolysis

6.1 Introduction

In the previous chapter, it was outlined how the rate limiting first stage in the hydrolysis of acyclic ortho esters may be exploited in order to uncover the preferred mechanism of acid catalysis. The impact of structural perturbations upon the rate of hydrolysis of both acyclic and cyclic systems was then examined, and qualitative predictions were made about the means through which FDII structure impacts upon the rate of hydrolysis. This chapter describes the more ambitious goal of developing *quantitative* links between molecular structure and corresponding rate of hydrolysis for a range of cyclic and acyclic ketals and ortho esters.

Brönsted became interested in the comparative rates for the hydrolysis of a range of acyclic acetals, ketals, ortho esters and carbonates as part of the wider development of his ground-braking theory of acid catalysis in the late 1920's (Brönsted & Wynne-Jones, 1929). Kinetic studies were performed using the dilatometric method in buffered aqueous solutions with ionic strengths and *p*H varying across the range 0.01-0.1 M and 6-8, respectively. Importantly, Brönsted noted the "salt effect", which describes an increase in the rate constant in proportion to the salt concentration, presumably because the increased polarity of the medium facilitates or stabilises carbocation formation. Quantitative data [*i.e.,* $\log(k/k_0)$] for the hydrolysis of a range of acyclic acetals, ketals and ortho esters in buffered mixtures of water, methanol, and dioxane have been reported using UV spectroscopy (Cordes & Bull, 1974); Kresge *et al.,* also discusses the hydrolysis of cyclic ortho esters in either aqueous HCl or buffer solutions using UV spectroscopy to measure the rate of carbonyl formation (1983). Not only is it difficult to draw upon such a disparate body of quantitative findings wherein data is gathered across a range of conditions, but it is anticipated that, for the purpose of developing FDII, less polar and non-buffered conditions should be considered.

Having already established ^{1}H NMR spectroscopy to be a fast, reproducible and flexible tool for investigating the kinetics of ortho ester hydrolysis (Section 5.2), it was decided to exploit this technique further. Rather than establish the absolute rate of hydrolysis for an individual molecule, it was deemed more useful to compare the relative rates of two or more compounds simultaneously, thereby accelerating the rate at which promising FDII may be screened. Furthermore, this methodology is unambiguous and minimises the experimental error between the pair of molecules under scrutiny.

Deslongchamps has reported the relative rate of hydrolysis for a limited range of six-membered ketals and ortho esters using ^{1}H NMR spectroscopy with such a "paired" kinetic approach (Deslongchamps *et al.*, 2000). Deslongchamps employed conditions which mimic more closely those potentially encountered in a fuel tank by a FDII *i.e.,* specific acid catalysis in a relatively apolar solvent similar to the fuel-water interface (D_2O/CD_3CN = 1:4). There are flaws in the work of Deslongchamps insofar that an attempt was made to compare the relative rates of hydrolysis of six-membered geminal ethers in D_2O/CD_3CN with those of acyclic derivatives measured in aqueous solutions drawn from the literature.

In the following sections this error is rectified. Using the rapid screening "paired" kinetic approach, quantitative rate data for the hydrolysis reactions of acyclic and novel cyclic derivatives are unified (*vide infra*), thereby enabling the assembly of a library of potential FDII, unambiguously organised according to their rates of hydrolysis.

6.2 Acyclic Ortho Esters

It was established earlier that TEOF **1** (Figure 28) performs as a highly efficient dehydrating agent for jet fuel both with, and importantly without an added acid catalyst (Section 3.5 and 4.3, respectively). In addition, NMR experiments upon **22** established that this molecule undergoes relatively fast specific acid catalysed hydrolysis as opposed to slower, general acid catalysed hydrolysis (Section 5.2). Comparing literature values for the hydroxonium catalytic coefficients for these acyclic ortho esters (*cf.* equation II, Section 5.2), Brönsted cites k_{H+} = 1.4 x10^4 $M^{-1}s^{-1}$ for **1** (Brönsted & Wynne-Jones, 1929), and Kresge reports k_{H+} = 1.2 x10^4 $M^{-1}s^{-1}$ for **22** (Kresge *et al.*, 1983). One might conclude from this data that both ortho esters react with water at a similar rate. This might appear surprising at first glance (Section 5.3); one would anticipate a significant acceleration in the rate of hydrolysis upon replacement of an H atom for a methyl group upon the central carbon atom (*i.e.,* **1** → **22**), whereas a modest acceleration might be anticipated when exchanging MeO- for EtO- (*i.e.,* **22** → **1**) [pK_a = 15.5_{MeOH}; 15.9_{EtOH} respectively (Brown *et al.*, 2013)]. In order to disassemble these overlapping structural effects upon the rate of hydrolysis, this study presents for the first time an unambiguous comparison of the relative rates of hydrolysis for the following pairs of ortho esters (Figure 28):

- **22 & 23** substituted *v*. unsubstituted at the central carbon atom
- **1** & **23** EtO *v*. MeO – unsubstituted at the central carbon atom
- **22** & **24** EtO *v*. MeO – substituted at the central carbon atom

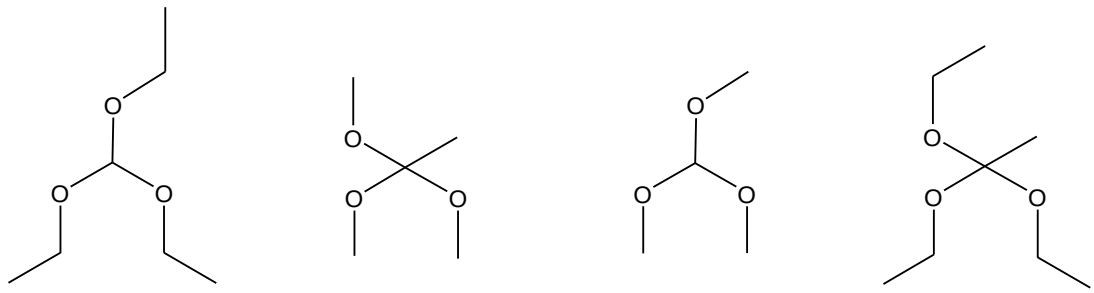

1 **22** **23** **24**

Figure 28. Acyclic ortho esters considered for kinetic experiments.

As discussed in Section 5.2, the disappearance of an ortho ester in the hydrolysis reaction follows first order kinetics (Equation I). In the case of acyclic ortho esters, stage 1 is the rate limiting step; therefore by measuring the consumption of starting materials it is possible to obtain the overall rate of reaction. Paired kinetic experiments were performed using ^{1}H NMR spectroscopy at 25ºC. The observed rate constants (k_{obs}) for both ortho esters were obtained by using the rate equation integrated over time (Equation IV - Section 5.2). The concentration of a given ortho ester was determined by measuring the integral beneath an appropriate resonance associated with hydrogen atoms of substituents upon the central carbon atom [*i.e.,* $(RO)_3CH$ or $(RO)_3CCH_3$]. By plotting the logarithm of the decrease in concentration over time, k_{obs} may be obtained. Although the solvent system used earlier to determine the specific and general acid catalytic coefficients for **22** (*i.e.,* acetone-d_6 and H_2O) would have been appropriate for these experiments, it was decided to use D_2O/CD_3CN (1:4, respectively). The decision was made primarily because H_2O solvent suppression in the ^{1}H NMR experiments might limit the range of ortho esters which could be analysed, and secondly to enable this work to be more closely correlated with the findings of Deslongchamps *et al*. (2000).

Having already established that specific acid catalysis is more likely to be the dominant mechanism operating in jet fuel/water mixtures (Section 5.2), the complications attending the use of buffered systems (and potential k_3 catalysis by A^-) could be obviated by using mineral acid (*i.e.,* HCl) directly. It was also established previously that k_{obs} is proportional to $[H^+]$ ($k_{obs} = k_{H+}[H^+]$; Figure 21) – that is to say, the observed rate of hydrolysis increases linearly with increasing catalyst concentration. It follows then that in order to correlate k_{obs} between different workers, and indeed across different acyclic and cyclic geminal ethers, some consistency for $[H^+]$ should be established *i.e.,* = 2 x 10^{-4} M. However, in the case of particularly slow hydrolysis reactions *i.e.,* those which take more than 12h to reach completion at this acid concentration, the $[H^+]$ has been increased to ensure completion of the reaction within a reasonable timescale *i.e.,* → 5 x 10^{-4} M. To illustrate the general approach adopted in this work, attention turns to the paired analysis of **22** and **23** (Figure 29).

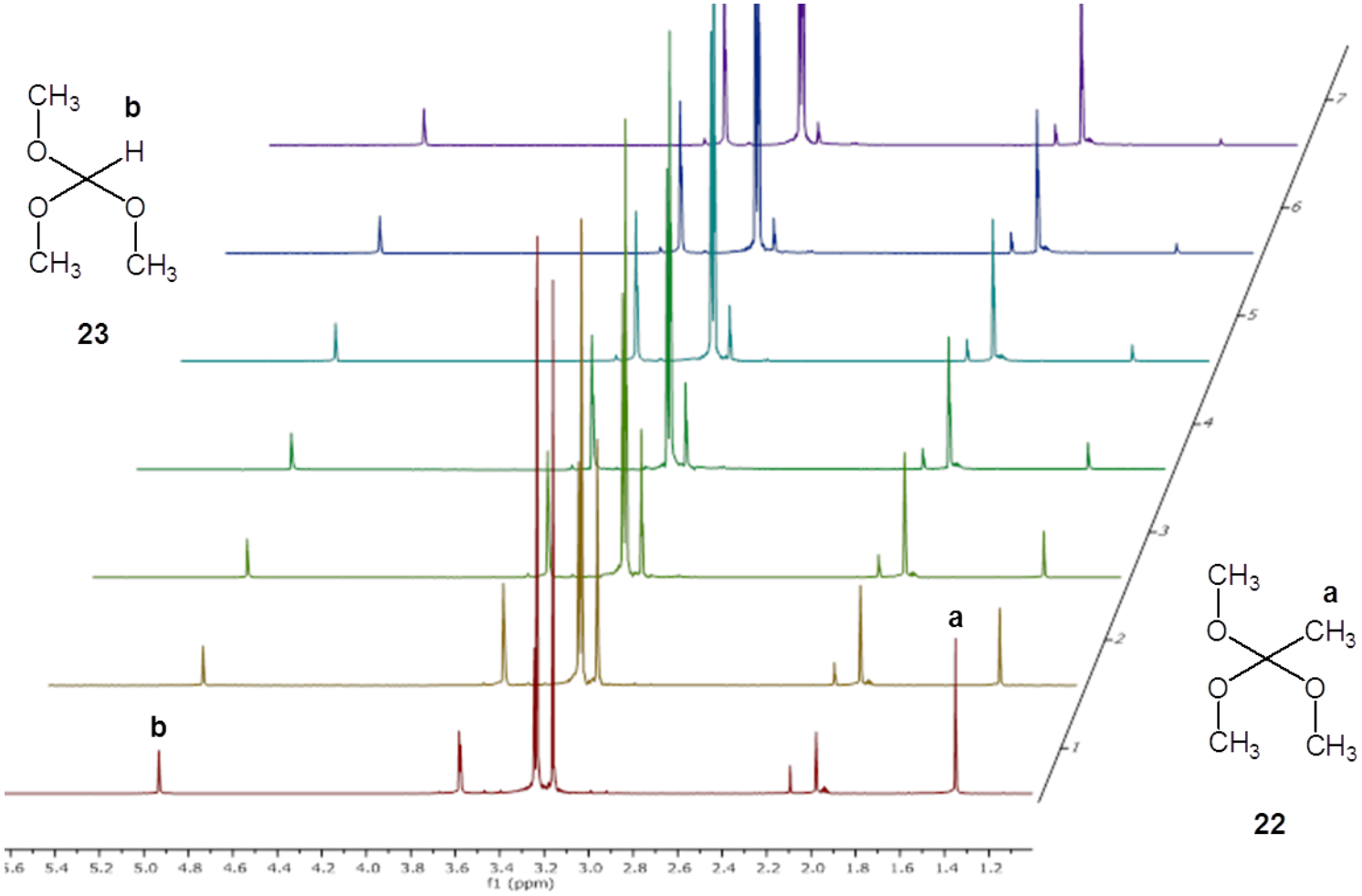

Figure 29. Stacked plot of **22** and **23** (300 MHz ^{1}H NMR in D_2O/CD_3CN (1:4), 625 s intervals, T= 25ºC, [HCl] = 9.56 x 10^{-5} M).

The hydrolysis reaction of **23** is almost imperceptible at $[H^+]$ = 2 x 10^{-4} M, requiring >24h in order to afford detectable amounts of product. For this reason a greater acid concentration of 4.78 x 10^{-4} M was used in order to examine the reaction pair of **23** and **22** on a reasonable timescale. The resonances used for comparison were those associated with methyl $(CH_3O)_3CCH_3$ (1.35ppm) for **22**, and methine $(CH_3O)_3CH$ (4.93ppm) for **23** (Figure 29 a and b, respectively). By plotting the logarithms of concentration for **22** and **23** with respect to time, it was possible to determine k_{obs} for both molecules (Figure 30). Further details can be found in the experimental section (Chapter 10 - Section 10.7).

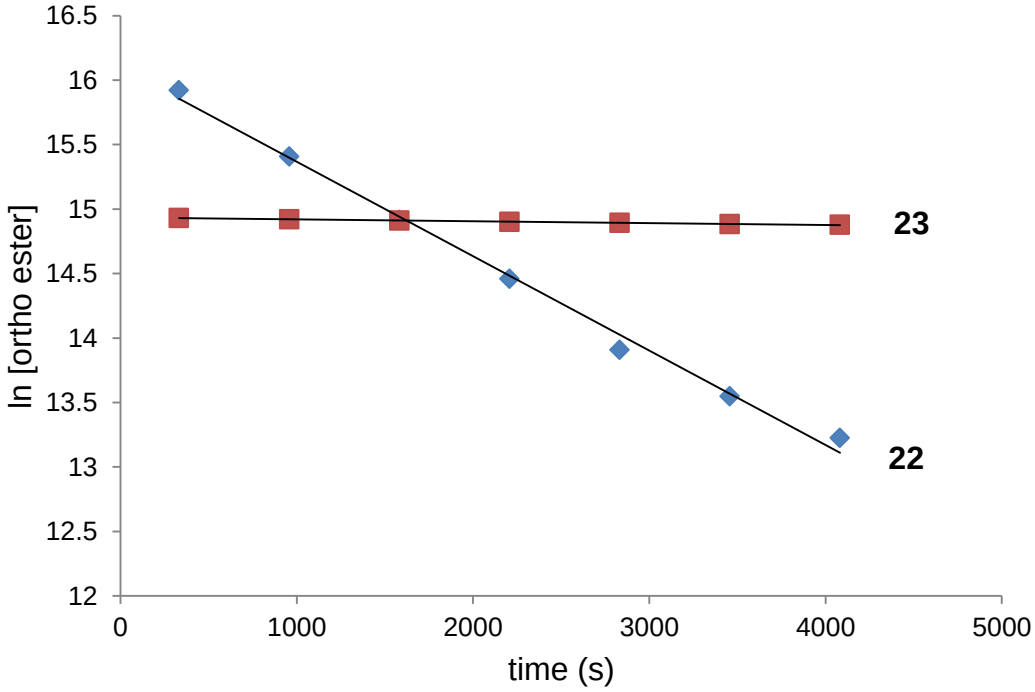

Figure 30. A plot of ln[**22**] (k_{obs} = 7 x 10^{-4}; R^2 = 0.9944), and ln[**23**] (k_{obs} = 1.46 x 10^{-5}; R^2 = 0.9932), *versus* time (s).

The value of k_{obs} for **22** and **23** obtained from the plots presented in Figure 30 may be divided by $[H^+]$ (*i.e.*, 9.56 x 10^{-5} M in the NMR tube after dilution by solvent) to afford k_{H+} = 7.32 $M^{-1}s^{-1}$ and 0.153 $M^{-1}s^{-1}$, respectively. The NMR kinetic experiments were repeated three times in order to afford average values of k_{H+} = 7.09 ± 0.31 $M^{-1}s^{-1}$ for **22**, and 0.15 ± 0.004 $M^{-1}s^{-1}$ for **23** (Section 10.7). Furthermore, in the case of **22** and **23** the experiments

were repeated at $[H^+]$ = 6.38 and 5.31 x 10^{-5} M in order to establish the consistency of k_{H+} thereby verifying our experimental technique (Table 4).

Table 4. Values of k_{obs} and k_{H+} for **22** and **23** at different acid concentrations.

Ortho ester	[HCl] x 10^{-5} M	k_{obs} x 10^{-6} s^{-1}	k_{H+} $M^{-1}s^{-1}$
22	9.56	678	7.09
22	6.38	447	7.01
22	5.31	363	6.84
23	9.56	14.6	0.150
23	6.38	9.4	0.147
23	5.31	7.7	0.145

As anticipated, k_{H+} remains constant throughout the range $[H^+] \approx 5 \rightarrow 10$ x 10^{-5} M, thereby confirming the verity of our experimental technique. Furthermore, it is only necessary to measure k_{obs} for a given value of $[H^+]$ in order to determine k_{H+}. Although the rate of hydrolysis of **1** and **23** were studied at $[H^+]$ = 9.56 x 10^{-5} M, whereas the rate of hydrolysis **22** and **24** were examined at the more dilute acid concentration of 3.96 x 10^{-5} M, one may reliably compare the relative reaction rates by considering k_{H+}. Each experiment was performed three times and the average values are presented in Table 5.

Table 5. Hydroxonium catalytic coefficients (k_{H+}) for **23**, **1**, **22** and **24**.

Ortho ester	k_{H+} $(M^{-1}s^{-1})$
23	0.15 ± 0.006
1	1.69 ± 0.04
22	7.04 ± 0.24
24	20.12 ± 0.93

An eleven-fold acceleration in rate accompanies the replacement of the MeO- with EtO- ether moieties within the orthoformate derivative **23** → **1** (Table 5). In contrast, a relatively modest three-fold acceleration in rate appears to accompany the analogous MeO- to EtO- pair for the corresponding orthoacetates **22** → **24**. This apparently modest acceleration in rate accompanying the replacement of MeO- for the slightly more basic EtO- ether within the orthoacetate series **22** → **24** must be seen in the context of a fifty-fold rate acceleration accompanying the replacement of the H atom of the central carbon atom of an orthoformate with a $–CH_3$ of the corresponding orthoacetate (*i.e.,* **23** → **22**). It appears then, that the inductive effect of R^1 (H → Me) has a greater accelerating influence upon the overall rate of hydrolysis compared to R^2 (Me → Et) (Figure 31). Oxocarbenium ion formation is rate limiting, and so both orthoformate and orthoacetate derived ions will benefit from inductively donating R^2 (Figure 31a), whereas the orthoacetate derived carbocation alone will additionally derive stabilisation from inductively donating R^1 (Figure 31b).

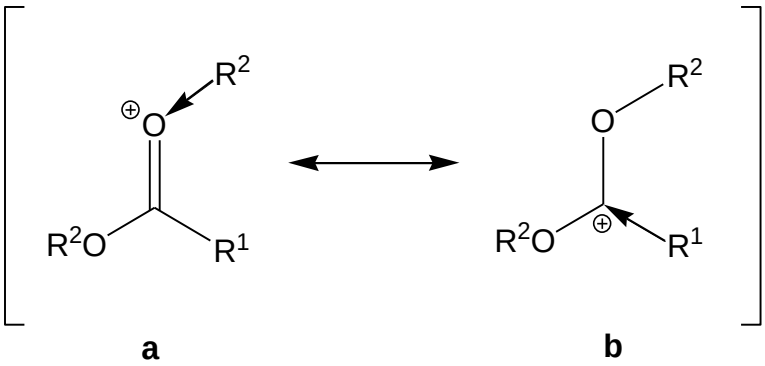

Figure 31. Cations stabilised ostensibly *via* (**a**) R^2 (= Me/Et); or (**b**) R^1 (= H/Me).

In conclusion, it has been established that ortho ester **22** reacts with water approximately four times faster than ortho ester **1**. Furthermore, in the case of acyclic systems, R^1 substituents have a greater role to play in accelerating the rate of hydrolysis (H → Me *ca*. x 50) compared to R^2 (Me → Et x 3-11), with the fastest rate of hydrolysis achieved by **24** (Table 5).

6.3 Cyclic Ortho Esters – Five *versus* Six Membered Rings

The same experimental procedure described in the previous section has been applied here in order to establish the relative rate of hydrolysis for the five- (**25**) and six-membered (**26**) cyclic ortho esters with respect to the acyclic orthoacetate **22** (Figure 32). For ease of ^{1}H NMR analysis, and to maintain structural consistency, acyclic **22** was examined alongside cyclic derivatives possessing an exocyclic methyl ether and a C(2) methyl substituent:

- **22** & **25** acyclic *v*. five-membered ring
- **22** & **26** acyclic *v*. six-membered ring

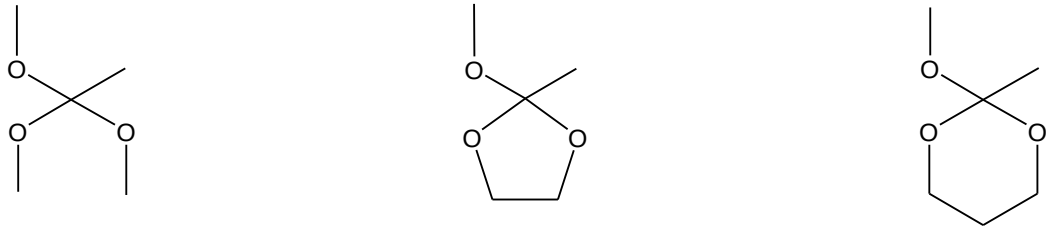

22 **25** **26**

Figure 32. Acyclic and cyclic ortho esters considered for kinetic analysis.

As discussed earlier, cyclic ortho esters undergo an apparent switch in rate limiting step (*i.e.,* $k_1 \leftrightarrow k_3$) within the *p*H range studied here (see Section 5.3). Consequently, it cannot be stated with a high level of certainty whether $k_1 = k_{obs}$ without further exhaustive kinetic studies which are beyond the scope of this present work. However, as "cross-over" of mechanisms takes place under the conditions in which this study is conducted, it is assumed that k_1 and k_3 will be of a similar order of magnitude, and therefore $k_1 \approx k_{obs}$. Compound **22** is commercially available, whereas cyclic ortho esters **25** and **26** required synthesis as part of this study (see Chapter 7 for discussion).

An interesting example of the experimental challenges encountered using NMR spectroscopy, and the means through which those challenges may be overcome may be illustrated by the case of the pair **22** and **25**. In the ^{1}H NMR spectra for these compounds at 300 MHz, the resonances associated with the hydrogen atoms of the non-etherial –C*H*$_3$ substituents for **22** and **25** (*i.e.,* singlets at 1.36 and 1.44ppm, respectively $\Delta\delta$ = 0.08ppm: Figure 33) are difficult to resolve, rendering accurate integration of the signals problematic. In order to achieve sufficient resolution for accurate kinetic analyses, ^{1}H NMR MHz experiments were performed at the much higher field of 500 MHz (singlets **a** and **b** for **22** and **25**, respectively Figure 34). By plotting the logarithms of concentration for **22** and **25** with respect to time, it was again possible to determine k_{obs} for both molecules (Figure 35).

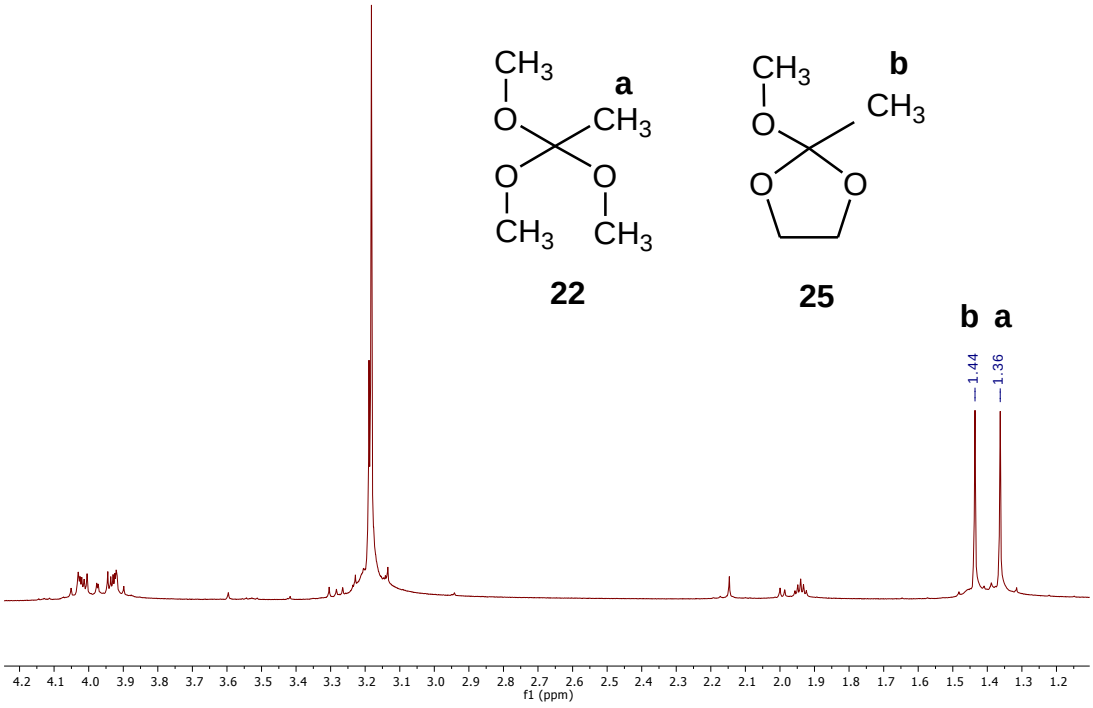

Figure 33. 300 MHz ^{1}H NMR spectrum of **22** (C–C*H*$_3$ = 1.36ppm) and **25** (C–C*H*$_3$ = 1.44ppm).

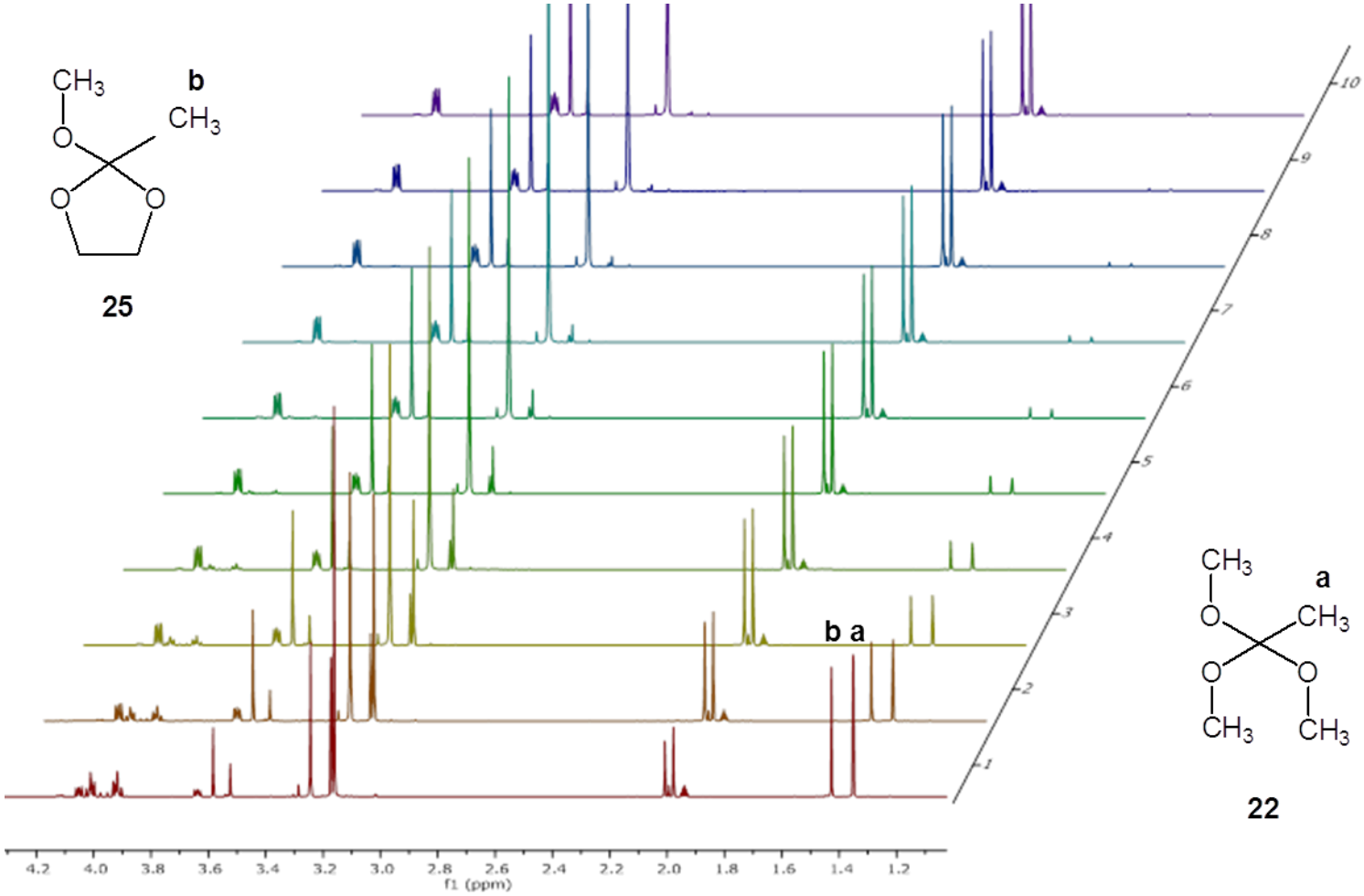

Figure 34. Stacked plot of **22** and **25** (500 MHz ^{1}H NMR in D_2O/CD_3CN=1:4, 1830 s intervals, T= 25ºC, [HCl]=3.96 x 10^{-5} M).

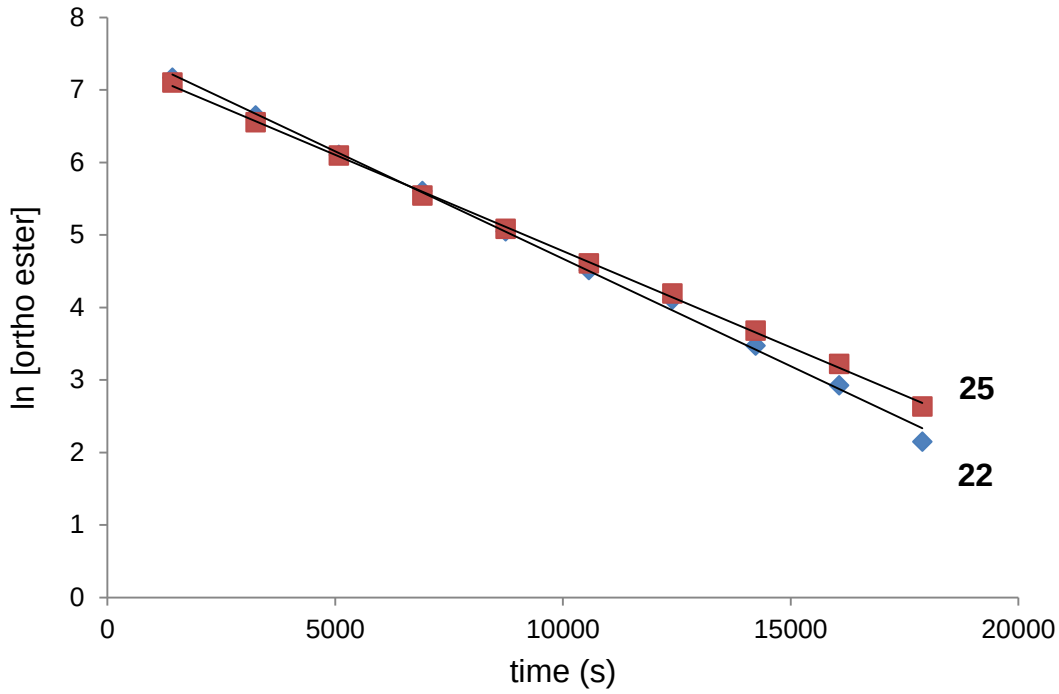

Figure 35. A plot of ln[**22**] (k_{obs} = 2.96 x 10^{-4}; R^2 = 0.9973), and ln[**25**] (k_{obs} = 2.65 x 10^{-4}; R^2 = 0.9992) *versus* time (s).

The values of k_{obs} for **22** and **25** obtained from Figure 35 (*i.e.,* 2.96 and 2.65 x 10^{-4}, respectively) were divided by [H^+] (*i.e.*, 3.96 x 10^{-5} M in the NMR tube after dilution by solvent) to afford k_{H+}. The experiment was repeated three times (see Section 10.7), and the average values are presented in Table 6.

Table 6. Hydroxonium catalytic coefficients for **22**, **25** and **26**.

Ortho ester	k_{H+} ($M^{-1}s^{-1}$)
25	6.53 ± 0.21
22	6.96 ± 0.35
26	9.78 ± 0.22

The five-membered 1,3-dioxolane derivative **25** appears to be hydrolysed by water at a marginally slower rate than the acyclic **22**; both would appear to react at a slower rate than the 6-membered 1,3-dioxane derivative **26**. In order to understand these somewhat unexpected results it is necessary to consider the conformations adopted by these molecules. To this end, the 2014 release of the Cambridge Structural Database was searched for 1,3-dioxolane ortho esters of type **25** (Allen, 2002); only one example has been reported to date, and the X-ray crystal structure (Figure 36 - ZICMED) of 2-phenoxy-2(trifluormethyl)-4,4,5,5-tetraphenyl-1,3-dioxolane (Figure 37a) is presented below (Zieger *et al.*, 1995).

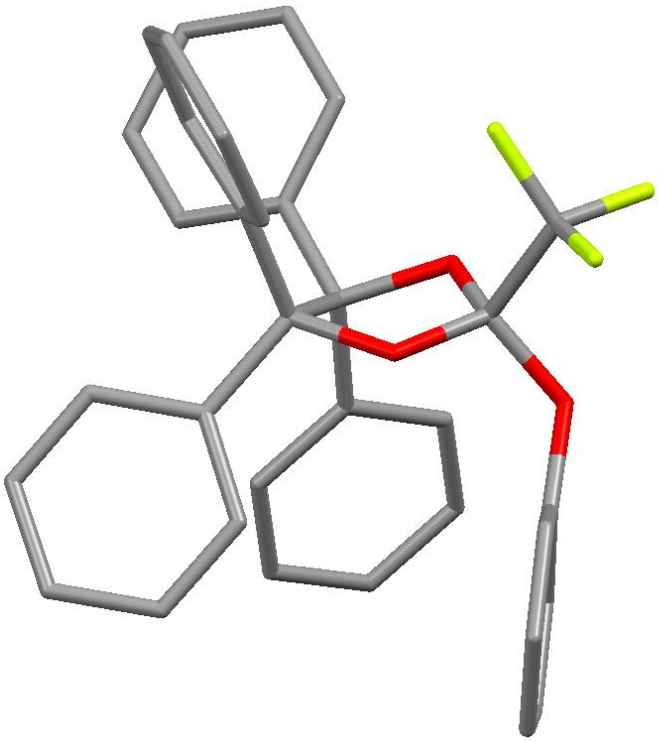

Figure 36. The X-ray crystal structure of 2-phenoxy-2(trifluormethyl)-4,4,5,5-tetraphenyl-1,3-dioxolane (ZICMED), viewed along C(4)—C(5) (Zieger *et al.*, 1995).

The first point to note about the solid-state structure of ZICMED is that the 1,3-dioxolane ring system adopts the half-chair (C_2) conformation. Cyclopentane is found to adopt the isoenergetic half chair or envelop (C_S)

conformations in solution, with a low barrier to the intermediate coplanar arrangement (4.3 kcal mol^{-1}), indicating that both conformational extremes lie within a broad energy well (Saebø *et al.*, 1983). Simple alkyl substituted 1,3-dioxolanes also undergo *facile* $C_2 \leftrightarrow C_S$ interconversion in solution (Willy *et al.*, 1970). Although the conformational preferences of 2-alkoxy-1,3-dioxolanes are relatively unexplored, Altona has noted that the steric characteristics of the exocyclic alkoxy substituent are implicated in the $C_2 \leftrightarrow C_S$ pseudorotation process; sterically demanding C(2)─OR groups appear to destabilise the half-chair C_2 arrangement in favour of the C_S envelope conformer (Altona & van der Veek, 1968). The literature is silent upon both the impact of alkyl substituents upon the $C_2 \leftrightarrow C_S$ pseudorotation of 2-alkoxy-1,3-dioxolanes, and of course upon how this influences the overall rate of hydrolysis. This hitherto neglected area of study is explored in greater detail in Section 6.5.

As can be clearly seen, the C(4/5)—C(*ipso*) bonds of the vicinal phenyl substituents do not adopt a perfectly staggered arrangement. A dihedral angle of 32° is observed for O—C(4)—C(5)—O (Figure 37b), as opposed to the value of 60° for the idealised half chair conformation (Figure 38a). This deformation may be accounted for by strong, non-bonded attractive interactions between vicinal phenyl rings, wherein the electron-deficient edge of one ring engages in a perpendicular T-shaped interaction with the electron rich face of another (Iverson & Martinez, 2012).

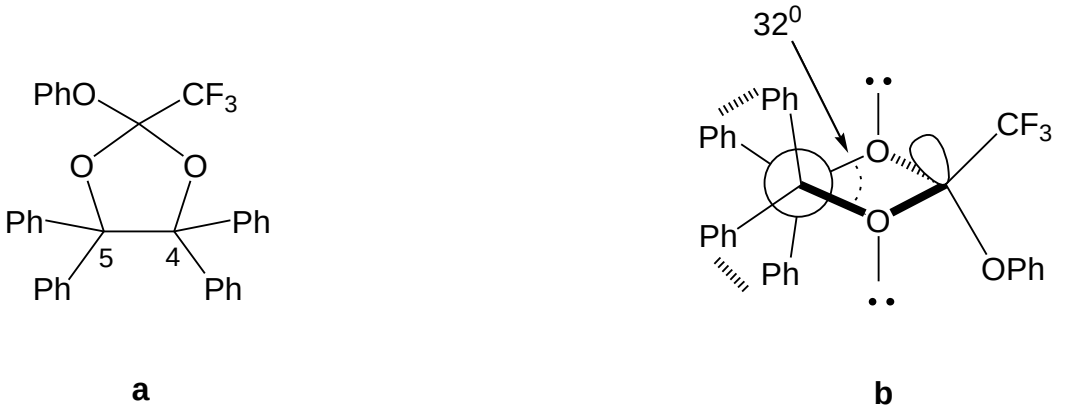

Figure 37. (a) The chemical structure of ZICMED, and (b) a Newman projection of ZICMED, viewed along C(4)—C(5).

In the absence of such intra-molecular π-π interactions which accompany multiple phenyl substituents upon the 1,3-dioxolane fragment, one would ordinarily anticipate that the lowest energy conformation of ortho esters of type **25** would resemble that depicted in Figure 38a. As the O—C(4)—C(5)—O dihedral angle approaches 60°, the pseudo-axial lone pairs of electrons (σ_{nb}) associated with the endocyclic oxygen atoms may adopt either an eclipsed or antiperiplanar orientation with respect to the exocyclic C(2)—OR substituent; it is only the former σ_{nb} which are geometrically disposed to engage in a through-space stabilising (*ca*. 2 kcal mol^{-1} (Grein & Deslongchamps, 1992) interaction with the eclipsing anti-bonding orbital (σ^*) of the leaving group *i.e.,* $\sigma_{nb} \rightarrow \sigma^*$ of C(2)$^{\cdots\cdots}$OR. It is argued then, that the geometrical constraints of the half chair C_2 conformation of 1,3-dioxolane ortho esters such as **25** enable only *one* of two oxygen lone pairs to participate in the developing π-system during elimination of exocyclic OR.

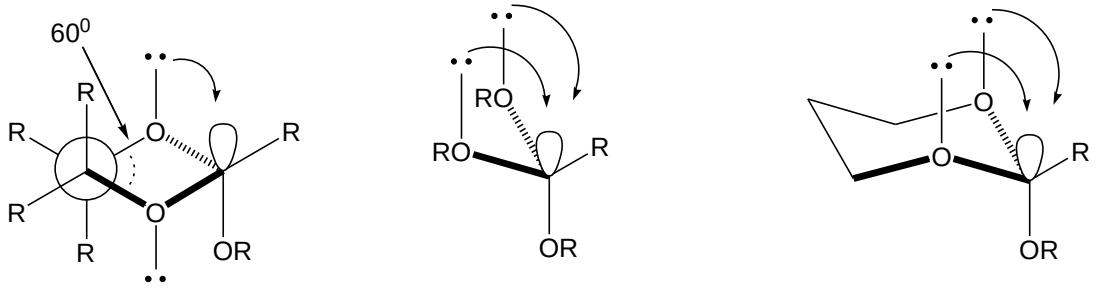

a **b** **c**

Figure 38. Stereoelectronic contributions ($\sigma_{nb} \rightarrow \sigma^*$) to ortho ester hydrolysis. (a) A Newman projection of a 1,3-dioxolane ortho ester of type **25** viewed along C(4)—C(5); (b) acyclic ortho ester of type **22**; (c) 1,3-dioxane ortho esters of type **26**.

The analogous, conformationally mobile acyclic ester **22** may readily orient two lone pairs parallel to the anti-bonding orbital of the antiperiplanar leaving group OR (*i.e.,* 2 x $\sigma_{nb} \rightarrow \sigma^*$; Figure 38b). It is proposed that the modest increase in the observed rate of hydrolysis on going from the 1,3-dioxolane

25 to acyclic **22** (Table 6; $\Delta \approx 7\%$) may be accounted for by the contribution of this double anomeric effect. The same argument applies to the corresponding hemi-ortho ester in stage 3 (*i.e.* **17**, Scheme 8). Finally, attention turns to the 36% increase in the rate of hydrolysis for 1,3-dioxane **26** with respect to acyclic **22** (Table 6). By constraining two oxygen atoms within an energetically favourable six-membered ring, two endocyclic lone pairs are now conformationally constrained to adopt an antiperiplanar arrangement with respect to the exocyclic leaving group OR (Deslongchamps *et al.*, 2000). Here, two oxygen σ_{nb} are geometrically constrained to participate in stabilising double anomeric $\sigma_{nb} \rightarrow \sigma^*$ interaction during elimination of exocyclic OR.

In conclusion, the relative rates of hydrolysis for analogous acyclic and cyclic ortho esters are of a similar magnitude *i.e.,* $k_{H+} \approx$ 6-10 M^{-1} s^{-1}; modest differences in the relative rates of hydrolysis can be accounted for using stereoelectronic arguments.

6.4 Six Membered Cyclic Ketals and Ortho Esters

Having carefully considered the differences between the hydrolysis rates of five and six-membered cyclic ortho esters, attention turns to a more detailed discussion of the case of six-membered geminal ethers. It was proposed earlier in Section 4.2 that *endo* and *exo/endo*-cyclic ketals presented themselves as promising candidates as FDII (*i.e.,* **27** and **28**, respectively Figure 39). Furthermore, *endo*- and *exo*-cyclic ortho esters were identified as promising FDII candidates (*i.e.,* **26** and **29**, respectively Figure 39). The hydroxonium catalytic coefficient for the *endo*-cyclic ortho ester **26** has been evaluated (Section 6.3, Table 6), and a rational proposed for the relative rate of reaction with respect to the analogous five-membered ring system **25**.

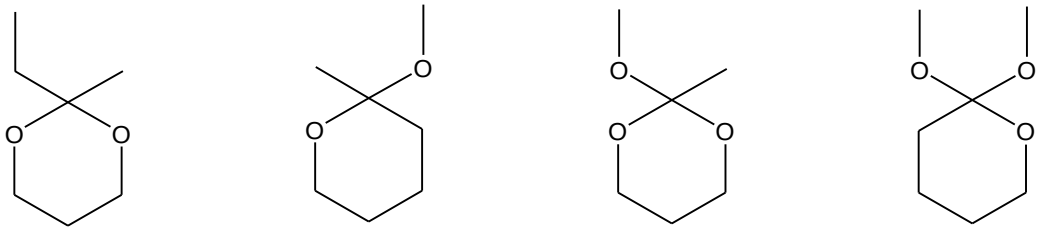

27 **28** **26** **29**

Figure 39. Six-membered geminal ethers as FDII candidates.

Fortunately, the relative rates of hydrolysis for **26**-**29** have been evaluated previously by Deslongchamps *et al.* (2000) under conditions similar to those considered here. Unfortunately, these workers do not report k_{H+} for **26**-**29**, merely citing instead unitless relative values (presented in Table 7) without offering a full explanation for their findings. Since an absolute numerical value of k_{H+} for **26** has been established, it becomes possible to calibrate and thereby estimate values of k_{H+} for **27**-**29** (Table 7). The importance of carrying-out this calibration will become clearer later, as progress is made towards assembling a library of candidate FDII, which are unambiguously ordered according to their hydroxonium catalytic coefficients.

Table 7. The relative rates of hydrolysis for **27**-**29** as reported by Deslongchamps *et al*. (2000)[a], and the estimated values[b] for k_{H+} calibrated against **26**, as determined in this study[c] (Table 6).

Ortho ester	Relative Rate[a]	k_{H+} ($M^{-1}s^{-1}$)
27	1	4.3×10^{-3} [b]
28	649	2.79[b]
26	2270	9.78[c]
29	11351	48.90[b]

It is clear to see that the *exo*-cyclic ortho ester **29** is the fastest reacting geminal ether of this series, and perhaps surprisingly, it hydrolyses at five times the rate of the constitutionally isomeric *endo*-cyclic ortho ester **26**. Despite the absence of an inductively accelerating oxygen atom, the *endo*/*exo*-cyclic ketal **28** hydrolyses at approximately 30% of the rate observed for **26**. Finally, the incorporation of both oxygen atoms of **28** within the ring affords *endo*-cyclic ketal **27**; this apparently minor change in molecular constitution is attended by a dramatic reduction (>99%) in rate. Given that the pairs **26**/**29** and **27**/**28** are constitutional isomers, one would not expect to explain the observed rate differences on the basis of inductive effects. Indeed, it is surprising to note that although **28** and **26** differ in the number of electronegative oxygen atoms, their rates of hydrolysis are of the same order of magnitude. In order to rationalise these relative rates, explanations are proposed based upon the equilibrium populations of conformers possessing favourable anomeric stabilisation.

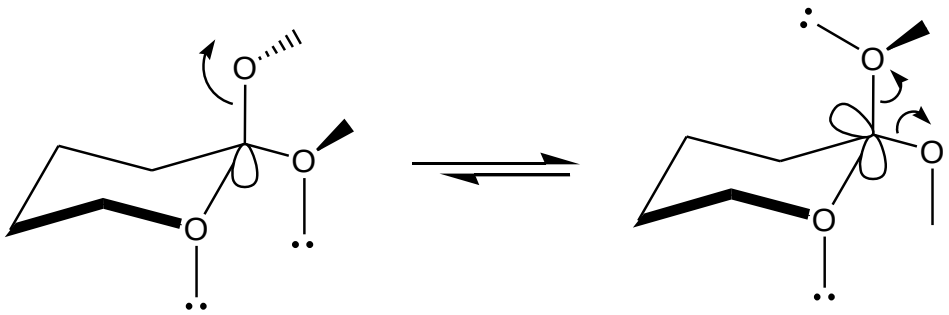

a (38%) **29** **b** (54%)

Figure 40. Equilibrium distributions of **29** in which (**a**) the axial alkoxy substituent is attended by 2 x $\sigma_{nb} \rightarrow \sigma^*$ stabilising interactions, and (**b**) both axial and equatorial alkoxy substituent are attended by a single $\sigma_{nb} \rightarrow \sigma^*$ stabilising interaction (Deslongchamps *et al.*, 2000).

All stable conformations of the *exo*-cyclic ortho ester **29** possess both an axial and equatorial MeO group; conformational equilibria exist only by virtue of the relative orientations of methyl ether groups (Figure 40).

Deslongchamps has calculated that the lowest energy conformation **29b** is present in 54%. As a consequence of the orientation of the methyl groups in **29b**, both axial and equatorial methoxy groups may adopt an energetically favourable antiperiplanar relationship with σ_{nb} of *endo*- and *exo*-cyclic oxygen atoms, respectively. In the case of conformer **29a**, which is calculated to be 0.2 kcal/mol higher in energy than **29b**, the axial methoxy group adopts an antiperiplanar relationship with the σ_{nb} of *both endo*- and *exo*-cyclic oxygen atoms. *In conclusion*, all orientations of both low energy conformers of **29** may benefit from acceleration in the rate of hydrolysis because of favourable stereoelectronic effects.

Without recourse to extensive variable temperature NMR experiments – which are beyond the scope of this current study – it is difficult to propose with any degree of certainty the equilibrium distribution of axial and equatorial conformers of **26** (Figure 41). However, using glucose derivatives as a guide to equilibrium distributions, it is reasonable to propose that the axial anomer will constitute the major conformer in solution (Kirby, 1996). With that said, the axial methoxy group may adopt an energetically favourable antiperiplanar relationship with σ_{nb} associated with both of the *endo*-cyclic oxygen atoms, thereby affording a stereoelectronic acceleration for hydrolysis. The absence of similar orbital overlaps, involving the oxygen σ_{nb} of the ring and the σ^* of an equatorially oriented MeO- group, will have an impact upon the overall rate of hydrolysis. Deslongchamps asserts that for ortho esters under acidic conditions, protonation of the most basic alkoxy group affords a conformationally constrained system unable to equilibrate as all oxygen atoms, and also the central carbon atom must be considered sp^2 hybridised (Deslongchamps *et al.*, 2000). The implication being that once subjected to acid, the overall rate of hydrolysis for **26** will reflect the equilibrium concentrations of axial and equatorial conformers in solution, thereby explaining the relative deceleration in the rate of hydrolysis of *endo*-**26** with respect to *exo*-**29**.

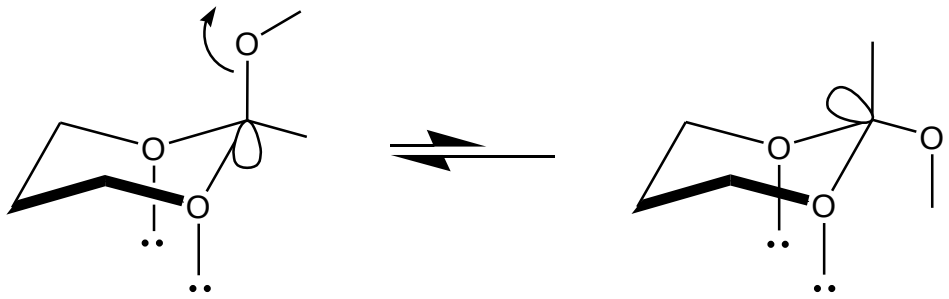

axial **26** equatorial

Figure 41. Proposed equilibrium distributions of **26** wherein the axial alkoxy substituent is attended by a double anomeric effect (*i.e.,* 2 x $\sigma_{nb} \rightarrow \sigma^*$), whereas the equatorial alkoxy substituent is devoid of such stabilising interactions.

One might anticipate that reducing the number of inductively donating oxygen atoms within the ortho ester **26** would lead to a dramatic rate deceleration. However, the importance of stereoelectronic acceleration upon the rate of hydrolysis would appear to be highlighted in the case of **26** → **28**. The stereoelectronic acceleration accompanying the donation of a single electron pair of one *endo*-cyclic oxygen atom in the axial conformer of **28** would appear to counteract the loss of an inductively donating oxygen atom.

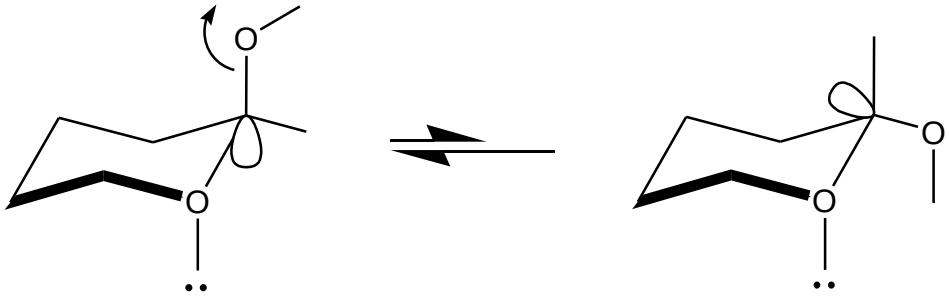

axial **28** equatorial

Figure 42. Proposed equilibrium distributions of **28** wherein the axial alkoxy substituent is attended by 1 x $\sigma_{nb} \rightarrow \sigma^*$ stabilising interactions, whereas the equatorial alkoxy substituent is devoid of such stabilising interactions.

Similar arguments, involving endocyclic $\sigma_{nb} \rightarrow \sigma^*$ stabilising interactions, may not be invoked for the constitutional isomer of *exo*/*endo*-ketal **26**, namely **27**, because by definition it does not possess an *exo*-cyclic alkoxy leaving group. An alternative factor is proposed in order to account for an overall 649 fold deceleration in the rate of hydrolysis of **27** with respect to **28**. Protonation of **27** will afford, after ring cleavage a cation (Figure 43a → b). Unlike other geminal ethers considered in this section, the leaving group is covalently tethered to the cationic species and so for entropic reasons, **27b** is more likely to undergo rapid 6-endo-trig cyclisation to reform cyclic **27a** (Baldwin, 1976). Because of the significant contribution of the cyclisation of **27b**, it is argued that the overall rate of hydrolysis of **27** appears to be relatively slow. If this analysis is correct, then Baldwin's rules also infer that ketals derived from 1,3-dioxolanes would undergo hydrolysis at a faster rate than their analogous 1,3-dioxanes, because the corresponding 5-endo-trig cyclisation is disfavoured.

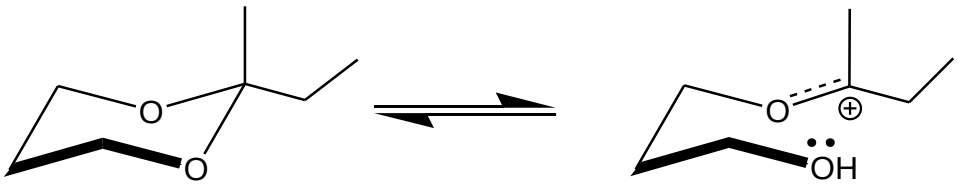

a **27** **b**

Figure 43. The acid catalysed cleavage, and re-cyclisation of **27**.

In conclusion, the work of Deslongchamps *et al.,* (2000) has been calibrated in order to estimate the relative rates of hydrolysis for a range of six-membered geminal ethers for inclusion in a library of candidate FDII. Furthermore, the role of stereoelectronic factors in the acceleration of hydrolysis reactions in six-membered rings has been extended, thereby developing the ability to optimise FDII performance.

6.5 Five Membered Cyclic Ortho Esters

Attention now returns to earlier discussions (Section 6.3) upon the impact of C(2) alkyl substituents upon the $C_2 \leftrightarrow C_S$ pseudorotation of 2-alkoxy-1,3-dioxolanes, and the concomitant influence upon the overall rates of hydrolysis. Once again, it is noted that although there has been activity elsewhere (McClelland *et al.*, 1988), the data has been gathered in a manner which renders quantitative comparison with this work difficult. A fuller account of the approach adopted in this study to calibrate the work of others is more appropriately presented in Section 6.5.2. The following discussion however, describes our findings upon the manner through which α-branching of C(2) alkyl substituents impacts upon the rate of hydrolysis of 2-methoxy-1,3-dioxolanes, and illustrates how transannular interactions may be exploited in order accelerate the hydrolysis reactions of FDII.

6.5.1 Exploiting α-strain *via* trans annular interactions – exploring vicinal substitution at C(4/5).

Attention now returns to the X-ray crystal structure of DOXYLP, which is the 1,3-dioxolan-2-ylium cation derived from 2-methoxy-2-methyl-1,3-dioxolane **25** (Figure 24). It is clear to see that the elimination of MeO- from **25** results in a change in hybridisation of O(1/3) and C(2) ($sp^3 \rightarrow sp^2$) to afford a planar cation (Figure 24). This change in ring geometry is expected to result in the relief of transannular strain in the starting material. The corresponding Newman projection of **25** - viewed along the H→Cα bond - is presented in Figure 44. It is reasonable to assume that replacing the H atoms upon Cα with sterically demanding Me groups (*i.e.,* **30**; Figure 44 viewed along Me→Cα) would increase transannular strain, leading to a dramatic acceleration in the rate of hydrolysis. However, a modest 20% rate acceleration for 2-methoxy-2-*tert*-butyl-1,3-dioxolane **30** is *estimated* (see Section 6.5.2; Table 9) compared to the experimentally determined value of k_{H+} for **25** reported in this work (Table 6). Indeed, McClelland *et al*. (1988) notes equally modest rate accelerations throughout a range of 2-methoxy-

1,3-dioxolanes possessing α-branched C(2) substituents, which leads to the conclusion that the transannular strain within these systems appears to be relatively ineffective. It seemed logical then to take the approach of increasing transannular strain by introducing sterically demanding substituents at C(4/5) (*i.e.,* **31-33**; Figure 44). In Section 5.3, X-ray crystallographic analyses were described which inferred that C(4/5) alkyl substituents upon the 1,3-dioxolan-2-ylium cation may support a separation of charge within the corresponding O(1/3)—C(4/5) bonds (Figure 25). It is anticipated that by inserting Me substituents upon C(4/5) of the 1,3-dioxolane core, one may probe the interplay of transannular steric demand upon Cα, and stereoelectronic effects upon the rate of hydrolysis, thereby accessing a novel range of FDII candidates.

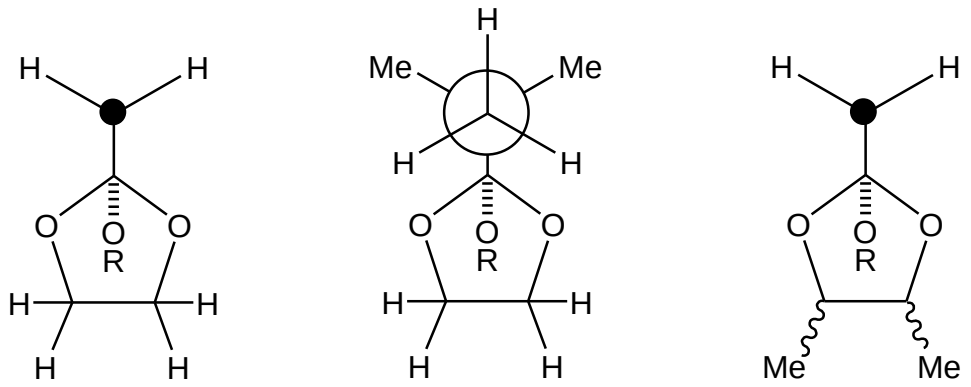

Figure 44. Newman projections of ortho ester 1,3-dioxolanes (where R = Me) viewed along the H→Cα (**25** and **31-33**) or Me→Cα (**30**) bonds, illustrating 1,3-transannular strain through substitution at either Cα (**30**) (*i.e.*, ^{t}Bu) or C(4/5) (**31-33**).

Alkyl substitution at positions C(4/5) introduces asymmetry into the 1,3-dioxolane core with the attendant challenges of preparing and separating stereoisomers (see Section 7.2). The synthesis of *trans* 2-methoxy-2,4,5-trimethyl-1,3-dioxolane **31** has been reported previously (van Maarseveen *et al.*, 2011). However, the *cis* 1,3-dioxolane derivatives **32**-**33** – which are epimeric at C(2) – are novel. Although preliminary studies towards the

stereoselective synthesis of *trans* **31** and *cis* **32**/**33** have been made as part of this study (Chapter 7), direct routes towards **32** and **33** are beyond the scope of this current study. Indeed, before investing in a synthetic challenge, it was considered wise to firstly determine the kinetic profile of these ortho esters as a mixture.

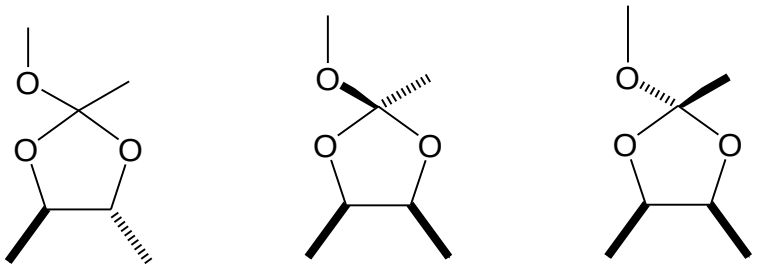

31 **32** **33**

Figure 45. The *trans* 2-methoxy-2,4,5-trimethyl-1,3-dioxolane **31**, and the epimeric *cis* 1,3-dioxolanes derivatives, with either C(2)─Me *anti* (**32**) or *syn* (**33**) to *Me*─C(4)─C(5)─*Me*.

It was demonstrated earlier that ^{1}H NMR spectroscopy is an effective and versatile tool for extracting kinetic data from complex mixtures of reactants. The preparation of **31-33** as a constitutionally homogeneous mixture of diastereoisomers is reported in some detail in Chapter 7. ^{1}H NMR spectroscopy has been used to unambiguously assign all three diastereoisomers **31-33** in solution. Valuable insights into the preferred conformations of **31-33** are arrived at using 1D NOESY spectroscopy, and finally a kinetic study of the acid catalysed hydrolysis reactions is presented.

The 500 MHz ^{1}H NMR spectrum (CD_3CN) of an analytically pure mixture of diastereoisomers **31**, **32** and **33**, in the ratio 3:1:3.2, respectively, is presented in Figure 46. The resonances associated the hydrogen atoms of (**a**) O─CH_3; (**b**) C(2)─CH_3; (**c**) C(4/5)─*H*, and (**d**) C(4/5)─CH_3 have been annotated within the spectrum. The C(4/5)–CH_3 and C(4/5)–*H* nuclei within *trans* **31** may not only be distinguished from each other, but they may be distinguished from the analogous nuclei within **32** and **33**.

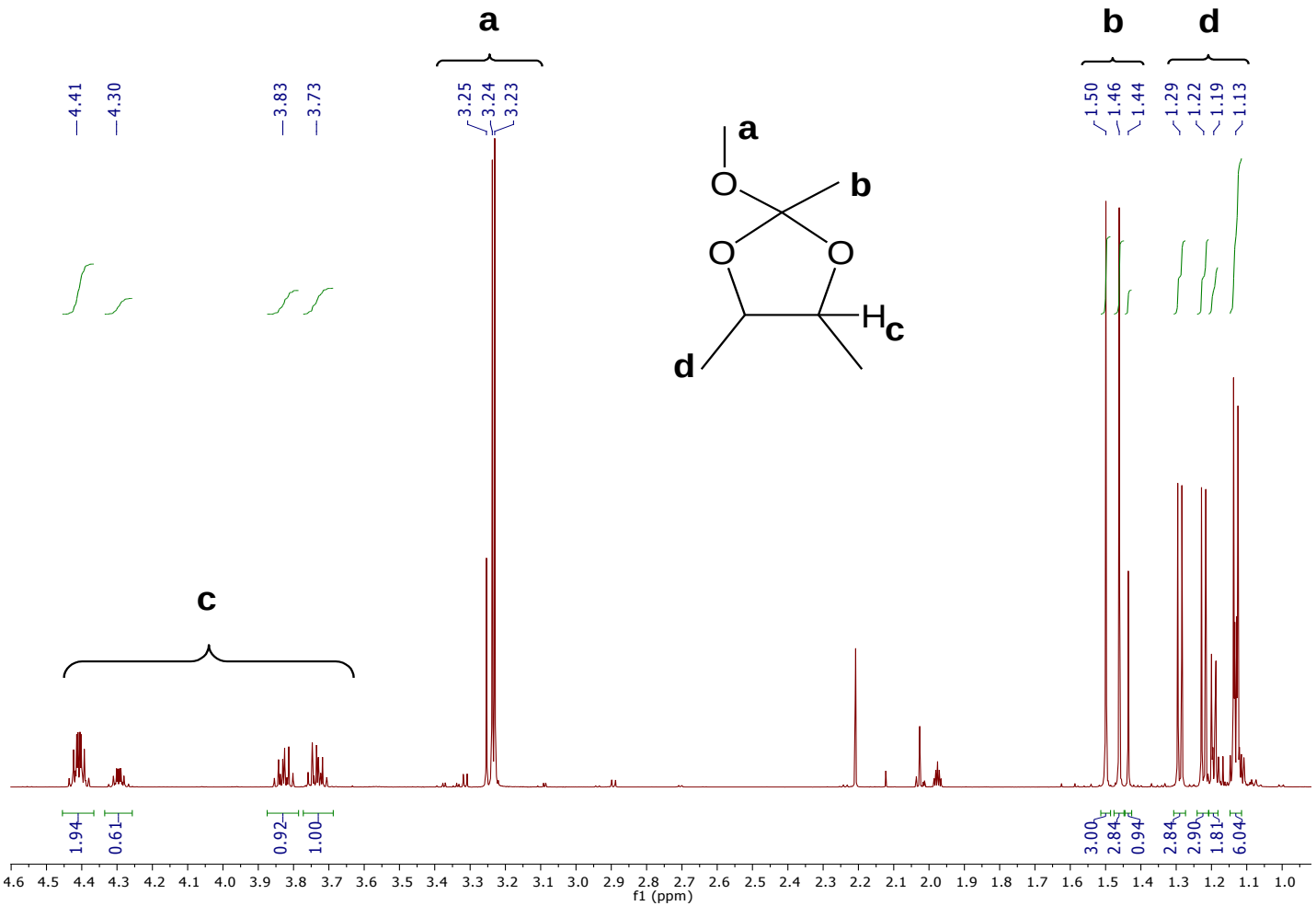

Figure 46. 500 MHz ^{1}H NMR spectrum of **31-33** in CD_3CN.

In this way it was possible to assign methyl C(4/5)–CH_3 [δ_{Me} = 1.22 and 1.29ppm (d, 3H, *J* 6.0Hz)], and methine C(4/5)–*H* [δ_H = 3.73 and 3.83ppm (m, 1H)] nuclei for **31**.

A pictorial representation of the calculated lowest energy conformation of **31**, along with the corresponding 500 MHz 1D-NOESY ^{1}H NMR spectrum is presented in Figure 47. Irradiation of the ^{1}H NMR singlet associated with the C(2)—CH_3 nuclei of **31** (at 1.46ppm) afforded a strong nuclear Overhauser enhancement (nOe) of the multiplet at 3.73ppm, and the singlet at 3.24ppm, which are consistent with the *syn* C(4/5)—*H*, and the geminal C(2)—OCH_3 nuclei, respectively (Figure 47). The observed nOe's support the calculations which imply that **31** adopts the half-chair conformation as shown in Figure 47, in which the C(2)—OCH_3 substituent may adopt the stereoelectronically favoured axial orientation.

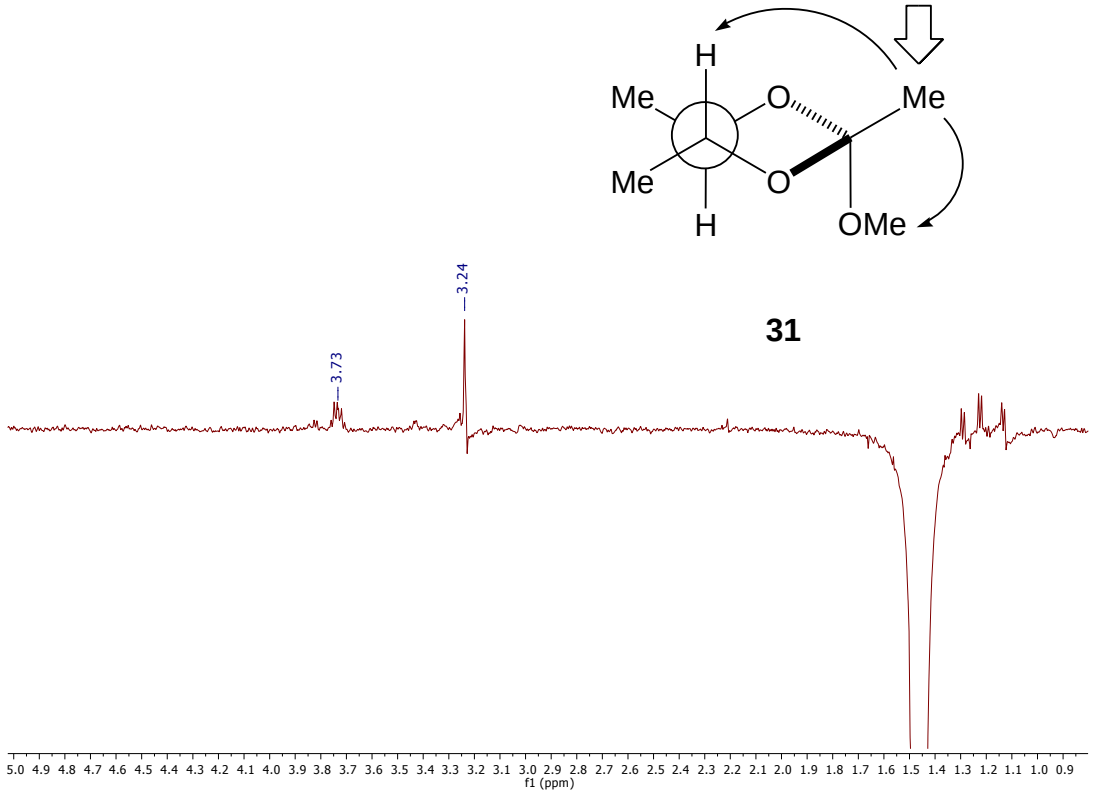

Figure 47. 1D-NOESY ^{1}H NMR spectrum of **31**, **32** and **33** (3:1:3.2, respectively) irradiated at 1.46ppm.

A pictorial representation of the calculated lowest energy conformation of **32**, along with the corresponding 500 MHz 1D-NOESY ^{1}H NMR spectrum is presented in Figure 48. Irradiation of the ^{1}H NMR singlet associated with the C(2)—CH_3 nuclei of **32** (1.44ppm) afforded a strong nOe of the multiplet at 4.30ppm, and the singlet at 3.25ppm, which have been attributed to the transannular C(4/5)—*H* and geminal C(2)—OCH_3 nuclei, respectively. The observed nOe's are once again consistent with the half chair conformation of **32** as presented in Figure 48, in which the C(2)—OCH_3 substituent may adopt the energetically favoured axial position.

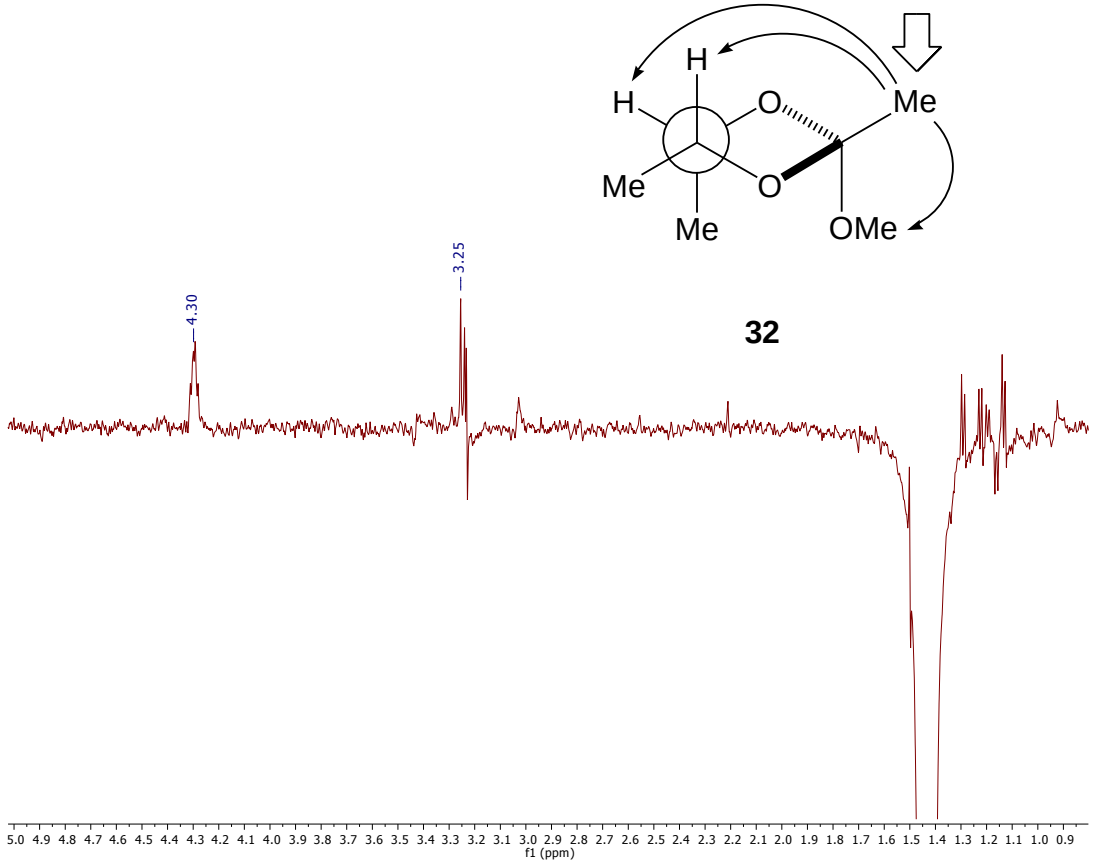

Figure 48. 1D-NOESY ^{1}H NMR spectrum of **31**, **32** and **33** (3:1:3.2, respectively) irradiated at 1.44ppm.

Finally, the 500 MHz 1D-NOESY ^{1}H NMR spectrum, along with the pictorial representation of the calculated lowest energy conformation of **33**, is presented in Figure 49. Irradiation of the singlet associated with the C(2)—CH_3 nuclei of **33** (1.50ppm) afforded a strong nOe of the singlet at 3.23ppm, and the doublet at 1.13ppm which have been attributed to the geminal C(2)—OCH_3 and the transannular C(4/5)—CH_3 nuclei, respectively. Again, the observed nOe's measured in solution are gratifyingly consistent with the conformation of **33** as presented, wherein the C(2)—OCH_3 substituent adopts the stereoelectronically favourable axial position.

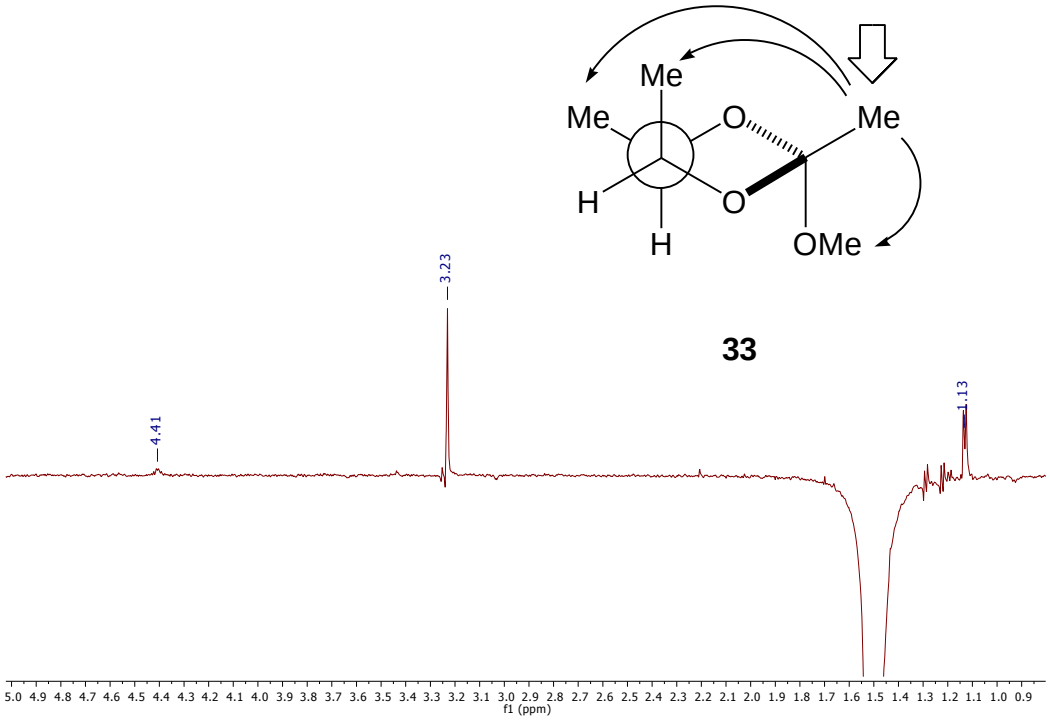

Figure 49. 1D-NOESY ^{1}H NMR spectrum of **31**, **32** and **33** (3:1:3.2, respectively) irradiated at 1.50ppm.

In conclusion, ^{1}H NMR spectroscopy has been used to unambiguously assign all resonances in the mixture of diastereoisomers **31-33**. Furthermore, 1D-NOESY experiments are consistent with calculations suggesting that 2-methoxy-2,4,5-trimethyl-1,3-dioxolanes adopt a half-chair conformation in solution wherein the C(2) methoxy moiety may be oriented in the axial position. Having unambiguously assigned the ^{1}H NMR spectra for **31-33**, and identifying clearly resolved resonances for each molecule [*i.e.,* C(2)-C*H*$_3$], it is now possible to proceed with our kinetic investigations of the acid catalysed hydrolysis of these ortho esters.

Kinetic experiments were performed with **31-33** alone, and with the acyclic ortho ester **22** added to the mixture; a stacked plot of the latter ^{1}H NMR kinetic experiment is presented in Figure 50. Here, the acid catalyst concentration was 3.96 x 10^{-5} M in the NMR tube after dilution by the solvent. In a manner similar to that discussed earlier, plotting the logarithms of concentration for **31-33** and **22** over time (Figure 51), afforded values of k_{obs} and thereafter k_{H+}. The kinetic experiment for **31-33** alone was performed twice, and the experiment involving **31-33** and **22** was repeated three times (see Section 10.7); the average values for k_{H+} are presented in Table 8 along with the value of **25** for reference (see Table 6).

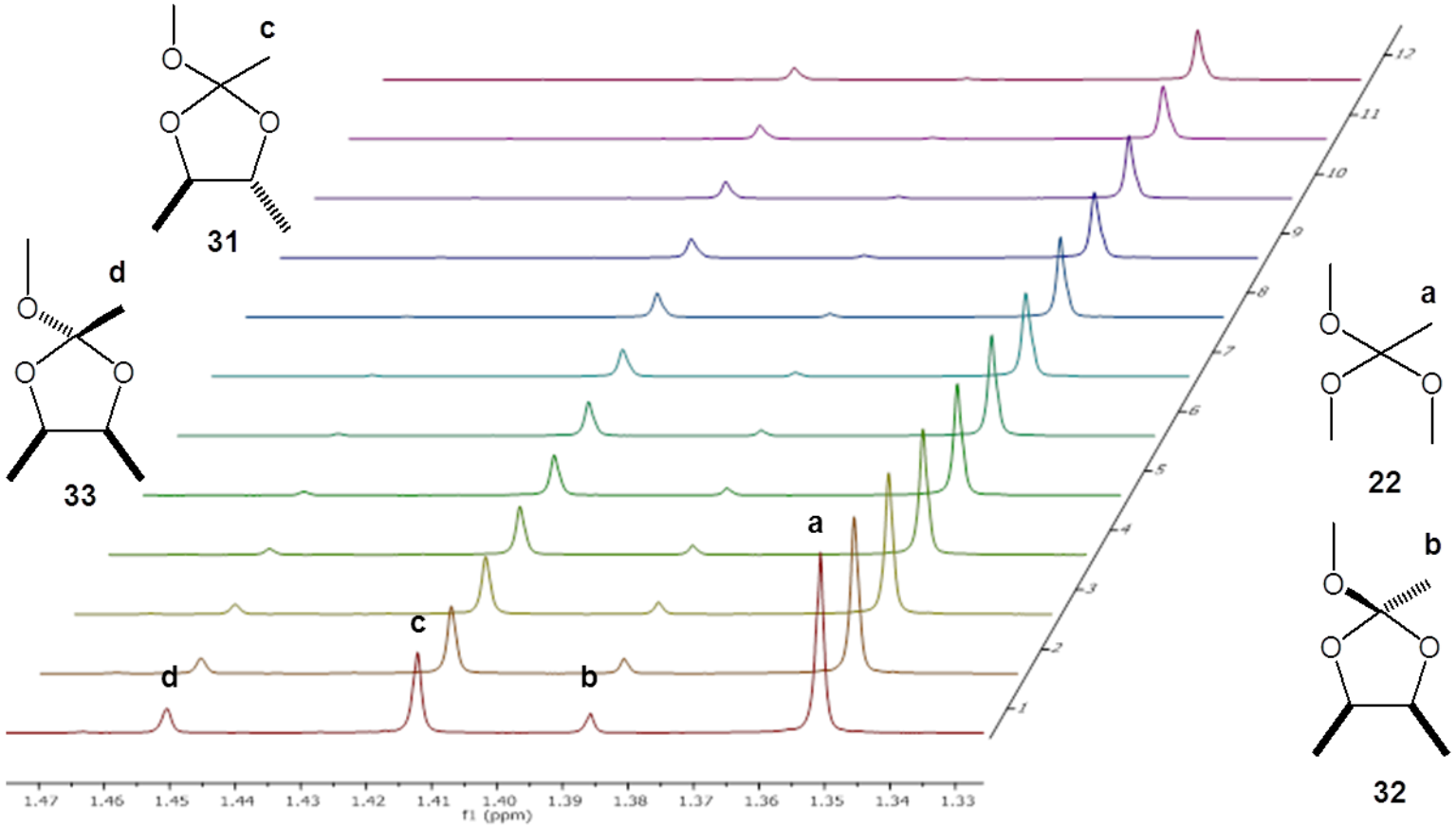

Figure 50. Stacked plot of **22** and **31-33** (500 MHz ^{1}H NMR in D_2O/CD_3CN=1:4, 305 s intervals, T= 25ºC, [HCl]=3.96 x 10^{-5} M).

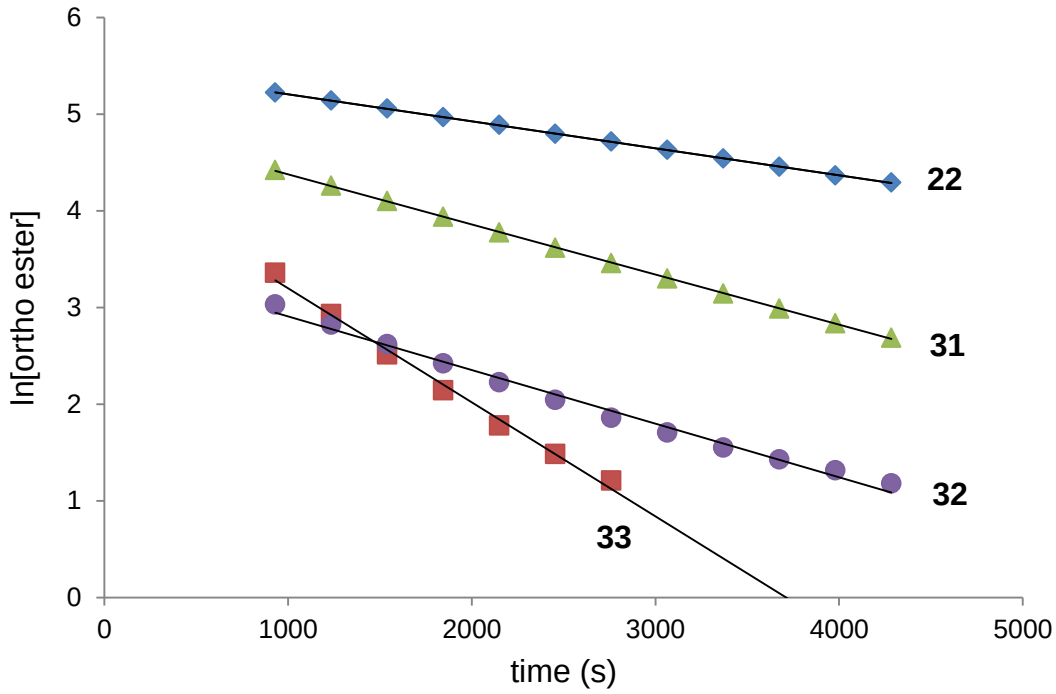

Figure 51. A plot of ln[**22**] (k_{obs} = 2.8 x 10^{-4}; R^2 = 0.9999), ln[**31**] (k_{obs} = 5.19 x 10^{-4}; R^2 = 0.9998), ln[**32**] (k_{obs} = 5.54 x 10^{-4}; R^2 = 0.991), and ln[**33**] (k_{obs} = 1.18 x 10^{-4}; R^2 = 0.9936) *versus* time (s).

Table 8. Values of k_{H+} for **22**, **25** and **31-33**.

Ortho ester	k_{H+} ($M^{-1}s^{-1}$)
25	6.53 ± 0.21
22	6.99 ± 0.09
31	12.08 ± 0.90
32	12.95 ± 0.97
33	27.93 ± 1.66

Earlier stereoelectronic arguments used to rationalise the marginal increase in the rate of hydrolysis of **25** → **22** will not be repeated here (see Section 6.3). It is useful to note here the approximately two-fold acceleration in rate of both **31** and **32** with respect to unsubstituted **25**. The predicted lowest energy conformers of both possess relatively unchallenging axial C(4/5)─H⋯⋯Me─C(2) transannular repulsive interactions. The conformation of **32** alone possesses a sterically demanding axial C(4/5)─Me moiety, and the relief of this strain appears to contribute to the marginally faster (10%) rate of hydrolysis. Overall then, a two-fold rate acceleration can be attributed to the inductively stabilising effect of C(4/5) alkyl substituents, as postulated earlier in Section 5.3. Finally, only one diastereoisomeric 2-methoxy-2,4,5-trimethyl-1,3-dioxolane, namely **33**, is predicted to adopt a low energy conformation wherein the C(2) methyl moiety presents a challenging C(4/5)─Me⋯⋯Me─C(2) transannular repulsive interaction (Figure 49). Assuming that a two-fold rate acceleration accompanies an inductively donating C(4/5) alkyl substituent, an additional two fold increase may be attributed to the relief of this 1,3-transannular repulsive interaction, thereby affording the overall observed value of $k_{H+} \approx 28\ M^{-1}\ s^{-1}$.

In conclusion, NMR spectroscopy, computer assisted conformational analyses, and kinetic studies suggest that for 2-alkoxy-2-alkyl-1,3-dioxolanes substituted at C(4/5), additive rate accelerations appears to derive from both the inductive effect, and the relief of 1,3-transannular repulsion. In the following section the effects of transannular steric demands upon substituents at the β position will be probed in some detail.

6.5.2 Exploiting β-strain - substitution at C(2).

Attention now turns to the effect upon the rates of hydrolysis attending the progressively sterically demanding substitution of the Cβ of 2-alkyl-2-alkoxy-1,3-dioxolanes **34** → **36**, as presented in Figure 52.

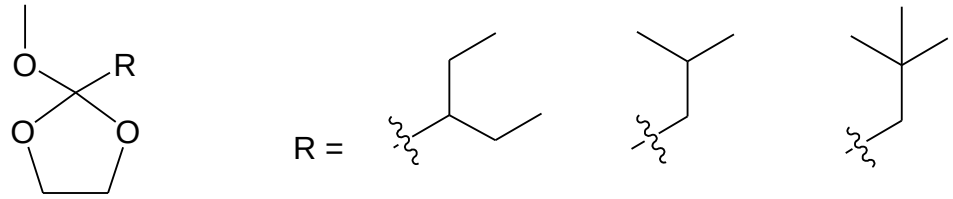

34 **35** **36**

Figure 52. Steric crowding at Cβ of 2-alkyl substituted 2-alkoxy-1,3-dioxolanes **34-36**.

McClelland *et al*. reported a spectrophotometric approach to obtain the catalytic coefficients k_{H+} for **25**, **30** (see Section 6.5.1), and **34-36**, by monitoring the appearance of the hydrolysis product for each molecule in phosphate buffer throughout the *p*H range 6-7, using an ionic strength of 0.1 M (1988). At this *p*H, McClelland assumes that the observed k_{H+} is equivalent to the rate limiting k_1 stage (*i.e.,* Figure 26). This work was performed in pure water, and the ionic strength of the solution was kept constant to correct for the use of buffer. Although it is anticipated that k_{H+} measured under these conditions will be effected by rate accelerating factors such as solvent and ionic strength, it will be assumed that the relative rates reported by McClelland *et al*. are internally consistent for **25**, **30**, **34-36**. Therefore, **25** and **36** were arbitrarily chosen for synthesis so that the relative rates of hydrolysis under the conditions employed in this study could be examined (for synthetic details, see Chapter 7). For internal consistency a paired kinetic approach was again used. The value of k_{H+} for **25** as determined under the conditions employed in this study has been reported in Section 6.3, and is presented in Table 9. A representative stacked plot of the ^{1}H NMR kinetic experiment for pair **22** and **36** is presented in Figure 53.

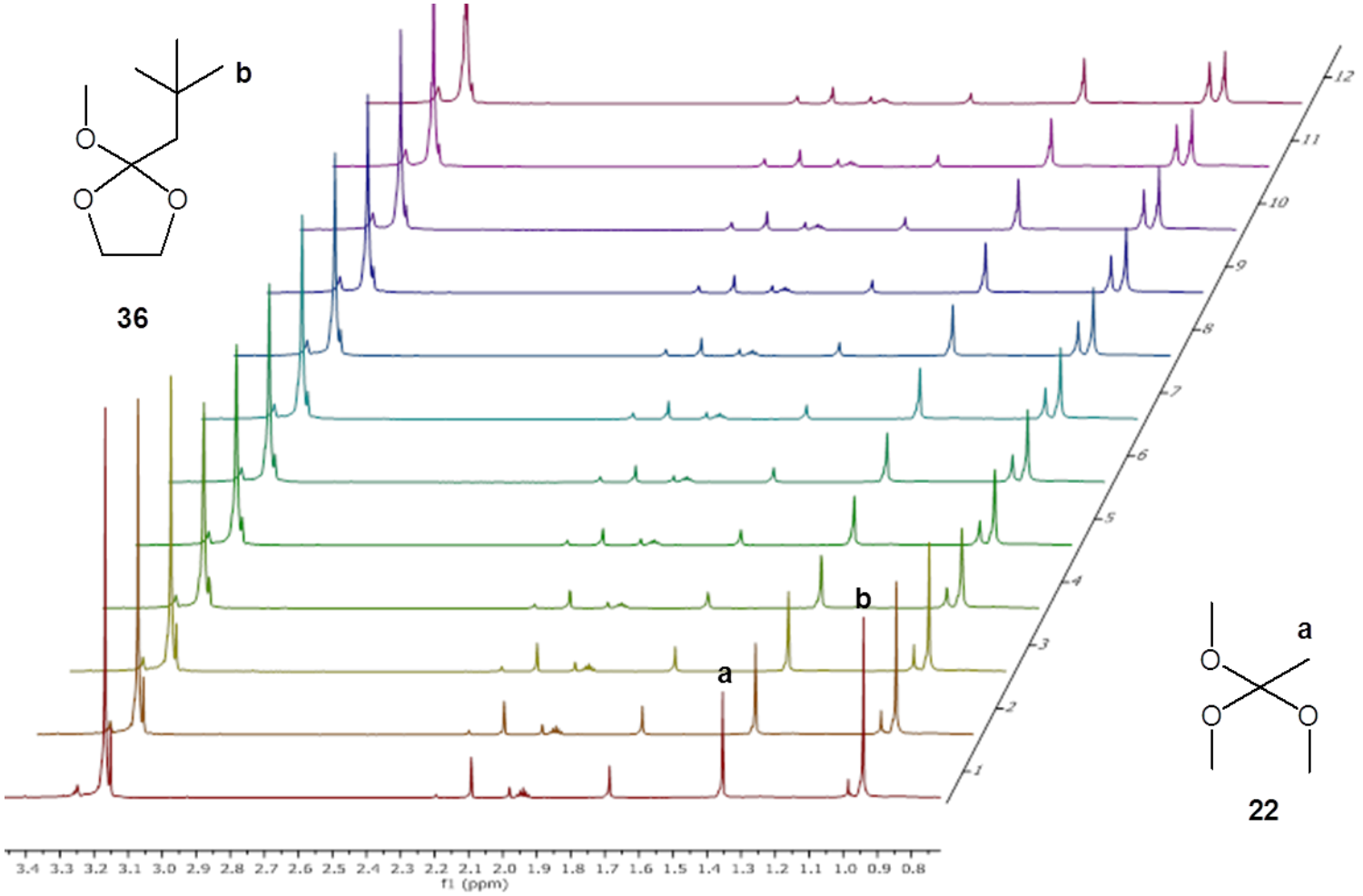

Figure 53. Stacked plot of **22** and **36** (300 MHz ^{1}H NMR in D_2O/CD_3CN=1:4, 625 s intervals, T= 25ºC, [HCl]= 2.5 x 10^{-6} M).

The ortho ester **36** was initially examined alongside **22** at [HCl] = 3.96 x 10^{-5} M in the NMR tube; however the rate at which **36** underwent hydrolysis under these conditions was too rapid, making an accurate determination of k_{H+} very difficult, testament to the unusual susceptibility of this molecule to hydrolysis. Ultimately, the lowest value of [H^+] used in this study *i.e.,* = 2.5 x 10^{-6} M in the NMR tube, proved to be more appropriate for the determination of k_{H+} for **36**. Plotting the logarithms of concentration for **36** and **22** over time (Figure 54), afforded values of k_{obs}, and thereafter k_{H+}.

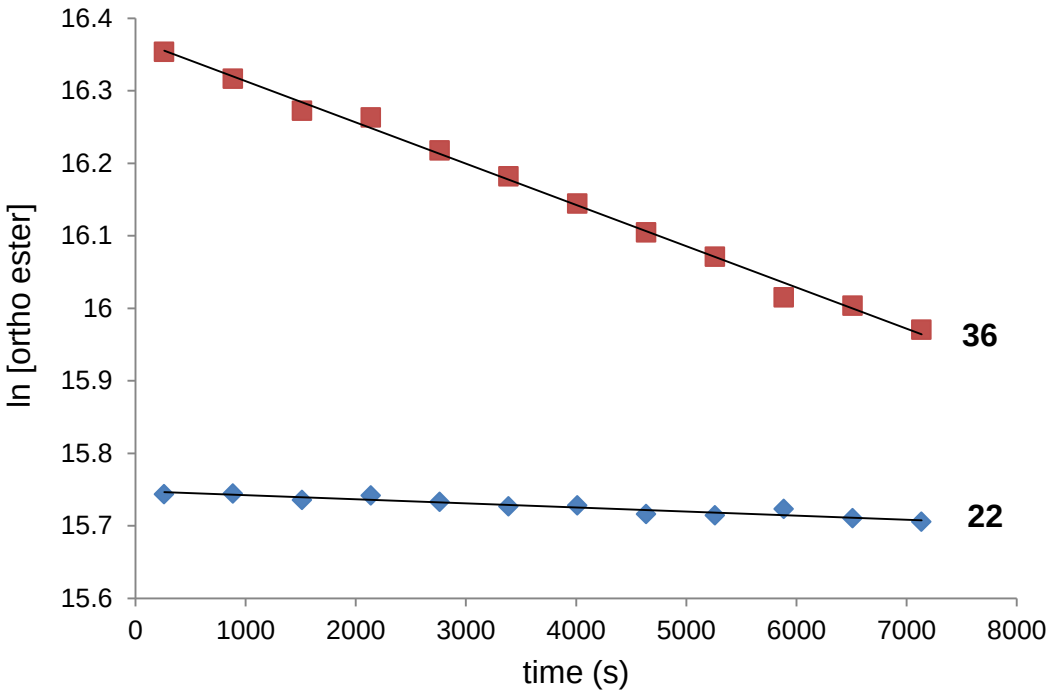

Figure 54. A plot of ln[**22**] (k_{obs} = 5.6 x 10^{-6}; R^2 = 0.9003), and ln[**36**] (k_{obs} = 5.69 x 10^{-5}; R^2 = 0.9952) *versus* time (s).

The paired kinetic experiments for **22** and **36** were performed three times (see Appendix B), and the average values of k_{H+} for each molecule determined in this study are presented in Table 9, alongside the value of **25** which was reported earlier (Table 6). The ratio[†2] of the values of k_{H+} (which has been assumed to be the rate limiting step) for **25, 30, 34**-**36**, as reported

[†2]The *ratio* of k_1^H (equivalent to k_{H+} in this work) are considered alone, as it is believed that this work may contain typographical errors in the exponential factors of reported values.

by McClelland *et al*., are also presented in Table 9 (1988). The ratios derived from McClelland *et al*. are firstly calibrated with respect to the value of **25** (*i.e.,* multiplied by k_{H+} = 6.53 $M^{-1}s^{-1}$), and secondly multiplied by a factor of 0.62 (*i.e.,* 76/123) in order to calibrate with respect to **36**, to finally afford the following values: **25** (6.53 $M^{-1}s^{-1}$), **30** (≈ 8 $M^{-1}s^{-1}$), **34** (≈ 11 $M^{-1}s^{-1}$), **35** (≈ 14 $M^{-1}s^{-1}$), and finally **36** (75.91 $M^{-1}s^{-1}$) (Table 9).

Table 9. The relative rates of hydrolysis for **25, 30, 34**-**36** as reported by McClelland *et al*. (1988)[a], calibrated firstly with respect to the k_{H+} of **25**[b], and secondly **36**[c] as determined in this study[d].

Ortho ester	k_{1H+} ratios[a]	k_{H+} ($M^{-1}s^{-1}$)[b]	k_{H+} ($M^{-1}s^{-1}$)[c]	k_{H+} ($M^{-1}s^{-1}$)[d]
25	1	6.53	-	6.53 ± 0.21
22	-	-	-	6.98 ± 0.23
30	2.0	≈ 13	≈ 8	-
34	2.6	≈ 17	≈ 11	-
35	3.4	≈ 22	≈ 14	-
36	18.8	≈ 123	≈ 76	75.91 ± 7.11

From the data above, one observes a relatively constant increase in the rate of hydrolysis of **25** → **30** (*ca.* 20%), **30** → **34** (*ca*. 40%), and **34** → **35** (*ca*. 30%), with a quite dramatic acceleration accompanying **35** → **36** (> 400%). Although McClelland has noted the relative order of hydrolyses as verified here, an explanation of the data has yet to be provided.

In order to rationalise the steady increase in the rate of hydrolysis associated with the series **25** → **30** → **34** → **35**, and the dramatic increase associated with **35** → **36**, it is useful to consider the relief of transannular strain within the starting materials. The rate acceleration for **25** → **30** was previously attributed to the modest degree of transannular strain associated with the progression from an H atom to a Me group upon Cα (Figure 44).

Attention now turns to the ≈ 40% rate acceleration associated with the progression **30** → **34**. A Newman projection – viewed along the Cβ─Cα bond of the C(2) substituent of **34** - is presented in Figure 55. In the case of **34**, the *gauche* conformation of the C(2) substituent minimises 1,3-transannular interactions with the C(4/5)─H atoms in much the same manner as **30** (Figure 44). However, the *gauche*-conformer of **34** is in all likelihood destabilised by vicinal Me$^{\cdots}$Et non-bonded repulsive interactions, possibly favouring the alternative *anti*-conformer. It is the *anti*-conformer which increases transannular steric pressure upon the C(4/5)─H atoms of the 1,3-dioxolane ring. The 30% rate acceleration accompanying the progression **34** → **35** may be explained using a similar argument. A Newman projection, viewed along the Cβ─Cα bond, of **35** is presented in Figure 55. It is proposed that the *iso*-propyl C(2) substituent within **35** adopts a staggered conformation which orients at least one Me group towards the C(4/5)─H atoms, thereby increasing the transannular steric pressure. Unlike the case of **34**, where 1,3-transannular repulsive interactions may be relieved *via anti* ↔ *gauche* interconversion, **35** is constrained to present at least one sterically demanding C(4/5)─H$^{\cdots}$Me interaction at all times.

The >400% rate acceleration accompanying the progression from *iso*-propyl **35** → *neo*-pentyl **36** is however, somewhat surprising. The corresponding Newman projection of **36** is presented in Figure 55. The nature of the Cβ substituent *i.e., tert*-butyl ensures that two sterically demanding Me groups permanently engage in 1,3-transannular repulsive interactions with the transannular C(4/5)─*H* atoms.

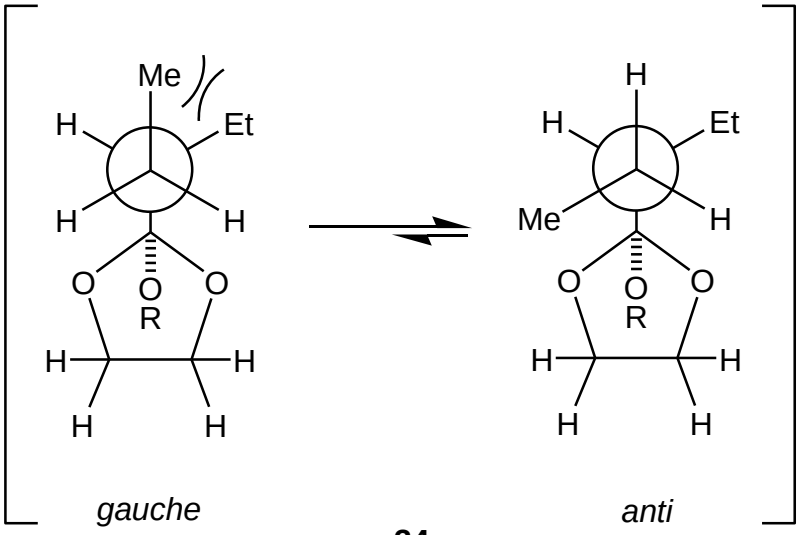

34

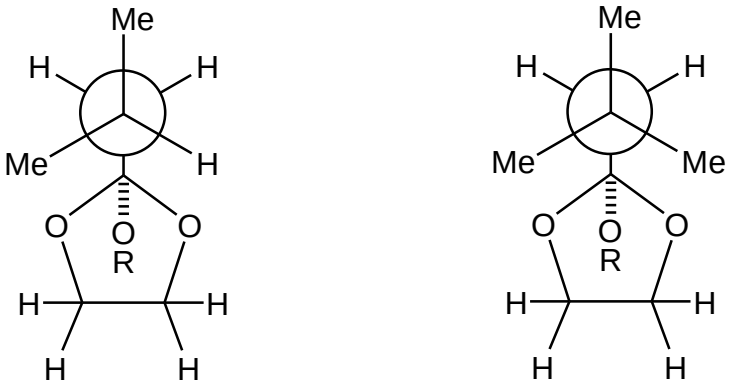

35 **36**

Figure 55. 1,3-Transannular steric strain through substitution at Cβ. Newman projections of ortho ester 1,3-dioxolanes (where R = Me) **34**-**36** viewed along the Cβ─Cα bond of the C(2) alkyl substituent.

However, interest was piqued about whether these interactions alone could account for the observed 400% rate acceleration of **36** with respect to **35**. It has been noted previously that nascent 1,3-transannular interactions are sufficient to prevent the cyclisation of certain 5-membered organometallic rings (Costello *et al.*, 2001). Furthermore, it has been established that the annular strain within *trans*-2,5-dimethyl tetrahydrofurans leads to a sufficient separation of charge, that the mechanism of ring cleavage switches from S_N2

→ S_N1 (Costello *et al.*, 2005). As the rate of reaction remains first order, there is no evidence of a change in mechanism; however it is still possible for the cation to become ambident *i.e.,* H_2O reacts at both C(2) and C(4/5). As discussed earlier (see Section 5.3, Scheme 9 and Figure 25), the products of hydrolytic attack at either C(2) or C(4/5) are constitutionally indistinguishable; however it *is* possible to distinguish between the products – and therefore the C(2) and C(4/5) pathways – using isotopically labelled H_2O^{18} (Scheme 10).

It is proposed that the generic 1,3-dioxolan-2-ylium cation **16** ordinarily undergoes hydrolytic attack at C(2) in order to afford the observed hydroxy ester **21**. In the presence of H_2O^{18}, hydrolytic attack at C(2) will afford, after ring cleavage, hydroxy ester **21** incorporating O^{18} at the carbonyl carbon atom, alone. The acid catalysed ring closure of **21** results in the elimination of the heavy isotope to generate **16** once again (Santry & McClelland, 1983). Alternatively, hydrolytic attack of H_2O^{18} upon C(4/5) will afford, after ring cleavage hydroxy ester **19** incorporating O^{18} within the OH function of either C(4/5). Ring closure of **19** will afford a 1,3-dioxolan-2-ylium cation **16a** incorporating O^{18}, which will exist alongside a constitutionally identical yet isotopically distinct mesomeric form *i.e.,* **16b**. Further hydrolytic attack by H_2O^{18} upon **16a** and **16b** will afford after ring fissure, hydroxy esters **19a** and **19b** respectively. It is important to note here that repetitive C(4/5) H_2O^{18} attacks of **16** will ultimately afford a hydroxy ester incorporating the heavy O^{18} isotope within the carbonyl, ethereal and hydroxy functions, whereas C(2) attack will afford incorporation of O^{18} at the carbonyl function alone (Scheme 10).

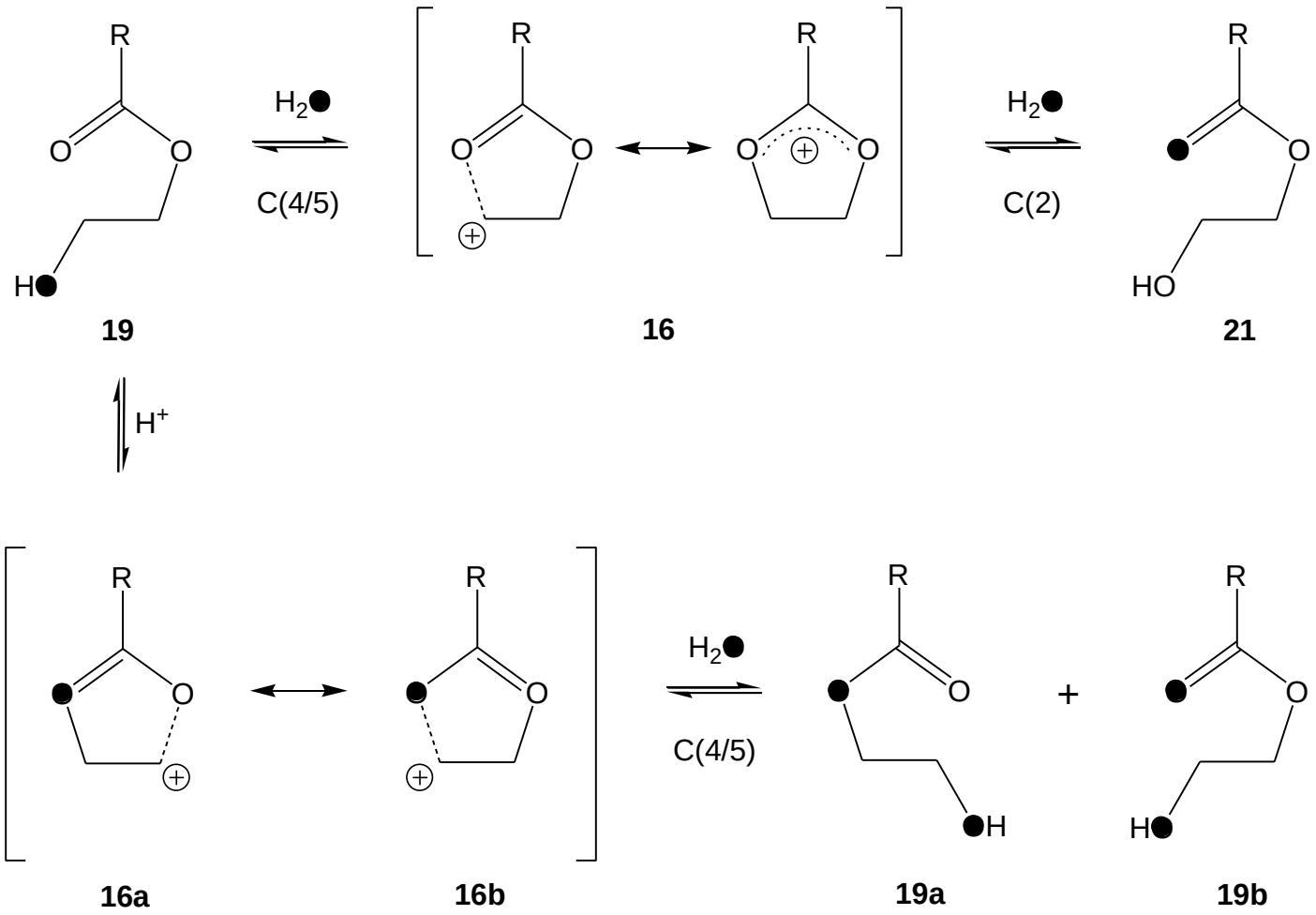

Scheme 10. Isotopomers **19a-b** and **21** derived from the C(2) or C(4/5) hydrolytic attack of a generic 1,3-dioxolan-2-ylium cation **16**, by H_20^{18} (the O^{18} isotope is represented by ●).

The choice was made to examine **25** alongside **36** as the former, which hydrolyses at 10% the rate of the latter, is not expected to possess sufficient separation of charge to undergo C(4/5) hydrolytic attack. The 1,3-dioxolan-2-ylium cations derived from **25** and **36** (*i.e.*, **25a** and **36a**) were prepared *via* an unambiguous route (see Chapter 7), and subsequently treated with H_2O^{18}. The crude mixtures were neutralised by passing them through an alumina frit. The process was repeated using H_2O^{16}, and the resulting mixtures were subjected to MS(CI) analyses. The MS(CI) spectrum of the hydroxy ester (**25ϕ**) derived from 2-methoxy-2-methyl-1,3-dioxolane is presented in Figure 56. The parent ion $[M+H]^+$ derived from the reaction of **25a** with H_2O^{16} *i.e.,* hydroxy ester **25ϕ** is clearly visible at m/z = 105.1. A single heavy isotope attributable to $[(M+2)+H]^+$ is observed at m/z = 107.1, indicating the incorporation of a single O^{18} atom. This is consistent with C(2) hydrolytic attack upon **25a**. Similarly, the MS(CI) spectrum of the hydroxy ester (**36ϕ**) derived from 2-methoxy-2-*neo*-pentyl-1,3-dioxolane reveals (Figure 57) m/z = 161.1 and 163.1, attributable to $[M+H]^+$, and $[(M+2)+H]^+$, respectively.

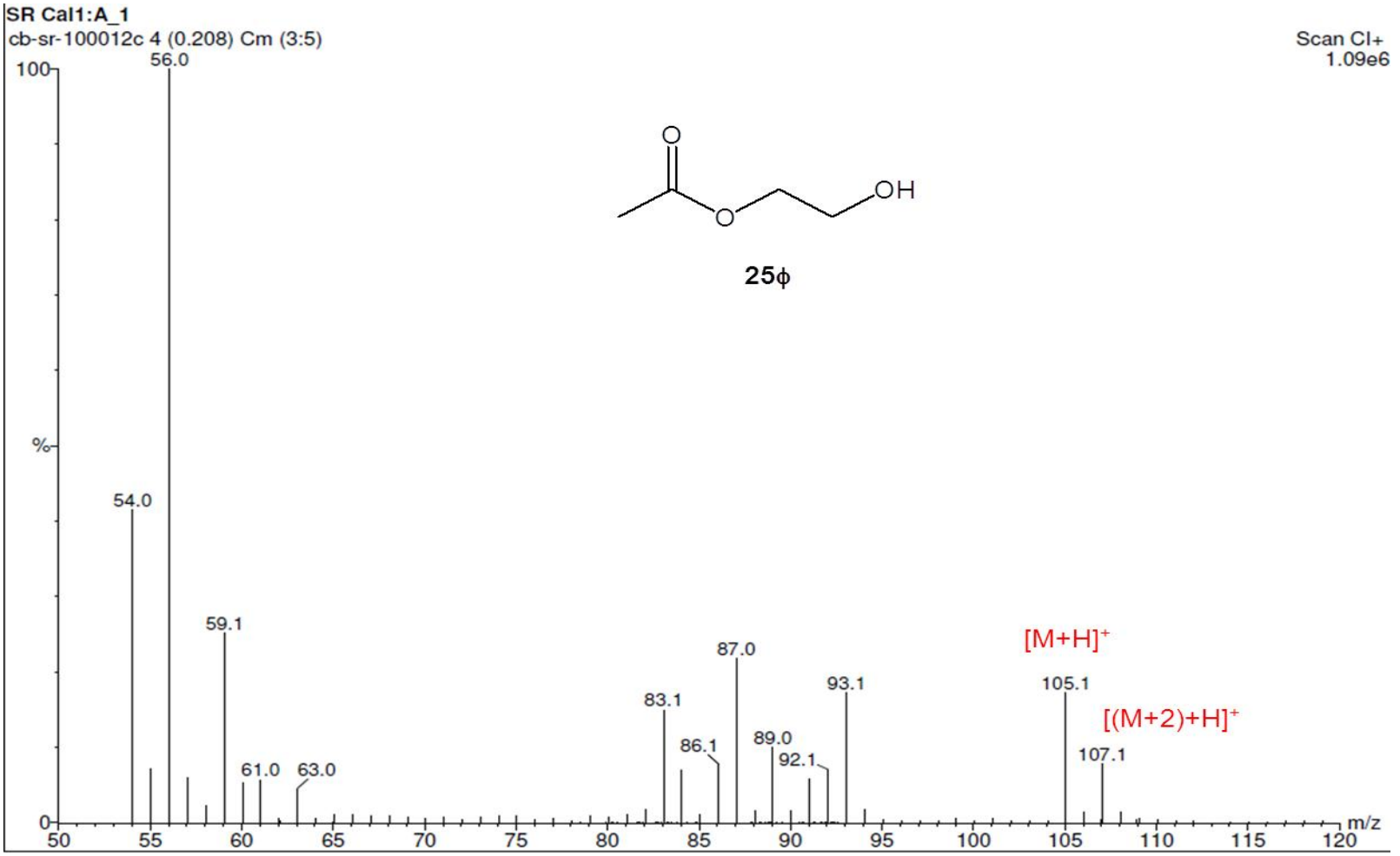

Figure 56. MS(CI) spectrum of hydroxy ester (**25ϕ**) derived from 1,3-dioxolan-2-ylium cation **25a** and $H_2O^{16/18}$.

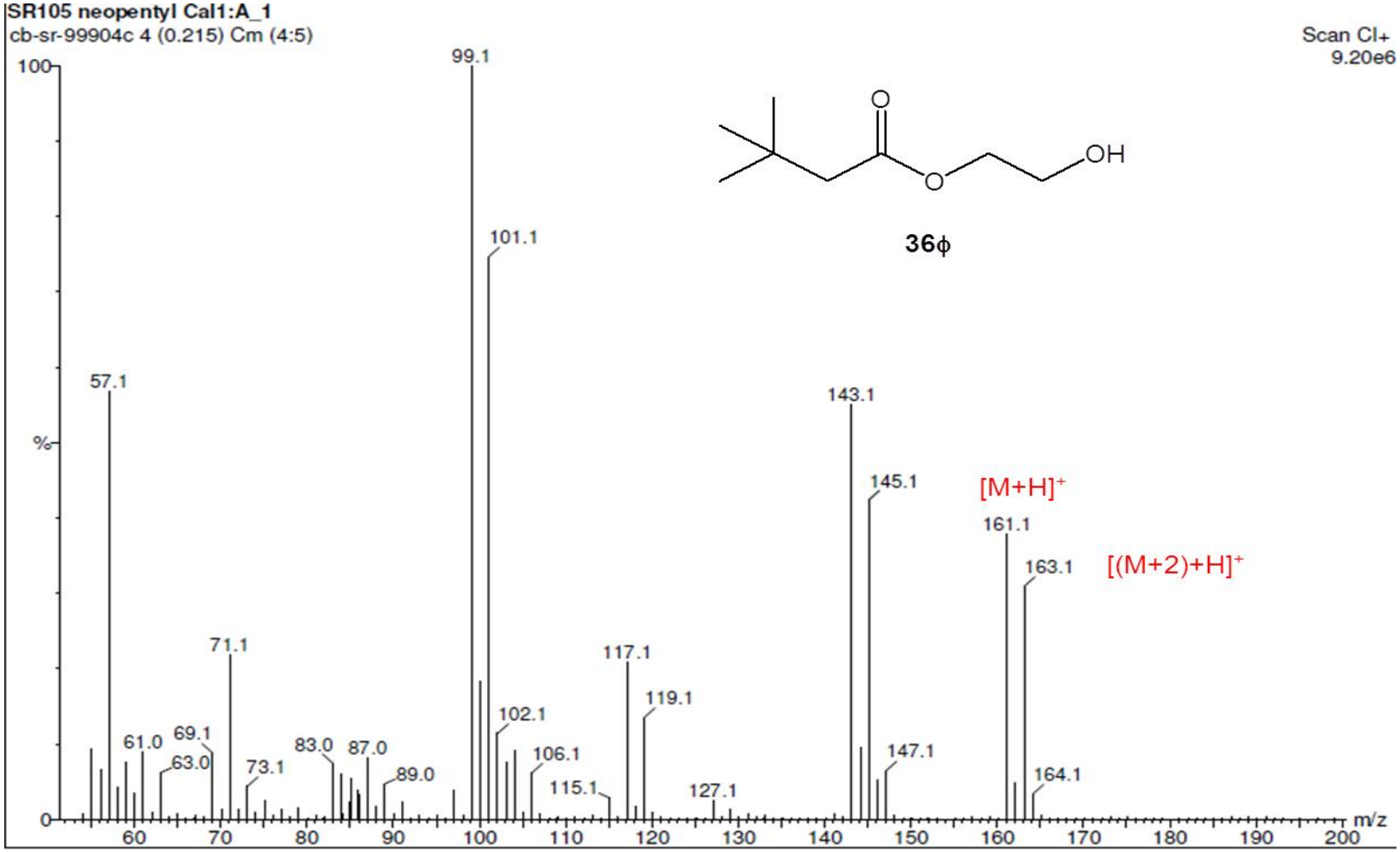

Figure57. MS(CI) spectrum of hydroxy ester (**36ϕ**) derived from 1,3-dioxolan-2-ylium cation **36a** and $H_2O^{16/18}$.

Although consistent with C(2) hydrolytic attack upon **36a**, it is not possible to dismiss the operation of the C(4/5) process. To unambiguously establish the site of isotope incorporation, the crude mixtures were examined *via* high field ^{13}C NMR spectroscopy in order to identify the characteristic upfield shifts induced by O^{18} substitution upon ^{13}C nuclei (Van Etten & Risley, 1980, 1979). The only resonance within the hydroxy ester derived from **25a**, to exhibit an isotopically induced upfield shift upon treatment with H_2O^{18} was that attributed to the carbonyl carbon atom ($\Delta\delta_C$ = +0.04ppm). The CIMS and ^{13}C NMR data confirm that **25a** undergoes C(2) hydrolytic attack alone. Surprisingly, both CIMS and ^{13}C NMR data also confirm that **36a** undergoes exclusive C(2) hydrolytic attack. This is confirmed by the ^{13}C NMR spectrum of the corresponding hydroxy ester (Figure 58), in which the signal attributed to the $^{13}C{=}O^{18}$ nucleus (δ_C = 172.76ppm) is isotopically shifted upfield of the corresponding $C{=}O^{16}$ resonance (δ_C = 172.80ppm *i.e.,* $\Delta\delta_C$ = +0.04ppm).

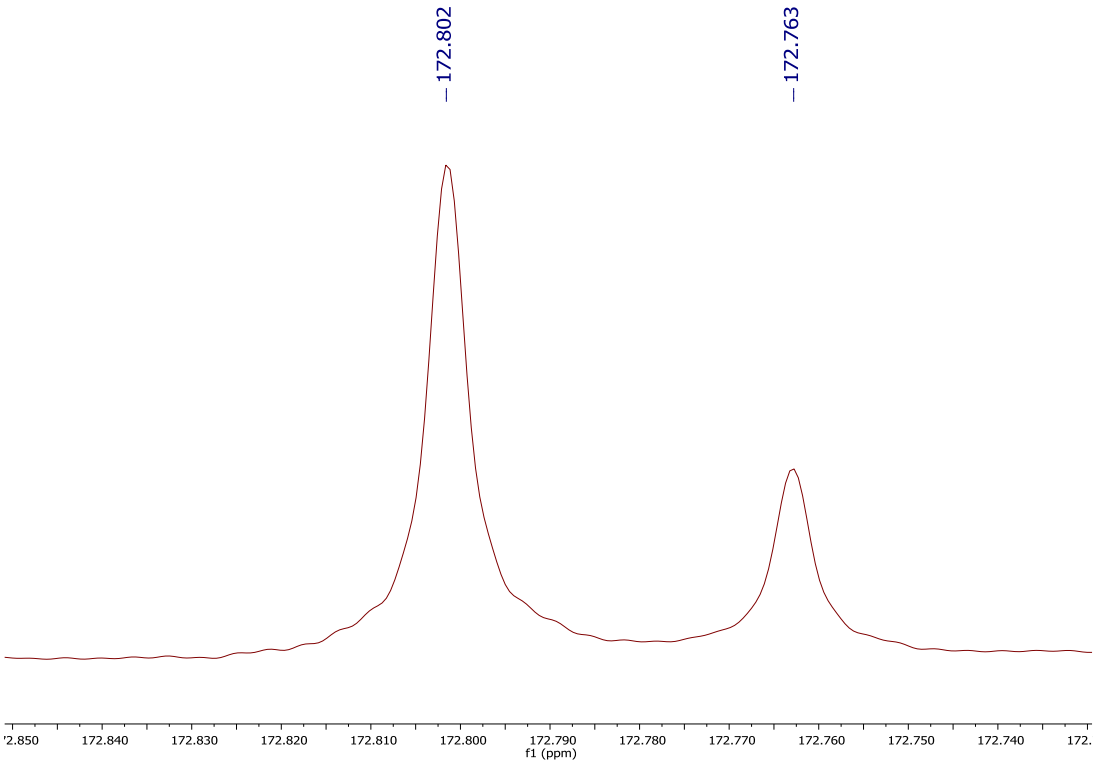

Figure 58. Partial ^{13}C NMR spectrum (125 MHz, $CDCl_3$) of hydroxy ester **36ϕ** illustrating resonances associated with $^{13}C{=}O^{18}$ (δ_C = 172.76ppm) and $^{13}C{=}O^{16}$ (δ_C = 172.80ppm *i.e.,* $\Delta\delta_C$ = +0.04ppm) nuclei.

It is tempting to attribute the rate acceleration observed for **36** to the relief of transannular strain alone, as there is little evidence to suggest that a change in mechanism through a separation of charge has occurred. However, attention turns to other factors which may govern the reactive conformations of 2-methoxy-2-alkyl-1,3-dioxolanes, leading to an acceleration of the reaction rate. Newman projections for a generic 2-methoxy-2-alkyl-1,3-dioxolane viewed along Cα─C(2), are presented in Figure 59. Although a concise analysis warrants extensive NMR and computational work beyond the scope of the current study, inspection of molecular models suggests that a half-chair arrangement of the 1,3-dioxolane ring may readily accommodate sterically undemanding groups, such as R = H (*i.e.,* **25**; Figure 59a). The half-chair is the preferred solid-state arrangement when R = F in 2-phenoxy-2(trifluormethyl)-4,4,5,5-tetraphenyl-1,3-dioxolane (ZICMED, Figure 36). Furthermore, calculations corroborate the view that for R = H, transannular interactions involving the axial C(4)─*H* moiety are insufficient to destabilise the half-chair (Figure 60). The stereoelectronic implications of the half chair arrangement have been addressed previously (Section 6.3). Only one oxygen σ_{nb} within the ring may adopt an *anti*-periplanar arrangement with respect to the axial C(2)─OMe moiety at any given time (*i.e.*, single anomeric effect).

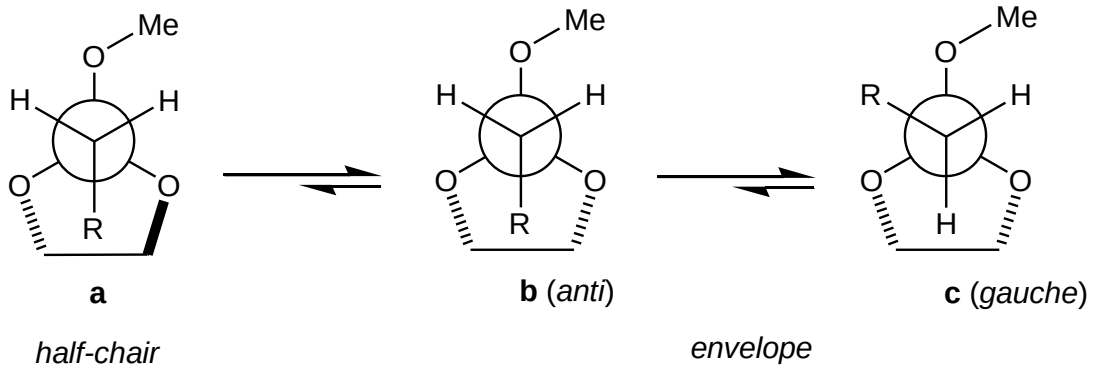

Figure 59. The progressive destabilisation of the *half-chair* (**a**) and *envelope* (**b-c**) arrangements of the 1,3-dioxolane ring, with progressively sterically demanding R (**a** → **b** → **c**).

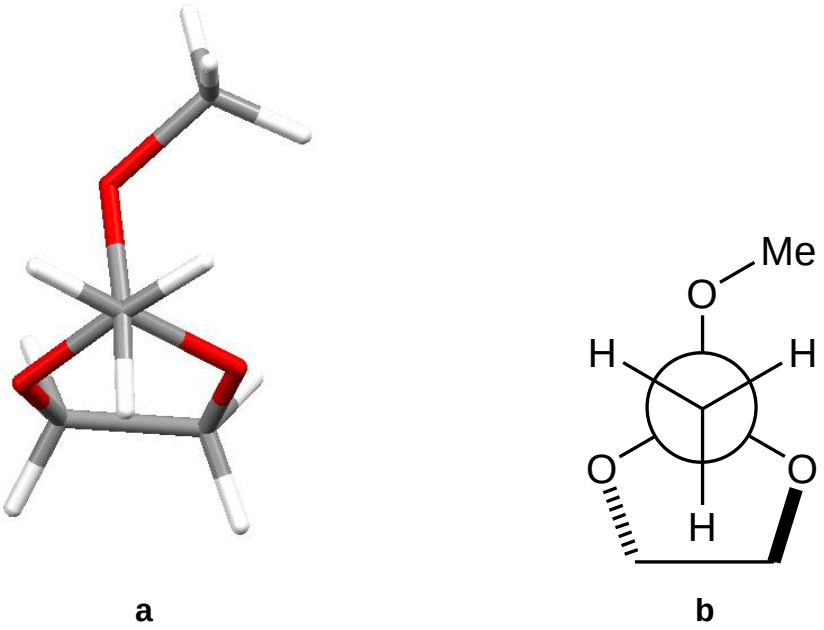

a **b**

Figure 60. Projections of **25** viewed along Cα─C(2), illustrating the, (a) calculated lowest energy half-chair arrangement for which the transannular interaction involving the axial C(4)─*H* moiety and R = H are clearly accommodated, and (b) corresponding Newman projection.

It is argued that as the R group becomes increasingly sterically demanding throughout the series **25** (R = -H) → **30** (R = -Me) → **34** (R = -Et) → **35** (R = *iso*-Pr), the transannular strain associated with the axial C(4)─*H* within the half-chair arrangement becomes progressively intolerable. This invokes a shift of the equilibrium toward the alternate envelope arrangement (Figure 59b). The stereoelectronic implications of the envelope arrangement are that two, as opposed to only one oxygen atom within the ring may orient σ_{nb} *anti* to the axial C(2)─OMe. The implications of this argument upon the rates of hydrolysis for **25**, **30** and **34-35** are consistent with experimental findings (Table 9). Finally, in the case of **36** (R = -*tert*-Bu), even the envelope arrangement of the 1,3-dioxolane ring is unable to relieve transannular steric pressure between the *tert*-Bu moiety and the C(4/5)─*H* atoms, and so R adopts the gauche conformer with respect to C(2)─OMe, effectively locking **36** into the envelope arrangement (Figure 59c). The calculated lowest energy conformation of **36** is presented in Figure 61.

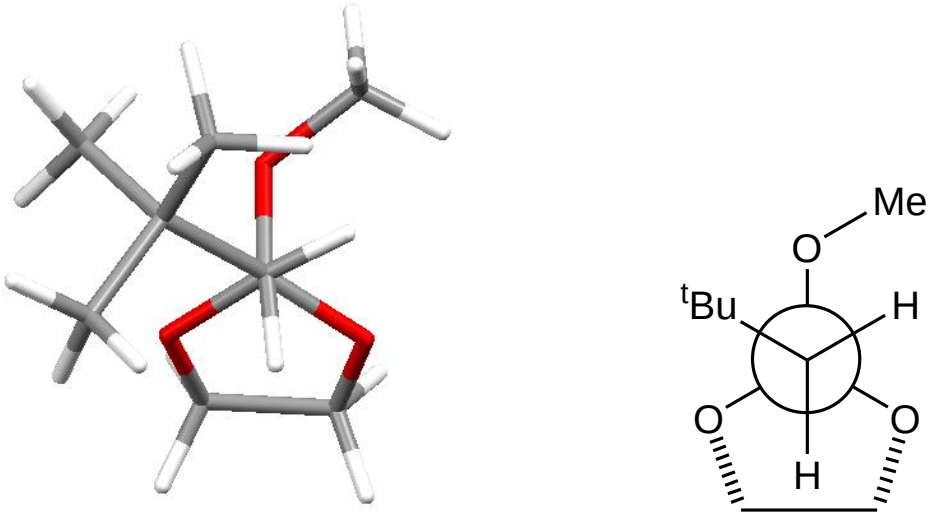

a **b**

Figure 61. Projections of **36** viewed along Cα–C(2) illustrating the, (a) calculated low energy *envelope* arrangement of the 1,3-dioxolane ring wherein the sterically demanding transannular strain is relieved by the *tert*-Bu group adopting a *gauche* arrangement with the C(2)–OMe moiety, and (b) the corresponding Newman projection.

Calculations upon **36** are consistent with this hypothesis, and the double anomeric effect accompanying the envelope arrangement is clearly illustrated in Figure 62. As can be seen, the *tert*-Bu group lies approximately in the same plane as the 1,3-dioxolane ring. As C(2) undergoes a change in hybridisation during hydrolysis step *i.e.,* $sp^3 \rightarrow sp^2$ so the steric pressure attending the *tert*-Bu moiety is released. It is concluded then, that the experimentally observed rate acceleration associated with **36** can be attributed to a strained 1,3-dioxolane ring locked into a conformation which affords a double anomeric effect.

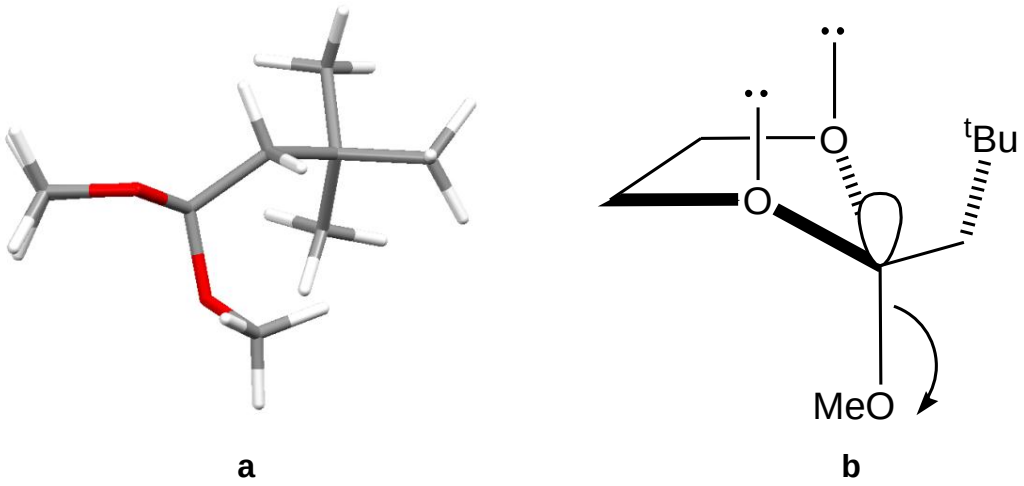

a **b**

Figure 62. Projections of **36** viewed along C(4)–C(5) illustrating the, (a) calculated low energy *envelope* arrangement wherein the sterically demanding *tert*-Bu group lies approximately in the same plane as the 1,3-dioxolane ring, and (b) the antiperiplanar arrangement of two oxygen σ_{nb} with respect to the axial C(2)–OMe leaving group.

6.6 Conclusions

A library of candidate FDII has been assembled and the catalytic coefficients k_{H+} of their hydrolysis reactions in CD_3CN/D_2O (4:1) are presented in Figure 63. The absolute values of k_{H+} reported herein can be expected to increase with both the polarity, and the ionic strength of the solvent; however, it is anticipated that the relative order of FDII reactivity will remain unchanged. Extensive $^{1}H/^{13}C$ NMR kinetic studies, alongside computational and conformational analyses have been used to uncover the key structural features which contribute towards the relative rates of hydrolysis. The key points are summarised below.

- In the case of acyclic systems, alkyl substituents have a greater role to play in accelerating the rate of hydrolysis compared to alkoxy substituents (Section 6.2).

- The relative rates for the hydrolysis of analogous acyclic and cyclic ortho esters are of a similar magnitude; modest differences in the relative rates of hydrolysis can be accounted for using stereoelectronic arguments (Section 6.3).

- Six membered *exo*-cyclic ortho esters are hydrolysed much faster than their *endo*-cyclic counterparts. Both react faster than the corresponding ketals. For the first time, a coherent explanation based upon conformational analyses has been proposed to explain these differences (Section 6.4).

- For five membered *endo*-cyclic ortho esters substituted at C(4/5), cumulative rate acceleration appears to derive from both the inductive effect, and the relief of 1,3-transannular repulsion (Section 6.5.1).

- Rate accelerations within five membered *endo*-cyclic ortho esters accompany increasingly bulky C(2) alkyl substitution. Dramatic increases in the rate of hydrolysis are observed for Cβ branching at C(2), which can lead to conformational locking of the ring into stereoelectronically favourable envelope arrangements (Section 6.5.2).

- All of the above factors promote the “spontaneity” of the departure of the alkoxy group (Section 5.3), either through 1,3-transannular strain or single/double anomeric effects (Chapter 6).

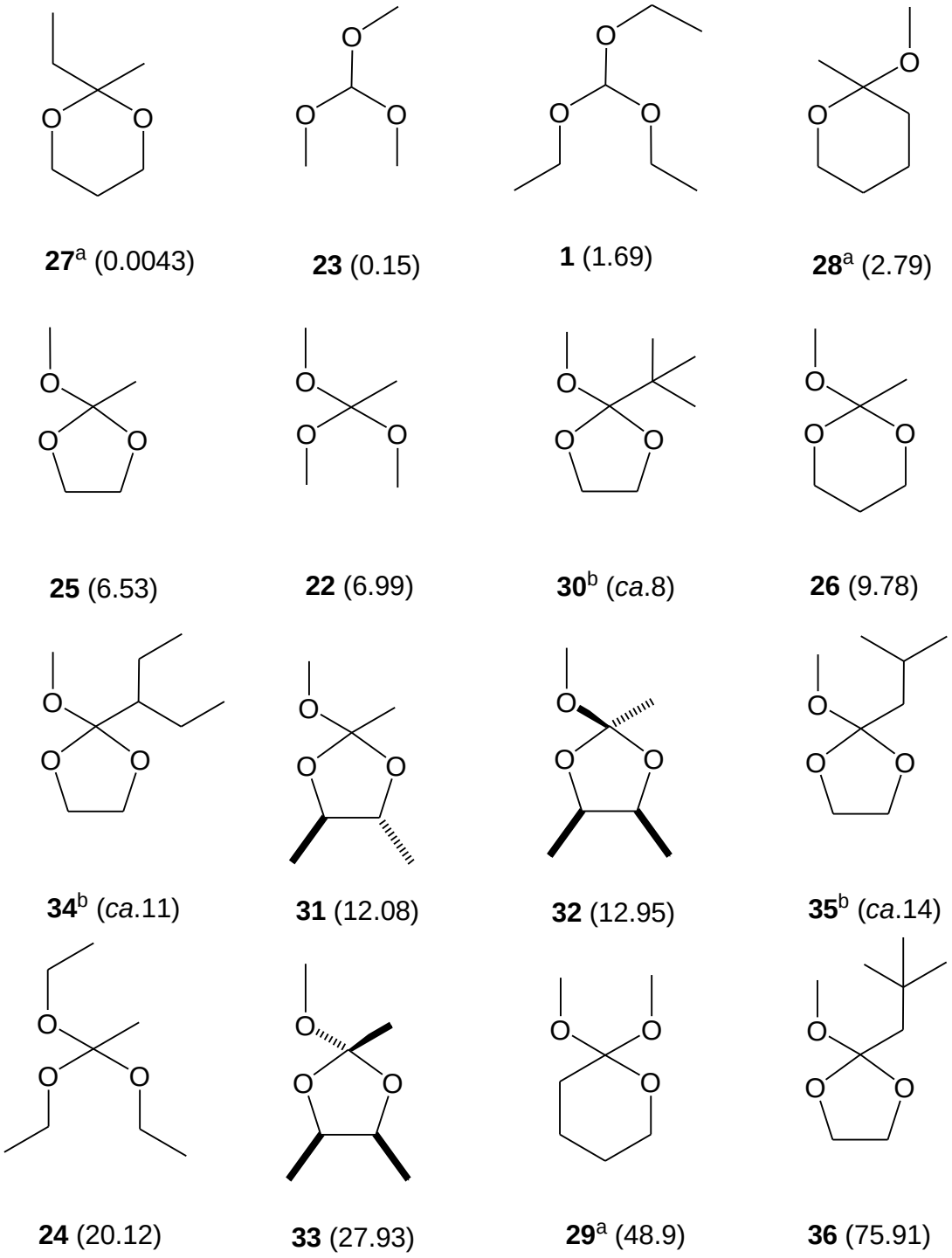

Figure 63. The catalytic coefficients [k_{H+} ($M^{-1}s^{-1}$) in parentheses] for the hydrolysis reactions of the molecules considered in this study.

Chapter 7

The Preparation of FDII

7.1 Introduction

Because ortho esters are stable towards bases and resistant to strong nucleophiles, most current applications are limited to their use as protecting groups for carboxylic acids or esters in organic synthesis (Kocienski, 2005; Corey & Raju, 1983). With respect to the parent carboxylic acid, an ortho ester attenuates the electrophilic carbonyl atom, eliminates the acidic hydroxyl hydrogen atom, and reduces the acidity of α-hydrogen atoms. The broad application of ortho esters in organic synthesis has been limited historically by the difficulty and low yields associated with their preparation. Routes to acyclic ortho esters, such as *via* the action of Grignard reagents upon ortho carbonates (Tschitschibabin, 1905), or the oxidation of aromatic alkyl substituents with $NaClO_4$ (Brinkhaus *et al*., 1986), have been largely superseded by the Pinner reaction (Noè *et al.*, 2013). In the first step of this procedure, alkyl or aryl nitriles are converted to the corresponding imidate hydrochlorides (>90%), which upon alcoholysis afford ortho esters **10** in good yields (*ca*. 60%) (Scheme 11). The Pinner route to acyclic ortho esters, followed by an exchange reaction with either a diol or triol, represents the most useful general strategy for the synthesis of cyclic derivatives.

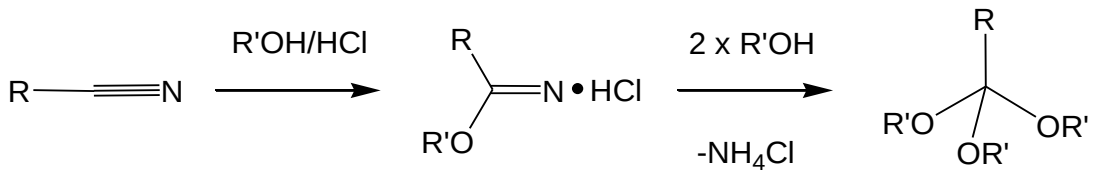

10

Scheme 11. The Pinner reaction for the preparation of ortho esters **10**.

The zirconocene dichloride (Cp_2ZrCl_2) catalysed rearrangement of epoxy esters provides ready access to bicylic ortho esters *via* the intramolecular capture of the intermediate 1,3-dioxan-2-ylium cation (Scheme 12). This reaction provides opportunities for the wider use of ortho esters in organic synthesis (Wipf *et al.*, 1997).

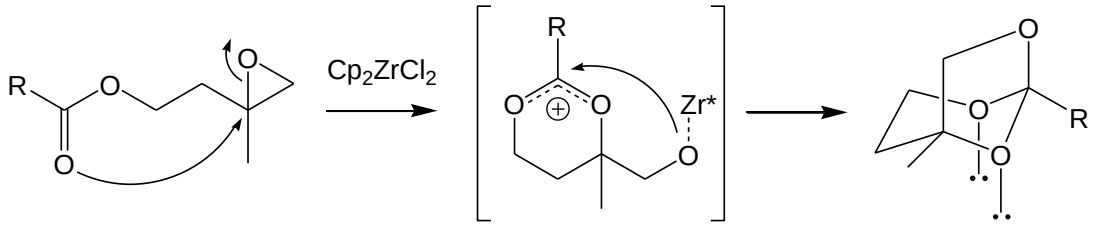

Scheme 12. Cationic zirconocene-catalysed rearrangement of epoxy esters to form bicyclic ortho esters. $Zr^* = Cp_2(Cl)Zr^+$.

The X-ray crystallographic analysis of bicyclic ortho esters indicates an unusually elongated axial C─O bond. This, along with the preferential reactivity of the axial ether towards Lewis acids (Wipf *et al.*, 1999), indicates a double anomeric effect (*i.e.,* 2 x $\sigma_{nb} \rightarrow \sigma^*$) in the chair conformation of the 1,3-dioxane, as indicated in Scheme 12. These observations are entirely consistent with the kinetic acceleration of hydrolyses for the axially oriented MeO- conformer of **26**, as discussed earlier in Section 6.4.

7.2 Cyclic Ortho Esters *via* Transesterification Reactions.

Exo-cyclic ortho esters (**8**, Scheme 5) may be prepared from the corresponding γ/δ-lactone using a strong alkylating agent, followed by treatment with an appropriate sodium alkoxide (Meerwein *et al.*, 1956). However, relatively simple C(2) alkyl and aryl *endo*-cyclic ortho esters (**7**, Scheme 5) are readily prepared *via* the acid catalysed transesterification reaction of commercially available acyclic ortho esters with the appropriate diol (Kresge *et al.*, 1974; McClelland *et al*., 1981; McClelland *et al.*, 1988; van Maarseveen *et al.*, 2011). The C(2) methyl ortho esters used in this study *i.e.,* **25**, **26**, and **31-33**, were prepared *via* this method using trimethyl orthoacetate **22**, and the appropriate 1,2- or 1,3-diols (see Section 10.8). Isolated yields - which were not optimised – were found to be in the order 40-70%.

The exchange reaction of **22** with *dl*/*meso*-2,3-butane diol[3] to afford a mixture of (±)-**31** (≈ 30%), (±)-**32** (≈ 20%) and (±)-**33** (≈ 50%) in 40% overall recovered yield, warrants some comments. This is because **33**, which appears to have been formed in the greatest quantity, was in fact found to react with water at twice the rate of the other two molecules (see summary in Figure 63).

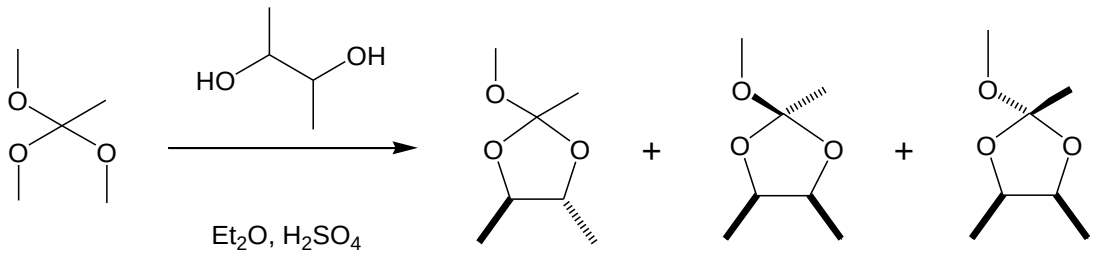

22 (±)-**31** (±)-**32** (±)-**33**

Scheme 13. Transesterification reaction of **22** with *dl*/*meso*-2,3-butane diol to afford the mixture **31** (≈ 30%), **32** (≈ 20%) and **33** (≈ 50%).

[3]The terms *dl*, racemic, and the symbol (±) are often used interchangeably to mean a 1:1 mixture of enantiomers.

The first anomaly is that the ratio of the products derived from the reaction of *meso*-2,3-butane diol (*i.e.,* **32** and **33** ≈ 70%), appears to exceed the amount of product derived from *dl*-2,3-butane diol (*i.e.,* **31** ≈ 30%). The second anomaly is the apparent formation of the most strained diastereoisomer **33** in the greatest overall relative amount (≈ 50%). In order to investigate these anomalies, the exchange reaction of **22** with *dl*/*meso*-2,3-butane diol was repeated three times at 20°, 0° and -10°C, and the reaction quenched in each case with an excess of anhydrous imidazole. The starting sample of 2,3-butane diol, along with the crude reaction mixtures obtained at all three temperatures, were analysed using GC-MS and ^{1}H NMR (500MHz). Both GC-MS and ^{1}H NMR (Gallwey *et al.*, 1990) analyses confirmed that the sample of 2,3-butane diol used for these experiments was in fact a 4:1 mixture of the *meso* (= *erythro*) and *dl* (= *threo*) diastereoisomers, respectively.

^{1}H NMR (500MHz) and GC-MS analyses of the crude reaction mixtures failed to indicate any particular temperature dependence for the transfer reactions, with the average value of the product ratios remaining of the order indicated earlier *i.e.,* **31** (32%), **32** (18%), and **33** (50%), with a conversion of 60%. The small disparity between the experimentally determined diastereoisomeric ratio of 2,3-butane diol (*meso*/*dl* = 77:23), and the ratio of **32**+**33**/**31** (*meso*/*dl* = 68:32) indicates that the *dl*- isomer reacts at a marginally faster rate than the *meso*. Because the observed product ratios are governed by the mass action effect, the most reliable method to determine relative rates of formation of **31-33** would be to repeat the reaction using a 1:1 mixture of *meso* and *dl* 2,3-butane diol. However, the observed ratio of **31** and **32**/**33** using a 4:1 mixture of diol can be arithmetically adjusted (*i.e.,* x 2 and x ½, respectively) to estimate the relative rates of formation using a 1:1 mixture of diols, *i.e.,* **31** (65%), **32** (10%), and **33** (25%).

The cyclisation of the mono-functionalised glycol formed during the transesterification reaction between ethylene glycol and trimethyl orthoacetate **22**, *en route* to **25**, is depicted in Figure 63.

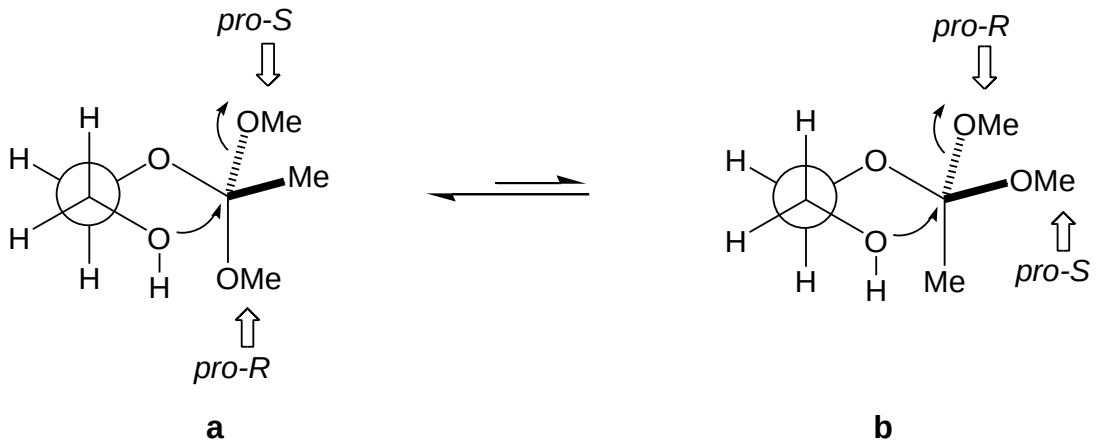

Figure 63. Cyclisation of the mono-functionalised ethylene glycol, *en route* to **25**, *via* the intramolecular S_N2 displacement of either; (a) *pro-S* MeO–, or (b) *pro-R* MeO–.

The half chair arrangement of the mono-functionalised glycol may orient the *pro-R* MeO– in a stereoelectronically favoured axial position, thereby allowing the *pro-S* MeO– to undergo S_N2 displacement ($O\sigma_{nb}$ *pro-R* → $O\sigma^*$ *pro-S*; Figure 63a). Conversely, S_N2 displacement of the *pro-R* MeO– orients the Me– group axial, thereby increasing transannular demand, whilst diminishing the possibility of stereoelectronic stabilisation during the course of the substitution process (Figure 63b). It is argued then, that the cyclisation of mono-functionalised glycols proceeds *via* the stereoelectronically favoured expulsion of the *pro-S* MeO– group. This assumption provides the basis for an explanation for the experimentally observed distribution of ortho esters **31**-**33** (Figure 64).

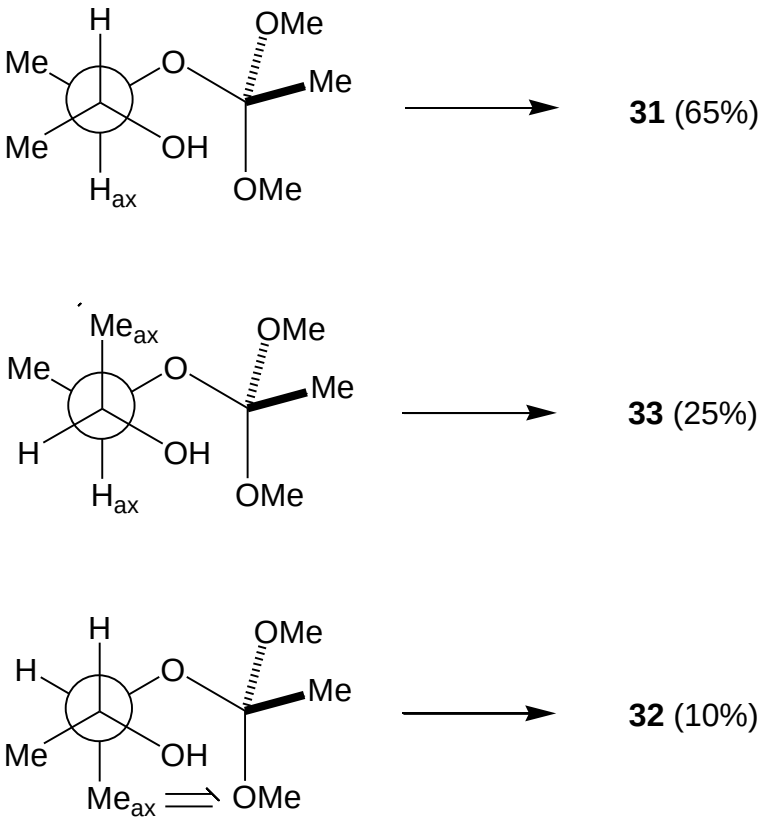

Figure 64. Stereoelectronically favourable conformations of mono-functionalised 2,3-butane diols *en route* to **31**-**33**. Reacting ratios adjusted to reflect the use of a 1:1 mixture of *dl*/*meso*-2,3-butane diol are presented in parenthesis.

The half chair arrangement of the mono-functionalised *dl*-2,3-butane diol *en route* to **31**, may orient the *pro*-*R* MeO– in a stereoelectronically favoured axial position without incurring any notable repulsive interactions with respect to the *pseudo*-transannular H_{ax} (Figure 64). The same may be said for the axially oriented *pro*-*R* MeO– of the mono-functionalised *meso*-2,3-butane diol *en route* to **33**. It would appear however, that *pseudo*-transannular repulsion between the developing C(2)—*Me* and Me_{ax} groups attenuates the rate of formation of **33** slightly. Finally, it is clear that the axial *pro*-*R* MeO– of the mono-functionalised *meso*-2,3-butane diol *en route* to **32** incurs serious *pseudo*-transannular repulsion with the Me_{ax} group, the results of which are expressed in the observed relative rate of formation.

7.3 Cyclic Ortho Esters *via* 1,3-Dioxolan-2-ylium Cation 36a.

Ortho esters bearing the *neo*-pentyl substituent upon C(2) *i.e.,* **36**, were not prepared *via* the acid catalysed transesterification procedure since the corresponding acyclic ortho ester [*i.e.,* $^{t}BuCH_2C(OMe)_3$] is not commercially available. However, a flexible general approach to 2-alkyl-2-alkoxy-1,3-dioxolanes **7** – strategically similar to that outlined earlier in Scheme 12 - involves the preparation of the precursor 1,3-dioxolan-2-ylium cation **16** and subsequent reaction with the alkoxy anion (Scheme 14). There are several routes to 1,3-dioxolan-2-ylium cations **16**; namely, the Lewis acid mediated cyclisation of halo esters [**37** X = Cl ($SbCl_5$); Br ($AgBF_4$) (Meerwein *et al.*, 1955)], methyl ether esters [**37** X = MeO ($Et_3O{:}BF_4$) (McClelland *et al*., 1988)], or alternatively *via* the C(2) hydrogen atom abstraction from the corresponding 2-alkyl-1,3-dioxolane **2** (Scheme 14).

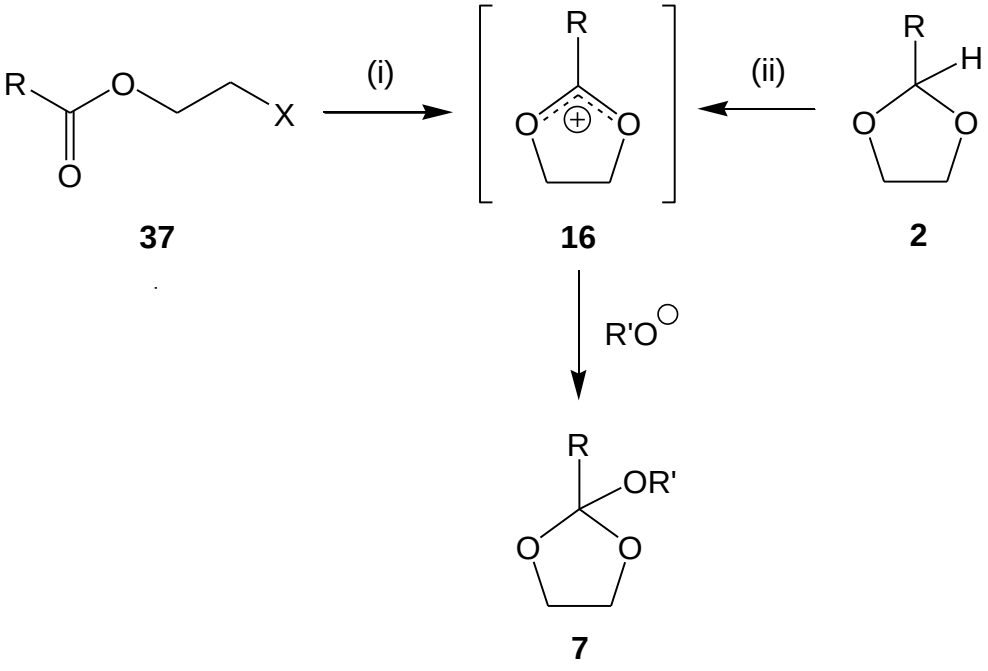

Scheme 14. General routes to **7** *via* esters **37** (i) X = Cl ($SbCl_5$); Br ($AgBF_4$); MeO ($Et_3O{:}BF_4$), or cyclic acetals **2** using (ii) $Ph_3C{:}BF_4$.

As 3,3-dimethyl-butanoyl chloride ($^{t}BuCH_2COCl$) **38** is commercially available, we chose to prepare cation **36a** (*i.e.,* **16** Scheme 14; where R = $^{t}BuCH_2$-) *via* the bromo ester **39** (*i.e.,* **37** Scheme 14; where R = $^{t}BuCH_2$-, X = Br), which was readily prepared in high yield (>80%) by the reaction of $^{t}BuCH_2COCl$ **38** with 2-bromoethanol. Treatment of **39** with $AgBF_4$ in anhydrous MeCN afforded the cation **36a** which was not isolated, but treated *in situ* with sodium methoxide to afford the *neo*-pentyl ortho ester **36** (*i.e.,* **7** Scheme 14; where R = $^{t}BuCH_2$-, R' = -OMe) in excellent yield (> 80%).

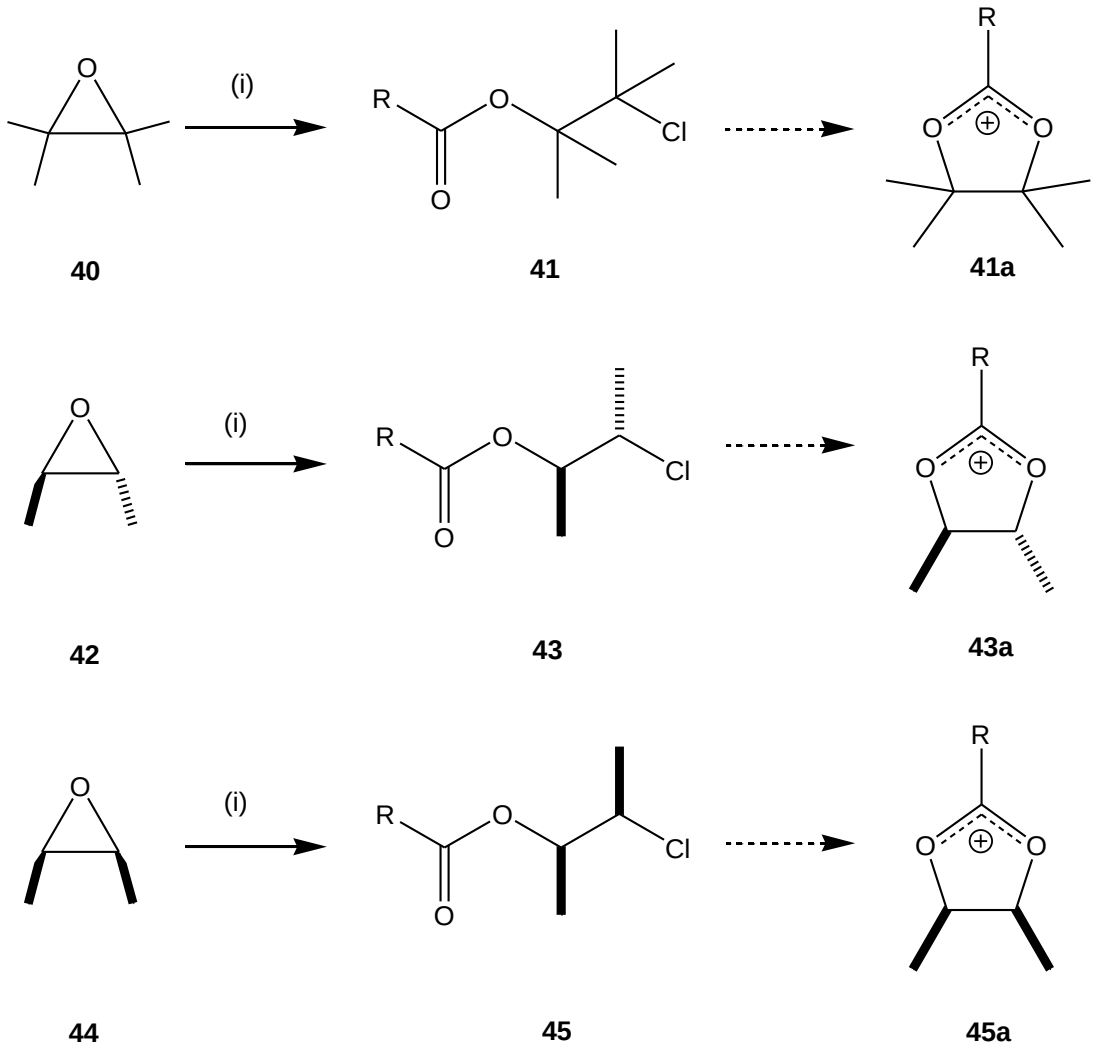

Scheme 15. Routes to C(4/5) alkyl substituted 1,3-dioxolan-2-ylium cations **41a**, **43a** and **45a** (R = $^{t}BuCH_2$-), *via* the corresponding β-chloro esters **41**, **43**, and **45**. Reagents: (i) $BiCl_3$ (5%), **38** ($^{t}BuCH_2COCl$).

Kinetic studies which clearly demonstrate that 2-*neo*-pentyl-2-methoxy-1,3-dioxolane **36** is highly reactive towards acid catalysed hydrolysis were presented earlier (Section 6.5.2). It was reasoned that C(4/5) alkyl substituted analogues of **36** might possess even greater transannular strain, thereby further accelerating the rate of hydrolysis. To this end, preliminary studies were undertaken to explore synthetic routes to the *neo*-pentyl cations **41a**, **43a** and **45a**, which in principle can be converted to the corresponding ortho esters by reaction with sodium methoxide (see Scheme 14). As *neo*-pentyl cations **41a**, **43a** and **45a** derive from the $AgBF_4$ facilitated cyclisation of the corresponding β-halo esters (*i.e.,* **41**, **44** and **45** respectively), it became necessary then to identify efficient, mild, high yielding, stereospecific (*i.e.,* particularly for **43** and **45**) routes to these compounds.

Stereospecific, yet experimentally arduous routes to β-halo esters *via* the chlorination of *E*/*Z* butenes have been known for some time (Fahey & Schubert, 1965). The cleavage of epoxides in the presence of an activated acyl equivalent to afford the corresponding β-chloro ester has been achieved using air sensitive ($TiCl_4$; Iranpoor & Zeynizadeh, 1998), expensive (Eu; Taniguchi *et al.*, 1998), or toxic (Hg/Al; Luzzio & Bobb, 1999) Lewis acids. A one-pot approach has been reported which uses a stoichiometric quantity of *tert*-butyldimethylsilyl chloride, along with a Cu catalyst (Singh *et al.*, 2002). However, the previously reported (Costello *et al.*, 2005) Bi(III) catalysed *O*-acylative cleavage of tetrahydrofurans has been successfully extended as part of this study. For the first time, epoxides have been shown to undergo a Bi(III) catalysed *O*-acylative cleavage in order to furnish a highly efficient, one-pot, stereospecific (*i.e.,* **43** and **45**) route to β-chloro esters (Scheme 15).

The novel 2,2,3,3-tetramethyl β-chloro ester **41** has been prepared in excellent yield (85%) by treating a mixture of epoxide **40** and $^{t}BuCH_2COCl$ (**38**), with $BiCl_3$ (5%) (Scheme 15). It should be pointed out that the corresponding β-bromo ester may in principle be prepared using the $^{t}BuCH_2COBr/BiBr_3$ combination. Furthermore, *trans* (±)-**42**, and *cis* (±)-**44** epoxides are quantitatively converted to the similarly novel *erythro* (±)-**43** and *threo* (±)-**45** diastereoisomers with excellent stereocontrol (*i.e.,* de > 97%). The relative stereochemistry of **43** and **45** are assigned on the basis of the similarity of the NMR data with respect to closely related diastereoisomerically pure compounds [*i.e.,* 3-chloro-2-butyl acetate (Fahey & Schubert, 1965), 3-bromo-2-butyl acetate (Högberg *et al.*, 1981), 3-hydroxy-2-butyl acetate (Atto *et al.*, 1983)]. The implication of this observed stereospecificity is that the Bi(III) catalysed *O*-acylative cleavage of epoxides **42** and **44** is consistent with a concerted S_N2 process wherein the ethereal C—O bond of the intermediate acyloxy:$BiCl_4^-$ ion pair becomes significantly polarised without actual cleavage prior to attack by the chloride anion (Figure 65) (Costello, and Draffin, 2005).

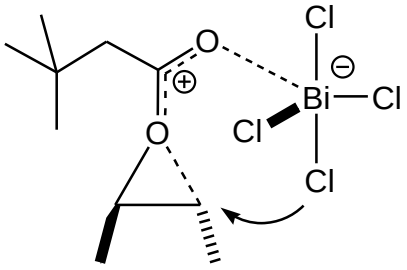

42

Figure 65. Proposed acyloxy:$BiCl_4^-$ ion pair intermediate consistent with *O*-acylative cleavage of epoxides (**42** shown).

Further work upon enhancing the reaction rates of *neo*-pentyl ortho esters by increasing the transannular demands of C(4/5) substituents will not be hindered by the synthetic demands of accessing halo esters **41**, **43** or **45**.

Chapter 8

The Partitioning Behaviour of Fuel Dehydrating / Icing Inhibitors

8.1 Introduction

Cyclic ortho esters present themselves as exciting, dual purpose agents because upon hydrolysis, the heterocyclic ring cleaves to afford hydrophilic alcohols which potentially incorporate as many sites for hydrogen bonding as the ice-inhibitor di-EGME (Figure 4). In order for the products of hydrolysis to express ice-inhibition properties, they must be sufficiently hydrophilic in order to partition preferentially into residual free water (Chang *et al.*, 1998). There will clearly be a tipping point for the ideal dual-reagent as the lipophilicity of the fuel dehydrating agent, and hydrophilicity of the potential icing inhibitor are inextricably linked. It has already been demonstrated that the rate at which a fuel dehydrating agent reacts with water is inextricably linked to molecular structure. Attention now turns to the relationship between the structure of the water scavenger, the structure of the resulting icing inhibitor, and the capacity of both to partition preferentially between the fuel and aqueous phases, respectively.

The octanol-water partition coefficient (K_{OW}) is a physical property extensively used to describe the lipophilic or hydrophilic properties of a molecule. It is the ratio of the concentrations of a given substance across the octanol-water phase when at equilibrium. Since values range across many orders of magnitude, the logarithm is commonly employed ($\log K_{OW}$). It is a valuable parameter in numerous quantitative structure-activity relationships (QSAR) that have been developed for the pharmaceutical, environmental, biochemical, and toxicological sciences (Hansch & Leo, 1995). Two well established computational methods [*i.e.*, KOWWIN™ of the US Environmental Protection Agency, and LogP (AB/LogP v2.0) of the National Chemical Database Service] have been used here to calculate $\log K_{OW}$ at 25°C. The effect of temperature on K_{OW} is usually in the order of 0.001 to 0.01 $\log K_{OW}$ units per degree, and may be either positive or negative. Both computational methods predict the log octanol-water partition coefficient by using an atom/fragment contribution method which can estimate $\log K_{OW}$ within ± 0.8 log units for over 96% of an experimental

dataset of >8000 compounds (Meylan & Howard, 1995). The fuel dehydrating agents discussed in Chapter 6 (Figure 63) are presented in ascending order of catalytic coefficient k_{H+} in Table 10. The corresponding hydrolysis products (*i.e.,* potential icing inhibitors) are listed alongside the fuel dehydrating agents. The average and the standard deviation of the calculated values of logK_{OW} for each structure, as determined using the KOWWIN™ and LogP computational programmes, are also presented in Table 10.

Table 10. Fuel dehydrating agents (FDA) presented in ascending order of catalytic coefficient k_{H+} (reported in Figure 63), along with the corresponding hydrolysis products. Calculated logK_{OW} and standard deviation presented alongside the structures. Experimentally determined values in parentheses (Hansch & Leo, 1995).

	FDA	logK_{ow}	Icing Inhibitor	logK_{ow}
27	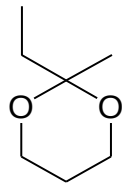	1.88 ± 0.52	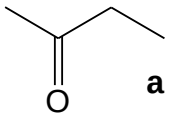 **a** 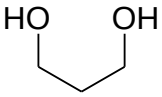 **b**	0.34 ± 0.11 (0.29) -0.89 ± 0.25 (-1.04)
23	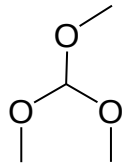	0.11 ± 0.19 (0.25)	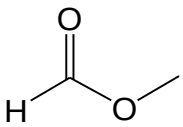	-0.12 ± 0.08 (0.03)
1	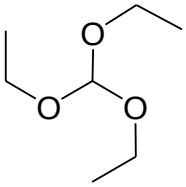	1.24 ± 0.30 (1.20)	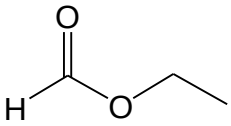	0.31 ± 0.02 (0.23)

28	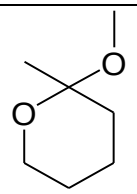	2.02 ± 0.33	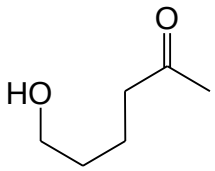	0.14 ± 0.52
25	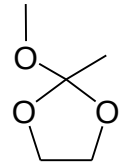	0.61 ± 0.59	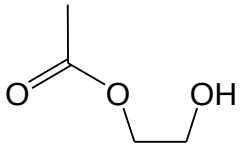	-0.55 ± 0.08
22	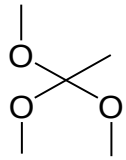	0.94 ± 0.28	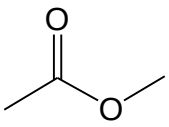	0.35 ± 0.04 (0.18)
30	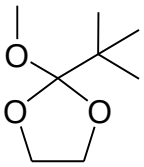	1.70 ± 0.96	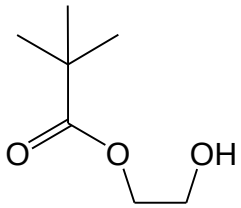	0.80 ± 0.05
26	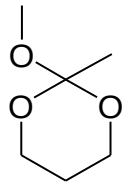	1.07 ± 0.62	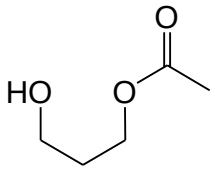	-0.14 ± 0.04
34	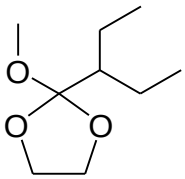	2.23 ± 0.97	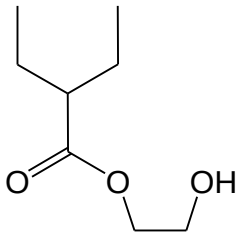	1.30 ± 0.01
31	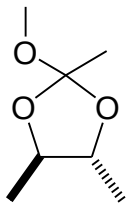	1.35 ± 0.71	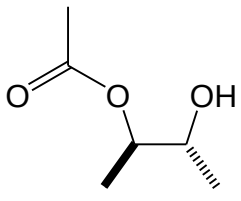	0.20 ± 0.05

32	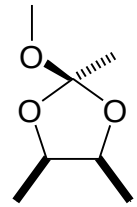	1.35 ± 0.71	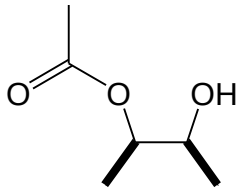	0.20 ± 0.05
35	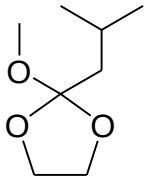	1.76 ± 0.94	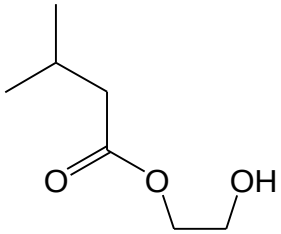	0.81 ± 0.01
24	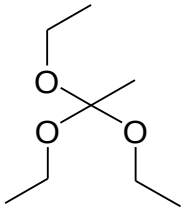	2.08 ± 0.74	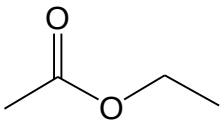	0.88 ± 0.02 (0.73)
33	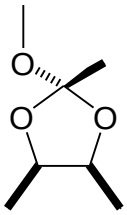	1.35 ± 0.71	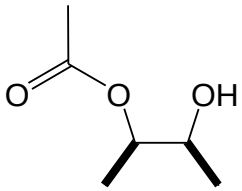	0.20 ± 0.05
29	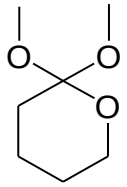	1.67 ± 0.47	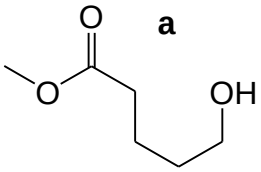 **a** 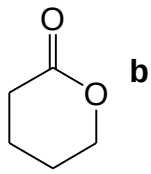 **b**	0.34 ± 0.06 0.05 ± 0.20 (-0.35)
36	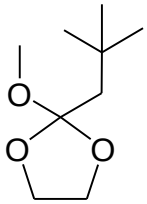	2.17 ± 1.00	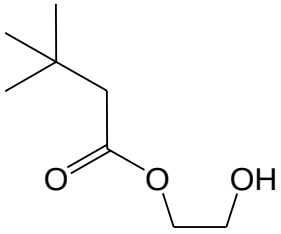	1.15 ± 0.15

A graphical representation of the logarithms of the relative rates of hydrolysis for the fuel dehydrating agents studied here (Figure 63), along with the corresponding values of logK_{ow} (Table 10), are presented in Figure 66. If it is assumed that octanol represents a reasonable surrogate for jet fuel, then a calculated value of logK_{ow} > 0 indicates a propensity to partition preferentially in the fuel phase. The x-axis in Figure 66 where logK_{ow} = 0, represents the boundary between the H_2O and fuel surrogate phases. Effective fuel system icing inhibitors are known to possess logK_{ow} approximately equal to, or certainly < 0 [di-EGME logK_{ow} = -0.68 (McDougal *et al.*, 2000)]. This is considered here to be a criteria for screening potential icing inhibitors (Stirling & Ripley, 1990).

It is clear to see then, that all fuel dehydrating agents considered in this study are predicted to partition preferentially into the fuel phase. If one were to screen FDII on the basis of hydrolysis products possessing logK_{ow} ≤ 0, then it is also clear that - in order of increasing logk_{H+} - **27**, **23**, **1**, **28**, **25**, **22**, **26**, **31-33**, and **29** are excellent candidates for further consideration. The preliminary study reported in Section 4.3 indicates that in the absence of added acid, FDII **1** undergoes 30% hydrolysis in just 30 minutes in Jet A-1. It is safe to say that FDII **27** and **23** will hydrolyse to a lesser extent during the same period of time. Equally, FDII occupying the top right quadrant of Figure 66 (expanded to afford Figure 67), will undergo hydrolysis to a greater extent during the same time period. Importantly, much like di-EGME, candidates **25**, **26**, **31-33**, and **29** possess one H-bond donor, and two H-bond acceptors, indicating their potential as effective icing inhibitors.

In summary, it is proposed that candidate FDII possess a sufficiently wide spectrum of performance enabling them to meet the equally broad range of operational requirements of the aviation industry.

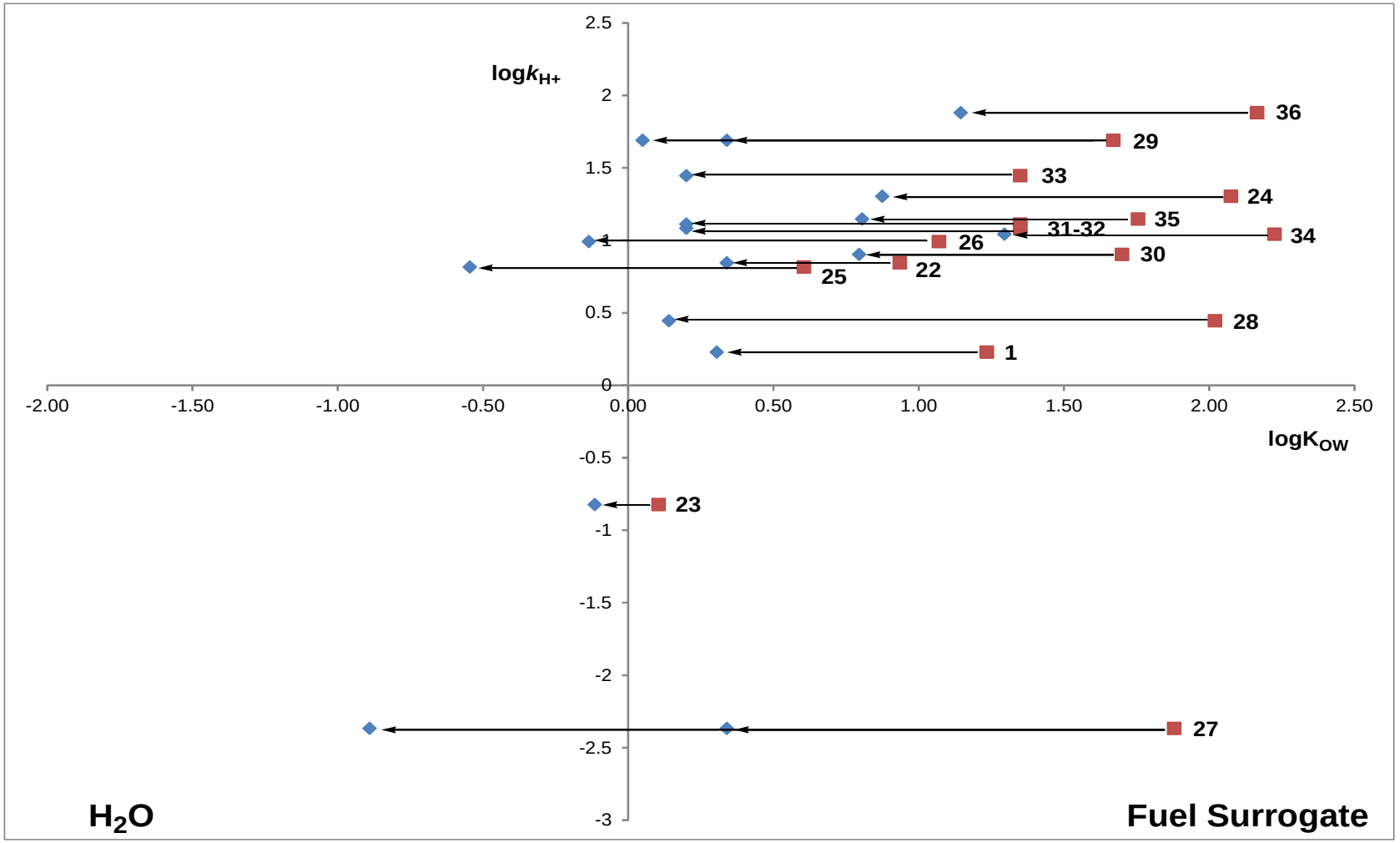

Figure 66. Graphical representation of logk_{H+} and logK_{ow} for candidate FDII ■ and hydrolysis products ◆ .

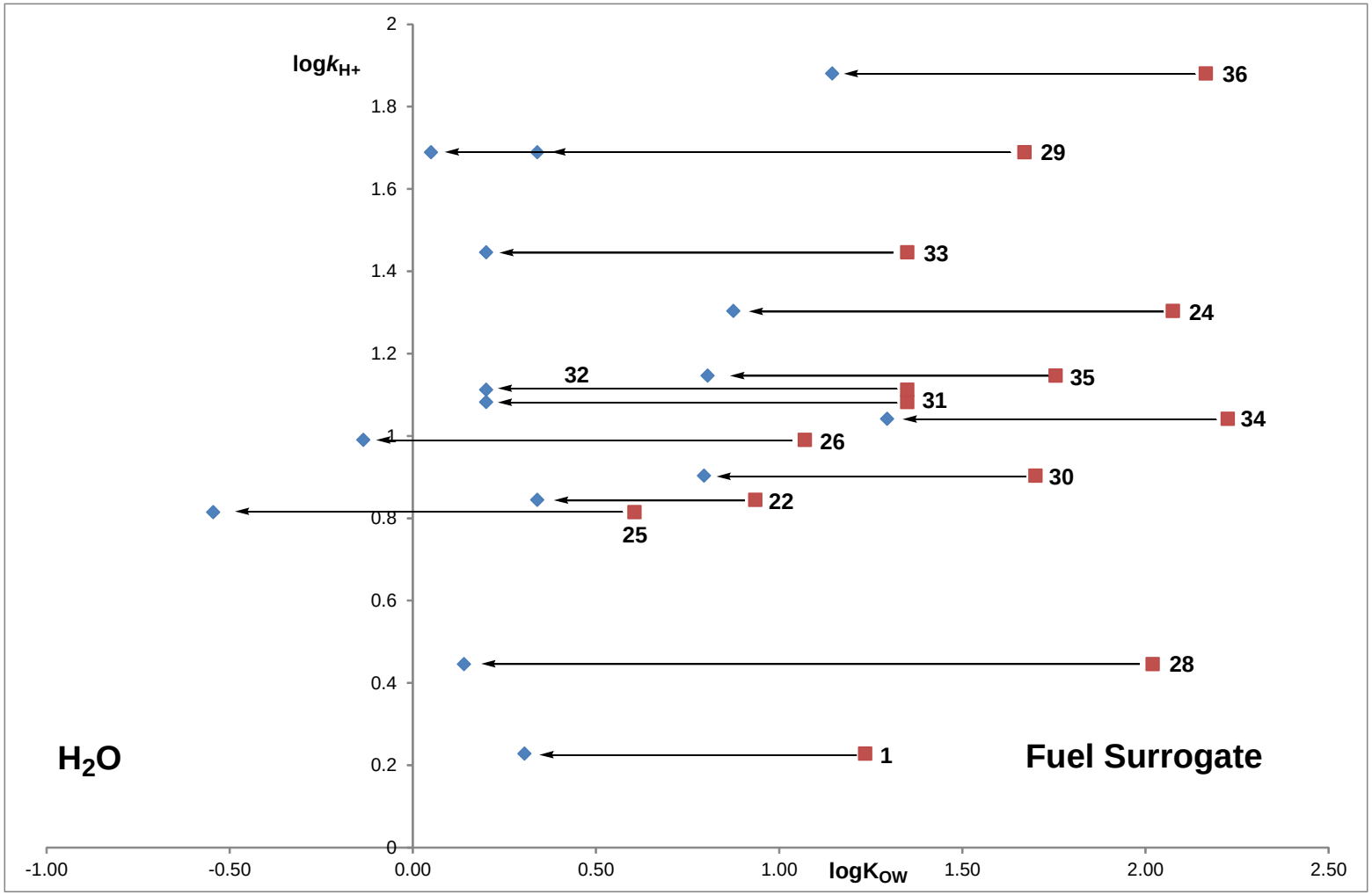

Figure 67. Expansion of the top right quadrant of Figure 66.

Chapter 9

Conclusions and Further Work

A clear and present need has been identified to reduce the risk of ice formation in aircraft fuel systems. This Thesis describes a novel approach to the management of water in jet fuel, based upon a dual-action fuel dehydrating/ice inhibition (FDII) strategy.

Preliminary studies to measure the water content of jet fuel using optical methods (UV-Vis and IR) indicate their potential for *in-situ* sensing systems in the future. However, further work is needed to develop these promising correlations into robust analytical methodologies which can overcome the challenges associated with the formation of emulsions (Chapter 3).

Jet fuel is a very complex organic solvent in which to optimise a chemical reaction. To ensure both clarity and reproducibility much of the work presented here has been performed in surrogates that mimic the fuel/water interface. The criteria for an ideal FDII were firstly identified, then used to screen a range of hydrolysable organic molecules, which led to a closer examination of water scavengers based upon geminal ethers. Indeed, such is the selectivity of germinal ethers towards water in jet fuel (see criterion outlined in Section 2.5), that the reaction constitutes a new method for the determination of water in jet fuel itself. This new analytical method has the potential to rival the industry standard KF titration. Further studies are required in order to determine the reproducibility and detection limits with respect to the KF titration method (Section 3.5).

Specifically, geminal ethers such as *exo*/*endo*-cyclic ketals of type **5**, and *endo*- and *exo*-cyclic ortho esters of type **7** and **8**, respectively, were identified as promising candidates (Section 4.2). These molecules and their products of hydrolysis, not only possess a low molecular mass, but they are expected to be highly combustible (see criteria outlined in Section 2.5). Preliminary studies confirmed for the first time that the inherent acidity of Jet A-1 was sufficient to catalyse the hydrolysis reactions of ortho esters (Section 4.3). This means that the FDII can be stored without degradation, even in the presence of water, and will only be activated when it comes into contact with acidic jet fuel. In this sense the FDII may be termed

"switchable", thereby meeting the criterion outlined in Section 2.5. Detailed kinetic measurements using ^{1}H NMR spectroscopy established that ortho esters are rapidly hydrolysed by dissociated acid catalysts, whilst a slower process occurs with an associated acid catalyst. The implications for the development of a water scavenger are that lipophilic ortho esters will hydrolyse slowly in jet fuel, yet rapidly at the interface with free water (Section 5.2).

In order to develop a kinetically fast system, a detailed and comprehensive qualitative analysis of the factors governing the rate of hydrolysis of geminal ethers has been presented. Furthermore, a unified and coherent overview of this highly complex field has been proposed (Chapter 5). A quantitative analysis of the factors influencing the rate of hydrolysis has been undertaken using reaction conditions relevant to the development of FDII. Detailed explanations have been provided in order to rationalise the data obtained. In doing so, we have been the first to invoke single and double anomeric effects to rationalise the reactivity of geminal ethers in five-membered ring systems (Chapter 6). To consolidate these stereoelectronic arguments, further kinetic analyses should be performed to verify the following predictions.

- Work here focusses upon five membered *endo*-cyclic ortho esters of type **7** because they are relatively easy to prepare (Section 7.2). However, we expect the corresponding *exo*-cyclic ortho esters of type **8** to undergo hydrolysis at a faster rate (Section 6.4).

- *Endo*-cyclic ketals of type **5** derived from 1,3-dioxolanes are expected to undergo hydrolysis at a faster rate than those derived from the corresponding 1,3-dioxanes (Section 6.4).

- Locking C(4/5) of 1,3-dioxolane **36** into a *trans* cyclohexane ring (derived from *trans*-1,2-cyclohexanediol) will attenuate half-chair ↔ envelope ring-flipping, and thereby prevent a double anomeric effect contributing towards the rate of hydrolysis (Section 6.5.2).

- The 1,3-dioxolane/-dioxane rings of the bicyclic ortho ester discussed in Scheme 12 are conformationally restricted through ring fusion. Although the hydrolysis reactions of these systems remain unexplored, a double anomeric effect and concomitant rate acceleration is anticipated to accompany the chair conformation of the 1,3-dioxane. Further advantages of this system include stoichiometry (*i.e.,* two molecules of water react with one molecule of scavenger), and the de-icing potential of the hydrolysis product (*i.e.,* 2 x HBD/A).

The synthesis of new compounds has been reported, and their stereochemistry has been unambiguously assigned using ^{1}H NMR spectroscopy. The anomeric effect is believed to play an important role in the transesterification reactions leading to novel ortho esters based upon C(4/5) substituted 1,3-dioxolanes (Section 7.2).

Another important factor in the choice of FDII has been the criterion of cheap and easy to synthesise; the synthesis of geminal ethers is based on inexpensive starting materials, simple steps, and high yields (Section 10.8). Furthermore, we have explored a new highly efficient, one-pot, stereospecific synthetic route to the precursors of novel C(4/5) substituted 1,3-dioxolane ortho esters (Section 7.3). Further study of these derivatives will deepen our understanding of how the double anomeric effect may be harnessed in order to fine-tune reaction rates, without having to resort to such lipophilic C(2) substituents *i.e., neo*-pentyl.

A library of geminal ethers possessing effective water scavenging properties has been assembled (Section 6.6). Calculated partitioning coefficients have been used to screen potential FDII candidates for further study (Section 8.1). Although the stereoelectronic contribution to the reaction rate of five-membered ring systems may be optimised through bulky substituents, the impact upon the lipophilicity of the hydrolysis products potentially undermines the partitioning properties of the de-icer (*i.e.,* **36**). Fuel/water partitioning is a fundamental criterion for the development of effective FDII. Having created a library of versatile water scavengers, focus can now shift towards the de-

icing properties of the hydrolysis products (Table 10). To this end, differential scanning calorimetry has been identified as the technique of choice for the preliminary examination of ice inhibition properties of the hydrolysis products in Jet A-1.

Although not discussed in this Thesis, preliminary calculations on the human/environmental toxicological profiling of geminal ethers with respect to Di-EGME have been published (Repetto *et al.*, 2013). Thermal stability and compatibility testing with all types of fuels, approved additives and materials, as per ASTM D4054, will be necessary to bring this novel solution to market.

In conclusion, an effective solution to a commercially important and technically challenging issue has been presented. All the criteria outlined in Section 2.5 have been met. Furthermore, a highly complex field has been unified, and a novel theoretical contribution to organic chemistry has been made.

Chapter 10

Experimental

10.1 General Experimental Procedures

Chemicals. The Jet A-1 fuel used throughout this study was obtained from Air BP, batch number BIS/HAL/12/035K. Concentrated HCl and H_2SO_4 were purchased from Fisher Scientific. All other materials were purchased from Sigma Aldrich to the highest level of purity, and used without further purification unless otherwise stated. Organic solvents *i.e.,* diethyl ether (Et_2O), dichloromethane (DCM) and acetonitrile (MeCN) were dried immediately prior to use by passing a commercially available pre-dried, oxygen-free formulation through an activated alumina column (Grubbs *et al.*, 1996).

Instrumentation. GC-MS measurements were carried-out using an Agilent 6890N GC system connected to an Agilent 5973N mass spectrometer. The GC column used was an Agilent HP-5MS capillary column (30m length x 0.25mm internal diameter coated with a film thickness of 0.25 µm of 5% phenyl and 95% dimethylpolysiloxane), with a helium flow rate of 1 mL/min. GC analyses were performed using an Agilent 5890 gas chromatograph equipped with a flame ionisation detector (FID). The GC column used was an Agilent HP-5MS capillary column, with a helium flow rate of 1.5 mL/min. HR-MS were performed by the mass spectrometry service at the School of Chemistry of the University of Bristol. Infrared analyses were performed using a Perkin Elmer FTIR spectrometer with NaCl plates in an Omni Specac cell with a pathlength of 1 mm. Sonication was performed using a Clifton DU-4 ultrasonic bath with operating frequency 30-40 kHz. UV-VIS spectrophotometric analyses were performed using an ATI Unicam UV2 spectrophotometer with quartz cuvettes. NMR spectra were recorded on a JEOL ECP Eclipse 300 spectrometer at 300 MHz (^1H), on a JEOL ECP Eclipse 400 spectrometer at 400 MHz (^1H) and 100 MHz (^{13}C) or on a Varian VNMRS500 spectrometer at 500 MHz (^1H) and 125 MHz (^{13}C) in anhydrous deuterated solvents at the University of Bristol.

All preparative operations and kinetic studies were performed at the synthetic laboratories of the School of Chemistry, University of Bristol. The yields of the reported synthetic preparations have not been optimised. Where an inert atmosphere of nitrogen was necessary, standard Schlenk line techniques were employed.

10.2 GC-MS Analysis of Jet A-1

This describes the experiments reported in Section 1.3.1.

A 10%v/v solution of Jet A-1 in hexane (1 µL) was injected into the GC port heated to 290ºC with a split ratio of 100:1. For this analysis, the oven temperature used was initially 50ºC held for 2 minutes. The temperature was then increased at a rate of 5ºC/min throughout the range 50 → 190ºC. The MS source temperature was 230ºC, with a scan range of 33-300 Daltons at 5.24 scans/s. The NIST MS Search 2.0 (National Institute of Standards and Technology, 2008) database was used for analysing the results. The software both forward matches and reverse matches the mass spectra of the actual components to the library spectra; it then calculates the probability of the accuracy of the assignments (Appendix B). Each peak was manually analysed, and background subtraction was used to maximise the identification of co-eluting compounds.

10.3 Water Content of Jet A-1 *via* Infrared Spectroscopy

This describes the experiments reported in Section 3.3.

Fuel was dried with 3Å molecular sieve for 12h and tested with a Coulometric Karl Fischer titrator before use. Standards of differing water content were prepared by adding measured volumes of distilled water *via* a SGE µl syringe, to anhydrous jet fuel (20 mL). The water was injected into the middle of the bulk of the fuel to minimise losses on the glassware. The

samples were ultrasonicated for 5 minutes prior to analysis to ensure the water was homogenously distributed. The absorbance was recorded (T = 21ºC); the averages of three analysis with corresponding standard deviation are reported in Table 11.

Table 11. Infrared frequencies and absorbance values for water/Jet A-1 solutions.

H_2O conc. (ppm v/v)	Frequency (cm^{-1})	Absorbance
10	3612	0.0010 ± 0.0001
	3707	0.0008 ± 0.0001
20	3612	0.0025 ± 0.0004
	3709	0.0018 ± 0.0002
30	3612	0.0039 ± 0.0005
	3709	0.0028 ± 0.0005
40	3607	0.0050 ± 0.0009
	3706	0.0032 ± 0.0003
250	3426	0.0377 ± 0.0140
500	3427	0.1563 ± 0.0300
1000	3430	0.2703 ± 0.0070
2000	3429	0.5167 ± 0.0120
3000	3431	0.5182 ± 0.2000

10.4 Water Content of Jet A-1 *via* Settling Rate (UV-VIS)

This describes the experiments reported in Section 3.4.

Aliquots of Jet fuel (dried overnight with 3Å molecular sieve), were placed in a 25 ml Schott Duran glass bottle, and deionised water was added using a SGE Analytical Science µl syringe. Just prior to analysis, the water was dispersed using sonication (5 minutes), and measurements recorded at one

minute intervals at λ = 370 nm. The procedure was repeated three times for each sample, and the data averaged to reduce experimental error. The gradients of the averaged settling curve (*i.e.*, absorbance *versus* time) for the first 20 minutes are reported in Table 12.

Table 12. Settling curve gradients (t = 0→20 min) for water/Jet A-1 solutions measure by UV-Vis spectrophotometry (λ = 370 nm).

H_2O conc. (ppm v/v)	Settling curve gradient
100	0.0013
250	0.0037
500	0.0061
750	0.0104
1000	0.0133

10.5 Water Content of Jet A-1 *via* Gas Chromatography

This describes the experiments reported in both Sections 3.5 and 4.3.

The following describes a modification of the procedure reported by Chen & Fritz (1991). The temperature of the detector and injector were fixed at 250ºC. The oven temperature used for the analysis was initially 80ºC held for 4 minutes. The oven temperature was increased at 20ºC/min to 240ºC and held for 2 minutes. Standards with different water concentrations (100-1250 ppm v/v) were prepared by adding measured volumes of distilled water by SGE µL syringes to anhydrous Jet A-1 (20 mL), taking extra care to inject the water into the middle of the solvent. Each standard was prepared just before use and sonicated for 5 minutes to ensure an equal distribution of water.

A reactant solution was prepared to enable a simple, one-step addition of all the necessary chemicals. Thus, triethyl orthoformate **1** (10 mL), 3-methylpentane (1 mL) and methanesulfonic acid (7.1 µL) were mixed in a 20 mL GC vial (Supelco Bellefonte, USA). Because of contamination from atmospheric moisture, it was necessary to prepare a new reactant solution each day. For the analysis, 100 µL of the reactant solution was added to 1 mL of a Jet A-1 sample in a 2 mL GC sample vial. The analysis was repeated three times for each sample and the average values of the RPA for ethanol (RT=1.68 min, see Figure 17) with the corresponding standard deviations are reported in Table 13.

Table 13. RPA of ethanol produced by the acid catalysed reaction of **1** with water/Jet A-1 solutions measured by GC-FID.

H_2O conc. (ppm v/v)	Ethanol RPA
100	0.0805 ± 0.0033
250	0.1273 ± 0.0024
400	0.1709 ± 0.0031
500	0.1958 ± 0.0033
750	0.2796 ± 0.0094
1000	0.3519 ± 0.0021
1250	0.4235 ± 0.0039

The same procedure was applied for the reaction of **1** with water/Jet A-1 solutions in the absence of added methanesulfonic acid (Section 4.3).

10.6 The Kinetic Analysis of the Acid Catalysed Hydrolysis of Trimethyl Orthoacetate (22)

This describes the experiments reported in Section 5.2.

Five buffered solutions of AcOH, and AcONa were prepared in de-ionised water (Table 14). As the ionic concentration of the solution has an impact on the rate of hydrolysis, NaCl was added to maintain the ionic strength at a constant value for all 5 solutions (Bunton & Reinheimer, 1970). Sodium chloride and sodium acetate were dried by heating them at 100ºC for 4 hours under vacuum.

Table 14. Buffer solutions in H_2O

Buffer	[AcOH] M	[AcONa] M	[NaCl] M
A	0.192	0.3947	0.3693
B	0.192	0.1920	0.5720
C	0.192	0.0658	0.6982
D	0.192	0.0480	0.7160
E	0.192	0.0185	0.7455

A solution of freshly distilled TMOA **22** (15 µL, 0.12 mmol) in anhydrous acetone–d_6 (500 µL) was added directly to a dry 5 mm NMR tube. The hydrolysis reaction was initiated by the addition of acetic acid/sodium acetate buffer solution (100 µL; A-E) to the NMR tube, which was gently agitated to ensure mixing. A 300 MHz NMR spectrometer was used to monitor the concentration of TMOA **22** with time (22ºC), by acquiring nine sequential ^{1}H NMR spectra every 600 s (actual delay time = 623 s). Pre-saturation solvent suppression technique was used to obscure the H_2O signal. An external reference was used by adding to the NMR tube a sealed capillary tube containing the sodium salt of 3-(trimethylsilyl)-1-propanesulfonic acid dissolved in D_2O (concentration = 0.1966 M).

The ^{1}H NMR spectrum of **22** consists of two singlets resonating at 3.15 and 1.33 ppm, assigned to the -OC*H*$_3$ and –C*H*$_3$ residues, respectively (integrating 3:1 – Figure 69). The relative peak area (RPA - proportional to concentration) was measured by comparing the –C*H*$_3$ resonance to that of the external reference.

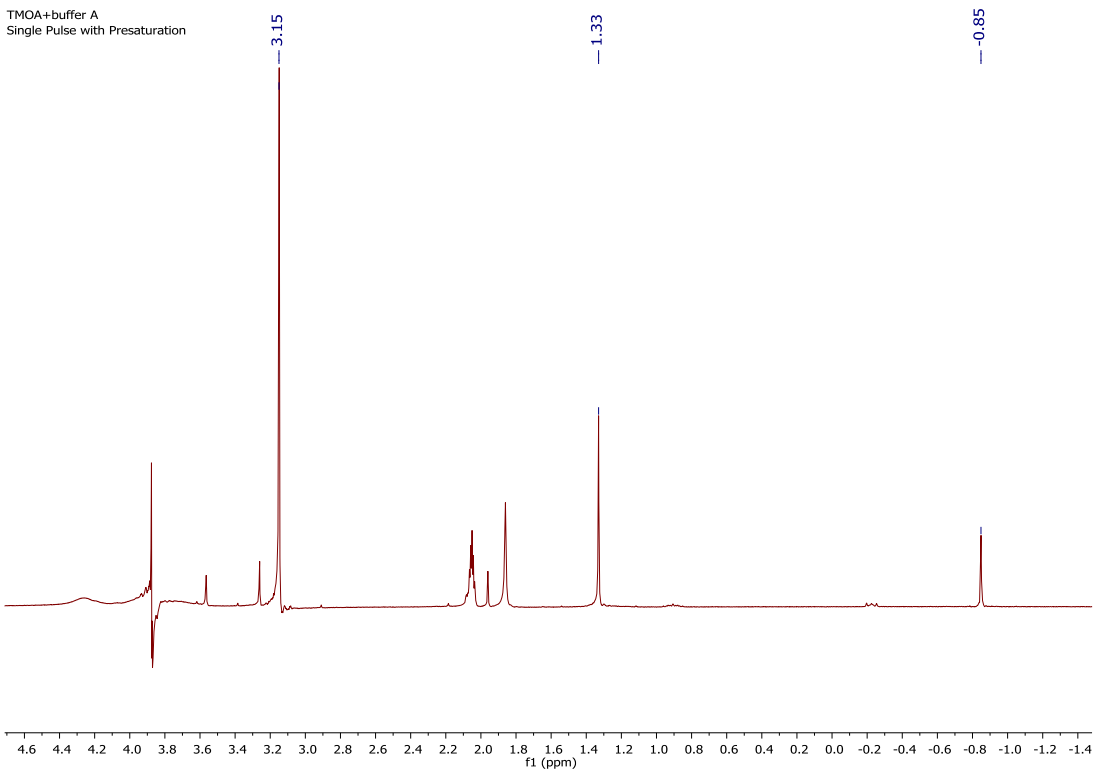

Figure 69. A typical ^{1}H NMR spectrum of **22** in acetone–d_6 with AcOH/AcONa buffer and TMS salt as external reference.

For the purposes of illustration, the data for buffer D (*p*H = 4.15) are tabulated in Table 15 and the corresponding plot is presented in Figure 70.

Table 15. Kinetic data for the hydrolysis of TMOA **22** using buffer D.

Time (s)	R.P.A.	ln(R.P.A.)
800	2.57	0.943906
1423	2.47	0.904218
2046	2.42	0.883768
2669	2.24	0.806476
3292	2.17	0.774727
3914	2.08	0.732368
4537	1.99	0.688135
5159	1.90	0.641854
5782	1.83	0.604316

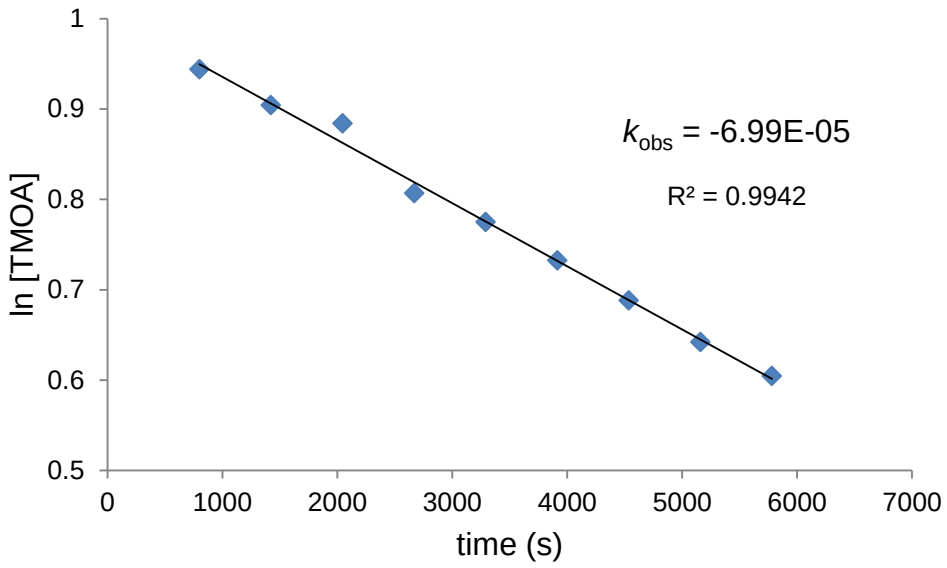

Figure 70. Plot of kinetic data for the reaction of TMOA with buffer D.

10.7 The Relative Rates of FDII Hydrolysis

This describes the experiments reported throughout Chapter 6. The acyclic ortho esters **1**, **22-24** are commercially available, whereas the cyclic derivatives **25**, **26**, **31-33**, and **36** were synthesised (see Section 10.8).

The reacting pair of **22** and **23** (Section 6.2) is used to illustrate a typical procedure. Modifications to the procedure to accommodate insufficient signal resolution at 300 MHz, were addressed by using higher fields (*i.e.,* 500 MHz). Adjustments to the acid catalyst concentration were made on an iterative basis in order to ensure the kinetic runs were complete within reasonable time-scales; these are presented in Table 16.

Freshly distilled **22** (38 µL, 0.3 mmol) and **23** (33 µL, 0.3 mmol) were added to anhydrous CD_3CN (1200 µL), and the resulting solution was equally divided into three dry 5 mm NMR tubes. ^1H NMR (300 MHz) spectroscopy was used to confirm the resulting 1:1 ratio of **22** and **23** in each sample. In order to minimise contamination by H_2O, acid solutions were prepared by the successive dilution of HCl (35% v/v) with D_2O. In this manner, a solution of $[H^+] = 4.78 \times 10^{-4}$ M was prepared. The hydrolysis reaction was initiated by the addition of HCl in D_2O (100 µL, 4.78×10^{-8} mol) to the NMR tube containing **22** and **23**. The solution was gently agitated to ensure mixing before being promptly returned to the ^1H NMR spectrometer where data was acquired every 625 s until the faster of the pair was consumed. A semi-logarithmic plot of the integral of the resonances associated with **22** (δ_H = 1.35ppm), and **23** (δ_H = 4.93ppm) against time (s) affords two straight lines with gradient = k_{obs}, which when divided by $[H^+]$, provides the catalytic coefficient k_{H+}. The process was repeated a further two times using the pre-prepared samples of **22** and **23**, and the results are presented below in Table 17.

Table 16. The concentration of acid catalyst used for determining values of k_{H+} for the following mixtures of reacting ortho esters.

Reacting Substrates	$[H^+] \times 10^{-4}$ M
22:23	4.78
1:23	4.78
22:24	1.98
22:25	1.98
22:26	1.98
22:31:32:33	1.98
22:36	0.125

Table 17. Corresponding values of k_{H+} ($M^{-1}s^{-1}$).

22	**23**
7.32	0.153
6.74	0.145
7.20	0.151

1	**23**
1.650	0.147
1.675	0.155
1.73	0.143

22	**24**
6.91	19.44
7.40	19.74
6.89	21.18

22	25
7.50	6.70
6.70	6.30
7.20	6.60

22	26
6.84	9.77
6.99	10.00
6.52	9.57

22	31	32	33
7.07	13.10	13.99	29.80
7.01	11.76	12.78	27.38
6.90	11.38	12.07	26.62

22	36
7.00	70.63
7.20	73.10
6.74	84.00

10.8 Synthesis of FDII

2-Methoxy-2-methyl-1,3-dioxolane (25)

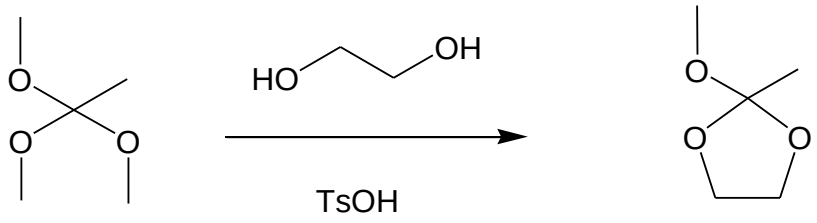

22 **25**

The cyclic ortho ester **25** was prepared *via* a modification of the method reported by McClelland *et al.* (1988), in order to improve the purity of the product. Thus, freshly distilled trimethyl orthoacetate **22** (18 g, 150 mmol) was added dropwise to a stirred solution of pre-dried ethylene glycol (9.5 g, 153 mmol), and toluene sulfonic acid (0.28 g, 1.5 mmol). The reaction mixture was stirred at room temperature for 2 hours under reduced pressure (water aspirator) to remove the methanol formed. The reaction was quenched by adding imidazole (0.1 g, 1.5 mmol), and distillation (105°C, 760 mmHg) of the crude reaction mixture afforded a clear colourless liquid characterised as 2-methoxy-2-methyl-1,3-dioxolane **25** (9.4 g, 53%); δ_H (400 MHz, $CDCl_3$) 1.54 (s, 3H), 3.27 (s, 3H), 3.95-4.11 (m, 4H); δ_C (100 MHz, $CDCl_3$) 21.6, 49.8, 65.0, 121.9. ^{1}H NMR data are in accord with the literature (McClelland *et al.*,1988; Yokoyama *et al.*, 1980).

2-Methoxy-2-methyl-1,3-dioxane (26)

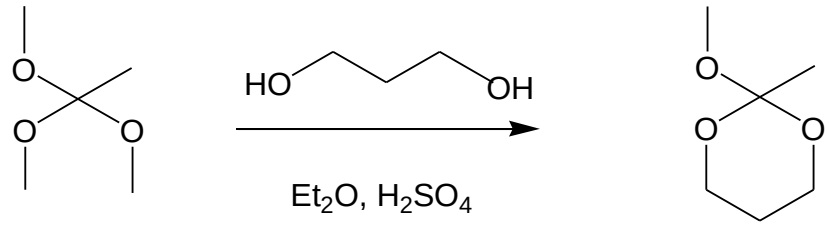

22 **26**

The cyclic ortho ester **26** was prepared *via* the method reported by van Maarseveen *et al.* (2011). Thus, freshly distilled **22** (20 mL, 157 mmol) was added with stirring to a pre-cooled (0°C) solution of 1,3-propanediol (8 mL, 110 mmol - freshly distilled from anhydrous K_2CO_3), and H_2SO_4 (240 µL, 4.5 mmol) in diethyl ether (60 mL) under nitrogen. The reaction mixture was allowed to warm to room temperature, whereupon triethylamine (2 mL, 14 mmol) was added, and the crude reaction mixture was washed with saturated aqueous $NaHCO_3$ solution (200 mL) and extracted with diethyl ether (3 x 50 mL). The combined ethereal extracts were dried (K_2CO_3), filtered, concentrated *in vacuo*, and distilled (30-32°C, 1 mmHg) to afford a clear colourless liquid characterised as 2-methoxy-2-methyl-1,3-dioxane **26** (9.7 g, 67%); δ_H (300 MHz, CD_3CN) 1.32 (s, 3H), 1.32-1.41 (m, $1H_{eq}$), 1.83-2.00 (m, $1H_{ax}$), 3.23 (s, 3H), 3.61-3.68 (m, $2H_{eq}$), 3.97-4.08 (m, $2H_{ax}$). ^1H NMR data are in accord with the literature (Lapuka *et al.*, 1981).

4(*RS*),5(*RS*)-2-Methoxy-2,4,5-trimethyl-1,3-dioxolane (31), *anti*-(32), and *syn*-4(*S*),5(*R*)-2-methoxy-2,4,5-trimethyl-1,3-dioxolane (33).

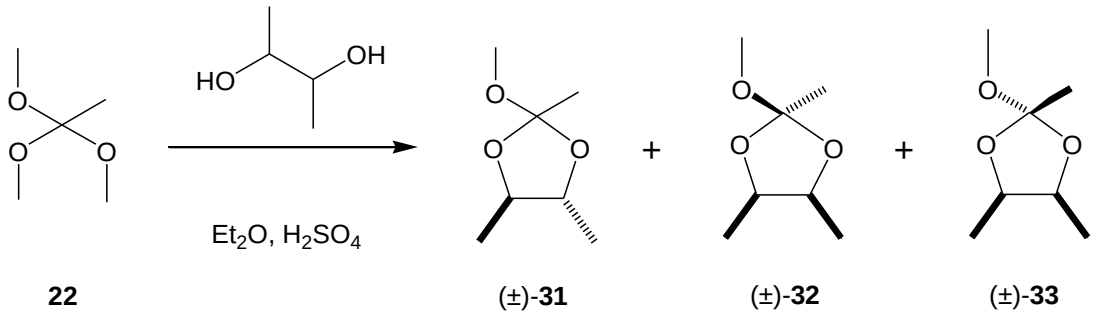

Freshly distilled **22** (9.3 mL, 73 mmol) was added with stirring to a pre-cooled (0°C) solution of 2,3-butanediol (6.6 g, 73 mmol), and H_2SO_4 (100 µL, 2.4 mmol) in diethyl ether (30 mL) under nitrogen. The reaction was quenched after 24 hours by the addition of imidazole (0.4 g, 6 mmol), and the resulting cloudy solution was washed with saturated aqueous $NaHCO_3$ (200 mL), filtered and extracted with diethyl ether (3 x 50 mL). The combined organic extracts were dried ($MgSO_4$), and concentrated *in vacuo* to afford a clear colourless liquid characterised (*via* 1D NOESY ^{1}H NMR spectroscopy) as a mixture of **31** (29%), **32** (19%) and **33** (52%) (4.3 g, 40%). Repeated distillations (37°C, 10 mmHg) failed to afford separation, and column chromatography (SiO_2, petroleum ether/ethyl acetate/triethylamine 15:4:1) simply resulted in the products of hydrolysis. δ_H (**31**) (500 MHz, $CDCl_3$) 1.25 (d, 3H, *J* 6.0 Hz), 1.30 (d, 3H, *J* 6.0 Hz), 1.53 (s, 3H), 3.29 (s, 3H), 3.72 (m, 1H), 3.84 (m, 1H); ^{1}H NMR data are in accord with the literature (van Maarseveen *et al.*, 2011). δ_H (**32**) (500 MHz, $CDCl_3$) 1.22 (m, 6H), 1.50 (s, 3H), 3.30 (s, 3H), 4.29 (m, 2H); δ_H (**33**) (500 MHz, $CDCl_3$) 1.15 (m, 6H), 1.56 (s, 3H), 3.28 (s, 3H), 4.41 (m, 2H). δ_C (**31-33**) (100 MHz, $CDCl_3$) 15.3, 15.5, 17.0, 17.4 [C(4/5)-*C*H_3)], 22.5, 23.3, 23.6 [C(2)-*C*H_3], 49.3*, 50.5 (-O*C*H_3), 73.9, 74.6, 79.1, 79.6 [*C*(4/5)], 120.0, 121.0 [*C*(2)]. *Signal splitting of $\Delta\delta$ = 0.09ppm observed. HR-MS(ESI) calculated for $[M+Na]^+$ 169.0835, found 169.0836.

(2'-Bromoethyl)-3,3-dimethylbutanoate (39)

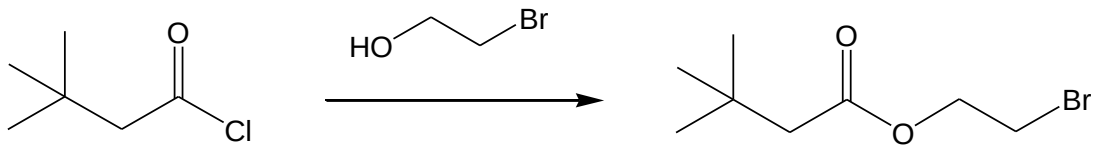

38 **39**

The ester **39** was prepared *via* a modification of the method reported by Liu *et al.* (2011). Freshly distilled 3,3-dimethyl-butanoyl chloride **38** (20 mL, 144 mmol) was added dropwise to 2-bromoethanol (10 mL, 130 mmol) under an atmosphere of dry nitrogen at 0ºC. The reaction was stirred for a further six hours at 0ºC, and then washed with saturated aqueous K_2CO_3 solution (2 x 30 mL), dried with anhydrous Na_2SO_4 and filtered to afford a light yellow oil characterised as (2'-bromoethyl)-3,3-dimethylbutanoate **39** (24 g, 83%); δ_H (400 MHz, $CDCl_3$) 1.04 (s, 9H), 2.24 (s, 2H), 3.51-4.38 (m, 4H); δ_C (100 MHz, CDCl3) 28.9, 29.8, 30.9, 47.9, 62.9, 172.0; HR-MS(CI) calculated for $[M+H]^+$ 223.0334, found 223.0328.

2-Methoxy-2-*neo*-pentyl-1,3-dioxolane (36)

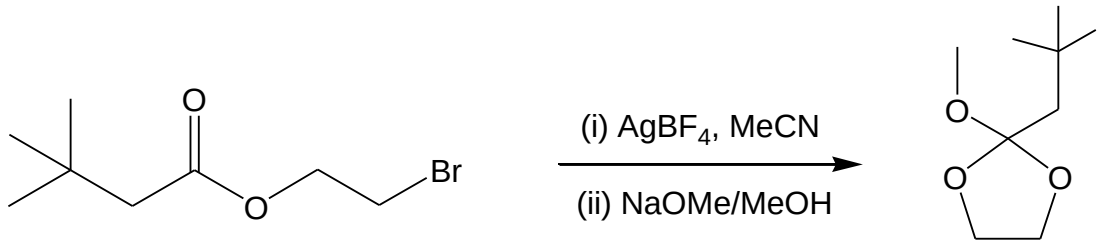

39 **36**

The ortho ester **36** was prepared *via* a modification of the method reported by Beringer and Galton (1967). The ester **39** (1.12 g, 5 mmol) was added to a stirred solution of anhydrous silver tetrafluoroborate (1.2 g, 6 mmol) in MeCN (50 mL) under an atmosphere of dry nitrogen for five hours. The supernatant of the resulting suspension was transferred *via* cannula directly to a stirred, cooled (0ºC) solution of sodium methoxide (0.5 g, 22 mmol of Na in 30 mL MeOH). The mixture was stirred under nitrogen for a further two hours. The crude reaction mixture was concentrated *in vacuo* to afford a slurry to which water was added (100 mL), and the resulting solution extracted with diethyl ether (3 x 40 mL). The combined extracts were dried with anhydrous K_2CO_3 and concentrated *in vacuo* to afford a yellow oil characterised as 2-methoxy-2-*neo*-pentyl-1,3-dioxolane **36** (0.7 g, 80%); δ_H (300 MHz, $CDCl_3$) 0.99 (s, 9H), 1.76 (s, 2H), 3.24 (s, 3H), 3.94-4.10 (m, 4H). ^{1}H NMR data are in accord with the literature (McClelland, *et al.*, 1988).

(2'-Chloro-1',1',2'-trimethylpropyl)-3,3-dimethylbutanoate (41)

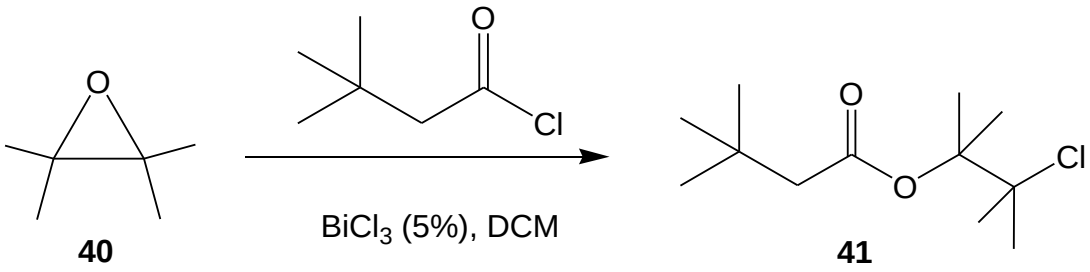

40 **41**

The ester **41** was prepared *via* a modification of the method reported by Costello *et al.* (2005). To a mixture of 3,3-dimethyl-butanoyl chloride (1.65 g, 12 mmol) and epoxide **40** (1.54 g, 15 mmol) in DCM (30 mL) was added $BiCl_3$ (0.3 g, 0.9 mmol) under an atmosphere of dry nitrogen. The solution was stirred at room temperature for 24 hours, after which time water (30 mL) was added to afford a suspension which was extracted with DCM (3 x 15 mL). The combined extracts were dried (K_2CO_3), filtered, concentrated *in vacuo* and distilled (50ºC, 8 mmHg) to afford an oil characterised as **41** (2.39 g, 85%); δ_H (400 MHz, $CDCl_3$) 1.03 (s, 9H), 1.63 (s, 6H), 1.68 (s, 6H), 2.13 (s, 2H); δ_C (100 MHz, $CDCl_3$) 21.1, 28.1, 29.9, 31.2, 49.5, 75.0, 85.8, 171.5. HR-MS(CI) calculated for $[M+H]^+$ 235.1465, found 235.1463.

[1'(*RS*),2'(*SR*),2'-Chloro-1'-methylpropyl]-3,3-dimethylbutanoate (43)

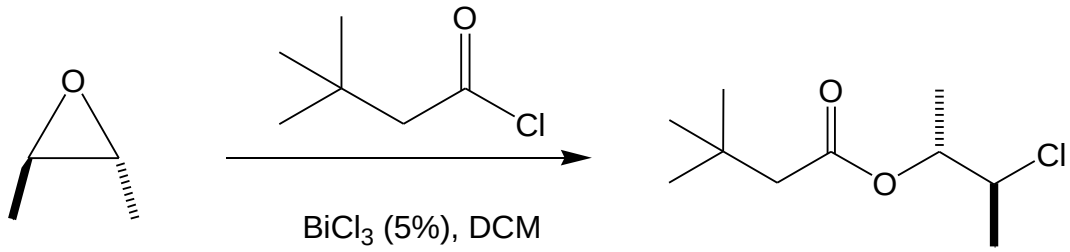

(±)-**42** (±)-**43**

To a mixture of 3,3-dimethyl-butanoyl chloride (0.85 g, 6.3 mmol) and *trans* epoxide (±)-**42** (0.46 g, 6.4 mmol) in DCM (20 mL) was added $BiCl_3$ (0.1 g, 0.32 mmol) under an atmosphere of dry nitrogen. The solution was stirred at room temperature for 24 hours, after which time the crude was concentrated *in vacuo* and extracted with $CHCl_3$ (3 x 15 mL). The combined extracts were dried (K_2CO_3), filtered through a plug of SiO_2, and concentrated *in vacuo* to afford a clear colourless oil characterised as (±)-**43** (1.13 g, 87%); δ_H (400 MHz, $CDCl_3$) 1.04 (s, 9H), 1.29 (d, 3H, *J* 6.4Hz), 1.48 (d, 3H, *J* 6.8Hz), 2.22 (s, 2H), 4.12 (dq, 1H, *J* 6.8, 4.2Hz), 4.99 (dq, 1H, *J* 6.4, 4.2Hz). δ_C (100 MHz, $CDCl_3$) 15.6, 20.8, 29.8, 31.0, 48.2, 59.5, 72.9, 171.8. HR-MS(CI) calculated for $[M+H]^+$ 207.1152, found 207.1149. GC retention times *anti* 12.44min and *syn* 12.56min; 37:1 respectively, de > 97%.

[1'(*RS*),2'(*RS*),2'-Chloro-1'-methylpropyl]-3,3-dimethylbutanoate (45)

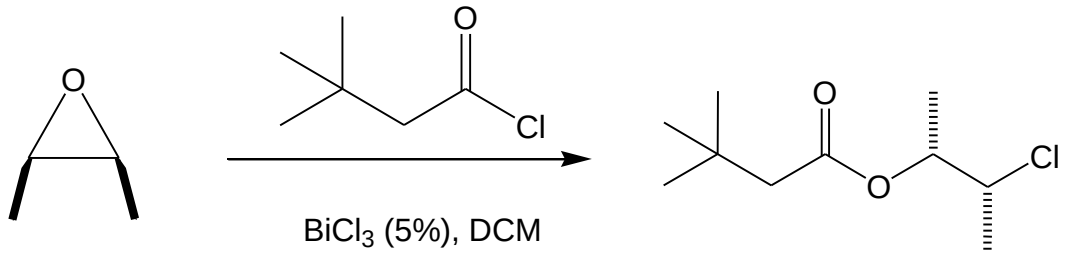

(±)-**44** (±)-**45**

To a mixture of 3,3-dimethyl-butanoyl chloride (1.87 g, 14 mmol) and (±)-**44** (0.98 g, 14 mmol) in DCM (20 mL) was added $BiCl_3$ (0.2 g, 0.6 mmol) under an atmosphere of dry nitrogen. The solution was stirred at room temperature for 24 hours, after which time the crude was concentrated *in vacuo* and extracted with $CHCl_3$ (3 x 15 mL). The combined extracts were dried (K_2CO_3), filtered through a plug of SiO_2, and concentrated *in vacuo* to afford a clear colourless oil characterised as (±)-**45** (2.6 g, 90%); δ_H (400 MHz, $CDCl_3$) 1.04 (s, 9H), 1.30 (d, 3H, *J* 6.4Hz), 1.49 (d, 3H, *J* 6.8Hz), 2.23 (s, 2H), 4.05 (dq, 1H, *J* 6.8, 4.5Hz), 5.04 (dq, 1H, *J* 6.4, 4.6Hz); δ_C (100 MHz, $CDCl_3$) 16.6, 20.7, 29.8, 31.0, 48.2, 58.9, 72.6, 171.7. HR-MS(CI) calculated for $[M+H]^+$ 207.1152, found 207.1145. GC retention times *anti* 12.44min and *syn* 12.56min; 1:44, respectively, de > 98%.

10.9 The Preparation of Isotopically Labelled Hydroxy Esters

This describes labelling experiments reported earlier in Section 6.5.2.

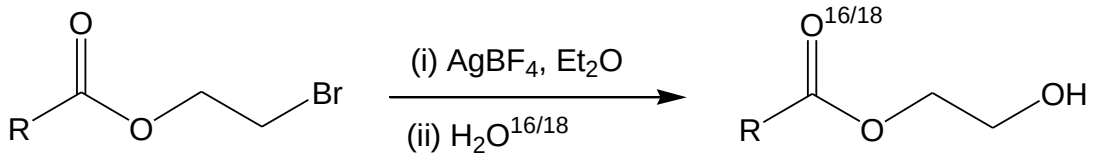

R = Me- (**46**);
R = *t*-BuCH_2(**39**)

R = Me- (**25ϕ**);
R = *t*-BuCH_2(**36ϕ**)

Ester **39** (0.09 g, 0.4 mmol) was added to a stirred solution of anhydrous silver tetrafluoroborate (0.12 g, 0.6 mmol) in Et_2O (5 mL) under an atmosphere of dry nitrogen for five hours. H_2O^{18} (15 μL, 0.8 mmol) was added directly to the reaction mixture which was stirred under nitrogen for a further hour. The crude reaction mixture was passed through a plug of basic alumina then concentrated *in vacuo* to afford a clear oil characterised as **36ϕ** (0.05g, 78%); δ_H (400 MHz, $CDCl_3$) 0.99 (s, 9H), 2.20 (s, 2H), 2.54 (br, 1H), 3.43 (m, 2H), 4.15 (m, 2H); δ_C (100 MHz, $CDCl_3$) 15.3, 30.8, 47.9, 61.2, 65.9, 172.8. HR-MS(CI) calculated for $[M+H-H_2O]^+$ 143.1067, found 143.1074.

The hydroxy ester **25ϕ** was prepared *via* a similar procedure starting from ester **46** (Liu *et al.*, 2011), and characterised accordingly. δ_H (400 MHz, $CDCl_3$) 2.06 (s, 3H), 3.10 (br, 1H), 3.82 (t, 2H), 4.20 (t, 2H); δ_C (100 MHz, $CDCl_3$) 20.6, 60.6, 65.9, 172.2. ^1H and ^{13}C NMR data are in accord with the literature (Wan & Muralidharan, 1988; Kizhakkedathu *et al*., 2012; Béguin *et al*., 1982).

10.10 Computational Techniques

X-Ray crystal structures were located in the 2014 release of the Cambridge Structural Database (CSD v 5.35, which contains 658, 007 entries) using the Conquest software (v 1.16) and visualised using the Mercury software package (v 3.1).

Molecular modelling calculations were performed using the Gaussian09 software package at the density functional level of theory, using the hybrid functional B3LYP/6-31G* to optimise structures (Becke, 1993; Lee, Yang & Parr, 1988).

LogK_{OW} values were calculated using two programs:

- KOWWIN™ from the EPI suite of the US Environmental Protection Agency (US EPA, 2013)
- LogP (AB/LogP v2.0) from the ACD/I-Lab of the National Chemical Database Service (Advanced Chemistry Development Inc, 2013).

The values reported in Table 10 are the average of the two results.

Reaxys is a fully indexed and organized database of around 16,000 periodicals containing 500 million published experimental facts, 37 million reactions and synthesis information for over 25 million substances, as well as bibliographic data. It was used to search for key chemical formulas, physicochemical properties, and experimental procedures reported in this Thesis (Elsevier Information Systems GmbH, 2014).

References

Adams, R.K., Zabarnick, S., West, Z.J., Striebich, R.C. & Johnson, D.W. (2013) Chemical Analysis of Jet Fuel Polar, Heteroatomic Species via High-Performance Liquid Chromatography with Electrospray Ionization–Mass Spectrometric Detection. *Energy & Fuels*, 27 (5), 2390–2398.

Advanced Chemistry Development Inc (2013) *ACD/I-Lab2 Predictor*.

Agosta, A., Cernansky, N., Miller, D., Faravelli, T. & Ranzi, E. (2004) Reference components of jet fuels: kinetic modeling and experimental results. *Experimental Thermal and Fluid Science*, 28 (7), 701–708.

Allen, F.H. (2002) The Cambridge Structural Database: a quarter of a million crystal structures and rising. *Acta Crystallographica Section B*., 58, 380–388.

Altona, C. & van der Veek, A.P.M. (1968) Conformation of non-aromatic ring compounds—XLIV. *Tetrahedron*, 24 (12), 4377–4391.

Amovilli, C. & Floris, F.M. (2003) Solubility of water in liquid hydrocarbons: a bridge between the polarizable continuum model and the mobile order theory. *Physical Chemistry Chemical Physics*, 5 (2), 363–368.

ASTM (2007) ASTM D6304 - 07 *Standard Test Method for Determination of Water in Petroleum Products, Lubricating Oils, and Additives by Coulometric Karl Fischer Titration.*

ASTM (2013) *ASTM D7566 - 13 Standard Specification for Aviation Turbine Fuel Containing Synthesized Hydrocarbons*.

Atkins, P. & de Paula, J. (2006) *Physical Chemistry*. W. H. Freeman.

Atto, S.Y., Tedder, J.M. & Walton, J.C. (1983) Free radical substitution. Part 38. The effect of solvent on the atomic chlorination and bromination of 2-substituted butanes and the importance of steric effects. *Journal of the Chemical Society, Perkin Transactions 2*, (5), 629–633.

Atwood, J.L., Hamada, F., Robinson, K.D., Orr, G.W. & Vincent, R.L. (1991) X-ray diffraction evidence for aromatic π hydrogen bonding to water. *Nature*, 349 (6311), 683–684.

Baena-Zambrana, S., Repetto, S.L., Lawson, C.P. & Lam, J.K.-W. (2013) Behaviour of water in jet fuel—A literature review. *Progress in Aerospace Sciences*, 60 35–44.

Baldwin, J.E. (1976) Rules for ring closure. *Journal of the Chemical Society, Chemical Communications*, (18), 734–736.

Becke, A.D. (1993) A new mixing of Hartree–Fock and local density-functional theories. *Journal of Chemical Physics*, 98 (2), 1372–1377.

Béguin, C., Barrelle, M. & Tessier, S. (1982) Carbon-13 NMR of oxygenated derivatives of polyoxyethylenes. *Organic Magnetic Resonance*, 19 (2), 102–104.

Berger, T.A. (1996) Separation of a gasoline on an open tubular column with 1.3 million effective plates. *Chromatographia*, 42 (1-2), 63–71.

Beringer, F. & Galton, S. (1967) 2-(2’,6'-Dimethoxyphenyl)-1,3-dioxolenium Fluoroborate. A Stable Carboxonium Salt. Reactions as an Alkylating Agent. *Journal of Organic Chemistry*. 32 (8), 2630–2632.

Boeing (2010) *Evaluation of Bio-Derived Synthetic Paraffinic Kerosenes (Bio-SPKs)*.

Brinkhaus, K.-H.G., Steckhan, E. & Degner, D. (1986) Indirect electrochemical side-chain oxidation of alkyl aromatic compounds - selective synthesis of methyl benzoates or ortho-benzoic acid trimethylesters. *Tetrahedron*, 42 (2), 553–560.

Brönsted, J.N. & Wynne-Jones, W.F.K. (1929) Acid catalysis in hydrolytic reactions. *Transactions of the Faraday Society*, 25, 59-76.

Brown, W., Iverson, B., Anslyn, E. & Foote, C. (2013) *Organic Chemistry*. Seventh Ed. Cengage Learning.

Buckley, N. & Oppenheimer, N.J. (1996) Reactions of Charged Substrates. 7. The Methoxymethyl Carbenium Ion Problem. 2. A Semiempirical Study of the Kinetic and Thermodynamic Stabilities of Linear and Cyclic Oxo- and Thiocarbenium Ions Generated from Aldehyde Hydrates, Hemiacetals, Acetals, and Methyl Ribosides and Glucosides. *Journal of Organic Chemistry*, 61 (23), 8048–8062.

Buergi, H.B. & Dunitz, J.D. (1983) From crystal statics to chemical dynamics. *Accounts of Chemical Research*, 16 (5), 153–161.

Bunton, C.A. & Reinheimer, J.D. (1970) Electrolyte effects on the hydrolysis of acetals and ortho esters. *Journal of Physical Chemistry*, 74 (26), 4457–4464.

C.R.C. (2004) *Handbook of Aviation Fuel Properties (CRC Report No. 635)*. 3rd edition.

Caira, M.R. & de Wet, J.F. (1981) 4,4,5,5-Tetramethyl-2-phenyl-1,3-dioxolan-2-ylium dichloroiodate(I). *Acta Crystallographica Section B: Structural Crystallography and Crystal Chemistry,* 37 (3), 709–711.

Carey, F.A. & Sundberg, R.J. (2007) *Advanced Organic Chemistry: Part A: Structure and Mechanisms*. Springer.

Carpenter, M.D., Hetherington, J.I., Lao, L., Ramshaw, C., Yeung, H., Lam, J.K.-W., Masters, S. & Barley, S. (2011) Behaviour of water in aviation fuels at low temperatures. *12th International Conference on Stability, Handling and Use of Liquid Fuels*, Sarasota, Florida, USA.

Chang, J.H., Beal, E.J., Stalick, W.M. & Mushrush, G. (1998) Fuel System Icing Inhibitors: the Synthesis of Esters of Oxaacids. *Petroleum Science and Technology*, 16 (9-10), 979–1000.

Chaplin, M. (2014) *Water structure and science*. Available from: http://www1.lsbu.ac.uk/water/.

Chen, J. & Fritz, J.S. (1991) Gas chromatographic determination of water after reaction with triethyl orthoformate. *Analytical Chemistry*, 63 (18), 2016–2020.

Childs, R.F., Orgias, R.M., Lock, C.J.L. & Mahendran, M. (1993) The structures of dioxolan-2-ylium cations; carbon–oxygen bond distances in acetoxonium ions. *Canadian Journal of Chemistry*, 71 (6), 836–845.

Colket, M., Edwards, T., Williams, S., Cernansky, N.P., Miller, D.L., Egolfopoulos, F., Lindstedt, P., Seshadri, K., Dryer, F.L., Law, C.K., Friend, D., Lehnert, D.B., Pitsch, H., Sarofim, A., et al. (2007) Development of an experimental database and kinetic models for surrogate jet fuels. *45th American Institute of Aeronautics and Astronautics Aerospace Sciences Meeting and Exhibit*, Reno, Nevada, USA.

Conrad, M.P. & Strauss, H.L. (1987) Nearly free rotation of water and ammonia in alkanes and other weakly interacting solvents. *Journal of Physical Chemistry*, 91 (6), 1668–1673.

Cordes, E.H. & Bull, H.G. (1974) Mechanism and catalysis for hydrolysis of acetals, ketals, and ortho esters. *Chemical Reviews*, 74 (5), 581–603.

Corey, E.J. & Raju, N. (1983) A new general synthetic route to bridged carboxylic ortho esters. *Tetrahedron Letters*, 24 (50), 5571–5574.

Costello, J.F., Barucki, H., Coles, S.J. & Hursthouse, M.B. (2001) Synthesis and structure of organoantimony (V) cyclometallates: transannular interactions and the barrier to cyclisation. *Journal of Organometallic Chemistry*, 622 (1-2), 265–273.

Costello, J.F., Coles, S.J., Draffin, W.N., Hursthouse, M.B. & Paver, S.P. (2005) Bi(III) halides as efficient catalysts for the O-acylative cleavage of tetrahydrofurans: an expeditious entry to tetralins. *Tetrahedron*, 61 (18), 4447–4452.

Costello, J.F., Draffin, W.N. & Paver, S.P. (2005) Bi(III) Catalysed O-acylative cleavage of 2,5-dimethyltetrahydrofuran: a substrate dependent borderline mechanism. *Tetrahedron*, 61 (28), 6715–6719.

Cox, B.G. (1994) *Modern Liquid Phase Kinetics*. Oxford University Press, Incorporated.

Dagaut, P., Reuillon, M., Boettner, J.-C. & Cathonnet, M. (1994) Kerosene combustion at pressures up to 40 atm: Experimental study and detailed chemical kinetic modeling. *Symposium (International) on Combustion*, 25 (1), 919–926.

Deslongchamps, P. (1975) Stereoelectronic control in the cleavage of tetrahedral intermediates in the hydrolysis of esters and amides. *Tetrahedron*, 31 (20), 2463–2490.

Deslongchamps, P., Dory, Y.L. & Li, S. (2000) The Relative Rate of Hydrolysis of a Series of Acyclic and Six-Membered Cyclic Acetals, Ketals, Orthoesters, and Orthocarbonates. *Tetrahedron*, 56 (22), 3533–3537.

Deslongchamps, P., Lessard, J. & Nadeau, Y. (1985) The products of hydrolysis of cyclic orthoesters as a function of pH and the theory of stereoelectronic control. *Canadian Journal of Chemistry*, 63 (9), 2485–2492.

Economou, I.G. & Tsonopoulos, C. (1997) Associating models and mixing rules in equations of state for water/hydrocarbon mixtures. *Chemical Engineering Science*, 52 (4), 511–525.

Eisenberg, D. & Kauzmann, W. (2005) *The Structure and Properties of Water*. Oxford University Press Incorporated.

Elsevier Information Systems GmbH (2014) *Reaxys*.

Van Etten, R.L. & Risley, J.M. (1979) An oxygen-18 isotope shift upon carbon-13 NMR spectra and its application to the study of oxygen exchange kinetics. *Journal of the American Chemical Society*, 101 (1), 252–253.

Van Etten, R.L. & Risley, J.M. (1980) Oxygen-18 isotope effect in carbon-13 nuclear magnetic resonance spectroscopy. 2. The effect of structure. *Journal of the American Chemical Society*, 102 (14), 4609–4614.

Fahey, R.C. & Schubert, C. (1965) Polar Additions to Olefins. I. The Chlorination of 2-Butene and 1-Phenylpropene. *Journal of the American Chemical Society*, 87 (22), 5172–5179.

Feller, D. (1999) Strength of the Benzene−Water Hydrogen Bond. *Journal of Physical Chemistry A*, 103 (38), 7558–7561.

Fife, T.H. (1972) General acid catalysis of acetal, ketal, and ortho ester hydrolysis. *Accounts of Chemical Research*, 5 (8), 264–272.

Fife, T.H. (1967) Participation of solvent and general acids in acetal hydrolysis. Hydrolysis of 2-(para-substituted phenyl)-4,4,5,5-tetramethyl-1,3-dioxolanes. *Journal of the American Chemical Society*, 89 (13), 3228–3231.

Fife, T.H., Bembi, R. & Natarajan, R. (1996) Neighboring Carboxyl Group Participation in the Hydrolysis of Acetals. Hydrolysis of o -Carboxybenzaldehyde cis - and trans -1,2-Cyclohexanediyl Acetals. *Journal of the American Chemical Society*, 118 (51), 12956–12963.

Frysinger, G.S. & Gaines, R.B. (1999) Comprehensive Two-Dimensional Gas Chromatography with Mass Spectrometric Detection (GC × GC/MS) Applied to the Analysis of Petroleum. *Journal of High Resolution Chromatography*, 22 (5), 251–255.

Gallwey, F.B., Hawkes, J.E., Haycock, P. & Lewis, D. (1990) 1H NMR spectra and conformations of propane-1,2-diol, meso- and racemic butane-2,3-diols, and some alditols in non-aqueous media. *Journal of the Chemical Society, Perkin Transactions 2*, (11), 1979.

Goodger, E.M. (2000) *Transport Fuels Technology: From Well to Wheels, Wings, and Water*. Landfall Press.

Grein, F. & Deslongchamps, P. (1992) The anomeric and reverse anomeric effect. A simple energy decomposition model for acetals and protonated acetals. *Canadian Journal of Chemistry*, 70 (5), 1562–1572.

Grob, R.L. & Barry, E.F. (2004) *Modern Practice of Gas Chromatography*. John Wiley & Sons.

Grubbs, R.H., Pangborn, A.B., Giardello, M.A., Rosen, R.K. & Timmers, F.J. (1996) Safe and Convenient Procedure for Solvent Purification. *Organometallics*, 15 (5), 1518–1520.

Guéret, C., Cathonnet, M., Boettner, J.-C. & Gaillard, F. (1991) Experimental study and modeling of kerosene oxidation in a jet-stirred flow reactor. *Symposium (International) on Combustion*, 23 (1), 211–216.

Guthrie, J.P. (1980) Energetic restrictions on the allowed range of catalyst pKas for general-acid- or general-base-catalyzed reactions of carbonyl compounds. *Journal of the American Chemical Society*, 102 (16), 5286–5293.

Hansch, C. & Leo, A. (1995) *Exploring Qsar: Hydrophobic, Electronic, and Steric Constants*. American Chemical Society.

Hemighaus, G., Boval, T., Bacha, J., Barnes, F., Franklin, M., Gibbs, L., Hogue, N., Jones, J., Lesnini, D., Lind, J. & Morris, J. (2006a) *Aviation Fuels Technical Review.* Chevron Corporation.

Hemighaus, G., Boval, T., Bosley, C., Organ, R., Lind, J., Brouette, R., Thompson, T., Lynch, J. & Jones, J. (2006b) *Alternative Jet Fuels. Technical Report.* Chevron Corporation.

Hill, T. (2003) Microbial growth in aviation fuel. *Aircraft Engineering and Aerospace Technology*, 75 (5), 497–502.

Högberg, H.-E., Byström, S. & Norin, T. (1981) Chiral synthesis of (2s,3s,7s)-3,7-dimethylpentadecan-2-yl acetate and propionate, potential sex pheromone components of the pine saw-fly neodiprion sertifer (geoff.). *Tetrahedron*, 37 (12), 2249–2254.

I.A.T.A. (2011) *IATA 2011 Report on alternative fuels. Technical Report*.

I.A.T.A. (2013) *Press release n. 72*.

Innospec (2010) *Material Safety Data Sheet Stadis (R) 450*. Available from: http://www.petrochemenergy.com/products.aspx.

Iranpoor, N. & Zeynizadeh, B. (1998) Efficient and Regioselective Conversion of Epoxides into Vicinal Chloroesters with TiCl4 and Imidazole in Ethyl Acetate. *Journal of Chemical Research*, (9), 582–583.

Iverson, B.L. & Martinez, C.R. (2012) Rethinking the term “pi-stacking”. *Chemical Science*, 3 (7), 2191.

Jencks, W.P. (1972) General acid-base catalysis of complex reactions in water. *Chemical Reviews*, 72 (6), 705–718.

Jensen, J.L. & Wuhrman, W.B. (1983) Acid-catalyzed hydrolyses of 2-alkoxytetrahydropyrans: evidence for the changeover from an A-1 to an ASE2 mechanism. *Journal of Organic Chemistry*, 48 (24), 4686–4691.

Kankaanperä, A. (1969) Basicities of the Oxygen Atoms in Symmetrical and Unsymmetrical Acetals. Part I. The Determination of Base Strengths by Infrared Spectroscopy. *Acta Chemica Scandinavica*, 23, 1723–1727.

Kenkel, J. (2002) *Analytical Chemistry for Technicians*. Third Edition. CRC Press Book.

Kirby, A.J. (1996) *Stereoelectronic Effects*. Oxford University Press Incorporated.

Kirby, A.J., Hartwell, E. & Hodgson, D.R.W. (2000) Exploring the Limits of Efficiency of Proton-Transfer Catalysis in Models and Enzymes. *Journal of the American Chemical Society*, 122 (38), 9326–9327.

Kizhakkedathu, J.N., Shenoi, R.A. & Lai, B.F.L. (2012) Synthesis, characterization, and biocompatibility of biodegradable hyperbranched polyglycerols from acid-cleavable ketal group functionalized initiators. *Biomacromolecules*, 13 (10), 3018–3030.

Klamt, A. (2003) Prediction of the mutual solubilities of hydrocarbons and water with COSMO-RS. *Fluid Phase Equilibria*, 206 (1-2), 223–235.

Kocienski, P.J. (2005) *Protecting Groups*. Thieme.

Kresge, A.J., Ahmad, M., Bergstrom, R.G., Cashen, M.J., Chiang, Y., McClelland, R.A. & Powell, M.F. (1979a) Ortho ester hydrolysis: direct evidence for a three-stage reaction mechanism. *Journal of the American Chemical Society*, 101 (10), 2669–2677.

Kresge, A.J., Bergstrom, R.G., Cashen, M.J. & Chiang, Y. (1979b) Ortho ester hydrolysis: concerted nature of the dialkoxycarbonium ion forming stage. *Journal of Organic Chemistry*, 44 (10), 1639–1642.

Kresge, A.J., Burt, R.A., Chambers, C.A., Chiang, Y., Hillock, C.S. & Larsen, J.W. (1984) Heats of formation of 1,3-dioxolenium ions from ortho ester precursors in sulfuric acid solution: methyl vs. phenyl substitution at the pro-acyl carbon atom. *Journal of Organic Chemistry*, 49 (14), 2622–2624.

Kresge, A.J., Chiang, Y., Lahti, M.O. & Weeks, D.P. (1983) Hydrolysis of ortho esters: further investigation of the factors that control the rate-determining step. *Journal of the American Chemical Society*, 105 (23), 6852–6855.

Kresge, A.J., Chiang, Y., Salomaa, P. & Young, C.I. (1974) Effect of phenyl substitution on ortho ester hydrolysis. *Journal of the American Chemical Society*, 96 (14), 4494–4499.

Krynitsky, J.A., Crellin, J. & Carhart, H. (1950) *The behavior of water in jet fuels and the clogging of micronic filters at low temperatures. Naval Research Laboratory Report 3604.*

Lahti, M. (1987) Solvent Deuterium Isotope Effect on the Rate of the Uncatalyzed Hydrolysis of Phenyl Dimethyl Orthoformates. *Acta Chemica Scandinavica*, 41a, 93–97.

Lahti, M. & Kauppi, K. (1986) Rate-Equilibrium Relationship for General Acid-Catalyzed and Uncatalyzed Hydrolyses of Acetaldehyde Methyl Phenyl Acetals. *Acta Chemica Scandinavica*, 40a, 533–537.

Lam, J.K.-W., Carpenter, M.D., Williams, C.A. & Hetherington, J.I. (2014) Water solubility characteristics of current aviation jet fuels. *Fuel*, 133, 26–33.

Lao, L., Ramshaw, C., Yeung, H., Carpenter, M., Hetherington, J., Lam, J.K.-W. & Barley, S. (2011) Behaviour of Water in Jet Fuel in a Simulated Fuel Tank. *SAE Technical Paper 2011-01-2794*.

Lapuka, L.F., Chalova, O.B., Kantor, E.A., Kiladze, T.K. & Rakhmankulov, D.L. (1981) Synthesis and three-dimensional structure of 5,5-disubstituted 2-alkoxy-1,3-dioxanes. *Chemistry of Heterocyclic Compounds*, 17 (9), 876–879.

Lee, C., Yang, W. & Parr, R.G. (1988) Development of the Colle-Salvetti correlation-energy formula into a functional of the electron density. *Physical Review B*., 37 (2), 785–789.

Liu, M.-L., Feng, L.-S., Wang, S., Chai, Y., Lv, K., Shan, G.-Z., Cao, J., Li, S.-J. & Guo, H.-Y. (2011) Synthesis of naphthyridone derivatives containing 8-alkoxyimino-1,6-dizaspiro[3.4]octane scaffolds. *Tetrahedron*, 67 (43), 8264–8270.

Luzzio, F.A. & Bobb, R.A. (1999) Organomercury/aluminum-mediated acylative cleavage of cyclic ethers. *Tetrahedron*, 55 (7), 1851–1858.

Lykov, O.P., Slovetskii, V.I., Frolova, N. V., Kitashova, G. V. & Emel'yanov, V.E. (1989) Mechanism of action of alcohol-ester anti-icing additives in automotive gasolines. *Chemistry and Technology of Fuels and Oils*, 25 (9), 440–444.

Van Maarseveen, J.H., Detz, R.J., Abiri, Z., le Griel, R. & Hiemstra, H. (2011) Enantioselective copper-catalysed propargylic substitution: synthetic scope study and application in formal total syntheses of (+)-anisomycin and (-)-cytoxazone. *Chemistry European Journal*, 17 (21), 5921–5930.

Maniatis, K., Weitz, M., Zschocke, A., Schroecker, D., Deurwaarder, E. & Schild, P. (2013) *2 million tons per year: A performing biofuels supply chain for EU aviation. Technical Report.* European Commission.

McClelland, R.A., Ahmad, M., Bohonek, J. & Gedge, S. (1979) Carbonyl oxygen exchange of glycol monoesters. Rate and equilibrium constants for the formation of a tetrahedral intermediate. *Canadian Journal of Chemistry*, 57 (12), 1531–1540.

McClelland, R.A., Gedge, S. & Bohonek, J. (1981) Nature of the slow step in the hydrolysis of cyclic and bicyclic ortho esters containing 1,3-dioxane rings. *Journal of Organic Chemistry*, 46 (5), 886–891.

McClelland, R.A., Santry, L.J. & Azer, S. (1988) Alkyl group effects on the rate constants and equilibrium constants for formation of cyclic tetrahedral intermediates. *Journal of the American Chemical Society*, 110 (9), 2909–2914.

McDougal, J.N., Pollard, D.L., Weisman, W., Garrett, C.M. & Miller, T.E. (2000) Assessment of Skin Absorption and Penetration of JP-8 Jet Fuel and Its Components. *Toxicological Sciences*, 55 (2), 247–255.

Meerwein, H., Bodenbenner, K., Borner, P., Kunert, F., Müller, K.W., Sasse, H.J., Schrodt, H. & Spille, J. (1955) Organische Ionenreaktionen. *Angewandte Chemie*, 67 (14-15), 374–380.

Meerwein, H., Borner, P., Fuchs, O., Sasse, H.J., Schrodt, H. & Spille, J. (1956) Reaktionen mit Alkylkationen. *Chemische Berichte*, 89 (9), 2060–2079.

Mendham, J., Denney, R.C., Barnes, J.D. & Thomas, M.J.K. (2006) *Vogel's Textbook Of Quantitative Chemical Analysis*. Sixth Edition. Pearson Education.

Meshako, C.E., Bleckmann, C.A. & Goltz, M.N. (1999) Biodegradability and microbial toxicity of aircraft fuel system icing inhibitors. *Environmental Toxicology*, 14 (4), 383–390.

Meylan, W.M. & Howard, P.H. (1995) Atom/fragment contribution method for estimating octanol-water partition coefficients. *Journal of Pharmaceutical Sciences*, 84 (1), 83–92.

Ministry of Defence (2011) *Defence Standard 91-91, Issue 7. Turbine Fuel, Kerosine Type, Jet A-1 NATO Code: F-35 Joint Service Designation: AVTUR. Technical Report*.

Moses, C.A. (2008) *Comparative Evaluation of Semi-Synthetic Jet Fuels. Technical Report*.

Murray, B.J., Broadley, S.L. & Morris, G.J. (2011) Supercooling of water droplets in jet aviation fuel. *Fuel*., 90 (1), 433–435.

Murray, B.J., Broadley, S.L., Wilson, T.W., Bull, S.J., Wills, R.H., Christenson, H.K. & Murray, E.J. (2010) Kinetics of the homogeneous freezing of water. *Physical Chemistry Chemical Physics,* 12 (35), 10380–10387.

Mushrush, G.W., Beal, E.J., Hardy, D.R., Hughes, J.M. & Cummings, J.C. (1999) Jet Fuel System Icing Inhibitors: Synthesis and Characterization. *Industrial & Engineering Chemistry Research*, 38 (6), 2497–2502.

Mushrush, G.W., Stalick, W.M., Beal, E.J., Basu, S.C., Slone, J.E. & Cummings, J. (1997) The Synthesis of Acetals and Ketals of the Reduced Sugar Mannose as Fuel System Icing Inhibitors. *Petroleum Science and Technology*,15 (3-4), 237–244.

Natelson, R.H., Kurman, M.S., Cernansky, N.P. & Miller, D.L. (2008) Experimental investigation of surrogates for jet and diesel fuels. *Fuel*, 87 (10-11), 2339–2342.

National Institute of Standards and Technology (2008) *NIST MS Search*.

National Research Council (1997) *Aviation Fuels with Improved Fire Safety: A Proceedings, Part 3*. National Academies Press.

Nilsson, S.-O. (1986) Enthalpies of solution of water in benzene and in some n-alkanes. *Journal of Chemical Thermodynamics*, 18 (9), 877–884.

Noè, M., Perosa, A. & Selva, M. (2013) A flexible Pinner preparation of orthoesters: the model case of trimethylorthobenzoate. *Green Chemistry*, 15 (8), 2252–2260.

Ohno, K., Okimura, M., Akai, N. & Katsumoto, Y. (2005) The effect of cooperative hydrogen bonding on the OH stretching-band shift for water clusters studied by matrix-isolation infrared spectroscopy and density functional theory. *Physical Chemistry Chemical Physics,* 7 (16), 3005–3014.

Oliveira, M.B., Coutinho, J.A.P. & Queimada, A.J. (2007) Mutual solubilities of hydrocarbons and water with the CPA EoS. *Fluid Phase Equilibria*, 258 (1), 58–66.

Oreshenkov, a. V. (2004) Accumulation of Water in Jet Fuels. Mathematical Modeling of the Process. *Chemistry and Technology of Fuels and Oils*, 40 (5), 320–325.

Paulsen, H. (1971) *Advances in Carbohydrate Chemistry and Biochemistry*. Advances in Carbohydrate Chemistry and Biochemistry. Elsevier.

Paulsen, H. & Dammeyer, R. (1976) Carboxoniumverbindungen in der Kohlenhydratchemie, XXIX. Untersuchungen über die Ladungsverteilung bei 1,3-Dioxolan-2-ylium-Ionen. *Chemische Berichte*, 109 (5), 1837–1849.

Pittman, C.U., McManus, S.P. & Larsen, J.W. (1972) 1,3-Dioxolan-2-ylium and related heterocyclic cations. *Chemical Reviews*, 72 (4), 357–438.

Pittman, C.U., Patterson, T.B. & Kispert, L.D. (1973) Intermediate neglect of differential overlap theoretical studies. 2-Substituted 1,3-dioxolan-2-ylium ions. *Journal of Organic Chemistry*, 38 (3), 471–475.

Pohanish, R.P. (2011) *Sittig's Handbook of Toxic and Hazardous Chemicals and Carcinogens*. William Andrew.

Potts, R.A. & Schaller, R.A. (1993) Kinetics of the hydrolysis of orthoesters: A general acid-catalyzed reaction. An undergraduate physical organic chemistry experiment using NMR to determine both rate constants of a two-route mechanism. *Journal of Chemical Education*, 70 (5), 421–424.

Ragozin, N.A. (1961) *Jet propulsion fuels: translated from the Russian*. Pergamon Press.

Repetto, S.L., Costello, J.F., De Lacy Costello, B., Ratcliffe, N.M. & Lam, J.K.-W. (2013) The Development of Novel Fuel Dehydrating Icing Inhibitors. *SAE International Journal of Fuels and Lubricants*, 6 (3), 553–563.

Richard, J.P., Williams, K.B. & Amyes, T.L. (1999) Intrinsic Barriers for the Reactions of an Oxocarbenium Ion in Water. *Journal of the American Chemical Society*, 121 (36), 8403–8404.

Ruelle, P., Buchmann, M., Nam-Tran, H. & Kesselring, U.W. (1992) Enhancement of the solubilities of polycyclic aromatic hydrocarbons by weak hydrogen bonds with water. *Journal of Computer-Aided Molecular Design*, 6 (5), 431–448.

Ruelle, P. & Kesselring, U.W. (1996) Nonlinear dependence of the solubility of water in hydrocarbons on the molar volume of the hydrocarbon. *Journal of Solution Chemistry*, 25 (7), 657–665.

S.G.S. Oil (2012) *Jet A-1 Full Test Report. Test Certificate No:AV12-00033.001*.

Saebø, S., Cordell, F.R. & Boggs, J.E. (1983) Structures and conformations of cyclopentane, cyclopentene, and cyclopentadiene. *Journal of Molecular Structure: THEOCHEM*, 104 (1-2), 221–232.

Santry, L.J. & McClelland, R.A. (1983) Orientation effects on the rate and equilibrium constants for formation and decomposition of tetrahedral intermediates. *Journal of the American Chemical Society*, 105 (19), 6138–6141.

Schab, H.W. (1960) Problems associated with water contaminated jet fuels. *Journal of the American Society for Naval Engineers*, 72 (1), 41–60.

Schulz, H. (1999) Short history and present trends of Fischer–Tropsch synthesis. *Applied Catalysis A: General*, 186 (1-2), 3–12.

Seidov, S.I. & Prokhvatilova, L.I. (2008) Temperature dependence of IR absorption spectra of water in aromatic hydrocarbons. *Petroleum Chemistry*, 48 (4), 318–321.

Shafer, L., Striebich, R., Gomach, J. & Edwards, T. (2006) *Chemical Class Composition of Commercial Jet Fuels and Other Specialty Kerosene Fuels. AIAA Paper 2006-7972*.

Shaw, R.A., Durant, A.J. & Mi, Y. (2005) Heterogeneous surface crystallization observed in undercooled water. *Journal of Physical Chemistry B*., 109 (20), 9865–9868.

Singh, V.K., Chandra, K.L., Bisai, A. & Saravanan, P. (2002) A one-pot synthesis of β-chloro acetates/benzoates from epoxides. *Journal of Chemical Research*, 2002 (5), 221–223.

Sleight, P.A. & Carter, R.D.G. (2010) *Report on the accident to Boeing 777-236ER, G-YMMM, at London Heathrow Airport on 17 January 2008.* Air Accidents Investigation Branch, Department of Transport (UK).

Smith, M. (1970) *Aviation Fuels*. G. T. Foulis.

Stirling, K.Q. & Ripley, D.L. (1990) Partition Coefficients of Icing Inhibitors in JP-4 and JP-5 Jet Fuels, Final Report DEFC22-83FE60149. U.S. Department of Energy and Naval Air Propulsion Center.

Taniguchi, Y., Tanaka, S., Kitamura, T. & Fujiwara, Y. (1998) Lanthanoid-catalyzed ring-opening reaction of epoxides with acyl halides. *Tetrahedron Letters*, 39 (25), 4559–4560.

Taylor, S.E. (2008) Component Interactions in Jet Fuels: Fuel System Icing Inhibitor Additive. *Energy & Fuels*, 22 (4), 2396–2404.

Trohalaki, S., Pachter, R. & Cummings, J.R. (1999) Modeling of Fuel-System Icing Inhibitors. *Energy & Fuels*, 13 (5), 992–998.

Tschitschibabin, A.E. (1905) Ueber die Bildung von unvollständig hydrirten Pyridinen bei der Reaction von Wyschnegradsky-Ladenburg. *Berichte der deutschen chemischen Gesellschaft*, 38 (4), 3834–3834.

Tsonopoulos, C. (2001) Thermodynamic analysis of the mutual solubilities of hydrocarbons and water. *Fluid Phase Equilibria*, 186 (1-2), 185–206.

Tsonopoulos, C. (1999) Thermodynamic analysis of the mutual solubilities of normal alkanes and water. *Fluid Phase Equilibri,* 156 (1-2), 21–33.

US EPA (2013) *Estimation Programs Interface Suite™ for Microsoft® Windows*.

USA Department of Defence (2012) *Detail Specification: Turbine Fuel, Aviation, Kerosene Type, JP-8 (NATO F-34), NATO F-35, and JP-8+100 (NATO F-37). MIL-DTL-83133H, Amendment 1*.

Violi, A., Yan, S., Eddings, E.G., Sarofim, A.F., Granata, S., Faravelli, T. & Ranzi, E. (2002) Experimental formulation and kinetic model for JP-8 surrogate mixtures. *Combustion Science and Technology*, 174 (11-12), 399–417.

Wagner, R., Benz, S., Möhler, O., Saathoff, H., Schnaiter, M. & Schurath, U. (2005) Mid-infrared extinction spectra and optical constants of supercooled water droplets. *Journal of Physical Chemistry A*., 109 (32), 7099–7112.

Wan, P. & Muralidharan, S. (1988) Structure and mechanism in the photo-retro-aldol type reactions of nitrobenzyl derivatives. Photochemical heterolytic cleavage of carbon-carbon bonds. *Journal of the American Chemical Society*, 110 (13), 4336–4345.

Wenthe, A.M. & Cordes, E.H. (1965) Concerning the Mechanism of Acid-Catalyzed Hydrolysis of Ketals, Ortho Esters, and Orthocarbonates 1. *Journal of the American Chemical Society*, 87 (14), 3173–3180.

West, F.G., Bender, J.A. & Daves, S. (1998) 1,3-Dioxolan-2-ylium cations from acylfurans: Conversion of furyl ketones to esters under nonoxidative conditions. *Tetrahedron Letters*, 39 (15), 2051–2054.

Van der Westhuizen, R., Ajam, M., De Coning, P., Beens, J., de Villiers, A. & Sandra, P. (2011) Comprehensive two-dimensional gas chromatography for the analysis of synthetic and crude-derived jet fuels. *Journal of Chromatography A*., 1218 (28), 4478–4486.

Wiberg, K.B., Martin, E.J. & Squires, R.R. (1985) Thermochemical studies of carbonyl compounds. 3. Enthalpies of hydrolysis of ortho esters. *Journal of Organic Chemistry*, 50 (24), 4717–4720.

Willy, W.E., Binsch, G. & Eliel, E.L. (1970) Conformational analysis. XXIII. 1,3-Dioxolanes. *Journal of the American Chemical Society*, 92 (18), 5394–5402.

Winstein, S., Anderson, C.B. & Friedrich, E.C. (1963) The cis-cyclohexene acetoxonium ion. 2-methyl-cis-4,5-tetramethylene-1,3-dioxolenium tetrafluoroborate. *Tetrahedron Letters*, 4 (29), 2037–2044.

Winstein, S. & Buckles, R.E. (1942) The Role of Neighboring Groups in Replacement Reactions. I. Retention of Configuration in the Reaction of Some Dihalides and Acetoxyhalides with Silver Acetate. *Journal of the American Chemical Society*, 64 (12), 2780–2786.

Wipf, P., Tsuchimoto, T. & Takahashi, H. (1999) Synthetic applications of ortho esters. *Pure and Applied Chemistry*, 71 (3), 415–421.

Wipf, P., Xu, W., Kim, H. & Takahashi, H. (1997) Zirconocene-catalyzed epoxy ester - ortho ester rearrangement: A new method for the protection of polyfunctionalized carboxylic acids and the asymmetric synthesis of ortho esters. *Tetrahedron*, 53 (48), 16575–16596.

Wood, C.P., Mcdonell, V.G., Smith, R.A. & Samuelsen, G.S. (1989) Development and application of a surrogate distillate fuel. *Journal of Propulsion and Power*, 5 (4), 399–405.

Wood, J.F. & Hopkins, C.H. (1959) *Liquid fuel composition*. US Patent 2878109 A.

Wyatt, P. & Warren, S. (2013) *Organic Synthesis: Strategy and Control*. John Wiley & Sons.

Yokoyama, Y., Padias, A.B., De Blauwe, F. & Hall, H.K. (1980) Synthesis and Polymerization of 2,6,7-Trioxabicyclo[2.2.1]heptane and 1-Methyl-2,6,7-trioxabicyclo[2.2.1]heptane. *Macromolecules*, 13 (2), 252–261.

Young, P.R., Bogseth, R.C. & Rietz, E.G. (1980) Evidence for a solvent-induced change in rate-limiting step in the hydrolysis of benzaldehyde dimethyl acetal. *Journal of the American Chemical Society*, 102 (20), 6268–6271.

Zabarnick, S., DeWitt, M.J., Adams, R., West, Z.J., Shafer, L.M., Williams, T.F., Cook, R., Striebich, R., Balster, L.M., Delaney, C.L. & Phelps, D.K. (2010) *Evaluation of Triethylene Glycol Monomethyl Ether (TRIEGME) as an Alternative Fuel System Icing Inhibitor for JP-8 Fuel*.

Zanette, D., Belarmino, A.T.N., Froehner, S., Farah, J.P.S., Bunton, C.A. & Romsted, L.S. (2003) Effect of alkyl group size on the mechanism of acid hydrolyses of benzaldehyde acetals. *Journal of Organic Chemistry*, 68 (3), 1723–1727.

Zieger, H.E., Wo, S., Millar, M.M. & Koch, S.A. (1995) Synthesis of 2-Cyano-1,1,2,2-tetraphenylethyl Cation and Silver Ion Assisted Solvolysis of sym-Tetraphenylethylene Dichloride. *Journal of Organic Chemistry*, 60 (18), 5925–5930.

Appendix A

Prizes and Publications

- University of the West of England Research Forum Poster Winner (Bristol, 21 September 2012).

- Baena-Zambrana, S., Repetto, S.L., Lawson, C.P., & Lam, J.K.-W. (2013). Behaviour of Water in Jet Fuel - A Literature Review. *Progress in Aerospace Sciences*, 60, 35-44 [doi:10.1016/j.paerosci.2012.12.001].

- Fuel Additive. Repetto, S., Costello, J., De Lacy Costello, B., Ratcliffe, N. & Lam, J. Patent application number: 1307438.0. Patent application filing date: 25 April 2013.

- The Development of Novel Fuel Dehydrating Icing Inhibitors. *SAE AeroTech Congress and Exhibition* (24-26 September 2013) Montreal, Canada.

- John D. Bacha Research Award of Excellence (IASH, 2013).

- Towards Effective Fuel Dehydrating Icing Inhibitors. *13th International Conference on Stability, Handling and use of Liquid Fuels* (6-10 October 2013) Rhodes, Greece.

- Repetto, S., Costello, J., De Lacy Costello, B., Ratcliffe, N. & Lam, J. (2013). The Development of Novel Fuel Dehydrating Icing Inhibitors. *SAE International Journal of Fuels and Lubricants,* 6 (3), 553-563 [doi:10.4271/2013-01-2169].

- Airbus PhD Day Poster Winner (Bristol, 16 October 2013).

Appendix B

GC-MS analysis of Jet A-1

RT	Compound	Type	Match	Rev. Match	Peak Comment
3.105	Cyclohexane, methyl-	n	937	938	trace
3.165	Hexane, 2,5-dimethyl-	i	906	919	
3.195	Hexane, 2,4-dimethyl-	i	910	918	
3.239	Cyclopentane, ethyl-	n	937	942	
3.308	Cyclopentane, 1,2,4-trimethyl-	n	933	965	
3.416	Cyclopentane, 1,2,3-trimethyl-	n	940	942	
3.509	Hexane, 3,3-dimethyl-	i	815	896	trace
3.582	Heptane, 4-methyl-	i	912	923	
3.605	Pentane, 3-ethyl-2-methyl-	i	943	951	coeluting
3.663	Heptane, 2-methyl-	i	927	933	
3.686	Pentane, 2,3,4-trimethyl-	i	864	914	trace
3.726	Toluene	a	887	899	
3.791	Heptane, 3-methyl-	i	920	927	
3.831	Cyclopentane, 1,2,4-trimethyl-	n	755	905	coeluting
3.898	Cyclohexane, 1,3-dimethyl-	n	928	934	
3.917	Cyclohexane, 1,4-dimethyl-, trans	n	942	943	trace
4.036	Cyclohexane, 1,1-dimethyl-	n	915	916	
4.045	Cycloheptane, methyl-	n	898	902	coeluting
4.056	Cyclopentane, 1-ethyl-3-methyl-, trans	n	924	926	trace
4.123	Cyclopentane, 1-ethyl-3-methyl-, cis-	n	918	919	

4.184	Cyclopentane, 1-ethyl-1-methyl	n	871	883	
4.185	Cyclopentane, 1-ethyl-1-methyl-	n	874	881	trace
4.275	Octane	p	928	932	
4.382	Cyclohexane, 1,4-dimethyl-, cis	n	930	930	
4.451	Cyclopentane, 1,1,3,4-tetramethyl-, cis	n	858	863	
4.494	Cyclopentane, (1-methylethyl)-	n	883	889	
4.54	Hexane, 2,3,5-trimethyl-	i	875	888	trace
4.563	1-Undecene, 7-methyl-	o	830	837	
4.606	Heptane, 2,2-dimethyl-	i	912	916	
4.695	Heptane, 4,4-dimethyl-	i	848	932	
4.78	3-Tetradecene, (Z)-	o	806	808	coeluting
4.818	Heptane, 2,6-dimethyl-	i	896	897	coeluting
4.842	Octane, 2-methyl-	i	872	914	
4.925	Cyclohexane, 1,1,2-trimethyl-	n	813	820	coeluting
4.971	Cyclohexane, ethyl-	n	850	882	
4.995	Heptane, 3,5-dimethyl-	i	844	893	coeluting
5.042	Cyclohexane, 1,1,3-trimethyl-	n	868	880	
5.08	Cyclohexane, 1,1,4-trimethyl-	n	874	874	trace
5.145	Cyclohexane, 1-ethyl-2-methyl-	n	868	880	
5.252	1-Octene, 6-methyl-	o	822	826	
5.275	Cyclopentane, 1,2-Diethyl-, trans-	n	860	861	
5.361	Cyclohexane, 1,2,4-trimethyl-	n	932	940	

5.466	Heptane, 2,3-dimethyl-	i	836	903	
5.599	Ethylbenzene	a	842	934	
5.694	Octane, 4-methyl-	i	865	867	
5.831	p-Xylene	a	941	941	
5.858	Octane, 3-methyl-	i	870	896	coeluting
5.928	Cyclohexane, 1,2,3-trimethyl-	n	914	932	trace
5.956	Cyclohexane, 1,2,4-trimethyl-	n	915	927	
6.019	Cyclohexane, 1,3.5-trimethyl-	n	809	810	
6.086	Cyclohexane, 1,2,4-trimethyl-	n	915	931	
6.196	Cyclopentane, 1,3-Diethyl-, trans-	n	853	885	coeluting
6.254	Cyclohexane, 1-ethyl-3-methyl-, trans	n	923	923	
6.299	Cyclohexane, 1-ethyl-3-methyl-, cis	n	940	956	
6.383	o-Xylene	a	844	902	
6.616	Nonane	p	916	928	
6.749	Cyclohexane, 1-ethyl-4-methyl- trans	n	944	952	
6.811	Cyclohexane, 1-ethyl-4-methyl- cis	n	860	903	
6.968	Octane, 2,5,6-trimethyl-	i	838	851	coeluting
7.056	Pentalene, octahydro-, 2-methyl	n	828	843	
7.189	Benzene, 1-ethyl-2-methyl-	a	694	796	
7.345	Cyclohexane, propyl-	n	821	855	
7.458	Nonane, 3-methyl-	i	828	843	
7.646	Unknown 1 (57, 69, 43, 98, 111, 125, 140)				

7.77	Unknown 2 (67, 55, 82, 41, 125, 109, 140)				
7.891	Cyclohexane, 1,2-diethyl-, cis-	n	763	811	trace
7.999	Benzene, propyl-	a	707	859	
8.047	Cyclooctane, 1-methyl-3-propyl-	n	796	814	coeluting
8.237	Benzene, 1-ethyl-2-methyl-	a	733	838	coeluting
8.25	Nonane, 4-methyl-	i	633	773	
8.34	Nonane, 2-methyl-	i	825	841	
8.462	Benzene, 1,3,5-trimethyl-	a	703	834	
8.514	1-Decene, 4-methyl-	o	808	824	
8.563	Unknown 3 (55, 97, 81, 69, 111, 41, 140, 156)				
8.604	Cyclohexane, 2-ethyl-1,3-dimethyl-	n	777	797	coeluting
8.631	Cyclopentane,1-methyl-3-(2-methylpropyl	n	801	806	coeluting
8.736	Benzene, 1-ethyl-3-methyl-	a	891	935	
8.849	Cyclohexane, 1-methyl-2-propyl	n	855	891	
8.916	Cyclohexane, 1-methyl-3-propyl	n	795	812	
8.963	Unknown 4 (55, 69, 81, 96, 41, 111, 139, 124, 154)				
9.158	Benzene, 1,2,3-trimethyl-	a	890	921	
9.4	Decane	p	902	911	
9.494	Unknown 5 (55, 97, 81, 69, 41, 91, 111, 140, 152)				
9.547	Unknown 6 (91, 69, 95, 81, 55, 41, 111, 134, 152)				
9.628	Benzene, (1-methylpropyl)-	a	753	883	

9.715	Unknown 7 (57, 43, 85, 71, 95, 111, 123, 137)				
9.974	Benzene, 1,2-diethyl-	a	827	865	
10.118	Decane, 4-methyl-	i	774	850	
10.24	Cyclohexane, butyl-	n	838	859	
10.306	Benzene, 1-ethenyl-4-methyl-	a	653	810	
10.331	Benzene, cyclopropyl-	a	799	906	coeluting
10.42	Nonane, 3,7-dimethyl-	i	667	802	
10.554	Cyclohexane, 1-Ethyl-2,2,6-trimethyl-	n	786	854	
10.608	Cyclopentane, 1,2-dipropyl-	n	798	809	
10.805	Benzene, 1-methyl-3-propyl-	a	752	880	
10.908	Benzene, butyl-	a	749	840	
10.975	Benzene, 1-ethyl-2,4-dimethyl-	a	780	835	
11.013	Benzene, 2-ethyl-1,4-dimethyl-	a	792	910	coeluting
11.066	Nonane, 4-methyl-5-propyl-	i	732	869	
11.176	Decane, 2-methyl-	i	870	893	
11.239	Benzene, 1-methyl-4-propyl-	a	916	918	
11.36	Decane, 3-methyl-	i	824	899	
11.448	Cyclohexane, 1,2-diethyl-3-methyl-	n	791	824	
11.555	Benzene, 1-ethyl-3,5-dimethyl-	a	899	917	
11.597	Benzene, 1-methyl-4-(1-methylethyl)-	a	832	845	
11.747	Cyclohexane, 1-isopropyl-1-methyl-	n	759	826	coeluting
11.768	Benzene, 1-methyl-3-(1-methylethyl)-	a	745	879	
11.888	Cyclopentane, 1,2-dipropyl-	n	805	833	

11.945	Benzene, 2-ethyl-1,4-dimethyl-	a	794	864	
12.021	Cyclohexane, 2,4-diisopropyl -1,1-dimethyl-	n	773	782	coeluting
12.084	Cyclohexane, (1-methylbutyl)-	n	702	809	
12.303	Undecane	p	861	909	
12.376	Benzene, 1,3-diethyl-4-methyl-	a	687	849	
12.427	Octane, 5-ethyl-2-methyl-	i	651	835	
12.553	Decalin, 2-methyl-, trans-	n	822	839	
12.687	Benzene, 1,3-diethyl-5-methyl-	a	711	847	
12.812	Benzene, 1,2,4,5-tetramethyl-	a	782	885	
12.863	Octane, 2,6,6-trimethyl-	i	732	801	coeluting
12.973	Naphthalene, decahydro-2-methyl-	a	742	766	
12.988	Unknown 8 (71, 57, 43, 152, 95, 81, 67, 85, 137, 109, 166)				coeluting
13.191	Cyclohexane, pentyl-	n	800	852	
13.31	Cyclopentane, hexyl-	n	624	877	
13.471	Benzene, 1,3-diethyl-5-methyl-	a	739	902	
13.507	Benzene, 1-methyl-4-(1-methylpropyl)-	a	782	841	
13.592	Cyclohexane, 1-methyl-4-(1-methylbutyl)-	n	734	746	
13.637	1H-Indene, 2,3-dihydro-4-methyl-	o	882	888	

13.646	Benzene, 1-methyl-2-(2-propenyl)-	a	882	889	coeluting
13.721	Benzene, 1,3-diethyl-	a	668	760	
13.73	Undecane, 6-methyl-	i	635	800	coeluting
13.774	2,6-Dimethyldecane	i	796	859	
13.81	Decane, 2,6-dimethyl-	i	860	876	
13.871	Decane, 2,3-dimethyl-	i	697	861	coeluting
13.872	Benzene, (1-methylbutyl)-	a	737	789	
13.922	Undecane, 4-methyl-	i	650	878	
13.995	Naphthalene, 1,2,3,4-tetrahydro-	a	843	848	coeluting
14.052	Undecane, 2-methyl-	i	844	890	
14.094	Benzene, (1,2-dimethylpropyl)-	a	763	829	
14.226	Undecane, 3-methyl-	i	802	869	
14.367	Benzene, 1-methyl-4-(1-methylpropyl)-	a	743	809	
14.503	Naphthalene, decahydro-2,6-dimethyl-	a	758	770	coeluting
14.619	Naphthalene	a	843	909	
14.672	Cyclohexane, 1-methyl-2-pentyl-	n	795	798	
14.773	Cyclohexane, 1-methyl-4-(1-methylbutyl)-	n	758	787	
14.87	Benzene, 2,4-diethyl-1-methyl-	a	713	773	
15.019	1H-Indene,2,3-dihydro-2,2-dimethyl-	o	702	861	coeluting
15.153	Dodecane	p	872	908	
15.201	Unknown 9 (57, 71, 43, 119, 83, 95, 145, 151, 162, 166)				coeluting
15.243	Unknown 10 (55, 83, 41, 119, 95, 151, 162, 166, 180)				

15.36	Unknown 11 (57, 133, 43, 85, 71, 106, 148, 162, 166, 184)				coeluting
15.362	Benzene, 1-methyl-2-(1-ethylpropyl)-	a	613	643	
15.478	Undecane, 2,6-dimethyl-	i	809	948	
15.556	Decane, 4-ethyl-	i	545	808	
15.671	Unknown 12 (57, 43, 71, 85, 95, 109, 123, 166, 182)				
15.712	4-Nonene, 5-butyl-	o	737	750	
15.753	Naphthalene, 2-ethyldecahydro-	a	570	606	
15.798	Undecane, 4,7-dimethyl-	i	800	867	
15.995	Undecane, 2,9-dimethyl-	i	575	853	coeluting
16.054	Benzene, 1-ethyl-2,4,5-trimethyl-	a	720	863	
16.138	Cyclohexane, (4-methylpentyl)-	n	820	882	
16.221	Cyclododecane	n	781	835	
16.264	Benzene, 1-ethyl-4-(2-methylpropyl)-	a	683	786	coeluting
16.324	Unknown 13 (145, 120, 133, 162, 105, 55, 69, 180, 194)				
16.43	Benzene,1-cyclopropylmethyl-4-(1-methylethyl)-	a	631	696	coeluting
16.478	Dodecane, 6-methyl-	i	674	838	coeluting
16.512	Decane, 5-propyl-	i	598	774	
16.569	Unknown 14 (43, 85, 57, 71, 133, 97, 126, 162, 182, 194)				
16.704	Unknown 15 (71, 43, 57, 85, 105, 119, 165, 180)				

16.838	Dodecane, 4-methyl-	i	724	866	
16.896	Naphthalene,1,2,3,4-tetrahydro-6-methyl-	a	736	798	
17.036	Undecane, 6-ethyl-	i	807	861	coeluting
17.099	Undecane, 6,6-dimethyl-	i	790	882	
17.165	Unknown 16 (57, 145, 69, 41, 83, 131, 160, 176, 196)				
17.223	Unknown 17 (57, 119, 69, 41, 83, 133, 162, 196)				
17.334	Benzene, 1,3,5-trimethyl-2-propyl-	a	585	727	
17.523	Cyclotridecane	n	774	856	
17.716	Naphthalene, 1-methyl-	a	787	893	
17.899	Tridecane	p	874	884	
18.04	Dodecane, 2,4-dimethyl-	i	715	873	
18.166	Naphthalene, 2-methyl-	a	900	922	
18.283	Dodecane, 2,5-dimethyl-	i	804	835	
18.372	Benzocyclooctene,5,6,7,8,9,10-hexahydro-	a	788	840	
18.498	Unknown 18 (57, 69, 41, 97, 81, 159, 145, 133, 176, 196)				
18.592	Unknown 19 (145, 55, 69, 81, 97, 41, 160, 174, 180, 196)				
18.668	Unknown 20 (57, 41, 71, 97, 129, 145, 176, 196)				
18.74	Unknown 21 (129, 57, 119, 69, 41, 83, 158, 176, 194)				
18.935	Heptylcyclohexane	n	726	791	
18.994	Unknown 22 (69, 55, 83, 41, 97, 111, 145, 174, 182, 194)				
19.125	Tridecane, 6-methyl-	i	775	851	
19.203	Tridecane, 5-methyl-	i	628	861	coeluting

19.207	Benzene, 1-methyl-3-hexyl-	a	586	828	
19.336	Tridecane, 4-methyl-	i	751	897	
19.474	Tridecane, 2-methyl-	i	817	907	
19.639	Tridecane, 3-methyl-	i	724	865	
19.706	Unknown 23 (57, 97, 69, 41, 81, 119, 109, 123, 193, 208)				
19.825	Dodecane, 2,6,10-trimethyl-	i	842	895	
19.915	Biphenyl	a	797	882	
20.038	Cyclopentane, 1-butyl-2-pentyl-	n	668	783	
20.19	Cyclotetradecane	n	775	834	
20.288	Naphthalene, 2-ethyl-	a	743	885	
20.487	Tetradecane	p	866	904	
20.538	Naphthalene, 1,6-dimethyl-	a	702	753	
20.587	Naphthalene, 1,5-dimethyl-	a	872	911	
20.798	Tridecane, 5-propyl-	i	678	820	
20.96	Naphthalene, 1,7-dimethyl-	a	855	923	
21.053	Naphthalene, 2,6-dimethyl-	a	892	928	
21.214	Dodecane, 2-methyl-8-propyl-	i	656	779	coeluting
21.218	5,5-Dibutylnonane	i	609	872	
21.324	Unknown 24 (57, 119, 69, 41, 83, 97, 145, 159, 190, 208)				
21.447	Naphthalene, 1,8-dimethyl-	a	822	922	
21.531	Naphthalene, 1,3-dimethyl-	a	626	687	coeluting
21.581	Cyclohexane, octyl-	n	828	839	
21.698	Tetradecane, 5-methyl-	i	769	876	
21.827	Tetradecane, 4-methyl-	i	629	768	
21.957	Unknown 25 (57, 71, 43, 85, 99, 113, 141, 183, 193)				
22.072	Benzene, octyl-	a	658	753	
22.135	Tetradecane, 3-methyl-	i	845	908	

22.194	Benzene, (1-methylheptyl)-	a	708	764	
22.268	Unknown 26 (57, 69, 97, 41, 83, 111, 159, 173, 224)				coeluting
22.368	Unknown 27 (57, 71, 85, 43, 97, 119, 133, 159, 173, 188, 208)				
22.555	1,1'-Biphenyl, 3-methyl-	a	766	833	
22.633	Naphthalene, 1-propyl-	a	730	788	
22.699	Cyclopentadecane	n	722	822	
22.77	1,1'-Biphenyl, 4-methyl-	a	682	901	
22.895	Pentadecane	p	884	911	
23.024	Naphthalene, 2-(1-methylethyl)-	a	625	789	
23.147	Unknown 28 (155, 57, 170, 71, 43, 83, 97, 105, 128, 161, 188)				
23.288	Naphthalene, 1,4,6-trimethyl-	a	663	736	
23.429	Naphthalene, 1,2,3,4-tetrahydro-5,6,7,8-tetramethyl-	a	671	738	
23.532	Naphthalene, 1,6,7-trimethyl-	a	840	919	
23.647	Naphthalene, 2,3,6-trimethyl-	a	867	891	
23.857	Unknown 29 (55, 141, 69, 97, 105, 83, 41, 120, 133, 157, 204)				coeluting
23.93	Pentadecane, 7-methyl-	i	734	829	
24.067	n-Nonylcyclohexane	n	771	835	

24.105	Unknown 30 (57, 71, 43, 170, 155, 85, 97, 145, 188, 202)				coeluting
24.201	Tridecane, 7-hexyl-	i	742	835	
24.325	Pentadecane, 2-methyl-	i	817	871	
24.378	Unknown 31 (57, 71, 43, 85, 170, 155, 97, 127, 141, 197, 240)				
24.485	Pentadecane, 3-methyl-	i	805	885	
24.64	Hexane, 2-phenyl-3-propyl-	a	672	759	
24.856	Unknown 32 (165, 166, 155, 57, 184, 83, 69, 43, 97, 115, 179, 232)				
24.975	Unknown 33 (57, 170, 155, 43, 71, 85, 97, 141, 165, 182, 202, 216)				
25.182	Hexadecane	p	875	900	
25.306	Unknown 34 (57, 71, 43, 97, 83, 167, 182, 155, 218, 230, 253)				trace
25.625	Unknown 35 (155, 184, 169, 57,105,41,69,83,97,218,233				trace
25.752	Unknown 36 (169, 182, 57, 71, 43, 97, 83, 152, 236)				trace
26.188	Hexadecane, 7-methyl-	i	723	830	
26.267	Pentadecane, 2,6,10-trimethyl-	i	850	891	
26.434	Cyclohexane, decyl-	n	787	863	
26.58	Unknown 37 (57, 43, 71, 85, 97, 106, 169, 197, 218, 236)				trace
26.75	Unknown 38 (57, 71, 43, 85, 97, 111, 141, 211, 224)				trace

27.398	Heptadecane	p	855	893	
27.52	Hexadecane, 2,6,10-trimethyl-	i	822	892	
29.525	Octadecane	p	844		
29.71	Hexadecane, 2,6,10,14-tetramethyl-	i	839		trace